ULTRA-LEAN METHANE COMBUSTION IN POROUS BURNERS

ULTRA-LEAN METHANE COMBUSTION IN POROUS BURNERS

Mitigation of methane emissions, pilot-scale demonstration and computational fluid dynamics model

Susie Wood

Reference should be made to this work as follows: Wood S. 2010. Ultra-lean methane combustion in porous burners: Mitigation of methane emissions, pilot-scale demonstration and computational fluid dynamics model. PhD thesis, The University of Sydney.

For Dominic

ABSTRACT

Ultra-lean methane combustion in porous burners is investigated by means of a pilot-scale demonstration of the technology supported by a computational fluid dynamics (CFD) modelling study. The suitability of porous burners as a lean-burn technology for the mitigation of methane emissions is also evaluated.

Methane constitutes 14.3% of total global anthropogenic greenhouse gas emissions. The mitigation of these emissions could have a significant near-term effect on slowing global warming, and recovering and burning the methane would allow a wasted energy resource to be exploited. The typically low and fluctuating energy content of the emission streams makes combustion difficult; however porous burners—an advanced combustion technology capable of burning low-calorific value fuels below the conventional flammability limit—are a possible mitigation solution.

A pilot-scale porous burner is designed expressly for the purpose of ultra-lean methane combustion. The burner comprises a cylindrical combustion chamber filled with a porous bed of alumina saddles, combined with an arrangement of heat exchanger tubes for preheating the incoming methane/air mixture. A CFD model is developed to aid in the design process. Results illustrating the operating range and behaviour of the burner are presented. Running on natural gas, the stable lean flammability limit of the system is 2.3 vol%, a considerable extension of the conventional lean limit of 4.3 vol%; operating in the transient combustion regime allows the lean limit to be reduced further still, to 1.1 vol%. The heat exchanger arrangement is found to be effective; preheat temperatures of up to 800K are recorded. Emissions of carbon monoxide and unburned hydrocarbons are negligible. The process appears stable to fluctuations in fuel concentration and flow rate, typically taking several hours to react to any changes.

A CFD model of the porous burner is developed based on the commercial CFD code ANSYS CFX 12.0. The burner is modelled as a single 1-dimensional porous domain. Pressure loss due to the presence of the porous solid is accounted for using an isotropic loss model. Separate energy equations for the gas and solid phases are applied. Models for conductive heat transfer within the solid phase, and for convective heat transport between the gas and solid phases, are added. Combustion is modelled using a finite rate chemistry model; a skeletal mechanism for ultra-lean methane combustion is developed and incorporated into the model to describe the combustion reaction. Results from the model are presented and validated against experimental data; the model correctly predicts the main features of burner behaviour.

Porous burners are found to show potential as a methane mitigation technology.

CONTENTS

ACKNOWLEDGEMENTS

I gratefully acknowledge the financial support of the Australian Coal Association Research Program (ACARP), as well as the School of Chemical and Biomolecular Engineering at the University of Sydney for the award of a scholarship.

I also acknowledge the assistance of the team at BEST Energies Australia in designing and building the pilot-scale porous burner. I would particularly like to thank Adrian Dawson and Stephen Joseph for their input into the design process.

I am grateful to David Fletcher for his invaluable advice on CFD modelling. I would also like to thank him for his general support throughout the project, and in the preparation of this thesis.

I would like to thank Brian Haynes for his guidance on combustion chemistry and mechanism reduction, and Catharine Tierney for her assistance in implementing the heat transfer models in CFX.

I also acknowledge the advice of Juan Carlos Morales and Phil Stopford of ANSYS regarding the use of additional variables and the stiff chemistry solver respectively in the CFD model.

I would like to thank my supervisor, Andrew Harris, for his continued help and support throughout the project.

Finally, I would like to thank my husband Dominic for being there when I needed him over the past four years. And for proofreading all 268 pages of this thesis.

LIST OF FIGURES

LIST OF TABLES

NOMENCLATURE

Units are given in parentheses.

Acronyms

AGO	Australian Greenhouse Office
CAD	Computer aided design
CARS	Coherent anti-stokes Raman scattering
CBM	Coal bed methane
CCS	Carbon capture and storage
CCT	Clean coal technology
CFD	Computational fluid dynamics
CFRR	Catalytic flow reversal reactor
CHP	Combined heating and power
CCHP	Combined cooling, heating and power
CIAB	Coal Industry Advisory Board
CMM	Coal mine methane
CMR	Catalytic monolith reactor
CO_2-eq	Carbon dioxide equivalent
CSIRO	Commonwealth Scientific and Industrial Research Organisation
DCC	Department of Climate Change
DI&M	Direct inspection and maintenance
DTI	Department of Trade and Industry
ECBM	Enhanced coal bed methane
ECT	Electrical capacitance tomography
EFCC	Externally fired combined cycle
EGR	Exhaust gas recirculation
EPA	Environmental Protection Agency
FAO	Food and Agriculture Organization

FRR	Flow reversal reactor
GDP	Gross domestic product
GHG	Greenhouse gas
GUI	Graphical user interface
GWP	Global warming potential
HCCI	Homogeneous charge compression ignition
HHV	Higher heating value
IC	Internal combustion
IGCC	Integrated gasification combined cycle
IEA	International Energy Agency
IPCC	Intergovernmental Panel on Climate Change
ISAT	In-situ adaptive tabulation
LFG	Landfill gas
LHV	Lower heating value
LIF	Laser induced fluorescence
LNG	Liquefied natural gas
LPG	Liquefied petroleum gas
MAC	Marginal abatement cost
MBT	Mechanical biological treatment
MCFC	Molten carbonate fuel cell
MFC	Mass flow controller
MIMS	Mineral-insulated metal-sheathed
MIT	Massachusetts Institute of Technology
MSW	Municipal solid waste
MVA	Mine ventilation air
NG	Natural gas
NSW	New South Wales
NZ	New Zealand
P&ID	Piping and instrumentation diagram

PB	Porous burner
PCA	Principal component analysis
PE	Partial equilibrium
PF	Pulverised fuel
PFBC	Pressurised fluidised bed combustion
PFD	Process flow diagram
PFR	Plug flow reactor
ppb	Parts per billion
ppcm	Pores per centimetre
ppm	Parts per million
QSS	Quasi-steady state
R&D	Research and development
SEM	Scanning electron microscope
slpm	Standard litres per minute
SOFC	Solid oxide fuel cell
TFRR	Thermal flow reversal reactor
UHC	Unburned hydrocarbons
UN	United Nations
UNFCCC	United Nations Framework Convention on Climate Change
USC	Ultra-supercritical
VAM	Ventilation air methane
VOC	Volatile organic compound

Chemical formulae and abbreviations

Al_2O_3	Alumina
Ar	Argon
CFC	Chlorofluorocarbon
CH_2O	Formaldehyde
CH_3	Methyl radical

CH_4	Methane
C_2H_6	Ethane
C_3H_8	Propane
C_4H_{10}	Butane
C_5H_{12}	Pentane
C_6H_{14}	Hexane
Cl	Chlorine atom
CO	Carbon monoxide
CO_2	Carbon dioxide
H	Hydrogen radical
H_2	Hydrogen molecule
H_2O	Water
H_2S	Hydrogen sulphide
HCl	Hydrogen chloride
He	Helium
HFC	Hydrofluorocarbon
LAS	Lithium aluminium silicate
N_2	Nitrogen molecule
N_2O	Nitrous oxide
NO_X	Nitrogen oxides
O_2	Oxygen molecule
O_3	Ozone
OH	Hydroxyl radical
PAH	Polycyclic aromatic hydrocarbons
PFC	Perfluorocarbon
PSZ	Partially stabilised zirconia
SF_6	Sulphur hexafluoride
SiC	Silicon carbide

SiSiC	Silicon silicon carbide
SO_X	Sulphur oxides
YZA	Yttria-stabilised zirconia/alumina composite
ZrO_2	Zirconia
ZTA	Zirconia-toughened alumina
ZTM	Zirconia-toughened mullite

Roman symbols

A	Area (m^2)
A	Pre-exponential factor in the Arrhenius equation (mol cm s K)
A_v	Area density (m^{-1})
V	Volume (m^3)
c_p	Heat capacity at constant pressure ($Jkg^{-1}K^{-1}$)
D	Binary diffusion coefficient (m^2s^{-1})
d_h	Hydraulic diameter (m)
d_s	Equivalent spherical diameter (m)
E	Energy (J)
E_a	Activation energy (cal mol^{-1})
H	Enthalpy (J)
h	Heat transfer coefficient ($Wm^{-2}K^{-1}$)
h_s	Surface heat transfer coefficient ($Wm^{-2}K^{-1}$)
h_v	Volumetric heat transfer coefficient ($Wm^{-3}K^{-1}$)
k	Reaction rate coefficient (mol cm s)
k	Thermal conductivity ($Wm^{-1}K^{-1}$)
L	Length (m)
m	Hydraulic radius (m)
N_s	Number of chemical species
n	Coordinate in the normal direction (m)

Nu	Nusselt number
p	Pressure (Pa)
Pr	Prandtl number
Q	Volumetric flow rate (m^3s^{-1})
R	Ideal gas constant (cal $K^{-1}mol^{-1}$)
r	Reaction rate (mol $cm^{-3}s^{-1}$)
Re	Reynolds number
S_E	Energy source term (Wm^{-3})
$\mathbf{S}_M$	Momentum source term ($kgm^{-2}s^{-2}$)
T	Temperature (K)
t	Time (s)
u	Velocity (ms^{-1})
u	Velocity vector (ms^{-1})
W	Molecular weight (kg mol^{-1})
X	Mass fraction (-)

Greek symbols

β	Temperature exponent in the Arrhenius equation
κ	Permeability (m^2)
λ	Shape factor (-)
μ	Viscosity ($kgm^{-1}s^{-1}$)
ρ	Density (kgm^{-3})
σ_t	Model constant for the k-ε model (-)
Φ	Porosity (-)
ϕ	Equivalence ratio (-)
Γ	Diffusivity (m^2s^{-1})
υ	Stoichiometric coefficient
ω	Molar rate of production (mol $m^{-3}s^{-1}$)

Ψ	Diffusive variable (K)

Subscripts

g	Gas
in	Inlet
inf	Infinity
k	k^{th} species
m	m^{th} species
p	Porous
s	Solid
t	Turbulent

INTRODUCTION

Methane (CH_4) emissions constitute 14.3% of total global anthropogenic greenhouse gas emissions. As CH_4 has a global warming potential 25 times greater than that of carbon dioxide (CO_2), but a relatively short atmospheric lifetime of only 12 years, the mitigation of these emissions will likely have a significant near-term effect on slowing global warming. Also, as CH_4 is a clean burning fuel, in recovering and burning the emissions a hitherto wasted energy resource can be exploited. However, while CH_4 is emitted from a wide range of activities, including coal mining, gas distribution, agriculture and waste management, many of these emission sources are diffuse and hence not amenable to recovery. Furthermore, once captured, the extremely low and often fluctuating energy content of the emission stream makes combustion difficult.

Porous burners are a possible lean-burn mitigation technology with the potential to overcome these challenges. They operate on the principle that the presence of a porous solid, such as a packed bed, in the combustion chamber of the burner serves as a means of recirculating heat from the hot combustion products back to the incoming CH_4/air mixture; this preheating of the incoming mixture enables the burner to operate in 'ultra-lean' mode on gases with a CH_4 concentration below the conventional lean flammability limit (5 vol% CH_4 in air). Burner performance is also typically characterised by increased burning velocities, low emissions of combustion related pollutants, and stable operation over a wide range of conditions.

In this thesis, ultra-lean CH_4 combustion in porous burners is investigated by means of a pilot-scale demonstration of the technology supported by a computational fluid dynamics (CFD) modelling study. The suitability of porous burners as a lean-burn technology for the mitigation of anthropogenic CH_4 emissions is also assessed.

Part 1 of the thesis provides the necessary background to the problem. Chapter 1 discusses CH_4 emissions: the function of CH_4 in the atmosphere and its role as a greenhouse gas are explained; evidence of elevated atmospheric CH_4 concentrations is provided; and the various natural and anthropogenic emissions sources responsible discussed. Possible approaches to mitigating emissions from each source are then reviewed, and a technical analysis of the available options is performed.

Chapter 2 takes the form of a case study. The emissions and associated mitigation solutions for a single source—coal mining—are examined in more detail. Coal mining is one of the sectors with the greatest potential for CH_4 mitigation; it also serves as a useful case study because these emissions are some of the most challenging to mitigate from a technical perspective. The CH_4 in the mine ventilation air (MVA)—which accounts for the majority of the emissions—is present at extremely low concentrations

(typically less than 1 vol%); the mitigation of these emissions requires the development and commercialisation of advanced lean-burn combustion technologies.

Chapter 3 reviews the use of porous burners for lean-burn applications such as the combustion of MVA and other CH_4 emissions. However, although there is an extensive body of research relating to porous burners, the majority is directed towards their use for radiant heating rather than for ultra-lean combustion; they have not previously been considered for the mitigation of methane emissions.

Part 2 of the thesis describes a pilot-scale demonstration of a porous burner system. The main aims of the pilot-scale study are to demonstrate the concept of ultra-lean CH_4 combustion in porous burners; to determine the lowest lean flammability limit at which stable operation can be achieved in a practical system; and to obtain the performance data needed to evaluate porous burners as a potential CH_4 mitigation technology.

Demonstration at pilot-scale is a key phase in the technology development process. It allows issues relating to scale-up and adaptation for industrial utilisation to be explored more fully than at bench scale. Analytical and process control requirements can be determined, preliminary information on operating and maintenance procedures compiled, and any limitations in the equipment or process design identified. Most importantly, a pilot-scale study results in an invaluable database of operational and technical performance statistics, including data on the predictability and reliability of the process. This information is invaluable if an accurate system and economic analysis of a technology's suitability for a real-world application—such as CH_4 mitigation—is to be performed.

In the case of porous burners, there are also particular process issues that make a pilot-scale study appropriate. First, the length of the porous bed is thought to be a significant determinant of the stable operating range of the burner. Second, as the combustion chamber of the burner is filled with a porous solid in the form of a packed bed, the use of a larger cross-section avoids there being a low bed-to-particle diameter ratio, and thus prevents a situation where wall effects dominate the system. Third, a larger cross-section also means that the effect of radial heat losses on the combustion process will be less significant.

Chapter 4 describes the design and construction of the pilot-scale burner. The burner is designed expressly for the purpose of ultra-lean CH_4 combustion and hence a number of innovative features—identified as being relevant to the optimisation of burner performance for ultra-lean applications—are incorporated into the design. Foremost amongst these is the integration of a heat exchanger into the system to recuperate additional heat from the combustion process, and thus enhance the internal heat recirculation provided by the porous bed. In order to investigate ultra-lean combustion,

it is necessary to run the burner at the limits of its operating range; an even flow distribution is essential under these conditions. A CFD model is therefore developed to assist in the design process, by allowing the flow pattern of the gas through the proposed system to be simulated.

Chapter 5 describes the experimental set-up for the pilot-scale demonstration. Details of the equipment used for flow measurement and control, temperature measurement, data acquisition, and exhaust gas analysis are provided. An effective burner operating procedure is also developed.

A series of experiments is undertaken in which burner operating conditions are systematically varied and the temperature profile in the porous bed measured to determine if, and where in the bed, the flame stabilises. Chapter 6 presents the results of these experiments. The main features of burner behaviour are illustrated, and the performance of the system discussed. The key performance measure for the purpose of this study is the stable lean flammability limit of the system; a burner map illustrating the stable operating range is therefore developed. The emissions profile of the burner is also considered.

Part 3 of the thesis concerns the development of a CFD porous burner model. The ultimate aim is to create a comprehensive model capable of accurately describing ultra-lean CH_4 combustion in a porous burner. The model is intended to augment the experimental pilot-scale demonstration.

Numerical modelling can lead to better understanding of burner behaviour. It provides additional data—such as local gas and solid temperatures, and species concentrations—not readily available via experimental means, and can thus reveal physical features of the system that might otherwise go unrecognised. This is particularly the case for porous burners, because accurate measurements from within the combustion chamber are inherently difficult to obtain due to the restrictive presence of the porous solid. Modelling also allows for the investigation of parameters that it would not be possible or practical to study experimentally in a reasonable timeframe.

The motivation behind using CFD is that it will eventually allow for the realisation of a multi-dimensional model of sufficient complexity to simulate the operation of 'real' burners, rather than an idealised combustion process.

The processes of momentum, heat and mass transfer in any system are described by a set of partial differential equations known as the Navier-Stokes equations; these have no known general analytical solution, but can be solved numerically by CFD codes. CFD is therefore a powerful tool for the calculation of fluid flow, heat transfer and other physical processes, and has previously been used to assist in the design of industrial burners (Gershtein and Baukal 2001; Lockwood et al. 2000).

The aim in this thesis is to demonstrate the viability and general applicability of CFD to modelling porous burners. However, the modelling of complex physics—such as combustion—in extensive geometries is computationally demanding. There is consequently a risk, in employing a modelling approach based on CFD, that the high computational requirements will make it unfeasible.

In order to accurately describe combustion behaviour in a porous burner, it is necessary to use a relatively detailed multi-step chemical kinetic mechanism. However, as comprehensive mechanisms for CH_4 combustion typically contain several hundred elementary reactions, the use of full combustion chemistry in a CFD code would be prohibitively computationally expensive. It is therefore necessary to develop a suitable skeletal mechanism to use in the porous burner model. A skeletal mechanism is a subset of reactions extracted from a full mechanism by elimination of the inconsequential species and reactions, such that it is still able to predict the relevant features of the combustion process over the range of conditions of interest; this is a widely used approach for the efficient implementation of combustion chemistry. Chapter 7 describes the reduction of a comprehensive CH_4 oxidation mechanism to a skeletal mechanism for ultra-lean combustion.

Chapter 8 describes the development of the CFD model itself. The commercial CFD code ANSYS CFX 12.0 is used as the basis for the model. The use of any commercial code for non-standard applications inevitably poses challenges; in this case, because CFX does not support heat transfer in a porous solid, it is necessary to add models to describe conductive heat transfer within the solid, as well as convective heat transfer between the solid and gas. The means by which the combustion mechanism is incorporated into the model is also described. The CFD model is then validated against experimental data from the pilot-scale porous burner, and some initial results presented.

Based on the results from the pilot-scale demonstration and modelling study, the suitability of porous burners as a lean-burn technology for the mitigation of CH_4 emissions is evaluated. Limitations in the design of the pilot-scale system, and in the experimental and modelling approaches used, are then discussed. Finally, possible improvements are suggested and opportunities for future research are identified.

Part 1

BACKGROUND

Chapter 1

MITIGATION OF METHANE EMISSIONS

1.1 Introduction

The Intergovernmental Panel on Climate Change (IPCC) concluded in their Fourth Assessment Report: (1) that warming of the climate system is unequivocal, as is now evident from observations of increases in global average air and ocean temperatures, widespread melting of snow and ice and rising global average sea levels; (2) that most of the observed increase in global average temperatures since the mid-20th century is very likely due to the observed increase in anthropogenic greenhouse gas emissions; and (3) that this anthropogenic warming has likely had, and will continue to have, a discernible influence at the global scale on observed changes in many physical and biological systems (IPCC 2007c).

Australia is already experiencing impacts from recent climate change, as is evident in increasing stresses on water supply and agriculture, and changing natural ecosystems. Water security problems are predicted to intensify in Southern and Eastern Australia in the future as a result of reduced precipitation and increased evaporation; production from agriculture and forestry is also expected to decline in these areas due to increased drought and fire. Significant losses in biodiversity are projected to occur in some ecologically rich sites including the Great Barrier Reef and Queensland Wet Tropics. In areas such as South-East Queensland, ongoing coastal development and population growth are projected to exacerbate the risks from sea-level rise and increases in the severity and frequency of storms and coastal flooding (IPCC 2007a).

Global atmospheric concentrations of greenhouse gases (GHG) have increased markedly as a result of human activities since 1750 and now far exceed pre-industrial levels (IPCC 2007d). Most current discussions of greenhouse gas mitigation focus on energy-related carbon dioxide (CO_2) emissions. CO_2 is the largest contributor to climate change, so this emphasis is justified, however it is estimated that almost a third of the

enhanced greenhouse effect observed since pre-industrial times is actually due to non-CO_2 greenhouse gases (Hansen et al. 2000).

Foremost among these is methane (CH_4), an extremely potent but short-lived greenhouse gas that is emitted from a wide range of sources across the agricultural, energy, and waste management sectors, as well as from natural sources. This chapter discusses these emissions, and assesses the options available for their mitigation.

The first half of the chapter reviews the problem: First, the function of CH_4 in the atmosphere, including its role as a greenhouse gas, will be discussed. Second, evidence of elevated atmospheric CH_4 concentrations due to human activity, and the subsequent contribution of CH_4 to the enhanced greenhouse effect, will be reviewed. Third, the latest estimates of current and future CH_4 emissions will be presented, and the various individual emissions sources described.

The second half of the chapter analyses the solution. First, the motivation behind mitigating CH_4 emissions will be clarified, and the overall potential for emissions reductions assessed. Second, the mitigation options that exist for each emissions source will be reviewed. Third, an analysis of the different options will be performed, and some common approaches and key technologies, that apply across sources and sectors, identified. Finally, the barriers that prevent mitigation measures from being adopted will be described, and some means of overcoming these suggested.

1.2 Methane emissions

1.2.1 Atmospheric methane

The existence of CH_4 in the atmosphere has been known since about 1948 (Khalil 2000). It has subsequently been discovered that CH_4 is the most abundant reactive trace gas in the troposphere and that its reactivity is important in both tropospheric and stratospheric chemistry (IPCC 2007d; Khalil 2000; Wuebbles and Hayhoe 2002; Wuebbles, Hayhoe and Kotamarthi 2000).

Most CH_4 is removed from the atmosphere by reaction with hydroxyl free radicals (OH) in the troposphere. The oxidation of CH_4 by OH produces methyl radicals (CH_3)—which are subsequently oxidised further to form formaldehyde (CH_2O), and eventually CO_2—as well as water vapour, and ozone (O_3). In the presence of the elevated levels of nitrogen oxides (NO_X) typical of the more polluted Northern Hemisphere, carbon monoxide (CO) is also produced—this will in turn react with OH to form CO_2.

Some CH_4 also enters the stratosphere, where it is again oxidised by OH, thus increasing levels of stratospheric water vapour and O_3. It also reacts with free chlorine atoms (Cl) to produce the less reactive hydrogen chloride (HCl).

OH, which is formed from the photo-dissociation of tropospheric O_3 and water vapour, is crucial to atmospheric chemistry as it acts as the primary oxidant for most pollutants, including CO, NO_X, CH_4 and other organic compounds. By helping to control the level of OH, CH_4 plays a vital role in determining the oxidising capacity of the atmosphere.

CH_4 also plays a significant role in O_3 chemistry. Tropospheric O_3—concentrations of which increase roughly in line with CH_4 concentrations—is an oxidant that damages natural ecosystems, agriculture and materials, and adversely affects human health (West and Fiore 2005; West et al. 2006).

CH_4 itself has no appreciable effect on local or regional air pollution.

1.2.1.1 Methane as a greenhouse gas

This review is concerned primarily with the role of CH_4 as a greenhouse gas. Greenhouse gases effectively absorb thermal infrared radiation emitted from the earth's surface, thus trapping heat in the atmosphere. As a result the earth's surface temperature is estimated to be approximately 30ºC warmer than it would be if such gases were not present, allowing life on earth to flourish (Jardine et al. 2004).

Water vapour, CO_2, nitrous oxide (N_2O), CH_4 and O_3 are the primary greenhouse gases in the earth's atmosphere (IPCC 2007d). Although the atmospheric abundance of CH_4 is less than 0.5% that of CO_2, it has been estimated that the presence of CH_4 at current levels causes the average global surface temperature to be about 1.3ºC higher than it would otherwise be (Wuebbles and Hayhoe 2002).

CH_4 is one of the six Kyoto Protocol gases, identified by the IPCC (2007d) as contributing to the enhanced greenhouse effect[†]; the others are CO_2, N_2O, sulphur hexafluoride (SF_6), hydrofluorocarbons (HFCs), and perfluorocarbons (PFCs). Each of these gases has a different global warming potential (GWP)[‡] and atmospheric lifetime, as shown in Table 1.1, and so affects the extent and rate of global warming in different ways.

CH_4, which has a 100-year GWP of 25[§], traps heat in the atmosphere more effectively than CO_2, but has a relatively short atmospheric lifetime of only 12 years. Because CH_4 is potent yet short-lived it predominantly affects the short-term rate of global warming.

[†] The enhanced greenhouse effect is the increase in the natural greenhouse effect through increased concentrations of greenhouse gases as a result of human activities.

[‡] GWP is a measure of the cumulative radiative forcing per unit mass of a gas relative to that of CO_2 over a given time horizon. Radiative forcing is determined by the balance between the solar radiation absorbed and the infrared radiation emitted by the gas.

[§] The 100-year GWP is used by the Kyoto Protocol and other key policies, and is the one usually quoted.

Table 1.1 Atmospheric lifetimes and global warming potentials of the six Kyoto Protocol gases.

Gas	Lifetime (years)	GWP for given time horizon		
		20 years	100 years	500 years
CO_2	50–200	1	1	1
CH_4[a]	12	72	25	7.6
N_2O	114	289	298	153
SF_6	3,200	16,300	22,800	32,600
HFCs	1.4–270	437–12,000	124–14,800	38–12,200
PFCs	2,600–50,000	5,210–8,630	7,390–12,200	11,200–18,200

Source: IPCC 2007d.

[a] The lifetime specified for CH_4 is the perturbation lifetime, which accounts for the presence of feedback loops in the atmospheric chemistry of CH_4 that slow its removal from the atmosphere at higher concentrations.

The radiative forcing for CH_4 also has different spatial effects on climate than CO_2 (Wang et al. 1991).

As well as its direct radiative effect, CH_4 influences climate indirectly in a number of ways. First, as described previously, CH_4 enhances its own atmospheric lifetime via its effect on OH levels (increased concentrations of CH_4 depress OH levels, reducing oxidative capacity). Second, CH_4 oxidation produces tropospheric O_3, which is also a greenhouse gas. Third, CH_4 increases stratospheric water vapour, relatively small changes in which can affect radiative forcing, and which can additionally lead to increased formation of polar stratospheric clouds, which further enhance the greenhouse effect. Finally, CH_4 is eventually oxidised to CO_2, a greenhouse gas with a far longer lifetime (IPCC 2007b; Khalil 2000)[†].

Emissions of CO, NO_X and volatile organic compounds (VOCs) also exert an indirect effect on climate. Although having no greenhouse effect of their own, these gases are oxidised by OH, thus reducing this potential CH_4 sink and extending the lifetime of CH_4 in the atmosphere (Reilly, Jacoby and Prinn 2003; Prinn et al. 2007).

1.2.1.2 Atmospheric methane concentrations

The first suggestion that atmospheric CH_4 concentrations might be increasing as a result of human activities was made by Singer (1971).

[†] The GWP for methane includes the first three of these effects.

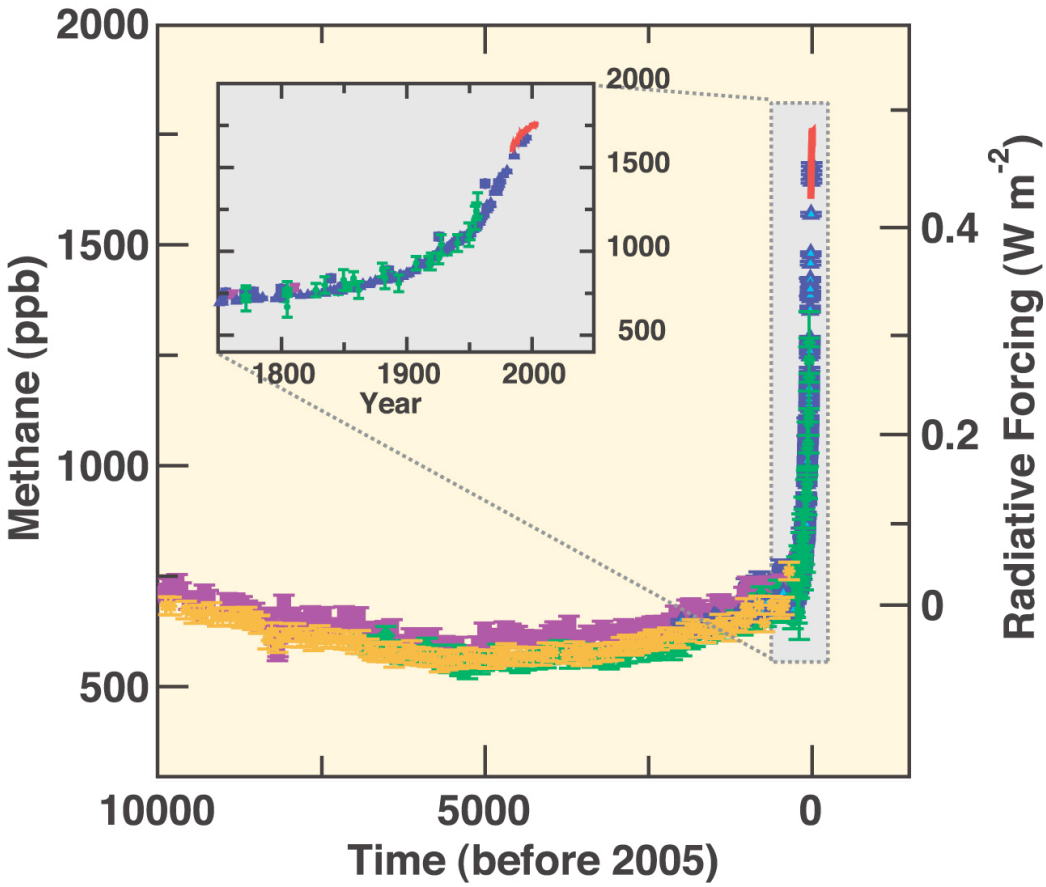

Figure 1.1 Atmospheric concentrations of CH_4 over the last 10,000 years and since 1750 (inset). Measurements are from ice cores (symbols with different colours representing different studies) and atmospheric samples (red lines). The corresponding radiative forcings are shown on the right hand axis of the main chart (Source: IPCC 2007d).

As can be seen from Figure 1.1, the atmospheric concentration of CH_4 has in fact more than doubled since 1750, from a pre-industrial value of about 715 ppb in 1750 to 1774 ppb in 2005. This far exceeds the natural range of the last 10,000 years (580 to 730 ppb). It is very likely that the observed increase is primarily due to an increase in anthropogenic sources (Chappellaz and Raynaud 2000; IPCC 2007b).

It has been observed that the increase in atmospheric CH_4 follows very closely the growth in human population since the industrial revolution (Houghton 2004), and it is also interesting to note that the rate of increase in atmospheric CH_4 concentration exceeds that of CO_2. Whilst increases in CO_2 concentration are due mainly to emissions from the combustion of fossil fuels and land use change, it is thought that those of CH_4 are primarily due to agriculture (IPCC 2007d).

Growth rates have declined since the early 1990s however, consistent with total (anthropogenic and natural) CH_4 emissions being nearly constant during this period (IPCC 2007d).

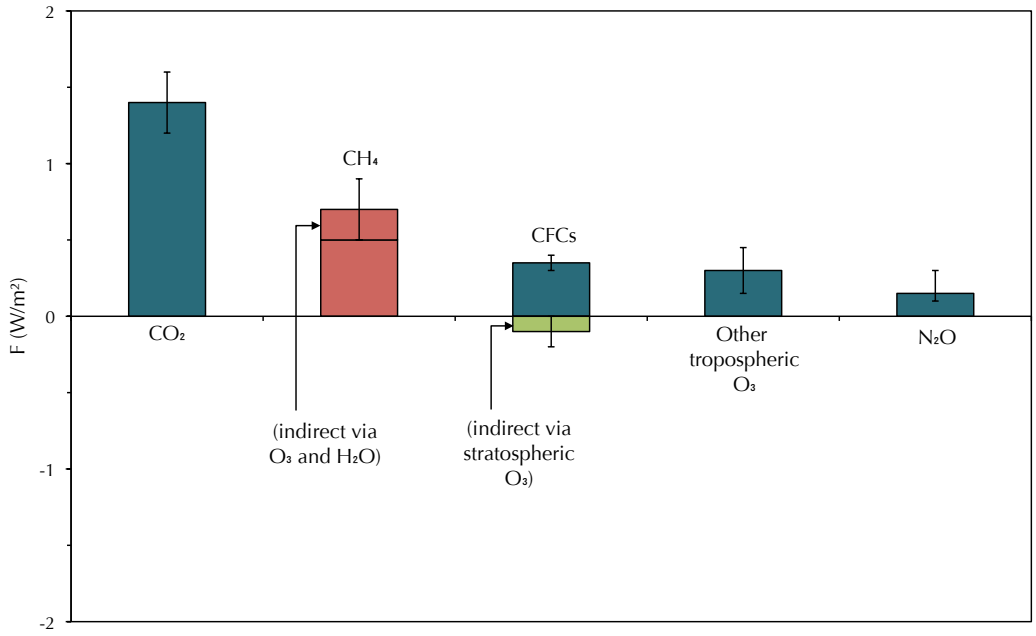

Figure 1.2 Estimated climate forcings for the period 1750 to 2000 (Source: adapted from Hansen et al. 2000).

Several drivers are thought to be responsible for this recent trend, including changing agricultural policies, specifically in the European Union, economic restructuring in the former Soviet Union and Eastern Europe, and the effects of non-climate driven regulations on waste management (EPA 2006a).

The latest measurements indicate renewed growth in atmospheric concentrations since the start of 2007 however. It has been suggested that this could be the first sign of a biospheric feedback to climate change, as wetland emissions increase in response to the climate warming (see later) (Rigby et al. 2008).

It is estimated that CH_4 accounts for approximately 25% of the enhanced greenhouse effect observed since pre-industrial times, as illustrated by Figure 1.2, which compares estimated radiative forcings on climate for the major greenhouse gases (Hansen et al. 2000).

1.2.2 Current and projected methane emissions

CH_4 emissions currently constitute 14.3% of total global anthropogenic greenhouse gas emissions, as shown in Figure 1.3. In total, more than 6,000 $MtCO_2$-eq[†] of CH_4 is emitted annually as a result of human activity.

[†] Million tonnes of carbon dioxide-equivalent. CO_2-equivalent emissions are calculated by multiplying the mass of methane emitted by its 100-year GWP. A value of 21 for the GWP is used. Whilst the latest figure of 25 reflects the current level of understanding, the older value of 21 from

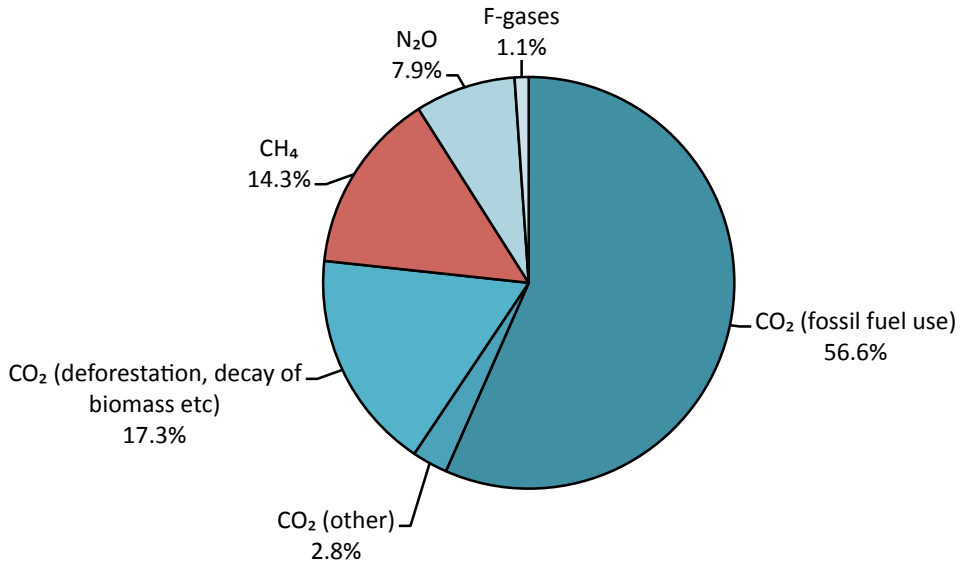

Figure 1.3 Global anthropogenic GHG emissions by gas in 2004. F-gases include HFCs, PFCs and SF_6 (Source: adapted from IPCC 2007b).

Emissions have risen by about 40% since 1970 (IPCC 2007b), and are projected to increase over the next century. This increase is expected to be less rapid than that of CO_2 however, as agricultural activity, the major source of CH_4 emissions, is predicted to expand less than energy use. Recent scenarios project that agricultural CH_4 emissions will continue to increase until the end of this century however, potentially doubling in some scenarios (IPCC 2007b).

As an example, Figure 1.4 shows emissions scenarios for CH_4, developed as part of a recent collaboration coordinated by Stanford University's Energy Modelling Forum, EMF-21, which looked specifically at non-CO_2 greenhouse gases (Weyant, de la Chesnaye and Blanford 2006). Projected increases in CH_4 emissions by 2030 range from 1.3 $GtCO_2$-eq to 7.5 $GtCO_2$-eq; by the end of the century the range of the projections is much larger. Future projections must account for changes in the magnitude of sources and sinks, including the consideration of feedback from climate change and emissions of other trace gases.

1.2.3 Methane sources and sinks

CH_4 is emitted from a wide range of natural and anthropogenic sources, and removed from the atmosphere by a variety of chemical and biological processes (sinks) (EPA 2006a; Jardine et al. 2004; Khalil and Shearer 2000; Khalil, Shearer and Rasmussen 2000).

---

the IPCC Second Assessment Report is still used for reporting under the UNFCCC, and will apply until the second Kyoto period (post-2013).

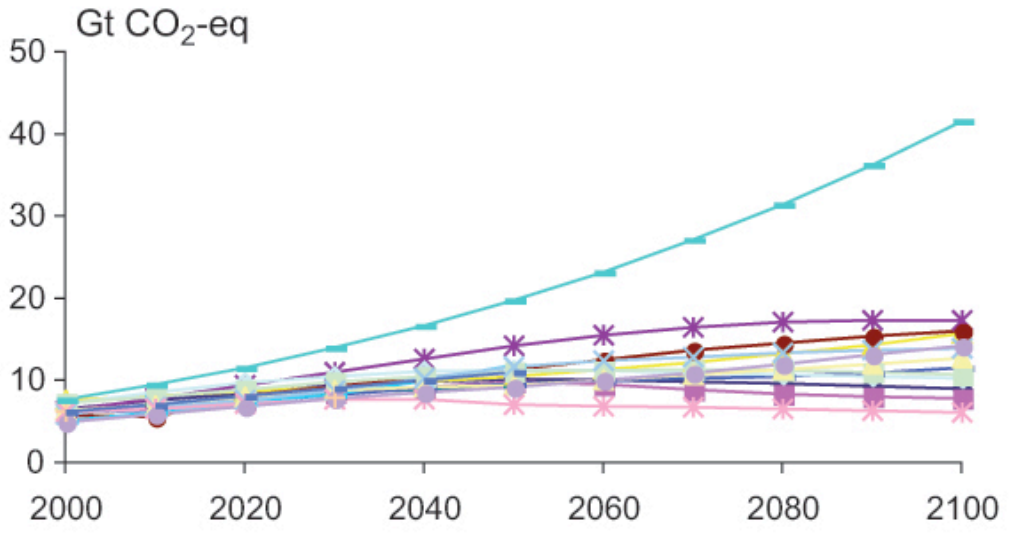

Figure 1.4 Baseline (without mitigation measures) emission scenarios for CH_4 developed by the Stanford University Energy Modeling Forum (EMF-21) (lines represent individual studies) (Source: IPCC 2007b).

The atmospheric concentration of CH_4 will depend on the relative capacities of each. Figure 1.5 shows a breakdown of the relative contributions of natural and anthropogenic sources, and sinks, to changes in atmospheric CH_4 concentrations over recent decades. It can be seen that anthropogenic sources dominate emissions.

CH_4 is produced either biogenically (by both natural and anthropogenic sources) or thermogenically. The contribution of thermogenic CH_4 from fossil fuel sources to the atmospheric inventory can be determined by measuring the abundance of the radioactive carbon-14 (^{14}C) isotope. Atmospheric carbon receives a constant input of ^{14}C, which is derived from cosmic ray neutrons; CH_4 produced biogenically contains contemporary levels of ^{14}C whereas CH_4 derived from fossil fuels contains none (Stevens and Whalen 2000).

There is still considerable uncertainty over the magnitude of emissions from individual sources however (IPCC 2007b). Unlike emissions of CO_2 from fossil fuel use, which can be readily estimated from market data on fuel use, CH_4 emissions are associated with a geographically disperse set of heterogeneous processes. The variability of many emissions over space and time also makes individual sources difficult to quantify. Wetland emissions for example, may vary by a few orders of magnitude over just a few metres, and are also seasonal (IPCC 2007d).

In addition, most biogenic sources are highly temperature dependant and therefore influenced by local climate, as well as global climate change (Wuebbles and Hayhoe 2002). So-called 'fugitive' emissions from coal mining and natural gas distribution are, by definition, elusive.

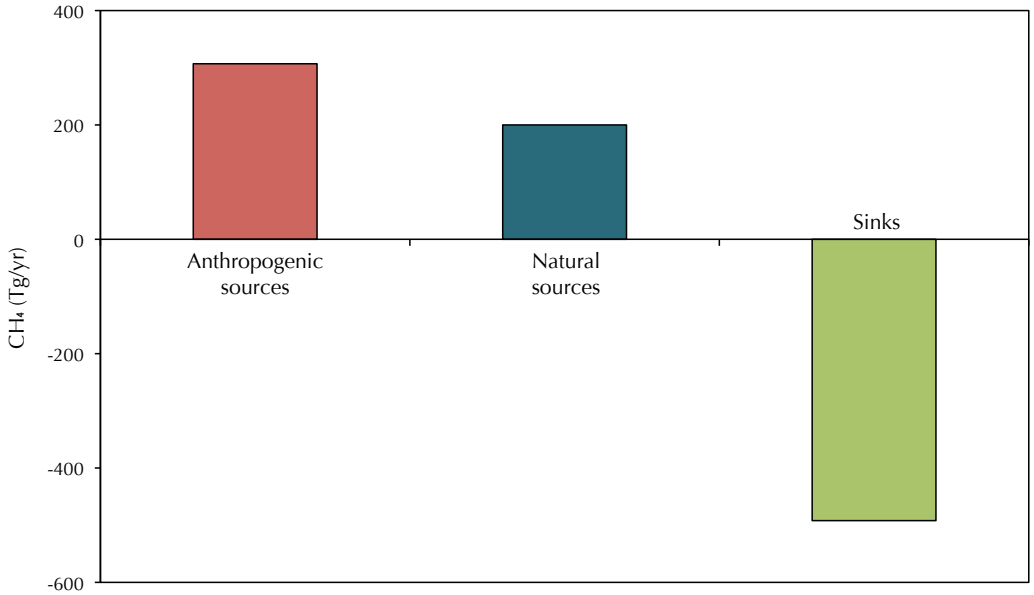

Figure 1.5 Sources and sinks of CH_4 for the period 1983 to 2004 (Source: adapted from IPCC 2007d).

1.2.3.1 Natural sources

CH_4 is emitted by a variety of natural sources, as shown in Figure 1.6.

Most natural emissions sources are biogenic; CH_4 plays an important role in the natural cycle of carbon (IPCC 2007b). Two classes of bacteria are involved in the CH_4 cycle: Methanogenic bacteria generate CH_4 by anaerobically breaking down organic matter, releasing both CH_4 and CO_2. Conversely, methanotrophic bacteria oxidise CH_4 to CO_2, either at high concentrations near the source of production ('low-affinity' oxidation), or at atmospheric concentrations ('high-affinity' oxidation) (Boone 2000; Jardine et al. 2004; Khalil 2000).

The main natural source of CH_4 to the atmosphere is wetlands, including areas of marsh, fen, peatland, permafrost and fresh water. These emissions are highly temperature dependent and seasonal (Matthews 2000).

Oceanic emissions occur because the oceans are slightly supersaturated with CH_4. The dissolved CH_4 is produced biogenically and may come from sediments, the decomposition of plants, or be generated in the gastrointestinal tracts of marine zooplankton and fish. Oceanic releases are spatially dependent, with high emissions occurring from nutrient rich estuaries for example (EPA 1999; Jardine et al. 2004).

Possible geological sources include biogenic CH_4 from organic-rich sediments; and thermogenic CH_4 from hydrocarbon bearing sediments, volcanic emissions, geothermal and hydrothermal sources, and the earth's mantle (released along deep-seated faults) (Judd 2000).

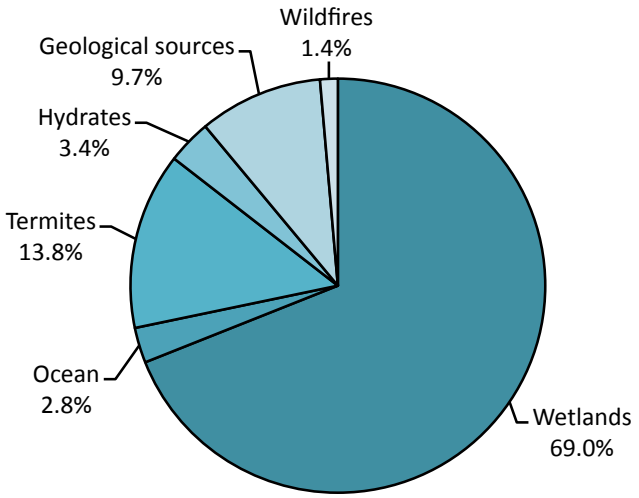

Figure 1.6 Global natural CH_4 emissions by source in 2000 (Source: adapted from Wuebbles and Hayhoe 2002).

Other natural sources include the CH_4 produced by microbes within the digestive system of termites; wildfires, which are caused primarily by lightning; and CH_4 hydrates[†], a crystalline solid mixture of water and CH_4 found in ocean floor sediments and arctic permafrost (Wuebbles and Hayhoe 2002).

As previously mentioned, biogenic emissions generally result from CH_4 production through bacterial action in anaerobic environments. Recently however, Keppler et al. (2006) reported the discovery that living terrestrial vegetation also emits CH_4, although the details of the production mechanism are not known.

This would add a potentially huge source (up to a third of total emissions) to the atmospheric CH_4 budget. The possibility also exists of further hitherto unidentified sources.

1.2.3.2 Anthropogenic sources

CH_4 is emitted from a wide range of human activities, as illustrated in Figure 1.7 and discussed individually below. Emissions occur predominantly from the agricultural, waste management, and energy (fossil fuels) sectors.

Due to the variety of sources, emission levels depend on a complex relationship between economic, social and technological factors. These include population and population distribution; agricultural practices; demand for energy and commodities; limitations imposed by land and resource availability; and climate (Khalil 2000).

[†] Methane hydrates are by far the largest store of CH_4 on the planet, accounting for 53% of all fossil fuels on earth (Lee and Holder 2001).

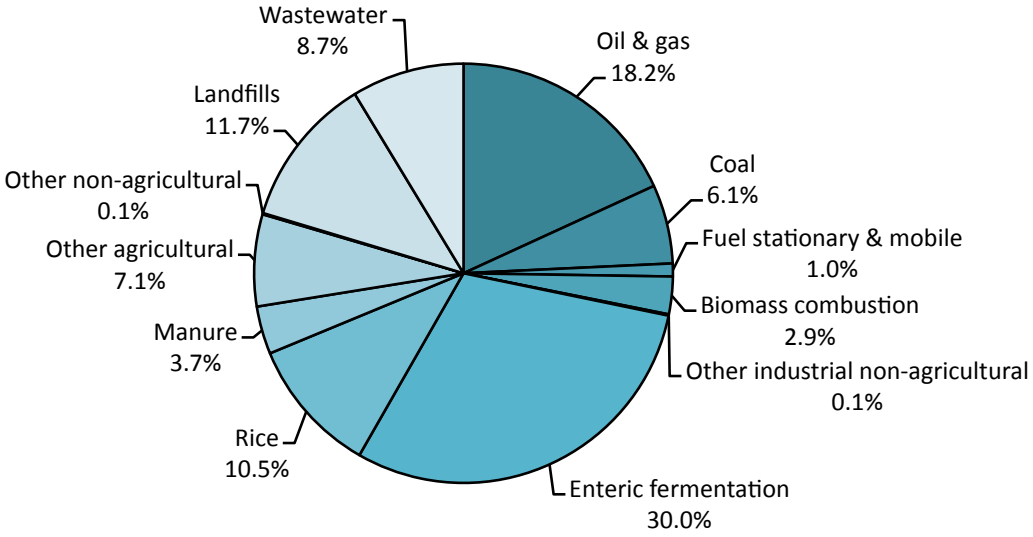

Figure 1.7 Global anthropogenic CH_4 emissions by source in 2005 (Source: adapted from EPA 2006a).

Oil and gas. Emissions in the natural gas industry occur during exploration, production (well drilling, extraction and field separation), processing, transmission, storage and distribution. Similarly, emissions from the oil sector result from activities associated with production, transportation and refining. They range from 'fugitive' emissions during normal operations and intermittent emissions from routine maintenance procedures, to system upsets and large-scale accidents.

Emission levels depend on the characteristics of a particular oil or gas field, operation and maintenance procedures, and equipment condition. Losses from the natural gas system are estimated at 1–2% for developed countries, but regional estimates have ranged as high as 15%, depending primarily on the quality of the pipelines and leakage control measures. Total emissions are of course tied to production levels, which are expected to increase, especially in the liquefied natural gas (LNG) sector.

Most emissions are either due to leakage from the gas distribution system or from upstream oil and gas activities. Leaks from pipelines are caused by corrosion, material and construction defects; leaks at valves, flanges and seals; and strains and cracks caused by earth movement. Upstream emissions are primarily from venting and flaring as part of safe process control, and emissions from oil wellheads when the CH_4 entrained in the oil is released as the pressure drops. Emissions from maintenance procedures include purges and venting of pipelines and vessels. Another significant source is venting from the high-bleed natural gas-powered pneumatic devices found throughout the transmission network (DCC 2008; IEA 2007a; EPA 2006a; Hayes 2004; Jardine et al. 2004; Kirchgessner 2000).

Coal. CH_4 is produced during the coalification process, and a small amount of that produced is retained in the coal seam and adjacent rock strata. Coal bed methane (CBM) is similar in composition to natural gas: generally 80–95% CH_4 (plus small quantities of other alkanes), the remainder being inerts (nitrogen (N_2), oxygen (O_2), CO_2 and argon (Ar)) and some other minor constituents (helium (He) and hydrogen (H_2)). The CBM content of coal depends primarily on its rank, depth and moisture, with greater volumes of gas—up to 25 m^3 per tonne of coal—found in higher rank coals with a low moisture content, in deeper coal seams. CBM is released when the pressure in the coal seam is reduced as a result of natural erosion, faulting and mining; that released as a result of mining is known as coal mine methane (CMM) (CIAB 1994; DCC 2008; EPA 2006a; Flores 1998; IEA 2007a; Jardine et al. 2004; Kirchgessner 2000).

Most CMM emissions occur from underground mines. A smaller amount of CH_4 is released from surface mining (surface mined coal seams tend to be shallower and low rank, so do not contain a significant amount of gas). Emissions also occur from post-mining handling activities and transportation, and from decommissioned mines (DTI 2004; Kirchgessner 2000).

CMM in underground mines is also a safety hazard, and mines must be well ventilated to reduce the risk of explosion. At some locations, a portion of the CMM is drained—and recovered for use as a fuel—prior to mining (see later). Most of the CH_4 released escapes to the atmosphere as fugitive emissions via the ventilation system however. The CH_4 in the mine ventilation air (MVA) is by necessity highly diluted, typically to concentrations of less than 1%. Between 4,000 and 25,000 m^3 of MVA is released per tonne of coal extracted. There is a correlation between mining activity and the amount of CH_4 produced, with emissions from a single shaft tending to decline over time as the mining operation progresses, and there can also be significant short-term fluctuations in both air flow and CH_4 concentration in the MVA.

CH_4 is also released by low temperature coal burning such as in home heating and cooking, particularly in developing countries (Khalil et al. 1993).

Biomass combustion. CH_4 is produced from the combustion of a variety of biomass sources, often in small-scale combustion devices in the developing world. Major contributors include fuel wood, charcoal, agricultural residues and waste, and municipal waste. CH_4 production results from incomplete combustion, for example a smouldering fire. The amount of CH_4 produced depends on the completeness of combustion as well as the original carbon content of the fuel (EPA 2006a; Levine, Cofer and Pinto 2000).

Enteric fermentation. CH_4 is produced as a natural product of incomplete digestion in animals. The fermentation of food by microbes in the animal's digestive system

produces CH_4 as a by-product, which is either exhaled or eructated by the animal. The amount of CH_4 produced depends primarily on the animal's digestive system. Ruminant animals (such as cattle, buffalo, sheep, goats and camels) are the major emitters. Non-ruminant animals do produce CH_4, but at far lower rates (AGO 2002; EPA 2006a; FAO 2006; Jardine et al. 2004; Johnson et al. 2000).

Emission levels are also dependent on diet, with a lower quality and higher intake of feed generally leading to greater CH_4 production. Other factors include animal type, age, function and productivity.

Rice. Most rice is grown in flooded paddy fields, which create conditions similar to those that exist in natural wetlands. When fields are flooded, decomposition of organic material gradually depletes the oxygen present in the soil and floodwater, leading to anaerobic conditions. The subsequent anaerobic decomposition of soil organic matter by methanogenic bacteria produces CH_4. Some of the CH_4 produced will be oxidised by aerobic methanotrophic bacteria, or leached away in floodwater. That remaining will be transported to the atmosphere, primarily via the rice plants, but also via diffusion and bubbling through the floodwater itself (AGO 2002; EPA 2006a; Jardine et al. 2004; Neue and Roger 2000; Shearer and Khalil 2000).

Emission levels are seasonal and depend on a combination of local conditions and cultivation practices. The floodwater system is the most important determining factor. CH_4 production is also affected by climate, soil characteristics, the use of fertilizers and other additives, and the variety of rice plant grown. Total emissions will then depend on the total area under cultivation, the number of crops each year and the yield, and, ultimately, the global demand for rice.

Manure. CH_4 is produced by the anaerobic decomposition of animal manure. Emission levels are therefore highly dependent on the manure handling system used. Significantly more CH_4 is produced when the manure is stored or treated in liquid systems (such as lagoons, ponds and tanks), which promote anaerobic decomposition, rather than when handled as a solid or spread directly on the land, or when produced by non-confined animals (the majority of the world's livestock), where it tends to decompose aerobically. Unfortunately, the trend is towards liquid systems in large industrial facilities in developed countries, particularly for large dairy and pig producers. The ambient temperature and storage time will also influence the amount of CH_4 produced. Manure composition also has an effect, and this in turn depends on animal type and diet. Animal manure also produces significant N_2O emissions (AGO 2002; EPA 2006a; FAO 2006; Jardine et al. 2004; Johnson et al. 2000; Thorneloe et al. 2000).

Other agricultural. Other agricultural sources include agricultural soils, field burning of agricultural residues, land clearance, and the prescribed burning of savannah (AGO 2002; EPA 2006a).

Landfills. CH_4 is produced from the anaerobic decomposition of organic material in landfills. Landfill gas (LFG) is 30–70% CH_4, the remainder being mainly CO_2. It is generally saturated and also contains traces of sulphur compounds such as hydrogen sulphide (H_2S); mercaptans and thiols; chlorinated compounds; and VOCs such as benzene, toluene and xylenes. Several of these are either toxic or carcinogenic, even at low concentrations, as well as being responsible for unpleasant odours.

The production of CH_4 depends on the amount of waste; its composition, age and pH; the local climate; and landfill design and operating practices, all of which affect the extent of anaerobic decomposition. More CH_4 will be generated if higher proportions of organic waste and increased levels of moisture are present. Municipal solid waste (MSW) contains a relatively high proportion of organic matter (compared to waste from the mining and construction industries, for example).

Paradoxically, modern 'sanitary' landfills where the waste is highly compacted—the norm in developed countries—produce more CH_4 than loosely compacted open dumps, as the latter are less conducive to the development of anaerobic conditions. LFG is generated over a period of several decades, usually beginning 1–2 years after the waste has been disposed of, but production rates are lower at the beginning and end of the life of the landfill, and possibly at intermediate periods due to variable gas production rates. If a soil cover is in place, about 10% of the generated CH_4 is oxidised by methanotrophic bacteria in the soil. If not collected, the remainder will be released to the atmosphere.

CH_4 in landfills is also a safety issue as subsurface migration to nearby structures can result in explosive mixtures. Regulations are in place in various countries to compel landfill owners to collect and combust the LFG (see later) in order to mitigate the risk of explosion and also to destroy toxic trace compounds (EPA 2006a,b; IEA 2007a; Isaacson 1991; Jardine et al. 2004; Nikiema et al. 2005; Thorneloe et al. 2000).

Wastewater. Treatment of wastewater (domestic sewage and industrial wastewater) involves the removal of soluble organic matter, suspended solids, pathogens and chemical contaminants. Biological processes are used to decompose the organic matter, and if the decomposition occurs under anaerobic conditions CH_4 is produced. Emissions depend on the organic content of the wastewater and the extent to which it is allowed to decompose under anaerobic conditions.

For domestic sewage, most developed countries employ central facilities with aerobic wastewater treatment systems followed by closed anaerobic sludge digesters, from

which the CH_4 produced can be captured (see later). Industrial wastewater is often treated onsite in either shallow lagoons or settling ponds, which promotes anaerobic decomposition. Industries producing large volumes of wastewater with a high organic content include the meat and poultry, produce (fruit and vegetable), and pulp and paper industries. Emissions also occur from small systems such as pit latrines, composting toilets and septic tanks. Wastewater is also a significant source of N_2O (EPA 2006a; Thorneloe et al. 2000).

Hydroelectric reservoirs. Hydroelectric reservoirs, particularly in tropical regions, constitute an additional source of CH_4 emissions, which has only recently been recognised. The CH_4 is produced from the decomposition of organic matter in the warm water, the main sources of which are the original vegetation that was flooded, dissolved and particulate matter flushed in neighbouring shores and drainage basins, and vegetation growing within the reservoir itself.

Most of the CH_4 produced is oxidised before it reaches the surface of the reservoir. However, as well as emissions from the surface, it has recently been suggested that there are more significant releases of CH_4 from the water passing through the turbines and spillways. The turbine intakes are typically located deep below the reservoir surface (to account for drought conditions), within the CH_4 saturation zone where bacterial oxidation is not yet complete. The water entering the turbines is therefore CH_4 enriched, and the CH_4 is degassed due to the sudden pressure drop in the turbine.

Although CH_4 production is highest in the first years of operation, due to the flooded vegetation, emissions will continue throughout the life of the reservoir (Bambace et al. 2007; Ramos et al. 2009).

Other minor sources. Other fossil fuel sources include coke production (CH_4 is produced as a by-product of the pyrolysis process), shale oil mining, and the CBM industry (Kirchgessner 2000).

Industrial emissions come predominantly from the iron and steel industry and chemical production. CH_4 is also released during metal production, mineral processing, petrochemical production, silicon carbide production, and solvent use (EPA 2006a).

1.2.3.3 Sinks

Once emitted, CH_4 is removed from the atmosphere by a variety of processes known as sinks, and the balance between sources and sinks (as shown earlier in Figure 1.5) ultimately determines atmospheric concentration and the length of time emissions will remain in the atmosphere.

The dominant sink is oxidation by OH in the troposphere. Stratospheric oxidation also plays a minor role, and together these reactions account for over 90% of the CH_4

removed. Other known minor sinks are reaction with Cl in the stratosphere and microbial oxidation in soils (IPCC 2007d; Khalil, Shearer and Rasmussen 2000; Wuebbles and Hayhoe 2002).

1.2.3.4 Anthropogenic effects on natural sources and sinks

Human activity can also influence natural sources and sinks, either directly, or indirectly via feedback loops in the atmospheric chemistry or climate.

Examples of direct influences on natural sources include the draining of wetlands, and changes in land use that alter emissions from termites. Emissions from the oceans also have an anthropogenic component in that populations of methanogenic bacteria are increased by high nutrient levels resulting from agricultural fertiliser run-off and waste treatment facilities (EPA 1999; Jardine et al. 2004).

Over 70% of emissions result from biogenic sources (both natural and anthropogenic). Biogenic emissions are strongly influenced by climate, in particular temperature and moisture. These emissions are therefore likely to increase as the climate warms. Wetland emissions in particular are highly sensitive to temperature (the optimal temperature for CH_4 release being 37–45ºC).

A more extreme example of climatic feedback is the potential release of large quantities of CH_4 due to the melting of the Arctic permafrost. At high levels of warming, CH_4 hydrates could also become destabilised, releasing huge amounts of CH_4 into the atmosphere. These events are considered to be potential 'tipping points' in the climate system (EPA 1999).

Wildfires are also more likely in the future due to an increase in extreme weather conditions, such as drought and storms, as a result of climate change.

Conversely, as atmospheric CH_4 concentrations increase, the proportion of CH_4 supersaturated in oceans and freshwaters will decline relative to atmospheric concentrations, reducing emissions from this source.

In relation to sinks, it has been shown that there exists a positive feedback loop in the atmospheric chemistry of CH_4 whereby increasing atmospheric CH_4 concentrations leads to a reduction in tropospheric OH levels—the major CH_4 sink—thus slowing the oxidation of CH_4, and thereby further enhancing the increase in atmospheric CH_4 concentration.

An example of a more direct influence on a natural sink is the use of artificial fertilisers containing ammonia. This is detrimental to the removal of CH_4 via soils, as high ammonium concentrations lead to the loss of methanotrophic bacteria (Khalil 2000; Wuebbles and Hayhoe 2002).

1.3 Mitigation of methane emissions

1.3.1 Motivation

The ultimate objective of the United Nations Framework Convention on Climate Change (UNFCCC) is stated as being to "stabilise greenhouse gas concentrations in the atmosphere at a level that would prevent dangerous anthropogenic interference with the climate system" (UN 1992). What constitutes 'dangerous anthropogenic interference' is clearly open to interpretation and involves numerous value judgements.

However, it can be calculated that an annual reduction in anthropogenic CH_4 emissions of just 5% (or 3% of total emissions) would be enough to stabilise CH_4 concentrations in the atmosphere at current levels (in other words such that sources and sinks are balanced). This target seems attainable, and would constitute a small but significant contribution to an overall climate change solution, as well as providing an encouraging example.

As previously discussed, CH_4, with a GWP of 25, traps heat in the atmosphere more effectively than CO_2: its mitigation should therefore be commensurately more effective at slowing global warming than the mitigation of CO_2. Also, because CH_4 has a relatively short atmospheric lifetime of only 12 years—compared with around 100 years for CO_2—the effect of such mitigation ought to be especially significant in the near term, as reductions in emissions will translate quickly into reductions in atmospheric concentrations, allowing a more rapid response to climate change.

The effectiveness of CH_4 mitigation in the near-term is enhanced compared to CO_2 mitigation by the fact that the benefits of reducing energy-related CO_2 emissions are partly offset in the near-term by the simultaneous reduction in energy-related aerosol emissions, which have a cooling effect on the climate (Lucas et al. 2007). On the other hand, reducing CO_2 emissions by reducing fossil fuel use would simultaneously reduce fossil fuel-related CH_4 emissions.

As mentioned previously, a feedback loop exists whereby CH_4 enhances its own atmospheric lifetime by reducing OH concentrations; this effect would be reversed were atmospheric concentrations of CH_4 to be reduced. The capacity of the atmosphere to oxidise other pollutants such as CO, NO_X and VOCs would also be increased, leading to improved local and regional air quality. Reducing the atmospheric concentration of CH_4 would also have an indirect effect on climate by reducing production of tropospheric O_3 and stratospheric water vapour, which also contribute to the greenhouse effect. Reducing tropospheric O_3 concentrations would also have benefits for air quality, agriculture, and public health.

CH_4 mitigation must be seen in the context of a comprehensive climate policy however: there is clearly also a risk in failing to control gases with very *long* lifetimes.

As well as being a potent greenhouse gas, CH_4 (the primary component of natural gas) is also a clean burning fuel, so one of the most obvious ways of mitigating emissions is to recover and burn them. Due to the stoichiometry of the combustion reaction and their relative GWPs, burning CH_4 to form CO_2 and water results in a net reduction in greenhouse gas emissions of 89%.

Furthermore, where it is possible to recover useful energy—for heating or electricity production—from the combustion process, an additional benefit is that a hitherto wasted energy resource is exploited, potentially offsetting emissions from more carbon-intensive forms of power generation such as coal or oil. This would have the added benefit of reducing emissions of other pollutants associated with the combustion of coal in particular, such as sulphur oxides (SO_X) and particulate matter. The utilisation of this additional energy resource would also enhance energy security and promote economic growth.

Owing to the flammable and explosive nature of the gas, CH_4 emissions are also a potential hazard, so their mitigation is often accompanied by safety improvements. The risk of explosion, when CH_4 from landfills or decommissioned mines migrates to nearby structures, can be reduced by controlling recovery of the CH_4 at the landfill or mine site, for example. Recovering CBM prior to mining improves mine safety as well as minimising MVA emissions.

Mitigation of CH_4 emissions can also be accompanied by improvements to the production or process efficiency of the emissions source. An obvious example would be reducing leaks from the natural gas system. Releases from livestock as a result of incomplete digestion also constitute a wasted energy resource, and changes to animal diet or management practices—intended to reduce emissions from enteric fermentation—can result in a concurrent increase in animal and farm productivity.

Including CH_4 (and other non-CO_2 greenhouse gases) in mitigation strategies, rather than focusing exclusively on CO_2, increases flexibility in meeting greenhouse gas reduction targets. (As does utilising carbon sinks by including land use and forestry mitigation options.) Such an approach can also be less politically sensitive as it allows countries to choose their own pathway to an overall target. This is particularly important where CO_2 is not the dominant gas for a particular economic sector or region (de la Chesnaye et al. 2007).

The diversity of CH_4 emissions sources means that an assortment of different mitigation options is available. As shall be seen, many mitigation measures simply involve more widespread implementation of current industry best practice, or a change in operating

or management procedures; or use technologies that are currently available, well demonstrated, relatively cheap to implement, and that do not require expensive new infrastructure, extensive reconfiguration of industry operations or turnover of major pieces of capital equipment. The IPCC (2007b) identify livestock and manure management to reduce CH_4 emissions, and landfill CH_4 recovery, as among the key mitigation technologies and practices already available.

Mitigation measures could therefore be implemented quickly. This is significant, as it has been shown that mitigation efforts over the next few decades will have a large impact on opportunities to achieve lower stabilisation levels (IPCC 2007b). Investment in CH_4 mitigation would also buy time for the development of cheaper CO_2 mitigation technologies, especially alternative energy sources, and provide time for CO_2 mitigation policies to be implemented.

1.3.2 Mitigation potential

The concept of mitigation potential assesses the scale of greenhouse gas reductions that could be made, relative to projected baseline emission scenarios, for a given carbon price (cost per unit of CO_2-eq emissions avoided or reduced). There is a large body of research indicating that there is substantial economic potential[†] for the mitigation of global greenhouse gas emissions over the coming decades, which could offset the projected growth of emissions, or reduce emissions below current levels (IPCC 2007b).

Furthermore, a number of economic modelling studies have concluded that a 'multi-gas' mitigation strategy, incorporating non-CO_2 greenhouse gases, reduces the economic cost of long-term emissions stabilisation (de la Chesnaye et al. 2001; EPA 2006b; Hayhoe et al. 1999; IPCC 2007b; Reilly et al. 1999; Reilly, Jacoby and Prinn 2003). A recent study by the US Environmental Protection Agency (EPA 2006b) found that of all the non-CO_2 greenhouse gases, CH_4 has the largest mitigation potential.

The concept of marginal abatement cost (MAC) is commonly used to estimate possible emission reductions at various carbon prices, or, conversely, the cost of achieving certain level of reductions. Figure 1.8 illustrates typical MAC curves for the mitigation of CH_4 and CO_2. The horizontal axis shows the quantity of emissions mitigated, and the vertical axis the breakeven price to achieve that level of mitigation.

[†] Mitigation potential can be differentiated in terms of *technical potential*, which is simply the amount by which it is possible to reduce greenhouse gas emissions by implementing an existing technology or practice; market *potential*, which is based on the private costs and discount rates which might be expected to occur under forecast market conditions and with current policies and measures in place, and assumes that various barriers limit actual uptake; and *economic potential*, which is based on social costs and benefits and social discount rates, and assumes that market efficiency is improved by policies and other measures, and that barriers are removed (IPCC 2007b).

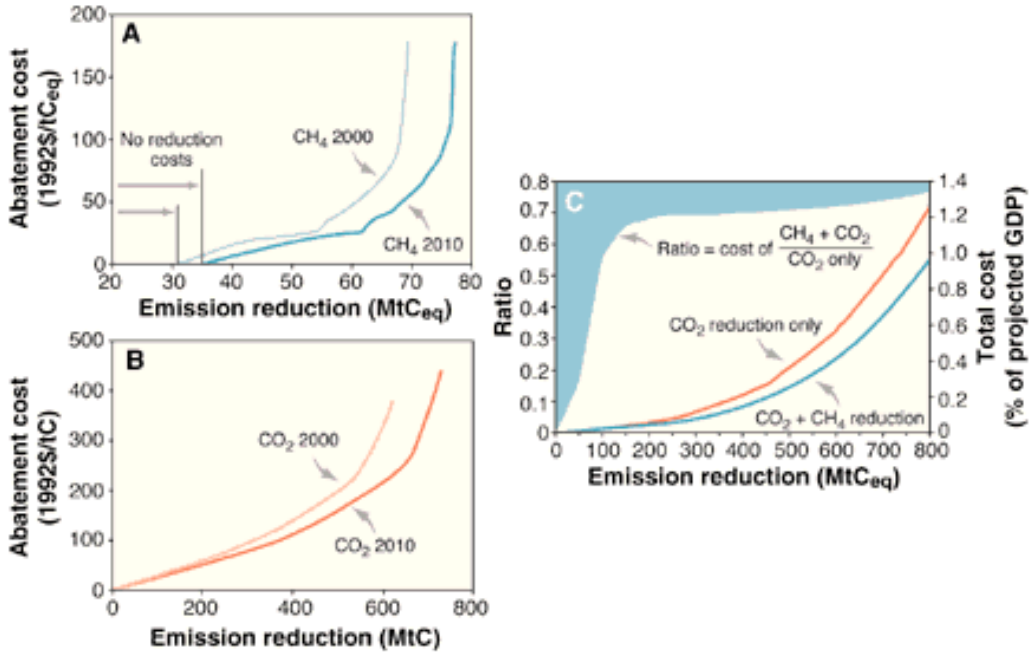

Figure 1.8 Marginal Abatement Cost (MAC) curves for (a) CH_4 in 2000 and 2010, (b) CO_2 in 2000 and 2010 and (c) CO_2 only compared to CO_2 and CH_4 together for 2010 (Source: Hayhoe et al. 1999).

Therefore, moving along the curve the lowest cost mitigation options are adopted first. The curve becomes vertical at the point of the maximum possible mitigation potential.

A number of significant features are evident from Figure 1.8. First, it can be seen from the MAC curve for CH_4 (Figure 1.8a) that a significant proportion of mitigation options lie 'below the line'. These are options that can be realised at zero cost or even at net benefit (given the costs and benefits considered), but have not yet been implemented due to the existence of nonmonetary barriers (see later), and are generally termed *no-regret* options. A more recent assessment by the US Environmental Protection Agency estimated that no-regret options account for nearly 500 $MtCO_2$-eq of mitigation potential (EPA 2006b). This is not the case for the CO_2 MAC curve, and is primarily a result of the potential value of CH_4 as a fuel.

Second, the MAC curve for CH_4 is much more non-linear than that for CO_2. This means that although the first increments of mitigation for CH_4 may be realised at a net benefit—or at zero or low cost—above a certain reduction level most mitigation opportunities are exhausted, even though a significant proportion of emissions remain unabated. To a certain extent this reflects the fact that MACs are estimated based on existing mitigation technologies, and do not account for technological change; in the long term, it is reasonable to assume that new technologies will emerge, and certain implementation barriers will become less important.

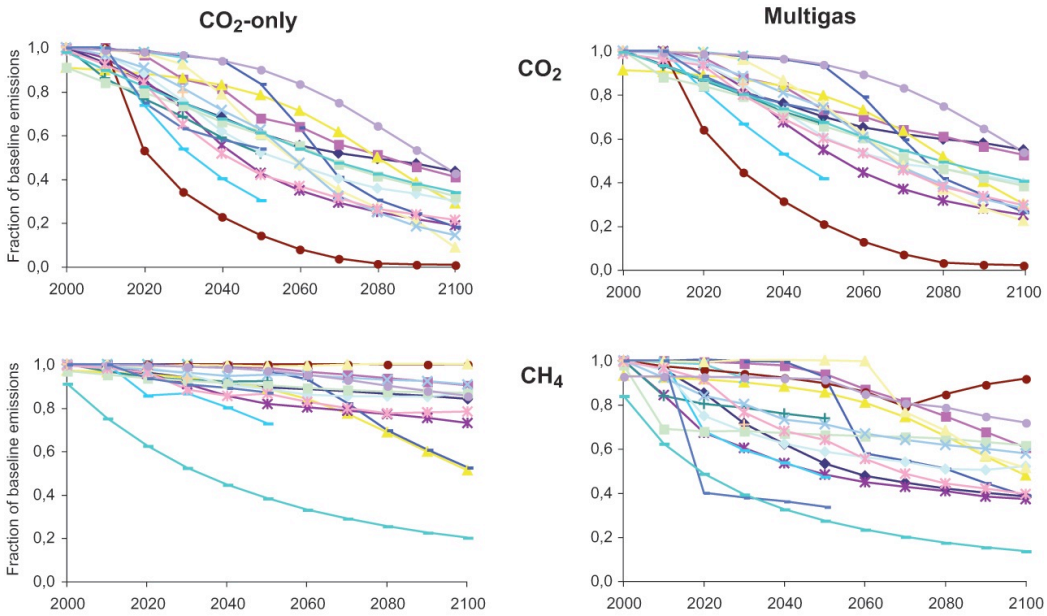

Figure 1.9 Emission reduction scenarios developed by the EMF-21, comparing CO_2-only versus multi-gas strategies (lines represent individual studies) (Source: IPCC 2007d).

Third, the maximum possible mitigation potential for CH_4 is an order of magnitude less than that for CO_2, as would be expected due to the relative sizes of the original emissions sources. Finally, it can be seen from Figure 1.8c that a given mitigation target can be achieved at a lower cost by mitigation of both CH_4 and CO_2 together (a multi-gas mitigation strategy), rather than CO_2 alone, as previously stated.

The last point is supported by the recent EMF-21 collaboration, summarised by Weyant, de la Chesnaye and Blanford (2006)[†], which found that on average the MAC of a multi-gas policy in 2025 is 48% lower than a CO_2-only policy, for the same long-term stabilisation target of 4.5 Wm^{-2} compared to pre-industrial levels[‡] (with the reduction ranging from 15–70% in individual studies).

A more recent meta-analysis of studies into the MACs of greenhouse gas mitigation by Kuik, Brander and Tol (2009) looked at 62 studies (based on 26 different models), including those from the EMF-21 forum, and, in near perfect agreement with the EMF-21 results, also found the difference in MAC with and without the inclusion of non-CO_2 greenhouse gases to be 48%[§].

[†] See the Energy Journal Multi-Greenhouse Gas Mitigation and Climate Policy Special Issue (2006) for individual studies.

[‡] This stabilisation level would correspond to a global average temperature increase of 3–4ºC above the pre-industrial temperature (IPCC 2007b).

[§] The cost estimates in the studies were also found to be sensitive to the stringency of the stabilisation target, the assumed emissions baseline, the method by which the time profile of emissions was determined in the model and the number of regions and energy sources included in the model.

Figure 1.9 shows the EMF-21 projections for reductions in emissions of both CO_2 and CH_4 over this century (the EMF-21 baseline emission scenarios for CH_4 were presented earlier in Figure 1.4), and compares the effect of employing a CO_2-only versus a multi-gas mitigation strategy.

It was previously suggested that an annual reduction in anthropogenic CH_4 emissions of just 5% would be enough to stabilise atmospheric CH_4 concentrations in the atmosphere. This target could be met by mitigating those emissions most easily captured from point sources, such as the ventilation air from underground coal mines and landfill gas.

Figure 1.10 breaks down the economic mitigation potential for CH_4 in 2010 by source (again based on the EMF-21 data). It can be seen that according to this analysis the greatest potential is indeed in the oil and gas, coal and landfill sectors.

1.3.3 Mitigation options by source

1.3.3.1 Oil and gas

When considering mitigation options in the oil and gas industry it is important to note that venting from rigs is a point source that can potentially be captured, whereas fugitive CH_4 emissions, such as leakages from pipelines, are a diffuse source that can only be reduced.

Emissions should be captured for use as an energy source if possible; if not, flaring is preferable to simply venting to the atmosphere. A further option in the oil sector is reinjection of the gas into the oil field, which can enhance future oil recovery.

As previously mentioned, fugitive releases occur from a wide variety of sources throughout the oil and gas systems. Mitigation of these emissions involves various improvements at the level of individual items of equipment (EPA 2006b; Fernandez et al. 2005; Gillis et al. 2007; IEA 2007a; Jardine et al. 2004; Robinson, Fernandez and Kantamaneni 2003). An obvious leak reduction measure is the upgrade and repair of pipelines; emissions from modern plastic pipes are lower than from the traditional cast iron version. Another mitigation opportunity is substituting compressed air for pressurized natural gas throughout the pneumatic control system.

Improvements in management practices and operational procedures can also reduce emissions, for example implementing direct inspection and maintenance (DI&M) programs to identify, quantify and reduce leaks, and employing pumpdown techniques to remove residual gas from sections of pipeline and compressors prior to maintenance.

A more comprehensive list of possible procedural and hardware improvements in the natural gas system can be found in Appendix A.

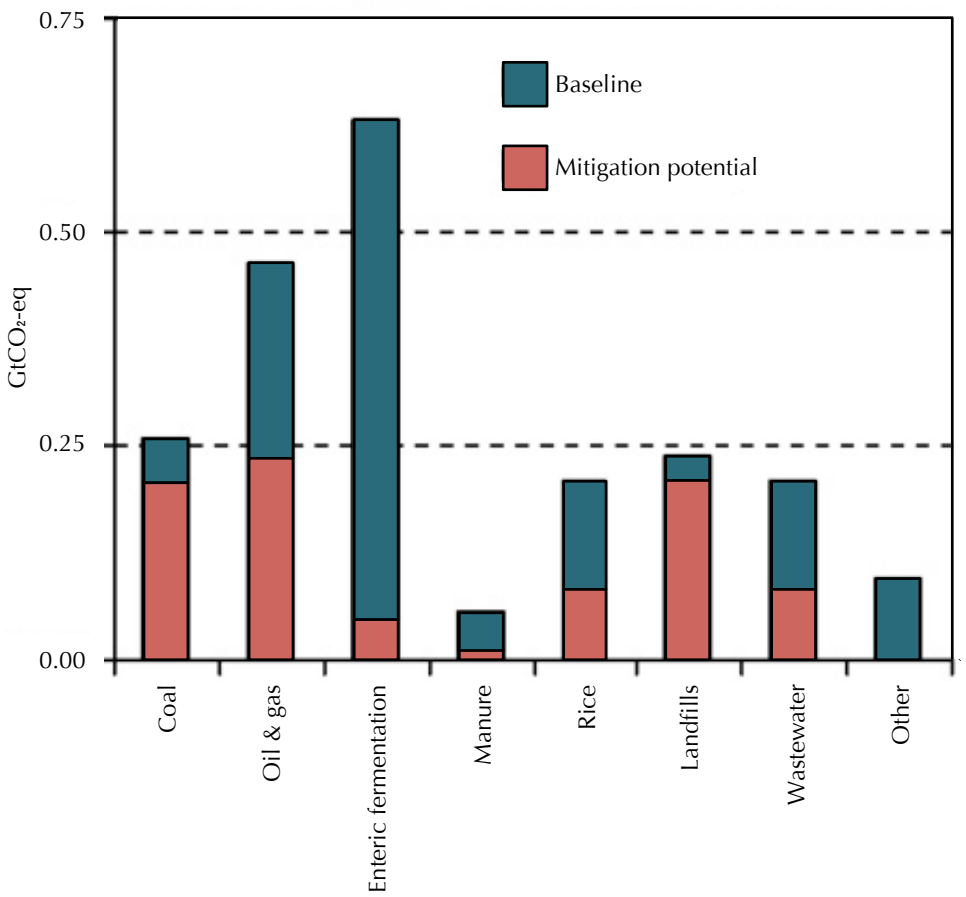

Figure 1.10 Emissions baseline and mitigation potential for CH_4 by source in 2010 (according to the EMF-21 data set) (Source: adapted from Lucas et al. 2007).

1.3.3.2 Coal

The most favourable mitigation option for coal-related emissions is drainage of the CMM prior to mining, via a degasification network of vertical and horizontal wells, boreholes and pipelines. The high quality gas can be recovered for use as a fuel. Pre-mining degasification also improves mine safety and reduces ventilation requirements. CMM can also be drained during or post-mining via gob wells, but the gob gas recovered tends to be of a lower quality. In the US, where the CMM industry is most developed, it is estimated that currently about 27% of gas is drained and recovered in this way; under ideal conditions the technical recovery potential is up to 70% (Brenkley and Bennet 1996; CIAB 1994; EPA 1999; EPA 2006b; Kirchgessner, Masemore and Piccot 2002).

Mitigation of CH_4 emissions in the MVA is more challenging due to the extremely low CH_4 concentrations and large volumes of gas involved. Because CH_4 concentrations are typically less than 1%, which is below the lean flammability limit (5% CH_4 in air for a free flame), flaring, or combustion of the emissions in conventional natural gas devices

such as gas turbines, is not possible. The variability in concentration and flow rate also hinders mitigation, and especially energy recovery (EPA 2000; Su et al. 2005).

One strategy for the mitigation of MVA emissions is to use the MVA as a replacement for the combustion air of a process in which some other fuel is the primary energy source. For example, a coal-fired power plant located at the mine site, or a gas-fired plant running on the higher quality drained CMM. However, this option depends on there being a suitable power generation facility in the proximity of the mine, limiting widespread applicability. Also, there must be a match between the large quantity of MVA produced by the mine and the combustion air requirements of the generation facility. Although this might be the case for a large coal fired power station, a plant running on the CMM drained from the mine would only be capable of using a fraction of the MVA produced, so a large amount of CH_4 would still be emitted.

An alternative MVA mitigation option is to combust the emissions using some form of more advanced lean-burn technology capable of burning below the conventional flammability limit, either with or without energy recovery. There are currently a number of such technologies under development, including thermal and catalytic flow reversal reactors and various designs of catalytic and recuperative lean-burn gas turbines. However none of these is yet commercially proven, and at very low CH_4 concentrations a supplementary fuel source (such as drained CMM) would still be required. Another option would be the co-combustion of MVA with waste coal, for example in a rotary kiln or fluidised bed.

Other approaches include the use of a concentrator to increase the CH_4 concentration in the MVA (or gob gas) to a level at which it could be used in either a conventional or lean-burn combustion device, however this is also still in the developmental stage. Some form of biological treatment process involving methanotrophic bacteria is also a future possibility.

Emissions from decommissioned mines can be reduced by inhibiting flow, sealing emission pathways (though this has safety implications), restricting flow from vents, and flooding the CH_4 producing mine workings. Alternatively, efforts similar to those for active mines can be made to recover and use the CH_4.

A reduction in the demand for coal, or a shift in production methods towards surface mining, would also reduce global emissions.

1.3.3.3 Enteric fermentation

There are a number of options for reducing emissions from enteric fermentation (AGO 2002; EPA 2006b; FAO 2006; IPCC 2007b; Jardine et al. 2004; Wuebbles and Hayhoe 2002). Most options involve changes to the animal's diet. These include increasing the

energy content and digestibility of the feed, feed supplementation to combat nutrient deficiencies (that prevent optimal use of the feed's energy content), or feed supplementation aimed at increasing the animal's productivity such as the use of growth hormones, steroids and antibiotics that enhance animal growth or lactation. Such measures are more easily applied at intensive farming operations. These options might actually increase emissions per animal, but increases in productivity would lead to reduced emissions per unit of product (meat, milk, etc).

Production efficiency can also be improved through changes to grazing practices and animal management procedures, for example changes in grazing management that improve the quality of pastures.

An alternative approach is to attempt to directly lower CH_4 production, either via dietary additives or vaccinations aimed at suppressing methanogenesis, or by genetic modification; in other words, selective breeding or genetic engineering of livestock for reduced CH_4 production.

Reducing livestock numbers by reducing demand for meat would ultimately reduce global emissions. Alternatively, non-ruminant animals could replace ruminants for meat production (for example farming kangaroos rather than cattle in Australia).

1.3.3.4 Rice

As previously discussed, the rice paddy floodwater system is the most important factor in determining CH_4 emission levels. Emissions can be reduced via modifications to the flooding regime. If water is drained periodically and the soil allowed to dry, CH_4 emissions are inhibited, both by suppressing CH_4 formation and by allowing the oxidation of existing CH_4 in the soil. Unfortunately such a regime has the potential to increase N_2O emissions. Another alternative is the use of shallow flooding.

Tillage, fertilisation and manure amendments to alter soil conditions in order to inhibit methanogenesis are also options, as is the selection of low-methane rice cultivars, or, ultimately, reducing rice consumption (EPA 2006b; Wuebbles and Hayhoe 2002).

1.3.3.5 Manure

Reducing CH_4 emissions from the handling of animal manure involves a move away from open lagoons towards less emission intense handling systems (EPA 2006b,c; FAO 2006; IPCC 2007b; Jardine et al. 2004). Purpose built anaerobic digestors would seem to be the most favourable solution in the majority of situations. They have the advantage that the CH_4 produced can be collected and used as an energy source. They also aid in controlling odour.

Emissions from tanks and lagoons can be reduced by the addition of a solid cover; CH_4 can also be captured for energy use from covered lagoons. CH_4 production from liquid-based systems is also decreased through the use of cooling and aeration, however these both require an additional energy input.

Switching to dry management systems is another option, however this can lead to increased surface and groundwater pollution. It may also be impractical for large farming operations for process design reasons.

Other alternatives are composting, with regular aeration to avoid anaerobic conditions (again requiring an energy input), or direct land application. These are both low-tech solutions, but they do require a certain amount of space, which may not be available in intensive farming facilities. Direct land application also increases the risk of eutrophication of nearby lakes and rivers due to nutrient rich run off.

Furthermore, promoting aerobic decomposition—either via direct land application, a switch to dry management, or aeration of liquid or compost systems—is associated with increased N_2O emissions.

1.3.3.6 Landfills

A number of mitigation options are available for methane from landfills (Calabrò 2009; De Gioannis et al. 2009; EPA 2006b; Haubrichs and Widmann 2006; IEA 2007a; IPCC 2007b; Isaacson 1991; Jardine et al. 2004; Jung et al. 2009; Philopoulos, Felske and McCartney 2008; Tillman and Harding 2004; Venkatraman and Ashwath 2009). The most widely applicable technological approach for reducing emissions is the collection and recovery of LFG for use as an energy source (or feedstock for chemical production). Basic systems are already in place in most landfills that aim to avoid lateral migration of the gas, thereby avoiding the risk of fire and explosion at nearby facilities. These often consist of impermeable liners and a capping layer, coupled with wells or trenches and vents through which the gas can escape. Often however, the gas is not captured, and is either vented to the atmosphere or flared. More advanced systems operate using a network of vertical and horizontal pipes and wells, combined with a fan or vacuum system to provide a favourable migration route for the gas to a point where it can be collected.

Emissions can also be reduced somewhat by improving the capping technology employed. Impermeable capping layers such as silts and clays are preferable to more permeable materials such as sand and gravel. Even the best caps are not 100% efficient however. Increased use of cover soils—or 'phytocapping', where selected plant species are established on the cover soil—or geomembrane composite covers, and practices such as applying a daily cover, can reduce emissions by increasing the amount of CH_4 that is oxidised by methanogens in the soil. A related approach, where a gas collection

system is in place, is the use of actively aerated biofilter systems, which enhance CH_4 oxidation compared to passive landfill covers.

An alternative approach to reducing CH_4 production is to attempt to create a less anaerobic environment in the landfill by improving aeration, however this is energy intensive and can create an explosion hazard.

The opposite approach involves the employment of a more extensive leachate management system to increase CH_4 production. The leachate is reinjected back into the landfill to increase moisture levels and alter pH. CH_4 production is thereby increased, enhancing its recoverability as an energy source, and the period of active gas production is compressed as the waste stabilises more quickly.

A related strategy is the use of purpose built closed anaerobic digestors incorporating CH_4 recovery as an alternative to landfills. These allow increased control over the CH_4 production process and have the advantage that a more regular supply of gas can be collected.

Thermal treatment technologies are another alternative to landfilling. These range from simple incineration of the waste to more advanced waste-to-energy technologies such as pyrolysis and gasification to produce syngas, although the later would require some prior separation of the waste.

Another treatment option is so-called mechanical biological treatment (MBT) of the waste, where mixed waste is subjected to a series of mechanical and biological operations to reduce volume and achieve partial stabilisation of the organic matter, reducing CH_4 production.

Finally, practices further up the waste management hierarchy can also play an important role in reducing CH_4 emissions from landfills, either by reducing the total amount of waste that needs to be landfilled, or reducing its organic component. These include recycling, reuse, composting, and, ultimately, waste prevention and minimisation. Mitigation of CH_4 emissions must be considered as a component of an overall waste management strategy.

1.3.3.7 Wastewater

The primary mitigation option in the wastewater treatment sector involves separation of the liquid and solid components of the waste and the use of a closed anaerobic digestor incorporating a gas capture system for the treatment of the resulting sewage sludge. Approximately 40–50% of the sludge can be converted to a methane-containing biogas and the remainder sent to landfill. The gas produced can be recovered as an energy resource. Such systems are already the norm for the treatment of domestic sewage in developed countries.

Another strategy is the aeration of lagoons to promote aerobic rather than anaerobic activity (EPA 2006b).

1.3.3.8 Hydroelectric reservoirs

A proposed mitigation strategy to reduce emissions from the water passing through the hydroelectric turbines is to erect a series of barriers around the turbine intake, designed to ensure that only shallow, CH_4 depleted waters enter the intake (Bambace et al. 2007).

An alternative approach is to recover the CH_4 as an energy resource. The CH_4 rich, pressurised waters are transported to the surface where the dissolved gas can be extracted by bubbling or by spraying droplets into a sealed vessel. If the water is collected at a great enough depth, within the CH_4 saturation zone, the gas recovered can have a CH_4 concentration of 30–80% (the remaining being mainly N_2 and CO_2). The greatest CH_4 recovery potential is during the first few years of reservoir operation, due to CH_4 produced from decomposition of the flooded vegetation (Bambace et al. 2007; Ramos et al. 2009).

1.3.3.9 Coke production

Coke oven gas is a medium-calorific value gas and as such can be recycled as a fuel for the coke ovens or else used to fuel other operations in the steel making process (Tillman and Harding 2004).

1.3.4 Analysis of mitigation options

As is evident from the previous section, the diversity of CH_4 emissions sources is mirrored by a correspondingly diverse range of mitigation solutions. Whilst certain mitigation options are specific to a particular source or sector, it is possible—and worthwhile—to identify some common themes and approaches, as well as a number of key technologies, that are applicable to a variety of sources across sectors.

It can be useful to think of the different approaches to mitigation in terms of a 'mitigation hierarchy' that echoes the well-known waste management hierarchy (prevention > minimisation > reuse > recycling > energy recovery > disposal). A schematic depicting the CH_4 mitigation hierarchy is shown in Figure 1.11.

According to the widely accepted principle that it is better to prevent waste than to treat it after it is formed (Anastas and Zimmerman 2003), mitigation approaches based on preventing or minimising CH_4 production by reducing demand for the product—or restructuring the process—responsible for the emissions, are preferable to 'end-of-pipe' strategies that rely on controlling or mitigating the final emissions.

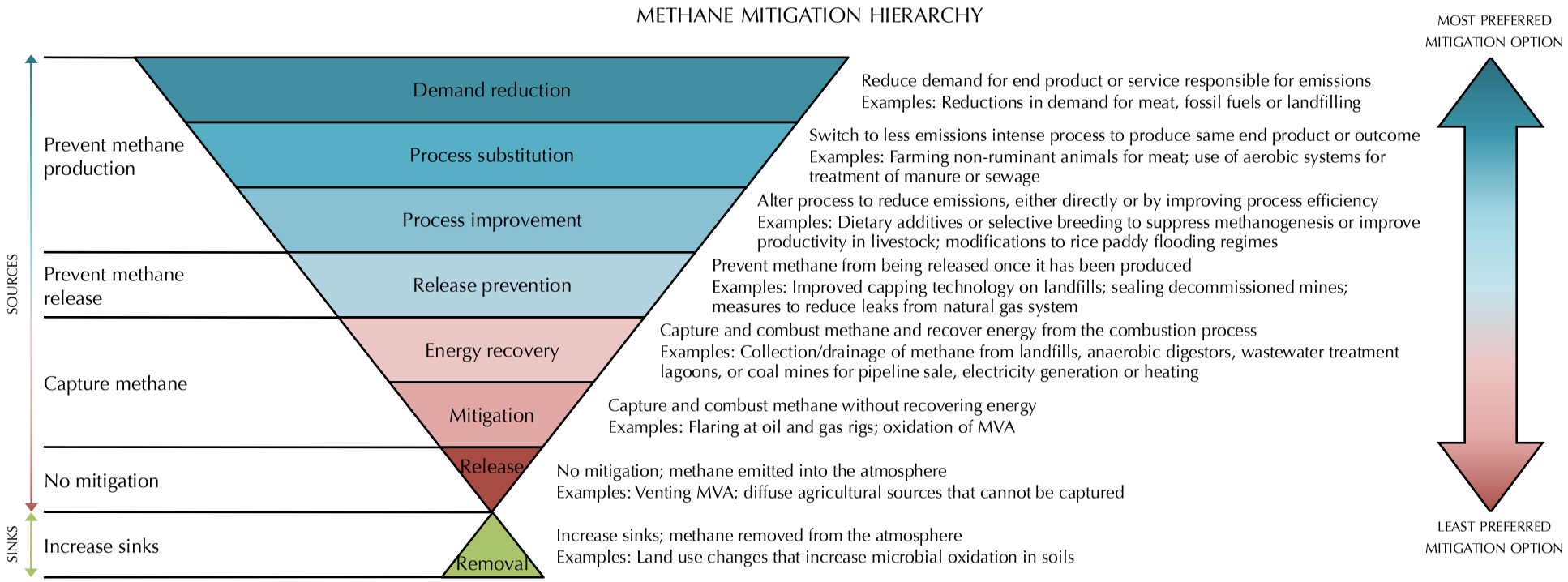

Figure 1.11 CH_4 mitigation hierarchy.

At the top of the hierarchy therefore are those approaches that aim to reduce emissions by preventing the CH_4 from being produced in the first place (or, in the case of fossil fuel-related emissions, by preventing it from being liberated from the relevant geological formation), or by minimising the amount produced.

This can be achieved either by reducing demand for the end product or service ultimately responsible for the emissions, by switching to a less emissions intense process to achieve the same end product or outcome, or by improving the process directly responsible for the emissions. The last can be accomplished either via interventions aimed explicitly at suppressing CH_4 production, or by improvements in productivity or process efficiency that that lead to lower emissions per unit of end product.

Further down the hierarchy are measures that aim to reduce emissions by preventing the *release* of the CH_4 once it has been produced, or by capturing and mitigating the emissions by combusting them. (As already shown, the combustion of CH_4 to form CO_2 and water results in a net reduction in greenhouse gas emissions of 89%). Approaches that simultaneously recover useful energy from the combustion process are clearly preferable.

At the bottom of the hierarchy are those cases where there is no mitigation measures are adopted and the CH_4 is emitted into the atmosphere; there are some emissions sources for which mitigation options currently do not exist.

Examples of each of the above approaches are included in Figure 1.11. It should be noted however that the categorisation of approaches in the hierarchy is somewhat arbitrary. For example, reducing leaks from the natural gas system is obviously an improvement to the efficiency of the gas distribution process, as well as being a leak prevention measure; switching from coal to renewable resources for electricity generation could be classified as demand reduction or process substitution depending on whether the end product is defined as ‘coal or ‘electricity’, in other words on where the system boundary is drawn.

As is the case for the waste hierarchy on which it is modelled, whilst the concept of a mitigation hierarchy is a useful guiding principle for evaluating the range of mitigation approaches available, it is overly simplistic. This is particularly true in the case of CH_4 emissions, due to the value of CH_4 as an energy resource.

In terms of technical mitigation potential, there is no inherent reason why preventative approaches are better. It is true that because CO_2 is also a greenhouse gas, the ‘mitigation efficiency’ of combusting CH_4 is only 89%; in other words only partial mitigation is achieved by this means. However, assuming the final demand for energy remains constant, utilising the CH_4 emissions in this way will—if energy can be

recovered from the combustion process—reduce the demand for some other more conventional fossil fuel source, and the CO_2 emissions thus prevented will offset the CO_2 released by burning the CH_4 emissions. If the CH_4 emissions act as a replacement for a more carbon-intense fuel such as coal, then the overall mitigation efficiency would in theory be over 100%. Furthermore, as mentioned previously, emissions of other pollutants associated with coal combustion, such as SO_X and particulates, would also be prevented.

Where applicable then, energy recovery could be the preferred option. In fact, a common theme that emerges across sectors is that *enhancement* and *control*—rather than inhibition—of CH_4 production, can form a viable part of a mitigation strategy. The use of more controlled environments, such as closed anaerobic digestors, allows conditions such as temperature and moisture level to be optimised to increase CH_4 production, and the CH_4 produced can be collected more easily. Furthermore, the gas produced is typically of a higher and less variable quality, and problems with supply continuity are reduced. Anaerobic digestors are therefore a key mitigation technology. Various digestor systems are currently commercially available, including complete-mix, plug-flow, fixed-film, covered-lagoon, dome-style, and even simple polyethylene bag digestors. The most appropriate design will depend primarily on the scale of the operation and the local climate (Chynoweth, Owens and Legrand 2001; EPA 2006b,c). Other examples of the 'enhance and control' approach are the use of leachate management systems in landfills, and the pre-mine drainage of CMM.

An additional complication related to mitigation efficiency is that some mitigation approaches, especially technology-based options, require an additional external input of energy. This might be explicit, for example the requirement for supplementary fuel in order to combust MVA containing especially low concentrations of CH_4. However, interventions such as the cooling or aeration of wastewater treatment lagoons, the aeration of landfills, the enrichment of MVA or gob gas prior to combustion, or simply the need for a collection and handling system if the CH_4 is to be recovered, also require an energy input. A further example from the agricultural sector would be the pumping requirements for the periodic draining of rice paddies. The additional energy required—and the associated CO_2 emissions—must be considered in evaluating the overall mitigation efficiency of any given approach, or indeed in determining if there is actually a net reduction in greenhouse gas emissions at all.

Other environmental costs and benefits also need to be considered. In the agricultural sector, for example, there is often a trade-off between CH_4 and N_2O emissions. A common mitigation approach across sectors is switching from anaerobic to more aerobic systems for the treatment of organic wastes, and although this reduces CH_4 production, production of N_2O is increased. This is also the case for the periodic

draining of rice paddies. Aerobic decomposition also produces more CO_2, which cannot be recovered as a fuel. Alternative manure handling systems such as direct land application can also lead to increased surface and groundwater pollution. Surface mining for coal produces less CH_4 than underground mining, but often has a greater negative impact on the local environment. On the other hand, some mitigation measures, such as reducing fossil fuel use, would have additional positive environmental effects. The mitigation of CH_4 emissions must therefore be seen in the context of an integrated climate change or environmental policy.

The likely adoption rate of a particular mitigation approach must also be considered, and this will depend on political and economic factors as well as the technical mitigation potential. The mitigation hierarchy does not consider economic costs and benefits; therefore it cannot help in assessing the economic affordability—or economic mitigation potential—of the different options. Reductions in emissions achieved through improvements in productivity or efficiency are likely to be accompanied by an increase in profits. Mitigation options involving the recovery of energy can generate an additional revenue stream either via gas pipeline or electricity sales; or reduce operating costs through the generation of electricity or production of heat for local onsite uses. The *economic* mitigation potential of these approaches might therefore be greater. No-regrets mitigation options, which can be realised at zero cost or net-benefit, are more likely to be implemented. Options that do not require major capital investment, or significant changes to infrastructure or current industry practice, and that are based on mature and proven technologies, are also more likely to be adopted.

It is also worth considering that although the most practical response to stabilising or reducing atmospheric CH_4 concentrations is preventing or mitigating emissions, a logical alternative would be to increase the capacity of existing CH_4 sinks (as also indicated by Figure 1.11). The potential for the control of the main atmospheric sink—oxidation by tropospheric OH—is minimal, although reductions in combustion related pollutants such as CO and NO_X, which are also oxidised by the OH radical, should result in a slight increase in the overall oxidative capacity of the troposphere, thereby enhancing CH_4 removal. Likewise, reductions in atmospheric nitrogen pollution could help to maintain the oxidative capacity of soils. Land use changes can have a more significant impact on the ability of soils to act as a CH_4 sink. For example, the reforestation of agricultural land tends to result in increased CH_4 oxidation as a result of decreased soil nitrogen concentrations (due to a cessation of fertiliser use) and changes to drainage patterns; forests also act as a sink for CO_2.

In practice, it is evident that not all mitigation approaches are applicable to all emissions sources. A key determinant of the most suitable strategy is whether or not an emissions source is diffuse and hence not amenable to recovery (many agricultural

emissions), or else a local or point source, in which case there is potential for the CH_4 to be captured and energy recovered. Another determinant is whether the CH_4 is biogenically or fossil fuel derived; other than the ultimate preventative measure of reducing fossil fuel demand, preventative approaches tend to be more applicable to biogenic sources.

Conversely, for a single emissions source or sector, an integrated mitigation strategy incorporating a combination of approaches from several levels of the hierarchy might be required. For coal-related emissions for example, such a strategy could incorporate a reduction in demand for coal; a shift in production towards surface mining; increased drainage and capture of—and energy recovery from—CMM before, during and post-mining; and capture and mitigation of the remaining CH_4 in the MVA.

1.3.4.1 Analysis of energy recovery options

For approaches based on capturing the CH_4, a number of technologies exist for its mitigation or use. Options include simple flaring, local thermal uses, electricity generation, cogeneration, use in fuel cells, pipeline sale and use as industrial feedstock. The technical applicability of any of these options will depend primarily on the quality of the gas recovered, and also on the continuity of the supply, the lifetime of the emissions source, the location of the emissions source, and the scale of the operation.

The concentration of CH_4 (and any other combustibles) in the emissions is the significant determinant in the viability of a particular technology, however other relevant characteristics of the emissions stream include its flow rate, moisture content (the emissions are often saturated), short and long-term variability in both energy content and flow rate, and the presence of impurities such as particulates (for example coal dust) or toxic trace compounds (as in landfill gas).

The simplest combustion option is flaring, by which means the emissions will be mitigated but no energy recovered. Flares can be of either the open or enclosed flame variety. This might be the only option for remote locations such as offshore oil platforms, if there is no local grid connection or pipeline network, and no local uses for any energy that could be recovered. It is not an option if the concentration of CH_4 in the emissions is under 5% (the lean flammability limit), as is the case for MVA, some emissions from decommissioned mines, or LFG at the beginning and end of the life of the landfill.

If the gas recovered is of a high enough quality, for example CMM drained pre-mining, it can be supplied to the gas pipeline network, assuming an appropriate network exists and there are not likely to be problems with gas continuity. Usually a minimum local pipeline quality (often 95% CH_4) will apply (Su et al. 2005).

Alternatively, the recovered CH_4 can be used to generate electricity onsite. If the quality of the gas is high enough, conventional gas combustion devices, such as gas turbines or internal combustion (IC) engines (Shrestha and Narayanan 2008), can be used. For smaller facilities, microturbines might be appropriate (EPA 2002). The electricity generated can be either sold to the grid or, if there is sufficient demand, used onsite, for example to power other mining or farming operations.

If the gas recovered is of a lower quality, then the options are to upgrade it, either for pipeline sale or onsite generation in a conventional gas-fired power plant, or to treat is 'as is' using more advanced lean-burn combustion technologies capable of burning low-calorific value fuels.

If the gas is to be upgraded, various commercial technologies are available to increase the CH_4 concentration, and remove moisture and particulates. These include nitrogen removal units, dehydrators, and wet scrubbers; and concentrators based on pressure-swing adsorption, solvent absorption, cryogenics, or membrane separation. Any pre-processing required will impose a negative energy cost however, and there will be a minimum gas quality below which the energy required for upgrading will exceed the inherent energy content of the recovered emissions. For emissions with extremely low CH_4 concentrations such as MVA, there is as yet no proven solution, although fluidised bed concentrators might be a possibility (Rasi et al. 2008; Shirley, Porto and Hawk 1996; Su et al. 2005).

If the emissions are to be used in a conventional gas combustion device, the addition of either additional fuel or air may be necessary to even out any fluctuations in energy content or flow rate. Given the variability of the fuel supply, there will also be increased need for diagnostic and performance monitoring, and a control strategy able to deal with transient behaviour.

An alternative for emissions sources with a very low energy content, such as MVA, is to treat the emissions using some form of lean-burn technology capable of burning below the conventional flammability limit. As already mentioned, a number of technologies, including thermal and catalytic flow reversal reactors, and various designs of catalytic and recuperative lean-burn gas turbines, are currently being developed specifically for MVA combustion (see Chapter 2 for further details), though non are yet in commercial operation (EPA 2000; Su et al. 2005). These could also be applicable to other CH_4 emissions. At very low CH_4 concentrations, energy recovery might not be possible, as the entire energy content of the fuel would go towards simply sustaining the combustion reaction, although the emissions would still be mitigated. Lean-burn combustion systems are another key mitigation technology, and there is much potential for additional research and development (R&D) in this area.

An alternative to electricity generation is direct thermal use of the energy recovered from the combustion process (either in conventional or lean-burn systems). Particularly in cases where the CH_4 emissions are of a low quality, so cannot be used for electricity generation, a large supply of *low-grade* heat is likely to be available. The available thermal resource must be matched to a corresponding local heating requirement. Apart from space and water heating for adjacent facilities, various opportunities exist. Where anaerobic digestors are used, waste heat can be recycled to heat the digestor to the optimal temperature for CH_4 production (approximately 60°C). It has recently been suggested that low-grade heat (again at approximately 60°C), can be used to operate a desalination process (Gude and Nirmalakhandan 2008). This would be suitable at coal mines for the desalination of mine wastewater, or could be incorporated into a municipal wastewater treatment facility. Other possible uses for heat at coal mines include coal drying and heating of the MVA prior to circulating it through the mines (Brenkley and Bennett 1996; EPA 2000).

Potential synergies also exist in the consolidation of waste streams, by co-combusting the recovered CH_4 with some other 'waste' material, thus allowing additional energy recovery as well as reducing waste. Examples include the combustion of CMM with waste coal fines, or combining the combustion of LFG with the thermal treatment of MSW. A related approach, where the CH_4 content is extremely low, is to use the emissions as a full or partial replacement for the combustion air of a process where some other fuel is the primary energy provider, for example the use of MVA as the combustion air for a coal-fired power station.

In locations where suitable markets for both electricity and heat exist another option would be cogeneration (combined heating and power (CHP)) or trigeneration (combined cooling, heating and power (CCHP)) (Hao, Yang and Zhang 2008). A further alternative is the use of CH_4 directly in solid oxide fuel cells (SOFC), or molten carbonate fuel cells (MCFC) (Lombardi, Carnevale and Corti 2006); however these require a high purity and are currently expensive.

The most profitable energy recovery option will depend on the relative local costs of gas and electricity, the potential savings to be made from electrical or thermal onsite use, and the existence of suitable local markets for gas, electricity or heat.

A final possibility is the use of the recovered CH_4 as an industrial feedstock, either for the production of transport fuel, or as a feedstock for chemical production, for example in the production of carbon black, ammonia, or organic chemicals (Bibler, Marshall and Pilcher 1998; CIAB 1994; EPA 1999).

1.3.5 Implementation of mitigation measures

It was previously shown that a significant proportion of CH_4 mitigation options could be implemented on a no-regrets basis, but have so far not been. There are a number of reasons why CH_4 recovery is not widespread, even where the technology exists, and a number of measures that could be taken to increase implementation.

1.3.5.1 Barriers

CH_4 is usually a secondary issue to the industrial process from which it is emitted (the exception being emissions from the natural gas industry). It is often regarded as a waste by-product to be disposed of, rather than as a resource. Historically, it may even have been viewed as a hazard. Those responsible for the emissions may therefore not be aware of the technologies available or profit potential; this is particularly the case for small-scale producers, or in developing countries.

Another problem is that CH_4 emissions can be difficult to identify and quantify, particularly in the agricultural sector, or in the case of fugitive emissions from the energy sector; measurement may be difficult if the CH_4 concentration is only slightly above ambient levels. This makes accurate measurement and monitoring of both baseline emissions and any reductions achieved difficult. In the agricultural sector, there is limited technical understanding of the relationships between management practices and emissions. Without such data it is not easy to incorporate CH_4 into mitigation policies such as emissions trading schemes. There are also uncertainties surrounding both monetary and nonmonetary mitigation costs and benefits. Furthermore, conventional fuel characterisation methods do not always provide sufficient information to evaluate CH_4 emissions as an energy resource. MVA, for example, has an energy content so low that it would not even be regarded as a fuel by conventional measures.

Many emissions sources, particularly agricultural sources, are diffuse and hence not amenable to recovery. Once captured, there are also technical barriers to mitigation, especially where the CH_4 is to be recovered as an energy resource, as previously discussed. Foremost among these is that the emission stream often has a very low energy content (and, conversely, high quantities of impurities and inerts) and as such makes a poor quality fuel (an extreme example is MVA); the dilute nature of such emissions also means that extremely large volumes of gas need to be treated. Emissions may also exhibit other properties typical of low-grade fuels, for example high levels of co-pollutants and moisture; LFG is a prime example of this. Furthermore, emissions even from a single source can be highly variable, often exhibiting significant fluctuations in both quality and quantity both in the short and long-term (over the lifetime of a landfill for example).

The remoteness of many emissions sources—including offshore oil and gas fields—also limits mitigation options. For example, where the CH_4 is recovered as a fuel, direct local use may be the only option due to otherwise prohibitive distribution costs, but local demand will not always match the resource available. Also, many mitigation strategies require the use of a central facility in order to benefit from economies of scale, for example treatment of domestic sewage or animal manure. This might necessitate the provision of additional infrastructure (for example a sewerage system), or result in prohibitively high transport costs if emission locations are distributed over a large area.

There are also various barriers that prevent the development and commercialisation of newer mitigation technologies. These include a lack of information and expertise, a lack of R&D expenditure, difficulties changing existing industry infrastructures, and the absence of incentives to overcome higher initial costs. The question of whether CH_4 can be classified as a renewable resource is central to determining its eligibility for certain financial incentives, and this is not always clear-cut, particularly for emissions associated with waste treatment. Also, more subtly, R&D can be inhibited by the fear that if suitable technologies were to become available there would be pressure to implement them. Furthermore, in many countries, poorly functioning energy markets and financially insolvent utilities fail to provide the private sector with a climate that will attract investment in CH_4 mitigation projects (Jardine et al. 2004; Watts 1997).

There are also issues of political and public acceptability to consider. For example, investing in technologies to mitigate emissions associated with coal mining might be seen by some parties to be unacceptable if it is seen to be prolonging the survival of a highly polluting industry. Suggestions that CH_4 emissions from livestock should be mitigated by reducing consumption of meat would also be unacceptable to large sections of the population. Furthermore, national governments are likely to be unwilling to apply measures that would affect the international competitiveness of an industry.

Finally, as already shown, emissions are frequently associated with a geographically dispersed set of heterogeneous processes. The range of economic sectors from which CH_4 emissions occur is also far larger and more diverse than for CO_2, and CH_4 sources also vary significantly among countries. Previously, it has been suggested that this diversity offers an advantage over CO_2 mitigation because it results in a wider variety of mitigation opportunities. It can also be an impediment to mitigation however, as more complex mitigation policies and schemes will be required: there can be no silver bullet solution.

A final point to appreciate is that individual minor sources—even though collectively significant—can seem inconsequential and thus not worth mitigating when considered in isolation.

1.3.5.2 Incentives

In order to encourage the adoption of CH_4 mitigation measures, government intervention—financial, legal, and political—is required.

For the development of new mitigation technologies, government financing of basic and applied R&D and initial demonstration projects is necessary. A public-private partnership approach, in which the cost is shared by industry and government, might also be a suitable support mechanism for pre-commercial technologies. Governments can also support industry innovation via intellectual property protection, R&D tax credits, and loan guarantees (CIAB 2008; IPCC 2007b; MIT 2007).

If mitigation technologies are to enter into widespread commercial use, various regulatory and economic pressures need to be applied to create a more receptive marketplace, in order to encourage producers to invest in mitigation technologies and processes.

An appropriate regulatory environment could include mandatory emissions limits. Regulatory standards can be technology-based, in which case limits on emissions are tied to the reductions achievable with existing technology, and the standards change in line with technological change; set with respect to a desired emissions stabilisation level regardless of the cost or technological feasibility of achieving that level; or involve an assessment of trade-offs between the risk to society of not mitigating the emissions, and the financial cost of doing so (MacDonald, Chadwick and Aslanian 1996).

The foremost economic pressure is to impose a real or implicit price on carbon. Market-based solutions include emissions trading schemes, such as cap-and-trade systems, or direct carbon taxes. Introducing feed-in tariffs for power generated from the recovered CH_4 based on the avoided emissions—and reducing barriers to distributed generation—could also encourage adoption of energy recovery approaches (CIAB 2008; de la Chesnaye et al. 2001; MIT 2007).

Other financial instruments include the provision of incentive programs and subsidies, and mandatory price supports, for example in the agricultural sector. The existence of reliable legal frameworks, and the necessary enabling infrastructure—for example a gas pipeline network—is also important (CIAB 2008; de la Chesnaye et al. 2001).

Voluntary contracts with industry are another policy tool. In the US, there are a number of existing voluntary CH_4 mitigation programs operated by the Environmental Protection Agency, for example the Coalbed Methane Outreach, Landfill Methane Outreach, Natural Gas Star and AgStar programs (EPA 2007). The Methane to Markets partnership, launched in 2004, is another an example of a voluntary agreement (Gunning 2005). It aims to advance project development in three major CH_4 source areas (landfills, underground coal mines, and oil and gas systems) by encouraging

collaborations that bring together technical and market expertise and match technology with financing. Raising awareness of the issue, and the provision of information, are also important.

Finally, the IPCC suggest that integrating climate policies—such as CH_4 mitigation—in broader development policies may make implementation and overcoming barriers easier (IPCC 2007b).

1.4 Conclusions

CH_4 is a powerful greenhouse gas with a GWP 25 times that of CO_2, and also plays an important role in atmospheric chemistry. It is responsible for approximately 25% of the enhanced greenhouse effect observed since pre-industrial times, and currently accounts for 14.3% of total global anthropogenic greenhouse gas emissions. Once emitted however, CH_4 has a relatively short lifetime of only 12 years, so reductions in emissions will translate quickly into reductions in atmospheric concentrations.

Many CH_4 mitigation measures involve technologies that are currently available, and that would be comparatively cheap and quick to implement. The mitigation of CH_4 emissions could therefore provide a relatively inexpensive supplement to CO_2 mitigation, and a cost-effective mitigation strategy would focus on CH_4 in the near-term.

CH_4 is emitted from a wide range of anthropogenic sources across the agricultural, energy, and waste management sectors, as well as from natural sources. There is a correspondingly diverse range of possible mitigation approaches, ranging from preventing CH_4 production at source to capturing and recovering energy from the emissions. Emissions from coal mining, landfills, and the oil and gas system show the greatest potential for mitigation.

Key mitigation technologies include anaerobic digestors, which allow greater control over CH_4 production and collection; and lean-burn combustion technologies, which allow energy to be recovered even from emissions with very low CH_4 concentrations, although further R&D is required in this area.

No technology offers universal applicability however, and there is no single unifying CH_4 mitigation policy. The next chapter takes the form of a case study, and will examine in more detail the emissions and associated mitigation solutions for a single source: coal mining.

Chapter 2

CASE STUDY: METHANE EMISSIONS FROM COAL

2.1 Introduction

In the previous chapter, emissions of methane (CH_4) from a diverse range of anthropogenic sources, and the many options available for their mitigation, were reviewed. This chapter takes the form of a case study, and focuses in more detail on the problem of emissions from a single source: coal mining.

Coal mining has been identified as one of the sectors with the greatest potential for CH_4 mitigation (Lucas et al. 2007). It also serves as a useful case study because these emissions are some of the most challenging to mitigate from a technical perspective, as the CH_4 in the mine ventilation air—which accounts for the majority of the emissions—is present at such extremely low concentrations. The mitigation solutions developed for coal mining will likely find application across other sources and sectors.

It is important that the issue of CH_4 emissions from mining be seen in the context of the environmental performance of the coal industry as a whole. The first part of this chapter therefore aims to provide the necessary background to the industry. The current environmental impacts of coal use, and ways of reducing these impacts—including developments in the fields of clean coal technology (CCT) and 'zero emissions' coal—will be described.

The problem of CH_4 emissions from coal mining activities will then be addressed in more detail. Estimates of current and projected emissions will be presented, and the economic potential for mitigation assessed. The characteristics of the emissions emanating from different phases in the mining process will then be described, and the options for mitigating these emissions—including recent advances in mitigation technologies—considered. Areas where further technological development is required will also be identified.

Where possible, examples from the Australian coal industry will be given.

2.2 The coal industry

The wide availability, supply security and comparatively low cost of coal means that it currently plays a key role in the global energy mix, and in the economies of many countries. Coal currently accounts for around 25% of primary energy supply and 40% of electricity generation (IEA 2007b). Global production was 6,781.2 Mt in 2008 and total reserves are estimated at 826,001 Mt (BP 2009).

In Australia, 401.5 Mt of coal was produced in 2008, and estimated reserves of 76,200 Mt are expected to sustain production for 200 years (BP 2009). Australia is the world's fourth largest producer of black coal[†], and its largest exporter (IEA 2007b); more than 70% of Australia's black coal is exported, accounting for over 10% of export revenues and making it the country's primary export (IEA 2005). Australia has more than 30 coal-fired power stations, with a combined capacity of approximately 30,000 MW. Coal is currently the lowest cost baseload power source in Australia, and, as it accounts for 75% of electricity generation, Australian electricity prices are among the lowest in the world. This has attracted several major energy-intensive industries (for example minerals mining and processing, and pulp and paper) that also make a significant contribution to exports (CIAB 2005). Unfortunately, Australia's reliance on coal also means its greenhouse gas emissions intensity is one of the highest in the world (IEA 2005).

Even if coal does not represent a long-term solution for the energy problem, it will undoubtedly be a strategic element in the mid-term, and will remain a part of the energy mix for many decades to come. This is particularly true in Australia, given its resource base and economic structure, and the key role coal plays in providing low energy prices and energy security. Improvements in the environmental performance of coal production and use are therefore essential.

2.2.1 The environmental impact of coal

Much current analysis of coal's environmental performance focuses on combustion-related carbon dioxide (CO_2) emissions. This is understandable given the severity of the global warming issue, and the magnitude of this particular emissions source. It is important to realise that greenhouse gas emissions, and other environmental impacts, arise throughout the coal cycle however, from exploration, extraction and beneficiation (refining and processing), to transportation, storage and finally conversion. Resource use throughout the cycle includes water, energy, materials, manpower and land; impacts may be global, regional or local (Chadwick, Highton and Lindman 1987).

[†] Brown coal production accounts for less than 10% of total production, and is used almost exclusively at mine mouth electricity generating stations, as its low energy and high moisture content make it uneconomic for export, or even for transport over significant distances internally.

The environmental impacts of coal mining include land disturbances—either scarring from surface mining or subsidence from underground mines—and surface waste deposits associated with pitheads. Mining produces wastewater and may adversely affect watercourses. Vegetation and wildlife may be harmed, and property damaged. Mining involves risks to the health and safety of the miners (Chadwick, Highton and Lindman 1987; Kirchgessner 2000). And, as shall be discussed further shortly, coal mining—particularly from underground mines—also results in significant releases of CH_4.

Impacts resulting from post-mining activities such as transportation and handling include the release of particulates and other air pollutants that adversely affect local air quality, human health, agriculture, and natural ecosystems; as well as emissions of CO_2 and other combustion-related pollutants from the vehicles used for transportation. Where slurry pipelines are used there is an additional demand for water, and the need to dispose of the wastewater—usually saline and loaded with coal fines—resulting from the dewatering of the slurry at the power plant; accidental release of slurry with subsequent damage to crops, other vegetation, aquatic systems and aquifers is also possible. There is the risk of accidents involving either industry employees or the public (Chadwick, Highton and Lindman 1987). Fugitive emissions of CH_4 also occur during coal transportation and handling activities.

CO_2 emissions from the combustion of coal for electricity generation constitute the most significant environmental impact however. As was shown in the previous chapter (Figure 1.3), CO_2 from fossil fuel use is responsible for 57% of global anthropogenic greenhouse gas emissions (IPCC 2007b). Of these, emissions from coal account for around 41%, which equates to annual emissions of approximately 11 Gt of CO_2 globally (IEA 2007b). In Australia, the combustion of coal was responsible for the release of just under 200 Mt of CO_2 in 2007 (DCC 2009).

The combustion process also results in emissions of nitrogen oxides (NO_X), sulphur oxides (SO_X) (depending on the sulphur content of the coal), and particulates. The last can contain potentially toxic or carcinogenic trace compounds, including hydrocarbons such as polycyclic aromatic hydrocarbons (PAH), heavy metals such as mercury, and radionuclides (Chadwick, Highton and Lindman 1987).

Liquid effluent, which can contain organic material, sulphuric acid, chloride, phosphate, boron and suspended solids, is also produced. Solid waste in the form of waste coal fines and ash (bottom ash and recovered fly ash) is produced as well, and can also contain potentially harmful trace elements (Chadwick, Highton and Lindman 1987).

Another significant environmental issue, especially in water-stressed regions—such as many areas of Australia—is fresh water consumption by coal-fired power stations. Coal-fired electricity generation consumes an average of 1.5 ML of water per GWh. Over 90% of this is used in the cooling system. The remainder comprises boiler make-up water and water used for ash management and disposal (Smart and Aspinall 2009).

2.2.2 Reducing the environmental impact of coal

Levels of CO_2 emissions form coal combustion depend on the type of generating technology employed. Pulverised fuel (PF) combustion is currently the dominant system. In Australia, almost all coal-fired power stations are of the conventional (subcritical steam generation) PF variety, which require less capital investment (CIAB 2005). Much research and development effort in the area of CCT is focused on either increasing the efficiency of PF power plants, or developing new generation technologies and alternative conversion pathways.

The maximum efficiency of conventional subcritical PF power stations is 36%[†] (however many older plants still in operation have efficiencies under 30%). Modern supercritical plants, such as InterGen's 850 MW Millmerran power station in Queensland, Australia (InterGen n.d.) are capable of achieving efficiencies of up to 40%. Ultra-supercritical (USC) plants can realise efficiencies of 47%. Combustion efficiencies are expected to improve further through the use of coal drying and higher power plant steam cycle temperatures, with efficiencies of over 50% predicted by 2020. Increased efficiencies result in reductions in CO_2 (and other) emissions per unit of energy generated (CIAB 2005; Diniz da Costa, Prasad and Pagan 2004; MIT 2007).

Alternative combustion technologies capable of reducing CO_2 emissions include pressurised fluidised bed combustion (PFBC) and oxy-fuel combustion, which uses pure O_2 and recycled flue gas as the oxidant instead of air. The integrated gasification combined cycle (IGCC) process, which gasifies coal to produce syngas, is an example of an alternative conversion pathway. The syngas can be used to generate electricity via gas turbine combustion, as a source of H_2 for fuel cells, or as a chemical feedstock. More developmental concepts include chemical looping combustion, dry ice co-generation, and the externally-fired combined cycle (EFCC) process (CIAB 2008; MIT 2007).

The long-term aim of clean coal research is to achieve 'zero emissions' generation by employing carbon capture and storage (CCS) (CIAB 2005, 2008; Diniz da Costa, Prasad and Pagan 2004; Franco and Diaz 2009; IEA 2002; IPCC 2005; MIT 2007; Wall 2007). Capture of CO_2 can be most readily achieved pre-combustion via the use of IGCC. Oxy-fuel combustion also lends itself to carbon capture as the exhaust stream contains CO_2

[†] All efficiencies are based on the lower heating value (LHV) of coal.

at high concentrations. Post-combustion capture from PF power plants—via absorption using solvents, pressure or temperature-swing adsorption, gas separation or absorption membranes, or cryogenic separation—is expensive and results in significant efficiency losses, especially when retrofitted to existing plants.

Carbon storage options include sequestration in geological formations such as depleted oil and gas fields, non-mineable coal seams (with simultaneous enhanced coal bed methane (ECBM) recovery (see later)), and deep saline aquifers. Geological sequestration would seem to be a viable option in Australia where there is a large underground storage potential. Alternative storage options include deep ocean storage, the enhancement of terrestrial carbon sinks such as forests, fixation with algae, and mineralisation. There are also a number of industrial uses for CO_2, but these only require small volumes of gas. Further research is required to ascertain that potential storage sites are effective, verifiably safe, and environmentally sound.

Other options for reducing CO_2 emissions include co-firing coal with biomass or waste, and combining coal and solar thermal generation. In-situ coal gasification might be another possibility in the future (CIAB 2005; Evans 2007).

Emissions of pollutants other than CO_2 are also dependent on the choice of combustion technology. PF combustion is characterised by relatively high dust and NO_X emissions. End-of-pipe emission control technologies must be applied to remove the hazardous compounds from the flue gas. Fluidised beds operate at a lower combustion temperature and so produce fewer NO_X emissions, and also allow for the possibility of adding carbonate material to the coal feed in order to bind sulphur against release to the atmosphere (Chadwick, Highton and Lindman 1987).

Improved coal preparation, including washing, beneficiation (to reduce ash and other impurities such as sulphur), drying and briquetting can also improve combustion efficiency and reduce emissions, as can the use of higher grade coal, or coal naturally low in sulphur (CIAB 2005, 2008).

Solid waste can be minimised if process wastes such as coal fines and coal washery rejects are recovered for power generation where possible. Fluidised beds, for example, are suitable for the combustion of waste coal. Alternatively, coal-water slurries can be co-fired with coal or as a substitute for heavy oil (Tillman and Harding 2004). Fly ash can also be reused—for example in cement making—to avoid disposal at landfill (CIAB 2005).

Water consumption can be reduced by the use of dry cooling systems—such as that employed by Millmerran power station—however this imposes an efficiency penalty and an associated increase in CO_2 emissions. Other options for reducing fresh water

requirements include the use of saline cooling systems and the recycling of wastewater (Smart and Aspinall 2009).

Finally, reducing the energy intensity of mining and post-mining operations can reduce CO_2 emissions from these stages in the coal cycle; the Australian mining sector is already relatively efficient in this respect however. In the following sections the issue of CH_4 emissions from mining activities will be discussed.

2.3 Methane emissions from coal mining

In the previous chapter it was suggested that because CH_4 is usually a secondary issue to the industrial process from which it is emitted, those responsible for the emissions may not be aware of the mitigation technologies available, or of the potential profits to be made, and that this constitutes a barrier to mitigation. In this context it is interesting to note that the majority of studies assessing the environmental impact of coal—and potential clean coal technologies—either do not mention CH_4 emissions at all, or do so in a cursory manner, even in the context of 'zero emissions' coal.

Coal bed methane (CBM) is formed as a by-product of the coalification process. About 1,300 m^3 of gas is produced per tonne of coal formed. Most of the gas produced escapes during coalification, but a small amount is retained in the coal seam, either as 'free gas' in fractures, adsorbed in pores in the coal, or in adjacent rock strata. The final gas content is up to 25 m^3 per tonne of coal. In general, the higher the rank of the coal, the deeper the coal seam, and the lower the moisture content, the greater the volume of gas. This residual CH_4 is released when the pressure within the coal seam is reduced, either as a result of natural erosion, faulting or mining. CH_4 released as a result of mining activities is known as coal mine methane (CMM) (Flores 1998; Kirchgessner 2000).

Most mining related CH_4 emissions are from underground mines. A substantial amount of CH_4 is also released from the strata above and below the active coal seam (CIAB 1994). The vast majority of the CH_4 released escapes to the atmosphere in the mine ventilation air (MVA).

Emissions from surface mines are lower as these seams are by definition shallow in depth, and tend to be low rank (lignite, sub-bituminous and low rank bituminous coal), so do not contain significant amounts of gas.

As well as the CH_4 released by the coal excavated and processed during mining, emissions occur from the coal and neighbouring strata exposed by mining activities, and from piles of waste coal stored on site (EPA 2008).

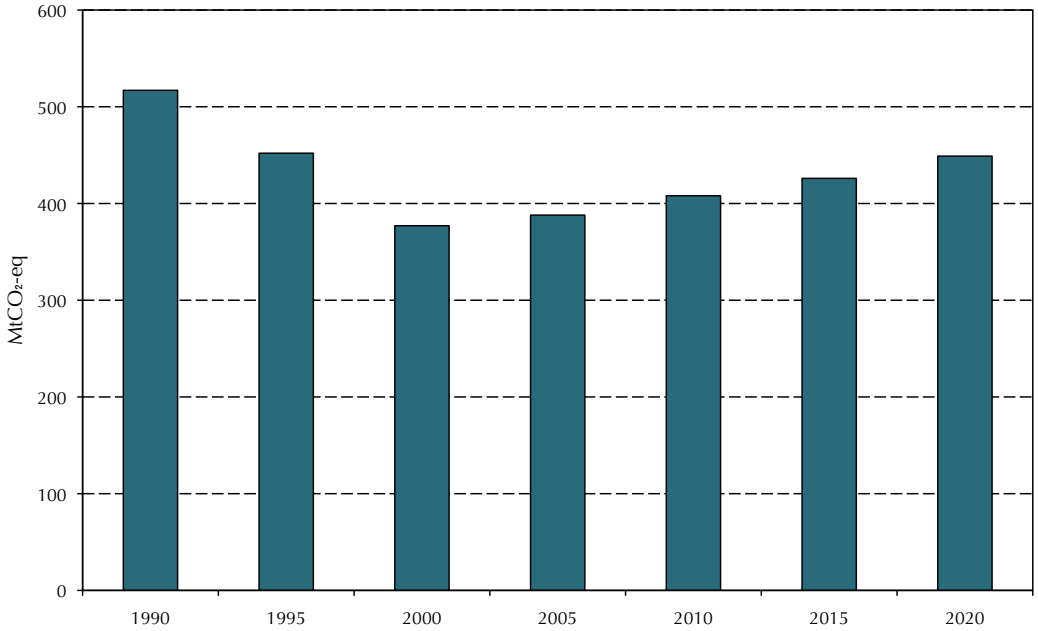

Figure 2.1 Global CH_4 emissions from coal mining activities for the period 1990 to 2020 (Source: adapted from EPA 2006a).

Emissions also occur from decommissioned mines, and from post mining handling activities, which include crushing, separation of impurities, size classification, drying, transportation and storage. The coal will continue to desorb gas until it's ultimately consumed (DTI 2004; Kirchgessner 2000).

As illustrated in Figure 1.7, emissions from coal mining constitute just over 6% of total anthropogenic CH_4 emissions. In 2005, 388 $MtCO_2$-eq of CH_4 was emitted from coal mining activities globally; 21.8 $MtCO_2$-eq of this in Australia (EPA 2006a; DCC 2008).

Figure 2.1 shows the recent global trend and future projections for these emissions. The decline in emissions from 1990 to 2000 is due to a number of factors including: changes in the Chinese coal industry, with many mines closing during this period and coal production slowing significantly; a rapid decline in coal production during the 1990s in both England and Germany; and restructuring of the energy industries in the former Soviet Union and Eastern Europe, which resulted in many of the gassiest underground mines closing. Emissions are projected to increase in the future due to a projected increase in coal production. These increases are likely to be modest however, due to a shift in production away from gassy underground mines and towards less capital-intensive surface mines (EPA 2006a).

This shift in production methods is already evident in Australia, as illustrated by Figure 2.2, which shows the equivalent Australian emissions up to 2007. Contributions from underground, surface and decommissioned mines, as well as post-mining activities, are indicated. The relationship between emissions and coal production is also illustrated.

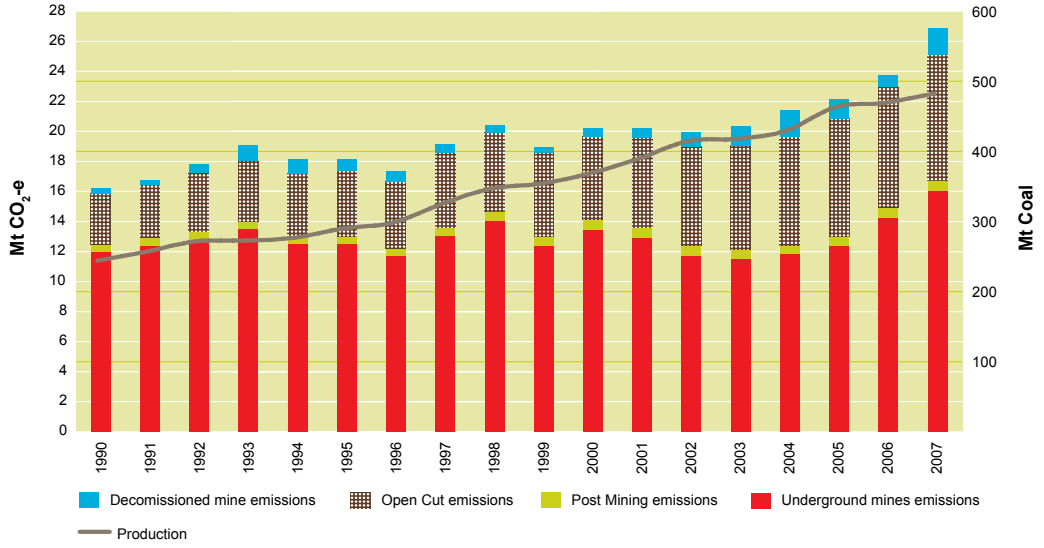

Figure 2.2 Australian CH_4 emissions from coal mining activities for the period 1990 to 2007 (Source: DCC 2009).

This highlights the effect of the relative increase in surface mines in moderating emissions; this is also apparent from the increase in emissions from surface mining and decommissioned mines (due to the closure of several gassy underground mines). Nevertheless, it can be seen that underground mining still accounts for the majority of coal related emissions, despite constituting only around 12% of production (DCC 2008, 2009). Moreover, it would be reasonable to assume that, in the longer term, underground mining is likely to expand once again, as surface mineable resources are exhausted.

An additional minor source of CH_4 from mining operations—unrelated to CBM—is from outbreaks of spontaneous combustion in spoil heaps at surface mines; CH_4 is produced if the combustion reaction occurs under reduced oxygen conditions (Carras et al. 2009).

2.4 Mitigation of methane emissions from coal mining

2.4.1 Motivation

Since the early 19th century, when improvements in technology allowed the construction of large, deep mines, mining engineers have treated CMM (or 'firedamp') as an explosive hazard (Flores 1998). (In surface mining, the released CH_4 is heavily diluted by its immediate exposure to the atmosphere, and therefore the risk of explosion is minimal.)

More recently, CMM has been recognised as a resource with a practical and profitable use.

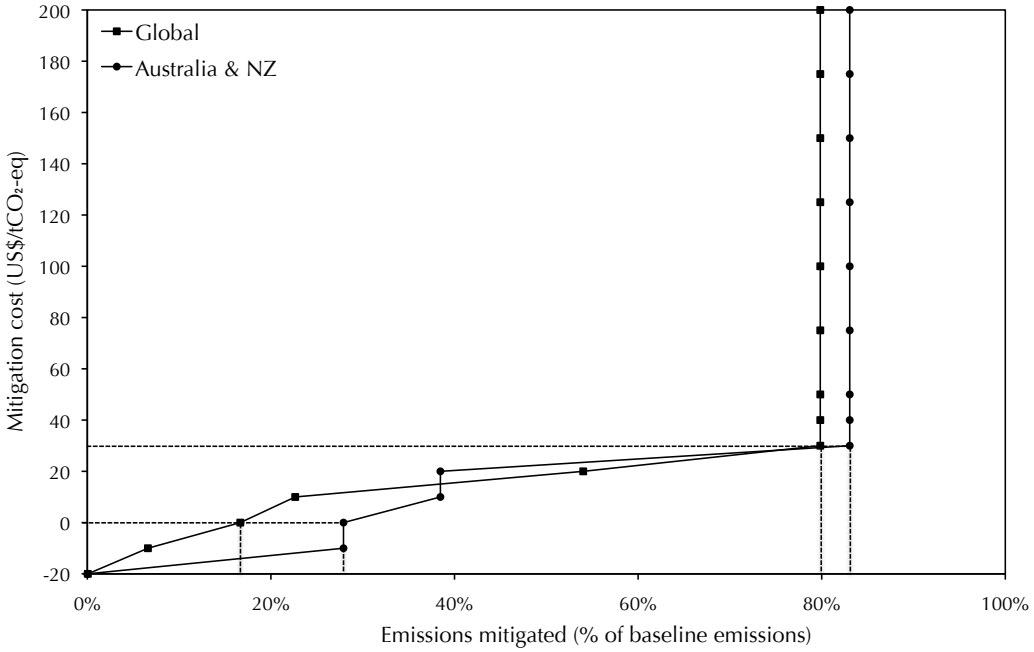

Figure 2.3 MAC curves for the mitigation of CH_4 from coal mining in 2010 (Source: adapted from EPA 2003b).

Undiluted, CBM is actually very similar to natural gas in composition and calorific value, and as such can be used interchangeably with natural gas in most applications. The quality of the gas varies depending on location, but it is usually composed principally of CH_4 plus small quantities of other alkanes (80–95%[†]), with the rest being mostly inerts (nitrogen (N_2), oxygen (O_2), CO_2 and argon (Ar)) and some other minor constituents (helium (He) and hydrogen (H_2)). Exceptions do occur: the gas from some Australian coal seams, for example, has a high CO_2 content (CIAB 1994; Flores 1998).

Lately, the role of CH_4 as a greenhouse gas, and its contribution to global climate change, as discussed in the previous chapter, has also been appreciated. As previously discussed (§1.3.1), combusting the CMM—whether or not energy is recovered from the combustion process—is an effective mitigation measure, resulting in a net reduction in greenhouse gas emissions of 89%. The motivation for the mitigation of CH_4 emissions from coal mining is therefore three-fold: mine safety improvement, economic advantage, and environmental benefit.

2.4.2 Mitigation potential

Marginal abatement cost (MAC) curves for the mitigation of CH_4 emissions from coal mining, based on data from a recent analysis by the US Environmental Protection Agency (EPA 2003b), are shown in Figure 2.3. It can be seen that, globally, 17% of

[†] All CH_4 concentrations are expressed as percentage by volume.

emissions could be mitigated at or below zero cost. In Australia and New Zealand, there is even greater potential, with no-regret options accounting for a 28% reduction in emissions. 80% of emissions could be mitigated at a cost of US$30 per tonne ($CO_2$-eq) of emissions or less.[†]

2.4.3 Mitigation options for underground mines

2.4.3.1 Recovery of coal mine methane

Given the value of CH_4 as a fuel, the most favourable mitigation strategy is to extract—or 'drain'—the CMM before mining commences (Bibler, Marshall and Pilcher 1998; Brenkley and Bennett 1996; CIAB 1994; EPA 1999, 2003a, 2006b; Kirchgessner 2000; Kirchgessner, Masemore and Piccot 2002).

This has the advantage that a high quality gas—often containing over 90% CH_4—can be recovered. Pre-mining degasification also improves mine safety, reduces ventilation air requirements, and increases productivity by reducing the amount of time the mine must curtail production due to explosions and gas outbursts. The degasification system consists of a network of vertical wells, horizontal boreholes and gas pipelines.

CMM can also be drained during or post-mining via gob wells (also known as goaf wells); however the quality of the gas recovered is more variable—CH_4 concentrations can be as low 30%—limiting utilisation options.

Under ideal conditions (deep gassy longwall mines) up to 60–70% of CMM at a mine can be recovered. For intermediate depth shafts, the potential may be closer to 30%. In Australia, the geology of underground reserves would likely support a technical recovery potential of 30–40%. Currently in the US, where the CMM industry is most developed, it is estimated that on average only about 27% of the gas is drained and used as a fuel, 7% is drained but released, and 66% escapes via the mine ventilation system.

Even with the expansion and improvement of degasification systems, a substantial quantity of CH_4 will still enter the ventilation system, so strategies for recovering and mitigating MVA emissions will be needed to complement drainage. Currently, most MVA is vented directly to the atmosphere. MVA mitigation is essentially an 'end-of-pipe' solution, and a far less favourable option than degasification. The CH_4 in the MVA is extremely diluted (concentrations of less than 1% are typical), making mitigation or utilisation of these emissions challenging.

[†] The analysis covered both drained CMM and MVA mitigation, and revenue from pipeline sales, electricity generation and space heating was considered. Data based on an assumed 10% discount rate and 40% tax rate was used in the construction of the MAC curves.

2.4.3.2 Utilisation of drained coal mine methane

The most appropriate use for the drained CMM will depend on the quality of the gas recovered. Because CMM recovered pre-mining is typically of a high quality and can be used interchangeably with conventional natural gas, there are number of options for its utilisation and energy recovery. Some of these were discussed in the previous chapter (§1.3.4.1), however it is worth summarising the options available in the context of CMM specifically.

Assuming an appropriate gas pipeline network exists, that there are no problems with supply continuity, and that it meets the local pipeline quality (usually 95% CH_4), the gas recovered can be supplied to the pipeline network in order to generate revenue; this would usually be the most profitable course of action (Su et al. 2005). In the US, it is estimated that 57% of the CH_4 recovered can be used directly for pipeline injection (EPA 1999).

Alternatively, the CMM can be used to generate electricity in an onsite gas fired power plant using conventional gas combustion devices such as gas turbines or internal combustion (IC) engines. The later approach was successfully demonstrated by two recent Australian projects: at BHP Billiton's Appin colliery in NSW, and Anglo Coal's German Creek mine in Queensland (CIAB 2006). The electricity generated can be either sold to the grid or used onsite to power mining processes and equipment such as conveyor belts, mining machines, desalination plants, coal preparation facilities and, in particular, ventilation fans, which have a large energy requirement. The CMM could alternatively be co-fired with coal to generate electricity (Bibler, Marshall and Pilcher 1998; CIAB 1994; Su et al. 2005).

Whilst pipeline sale or electricity generation are the most obvious energy recovery options, the CMM can also be used directly onsite to generate steam in order to heat mine facilities (EPA 2000). Other thermal uses include heating the mine ventilation air prior to circulating it through the mine[†] (EPA 2004a), and coal drying[‡] (Brenkley and Bennett 1996; EPA 1998, 2000). A factor to consider, however, is that onsite thermal uses are often seasonal, or non-continuous. The CMM could also be used to power the mine's vehicle fleet.

[†] Ventilation air is heated, especially in cold climates and during the winter months in milder climates, to increase worker comfort and productivity and reduce equipment problems.

[‡] Coal preparation usually involves drying, as reduced moisture facilitates handling, increases combustion efficiency and decreases transportation costs. Thermal dryers (such as rotary direct dryers, fluidized direct dryers, flash dryers, and indirect coal dryers), that produce a heated air stream that drives off moisture from the coal, are commonly used.

Depending on local circumstances, it could also be supplied as a fuel to adjacent industries. An example is Anglo Coal's Dawson mine (Queensland, Australia), which supplies drained CMM to an adjacent ammonium nitrate plant (CIAB 2006).

Gob gas (CMM recovered during or post-mining) on the other hand is often of a lower quality. The utilisation options are essentially the same as those above, however for pipeline injection or electricity-generation it may first be necessary to upgrade the gas using commercially available enrichment technologies. These include nitrogen removal units, dehydrators, pressure-swing adsorption, solvent absorption, cryogenics, and membrane separation (Shirley, Porto and Hawk 1996; Su et al. 2005). Enrichment of CMM drained pre-mining might also be appropriate to bring it up to pipeline quality. Enrichment requires an energy input however, which would lower both the net reduction in greenhouse gas emissions and the profit margin. For lower quality gas, direct thermal use on site might be more economic.

Alternatively, the drained CMM could simply be flared. Although this would be an effective mitigation method, and would still improve mine safety and reduce ventilation requirements, no energy would be recovered, and a potentially profitable resource would be wasted.

2.4.3.3 Mitigation and utilisation of mine ventilation air

Flaring can only be used where the concentration of CH_4 in the recovered gas is above the lean flammability limit of 5%. For MVA therefore, flaring is not a viable option, as the CH_4 concentration is too low.

Measured MVA CH_4 concentrations range from 0.1 to over 1%, but are typically between 0.3 and 0.5%. Such low concentrations are unavoidable, since effective mine ventilation is necessary for safety reasons, in order to mitigate the risk of explosion. Generally, the maximum allowable CH_4 concentrations in mine air are 1% in mine entries used by personnel, and 2% in areas less frequented by personnel. Fans ventilating active longwall panels typically reduce CH_4 concentrations to below 0.5% (CIAB 1994).

Between 4,000 and 25,000 m^3 of MVA, circulated by large fans, is released per tonne of coal extracted. Measured flow rates from individual shafts range from 47–470 m^3s^{-1} (Carothers, Schultz and Talkington 2004; EPA 2003a; Srivastava and Harpalani 2006; Su et al. 2005). In some countries, bleeder shafts are used to supplement the main ventilation shafts. The MVA from the bleeder shafts is typically characterised by slightly higher CH_4 concentrations and lower flow rates than the main shafts (Srivastava and Harpalani 2006). In Australia, the average MVA flow rate is estimated to be 225 m^3s^{-1}, and the average CH_4 concentration 0.4% (EPA 2003a).

The variation over time in both flow rate and concentration for a single shaft can also be significant. In one study, flow rates of 50–120 m^3s^{-1}, and concentrations of 0.5–0.7%, were measured from a single shaft over a two-year period (EPA 2003a). In another investigation, the maximum rate of variation in concentration was measured, and found to be 0.01% per hour (Su et al. 2005). It has been found that there is a fairly strong correlation between mining activity and the amount of CH_4 produced (Srivastava and Harpalani 2006). Furthermore, as mining advances one would expect the CH_4 concentration in the older shafts to diminish (CIAB 1994).

The large flow rates, low CH_4 concentrations, and short and long-term fluctuations in both flow rate and concentration, constitute significant challenges to the mitigation and utilisation of MVA.

The MVA must be treated at the mine site due to the large volumes of gas involved. Ideally, the mitigation system should be able to accept the entire flow from a single ventilation shaft. There must be a sufficiently large area to install the necessary equipment in the vicinity of the shaft exit. Furthermore, due to the changing location of the active ventilation shaft as the mining operation advances, the mitigation equipment should be reasonably portable. The ideal mitigation system would additionally be of rugged construction, have few moving parts and require little maintenance; and be resilient enough to cope with supply variability.

The integration of any mitigation system with the mine ventilation system must also be considered. A safe and effective interface, which does not impede on the venting of CH_4 from active mining operations, is required. One aspect of this is that either the pressure drop in the mitigation system must be low, to reduce the impact on the ventilation, or else extra fans—requiring additional energy to power them—would be needed to neutralise the additional resistance introduced.

A recent study characterising MVA flows found that the MVA contained significant levels of dust—consisting of coal fines, stone particles and ash—as well as moisture (Su et al. 2008). Particulate loading of the MVA could be a problem, particularly for mitigation systems where the MVA is substituted for the combustion air (see below). Pre-treatment might be required to eliminate coal fines; a commercial wet scrubber would be suitable for this purpose (EPA 2000).

MVA mitigation options can generally be classified as either *ancillary use* or *principal use* technologies.

Ancillary-use technologies. Ancillary-use technologies involve using the MVA as a full or partial replacement for the combustion air of a power generation process in which some other fuel acts as the primary energy source (EPA 2000; Su et al. 2005; Xiao, Sohrabi and Karim 2008). The CH_4 in the MVA acts as an ancillary energy supply. The most obvious

candidate to receive the MVA would be either a coal-fired power plant located adjacent to the mine, or a local gas-fired plant employing either turbines or IC engines running on the higher quality drained CMM (EPA 2004b). Alternatively, the MVA could be provided as the combustion air to a large fuel consumer, if one was located close to the mine (EPA 2000).

Adding the MVA to the combustion air of a coal-fired power station is technically straightforward and commercially proven, though it does increase the complexity of the process. There is no lower or upper limit on the CH_4 concentration in the MVA, although significant variations in concentration could affect stable operation. A modest air handling and transport system is required.

The applicability of this option does however depend on there being a suitable power generation facility in the proximity of the mine, limiting widespread implementation. In Australia, brown coal is used extensively at mine mouth electricity generating stations (as its low energy and high moisture content make transportation uneconomic). However, since it is extracted primarily using surface mining techniques, there is currently no practical way of recovering the CMM released by its production, which is in any case limited.

For turbines, the combustion air also performs a cooling function, and using MVA with CH_4 concentrations higher than 0.5% creates conditions where autoignition can occur in the turbine's cooling system: at elevated temperatures the CH_4 and water in the MVA react to form CO and hydrogen, which can then ignite (or cause hydrogen embrittlement). It may therefore be necessary to add additional ambient air to the process (Johnson et al. 1998).

The suitability of any given ancillary-use technology at a particular mine also relies on there being a match between the quantity of MVA produced at the mine and the combustion air requirements of the primary process. In practice, the quantity of MVA produced by a typical large underground mine *is* often well matched to the air requirements for a large coal fired power station. This is not the case for plants running on drained CMM however, which would only be capable of using a fraction of the MVA produced (Connell Wagner 2007; EPA 2000).

Principle-use technologies. Principle-use technologies involve using the MVA as the primary fuel for a process. As previously shown, the CH_4 concentration in MVA ranges from 0.1 to over 1%, but is typically 0.3–0.5%, which is below the conventional (for a free flame) lean flammability limit for CH_4 of 5% (or 4.3% for natural gas).

Conventional natural gas combustion devices such as turbines or IC engines are therefore not capable of using MVA as the primary fuel.

Figure 2.4 Pilot-scale VOCSIDIZER demonstration at Appin Colliery, NSW, Australia (Source: Danell, Nunn and Källstrand 2002).

Instead, some form of more advanced 'lean-burn' technology, capable of burning below the conventional limit—either with or without simultaneous recovery of the energy—is required. Lean-burn combustion typically involves either the use of a catalyst, which allows the CH_4 to ignite at a lower temperature; or some form of heat recuperation, whereby part or all of the energy released by the combustion reaction goes towards sustaining the reaction, rather than being recovered as useful energy from the system (Connell Wagner 2007; EPA 2000; Su et al. 2005).

Flow reversal reactors (FRR)—which can be of either the thermal (TFRR) or catalytic (CFRR) variety—were originally developed for the destruction of volatile organic compounds (VOCs), and are probably the mitigation technology closest to commercial use. They operate based on the principle of regenerative heat exchange between the MVA and a solid thermal storage medium—usually a porous ceramic bed, with the addition of a catalytic coating in the case of the CFRR—to preheat the incoming MVA and thus reduce the flammability limit of the system.

A TFRR developed by MEGTEC Systems (originally for VOC control, but adapted for use with MVA)—the 'VOCSIDIZER'—is reported to have a practical lower limit of 0.15%, and sustained operation with energy recovery is guaranteed down to 0.2% (MEGTEC 2008). A similar system developed by Biothermica Technologies—

'VAMOX'—has a reported lean limit of 0.2% (Duplessis 2009). The CFRR developed by Canadian Mineral and Energy Technologies (CANMET), has a reported lower limit of 0.1% (Litto et al. 2006; Sapoundjiev and Aubé 1999; Sapoundjiev, Aubé and Trottier 1999).

Useful energy can be extracted from FRRs by embedding heat exchanger tubes in the reactor. Either water or air can be used as the working fluid in the heat exchanger, and used to drive either a steam or gas turbine respectively. As already mentioned, energy recovery in this manner would not be possible at very low CH_4 concentrations, as all the energy released by the oxidation reaction would need to be regenerated to sustain the temperature in the reactor; as long as the oxidation process is complete, the CH_4 emissions would still be mitigated however.

A recent pilot-scale demonstration of the VOCSIDIZER at BHP Billiton's Appin colliery (NSW, Australia) (Figure 2.4) reportedly operated at CH_4 concentrations down to 0.19%—though it is not clear if operation was maintained for extended periods—with a CH_4 removal efficiency of over 97.5%. It was also reported that a large proportion of the energy in the MVA could be recovered (Danell, Nunn and Källstrand 2002; Mattus 2005).

Commercial-scale demonstrations of the VOCSIDIZER are currently being undertaken by BHP Billiton at Westcliff Colliery (NSW, Australia), and in the US by CONSOL Energy at an abandoned mine (with simulated MVA conditions) in West Virginia (CONSOL 2008; Kosmack, Winschel and Zak 2003). Also in the US, a commercial trial of the VAMOX system is currently underway at an Alabama mine owned by Jim Walter Resources (Duplessis 2009).

Various designs of lean-burn gas turbines are also under development. These include a lean-burn catalytic turbine—'VAMCAT'—developed by Australia's Commonwealth Scientific and Industrial Research Organisation (CSIRO), which has a reported minimum operating concentration of 1% CH_4. A pilot-scale VAMCAT demonstration is currently underway in China (CSIRO 2006). Other lean-burn turbines include catalytic microturbines developed by Ingersoll-Rand (minimum operating concentration 1%) and FlexEnergy (minimum operating concentration 1.3%); as well as EDL's recuperative gas turbine (minimum operating concentration 1.6%), which operates by recovering heat from the turbine exhaust gases (Carothers, Schultz and Talkington 2004; Su et al. 2005).

An alternative catalytic approach is a catalytic monolith reactor (CMR), again developed by the CSIRO, which is reported to have a minimum operating concentration of 0.4% (Su and Agnew 2006).

It has also been speculated that homogeneous charge compression ignition (HCCI) engines might be capable of operating on very lean mixtures. It has been predicted that such an engine could be designed for mixtures down to 0.3–0.7% (Connell Wagner 2007).

For any of these principle-use technologies, extracting useful energy from the process is difficult, as the fluctuating energy content of the MVA is likely to cause instability in the system. Drained CMM, or additional ambient air, could be used to even out the fluctuations. For those technologies where the minimum operating concentration is 1% or higher, supplementary fuel would almost certainly be required to sustain operation; again, higher quality drained CMM could be used for this purpose. In the case of FRRs with embedded heat exchangers, supplementary drained CMM could also be used to raise the temperature of the working fluid in the heat exchanger. However, for each technology there is a minimum MVA CH_4 concentration below which the requirements for supplementary fuel would result in more emissions being released than simply venting the MVA. It would be necessary to carry out a comprehensive energy and greenhouse gas balance for any proposed system. Any energy required to compress and redirect the MVA to the mitigation system would also need to be considered; this could potentially be higher than the inherent thermal energy content of the MVA.

Co-combustion technologies. A third approach, lying somewhere between the ancillary and principal-use options, is the co-combustion of MVA with a second low-quality 'waste' fuel such as coal mine waste, high ash or high sulphur coal, biomass or low quality gob gas. An example of a technology designed for this purpose is the rotary kiln combined with gas turbine developed by the CSIRO for hybrid waste coal-MVA combustion. A fluidised bed system might also be suitable for this sort of application (Connell Wagner 2007; Su et al. 2005; Wendt et al. 2003).

As with the ancillary-use options, availability of the necessary quantities of the second fuel to match the quantity of MVA produced is an issue. This option is particularly suited to mines, such as many in Australia, which generate a significant amount of high-ash content waste coal.

Enrichment. As with gob gas enrichment, some form of concentrator could be employed as an enabling technology to increase the CH_4 concentration in the MVA to a level at which it could be combusted in either a conventional natural gas combustion device, or in one of the lean-burn systems described above. Fluidised bed concentrators—originally developed for the concentration of VOCs prior to oxidation—would seem to be the most promising technology given the low starting concentrations involved; it has been suggested that final concentrations of 20% could be achievable, although this has not yet been proven. As previously mentioned, enrichment would however impose a negative energy cost on the overall process; this is particularly significant in the case of

MVA due to the extremely low inherent energy content of the emissions (Carothers, Schultz and Talkington 2004; Connell Wagner 2007; EPA 2003a; Su et al. 2005).

Biological treatment. Another option, still at the theoretical stage, is employing some form of biological treatment process to remove the CH_4 from the MVA. One proposal involves using the MVA as feedstock for the production of single-celled, methane-consuming proteins, the idea being that the protein would then be used as an animal feed supplement or as a feedstock for methanol production (Connell Wagner 2007). A bio-filter incorporating methanotrophic bacteria has also been suggested (Sly et al. 1993). It is unclear how well biological systems would handle the large flow rates characteristic of MVA however.

Greenhouses. Because MVA is also rich in CO_2 (2,000–3,000 ppm compared to atmospheric concentrations of 300–400 ppm) it has been suggested that it could be used in greenhouses located at the mine to stimulate plant growth. Also, MVA remains at a fairly constant temperature year-round, which could help maintain consistent greenhouse temperatures. Another benefit of locating greenhouses near mines is that, where the water quality is suitable, the mine wastewater could be used for irrigation (EPA 1997).

Utilisation of low-grade heat. Where the MVA emissions are of such a low CH_4 concentration that they cannot be used for electricity generation without excessive need for supplementary fuel, a supply of low-grade heat is still likely to be available from the combustion process. A possible mine site use for this 'waste' heat would be the heating of the MVA prior to circulation through the mine, as previously discussed in the context of drained CMM. Low-grade heat from the combustion of MVA could be used to heat the 'fresh' MVA directly (rather than by firing heaters in the ventilation duct) (EPA 2004a). Alternatively, the heated exhaust stream resulting from MVA combustion could be used directly for coal drying. A final option would be to use the supply of low-grade heat for the desalination of mine wastewater (Gude and Nirmalakhandan 2008).

A useful database, containing information on many of the mitigation technologies mentioned above, including commercial information and contacts, is available from the Methane to Markets partnership (Methane to Markets n.d.).

2.4.4 Mitigation options for surface mines

For surface mining, the only feasible mitigation approach would seem to be pre-mine drainage, using a degasification system similar to those employed at underground mines (EPA 2008). The utilisation options for the recovered gas would then be the same as those previously discussed for CMM drained from underground mines (§2.4.3.2).

2.4.5 Mitigation options for decommissioned mines

Emissions from decommissioned mines can be reduced by inhibiting flow; sealing pathways where CH_4 has been detected or is likely to be emitted (although this option is usually rejected on safety grounds); restricting flow from vents; and flooding the CH_4 producing areas of the mine (DTI 2004). Alternatively, as for working mines, efforts can be made to recover and use the CH_4. The most appropriate technology will depend primarily on the CH_4 concentration. This can range from under 1% to over 90%, and may be intermittent. Where the CH_4 concentration of the emissions is low, the various MVA mitigation technologies described in the previous section could potentially be applied to these emissions. Currently, the gas is typically flared when the concentration is above 5%, or released directly to the atmosphere where not.

2.4.6 Recovery of methane from non-mineable coal seams

Extraction of CBM from non-mineable virgin coal seams is also possible. Strictly speaking this cannot be classed as mitigation, as most of the CH_4 would never otherwise be released. Enhanced coal bed methane (ECBM) recovery involves sweeping the coal seam with CO_2. The CO_2 preferentially adsorbs in the pores of the coal, and the CH_4 is displaced, thus allowing the CH_4 to be recovered whilst simultaneously sequestering the CO_2 (Evans 2007; White et al. 2005). The gas produced is of a high quality, as with CMM drained pre-mining. A negative environmental impact associated with CBM recovery is the need to dispose of the large quantity of saline water that is co-located with the gas (Tillman and Harding 2004). This is a rapidly expanding industry however: CBM, like coal, is more widely distributed than conventional natural gas deposits, reducing transportation needs and increasing energy security (Evans 2007).

2.4.7 Implementation of mitigation measures

The barriers that prevent CMM mitigation measures from being adopted, and the means of overcoming these, are essentially the same as those described in the previous chapter for CH_4 mitigation generally (§1.3.5).

Historically, as previously mentioned, CH_4 has been viewed as a hazard, rather than as a resource. Current barriers to CMM use include lack of an appropriate policy framework; limited capital for investment in mitigation projects; the need for additional information and experience with technologies; and access to appropriate technologies. Many coal mines are situated in remote locations, so lack of a widespread pipeline network may also be an issue. For fugitive emissions from surface mines and post-mining activities especially, measuring and quantifying the emissions is difficult (Bibler, Marshall and Pilcher 1998; CIAB 1994; Methane to Markets 2006).

Access to appropriate technologies is an issue for the mitigation of MVA emissions in particular. The large flow rates, low CH_4 concentrations, and short and long-term fluctuations in both flow rate and concentration, constitute significant technical challenges to combustion of MVA. A number of technologies have been proposed, the closest to commercial use being flow reversal reactors, however a cost-effective, widely applicable solution has yet to be proven.

Also of concern in some regions are unresolved legal issues over ownership where the CH_4 is considered a resource. Previously, for example, the owners of the land, the coal, the oil and gas, and other minerals in an area have all asserted ownership of the CBM in that area (Gunning 2005; EPA 2008).

2.5 Conclusions

Much current analysis of coal's environmental performance focuses on combustion-related CO_2 emissions, however greenhouse gas emissions and other environmental impacts throughout the coal cycle should also be considered. A recent survey of coal industry attitudes towards sustainable development found that there is widespread support for reducing the environmental impacts of coal within a context of providing secure and low cost energy supply; including the development and use of new technologies that reduce greenhouse gas and other emissions from coal production and use (CIAB 2003). A comprehensive clean coal strategy for the future would address the issue of CH_4 emissions from coal mining, and their mitigation.

Sixty years ago, an official at the then UK Ministry of Fuel and Power suggested that the CH_4 occurring in small percentages in the ventilating upcasts from mines was sufficient—if it could be converted into useful energy—to run all the colliery machinery in Britain (Burgoyne and Hirsch 1954; Roxbee Cox 1951). More recently, an economic analysis by the US Environmental Protection Agency concluded: "large-scale ventilation air methane use offers a low-cost opportunity to reduce greenhouse gas emissions" (EPA 2003a).

The development—and commercialisation—of lean-burn combustion technologies capable of combusting MVA, and if possible, recovering useful energy from the process, is a key area where further work is still required.

Porous burners are a lean-burn combustion technology that has thus far not been investigated in the context of the mitigation of CH_4 emissions. In the following chapter, the use of porous burners for lean-burn applications will be reviewed.

Chapter 3

POROUS BURNERS FOR LEAN-BURN APPLICATIONS

3.1 Introduction

Porous burners are a potential lean-burn technology for the combustion of very low-calorific value fuels, such as certain methane emissions, that might otherwise not be flammable. In a porous burner a fuel/air mixture burns within the cavities of a solid porous matrix, rather than as a free flame at the burner exit, as is the case with conventional gas burners. The porous matrix serves as a means of recirculating heat from the hot combustion products to the incoming reactants, leading to higher flame speeds and extended flammability limits.

Porous burners are already commercially available (GoGas n.d.; Promeos n.d.). They find application in fields including space and water heating, metal heat-treating, coating and paint drying, glass and chemical processing, paper and wood drying, and food processing (Mößbauer, Pickenäcker and Trimis 1999; Rumminger 1996; von Issendorff et al. 2005). Since as early as the late 19th century (Trimis, Pickenäcker and Wawrzinek 2005), and particularly over the last three decades, combustion in porous media has been the subject of a significant amount of research and development, with a number of useful reviews published on the topic (Durst and Trimis 2002; Howell, Hall and Ellzey 1996; Kamal and Mohamad 2006a; Mohamad 2005; Mößbauer, Pickenäcker and Trimis 1999; Mujeebu et al. 2009b; Mujeebu et al. 2009c; Oliveira and Kaviany 2001; Pantangi and Mishra 2006; Trimis and Durst 1996; Trimis, Pickenäcker and Wawrzinek 2005; Viskanta 2005; Viskanta and Gore 2000).

The combustion of very low-calorific value fuels using porous burners, however, is a relatively unexplored field, though recent developments in this area include the investigation of the possibility of using porous burners to combust landfill gas, low-calorific syngas from waste pyrolysis, biogas and the anode off-gas from solid oxide fuel cells (Al-Hamamre et al. 2006; Voß, Al-Hamamre and Trimis 2007a,b). The use of

the technology specifically for lean-burn applications has yet to be demonstrated beyond the laboratory and pilot-scale.

This chapter reviews lean methane (CH_4) combustion in porous burners. Aspects of burner design and performance of practical significance to lean-burn applications, rather than the fundamental mechanisms of the combustion process, will be emphasised. Of particular interest is what may be described as 'ultra-lean' combustion, where the CH_4 concentration is at or below the lean flammability limit for a free flame (5% CH_4 by volume in air (Perry and Green 1997)).

The use of alternative fuels such as LPG (Bakry 2008; Liu and Hsieh 2004), hydrogen (H_2) (Saveliev et al. 1996; Voß et al. 2008), hydrogen sulphide (Bingue et al. 2002b) and syngas (Alavandi and Agrawal 2008; Gauthier, Lebas and Baillis 2007; Mendes, Pereira and Pereira 2008), liquid fuels such as heptane (Dixon et al. 2008; Kaplan and Hall 1995; Tseng and Howell 1996), iso-octane (Zhao, Wang and Xie 2009) kerosene (Jugjai and Phothiya 2007; Jugjai and Polmart 2003; Jugjai and Pongsai 2007; Jugjai et al. 2002; Newburn and Agrawal 2007; Sadasivani and Agrawal 2009; Takami et al. 1998; Vijaykant and Agrawal 2007), ethanol (Fuse, Kobayashi and Hasatani 2005), methanol (Pedersen-Mjaanes, Chan and Mastorakos 2005), vegetable oils (Bakry et al. 2000) and petrol (Pedersen-Mjaanes, Chan and Mastorakos 2005), or suspended solid particles such as coal dust (Kayal and Chakravarty 2007), will not be covered, but have all been the subjects of recent research; a review of liquid fuel combustion in porous burners is provided by Mujeebu et al. (2009). Neither will oxy-fuel combustion (Kesting et al. 1999; Qiu and Hayden 2009) be considered, nor the use of porous media reactors for processes such as syngas (Dixon et al. 2008; Drayton et al. 1998), hydrogen (Al-Hamamre, Voß and Trimis 2007, 2009; Bingue et al. 2002a; Bingue, Saveliev and Kennedy 2004; Dhamrat and Ellzey 2006; Dobrego et al. 2008b,c; Fay, Dhamrat and Ellzey 2005; Hall and Peroutka 1995; Pedersen-Mjaanes, Chan and Mastorakos 2005; Slimane et al. 2004; Toledo et al. 2009) or hydrochloric acid (HCl) (Wawrzinek et al. 2001) production, nitrogen oxide (NO_X) reburning (Afsharvahid, Ashman and Dally 2008; Bingue et al. 2007), or the destruction of volatile organic compounds (VOCs) (Bartz, Moreno and Duggan 1992; Gnesdilov et al. 2006). Additionally, the scope of this review will be limited to homogeneous combustion in inert porous media—research relating to catalytic combustion, or indeed systems involving the combustion of the porous bed itself, will not be included.

The structure of this chapter is as follows: First, the basic principles governing combustion in a porous medium will be explained, and the common characteristics of porous burners summarised. Second, specific examples of burner performance previously reported in the literature will be provided. Third, issues relating to porous material selection and other aspects of burner design will be explored. Finally, the

current status of research in the field will be reviewed, and some potential topics for future work identified.

3.2 Burner operating principles

3.2.1 Excess enthalpy combustion

For a laminar premixed flame the adiabatic flame temperature can be defined as the theoretical temperature obtained if all the heat released by the reaction is used to raise the temperature of the combustion products (Glassman 1996). It is therefore solely dependent on the initial reactant composition, in other words on the heating value of the fuel and the fuel/air ratio. However, if a means can be found of recirculating heat from the hot combustion products to the cold reactants, whilst at the same time avoiding dilution of the reactants with the products, it is theoretically possible to obtain flame temperatures in excess of the adiabatic flame temperature of the initial fuel/air mixture (Weinberg 1971).

The term 'excess enthalpy' burning is used to describe this process of 'borrowing' enthalpy from the combustion products to preheat the incoming reactants (Babkin, Wierzba and Karim 2003; Hardesty and Weinberg 1974). As it is characterised by flame temperatures and burning velocities greater than the corresponding adiabatic flame temperature and laminar burning velocity, it is also commonly referred to as 'super-adiabatic' combustion. The expression 'thermally stabilised' combustion is also appropriate (Churchill 1989).

The flammability limits for a fuel/air mixture are defined as the fuel concentrations within which a self-sustaining flame can form (Glassman 1996). Because the lean flammability limit of a fuel/air mixture decreases as the initial temperature of the mixture increases according to the Burgess-Wheeler law (Zabetakis 1965), excess enthalpy burning can lead to a reduction in this lower limit. Hardesty and Weinberg (1974) describe an idealised thermodynamic model of excess enthalpy burning and show that in moving towards the combustion of increasingly lean mixtures, heat losses from the system will become controlling, ultimately determining the lean limit that can be achieved.

Weinberg and colleagues suggested a number of schemes for the practical realisation of excess enthalpy burning in heat recirculating combustors involving various configurations of heat exchanger tubing surrounding the combustion chamber. Two of these are illustrated in Figure 3.1. In experiments using the 'double spiral' burner, they reported stable combustion for CH_4 concentrations as low as 1.6% (Hardesty and Weinberg 1974; Jones, Lloyd and Weinberg 1978; Lloyd and Weinberg 1974).

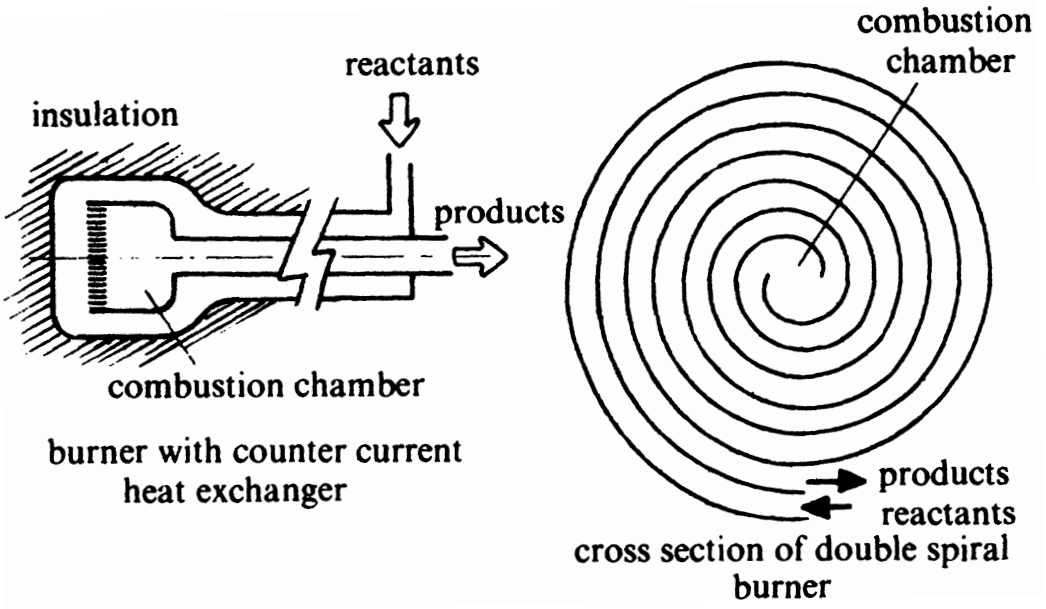

Figure 3.1 Examples of heat recirculating burners (Source: Jones, Lloyd and Weinberg 1978).

3.2.2 Combustion in a porous medium

An alternative means of achieving excess enthalpy combustion is to insert a porous solid with superior heat transfer properties into the combustion chamber. This provides a means of recirculating the heat *internally*. Rather than having an external heat exchanger surrounding the combustion chamber, the combustion takes place within the heat exchanger itself. This idea forms the basis of porous burner operation.

The concept was first demonstrated analytically by Takeno and Sato (1979). Subsequent investigations by Takeno and colleagues at the University of Tokyo confirmed their predictions experimentally (Kotani, Behbahani and Takeno 1984; Kotani and Takeno 1982). Using a burner combining both a combustion chamber containing a porous medium and an arrangement of heat exchanger tubes surrounding it, they were able to sustain combustion at flow velocities higher than could be attributed to the burning velocity of the externally preheated gases alone—the difference was credited to the contribution of the internal heat recirculation provided by the porous solid.

3.2.2.1 Heat recirculation

Heat recirculation in a porous medium involves a combination of all three modes of heat transfer—conduction, convection and radiation, as identified in Figures 3.2 and 3.3a. The process can be summarised as follows: Downstream of the reaction zone, the gas is hotter than the solid, and so heat is transferred convectively from the hot combustion products to the porous matrix; the hot solid conducts and radiates heat in the upstream direction; upstream of the reaction zone, the temperature of the solid

exceeds that of the gas, and so there is solid-to-gas convective heat transfer. The incoming gases are thus preheated until they reach the ignition temperature, reaction takes place, and the cycle continues.

The resulting temperature profiles for the solid and gas are shown in Figures 3.3b and 3.4. The profiles shown in Figure 3.4 were obtained using a 1-dimensional model containing full chemistry and accounting for the effects of solid and gas conduction, solid-to-solid radiation and convective heat transfer between solid and gas (Barra and Ellzey 2004). The preheating effect is clearly indicated, and it can be seen that although the reaction zone itself—indicated by the peak in the heat release rate—is similar in width to that for a premixed laminar flame, the 'preheat zone'—beginning where the gas temperature has increased by 1% of its original inlet value, and ending where the gas and solid temperatures are equal—is much wider.

Heat recirculation efficiency can be defined as the amount of solid-to-gas convection in the preheat zone compared with the firing rate. Based on this definition, Barra and Ellzey (2004) predicted efficiencies of up to 25% (for the particular burner configuration modelled). Additionally, it was found that the heat recirculation efficiency increases as the equivalence ratio (ϕ) decreases. The relative contributions of conduction and radiation to the recirculation process were also examined. It was found that at the lowest equivalence ratio investigated ($\phi = 0.55$), conduction is more important at lower flow velocities and vice versa at higher velocities. As the equivalence ratio (and hence temperature) increases, radiation becomes the dominant mechanism.

These findings corroborate those of an earlier study by Min and Shin (1991) using a 1-dimensional model that considered all three modes of heat transfer but modelled the combustion as a single-step irreversible reaction. It predicted that 28% of the total heat released would be recirculated to the incoming reactants, and that the contributions of conduction and radiation would be equivalent in magnitude (at $\phi = 0.55$).

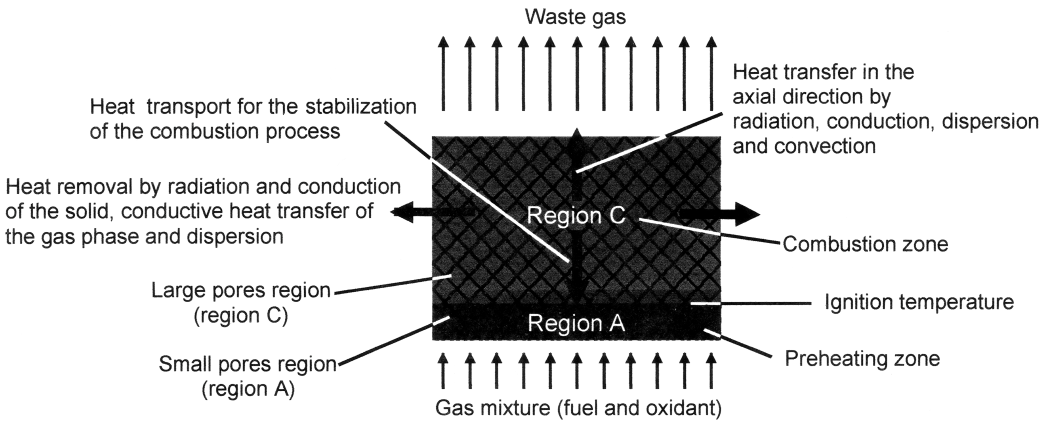

Figure 3.2 Heat transfer processes in a porous burner (Source: Durst and Trimis 2002).

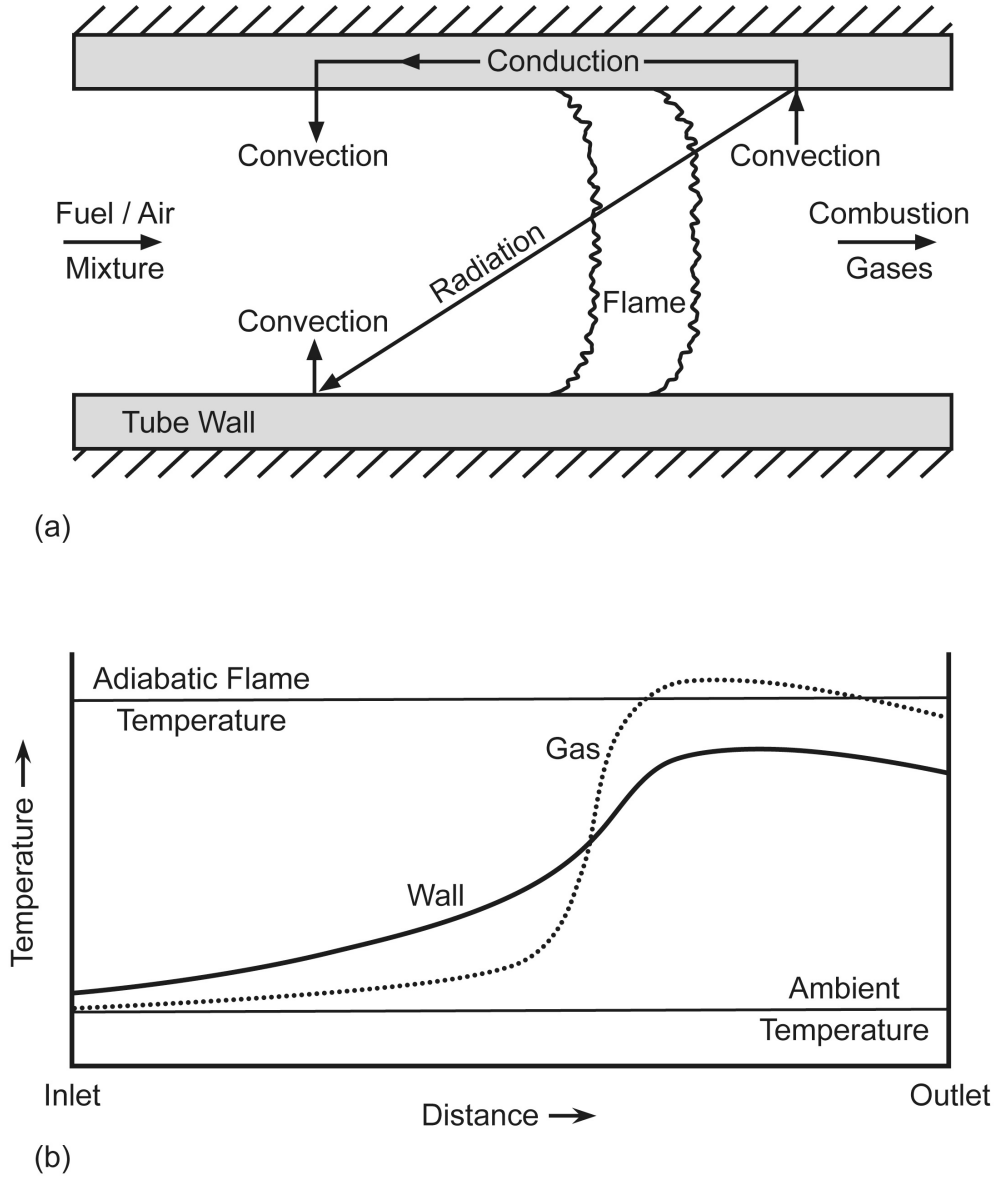

Figure 3.3 (a) Schematic representation of heat recirculation in a porous medium idealised as an insulated refractory tube and (b) the corresponding variation in gas and tube wall temperature with distance (Source: adapted from Viskanta and Gore 2000).

The degree of heat recirculation, and the role played by each of the heat transfer mechanisms, will obviously be highly dependent on the properties of the actual porous material being considered. The two previous examples modelled burners made of partially stabilised zirconia (PSZ) foam and a honeycomb ceramic respectively. The influence of porous material is discussed in more detail in §3.4.1.

If a porous material that promotes effective heat recirculation is selected, excess enthalpy or super-adiabatic combustion in the porous medium can be realised.

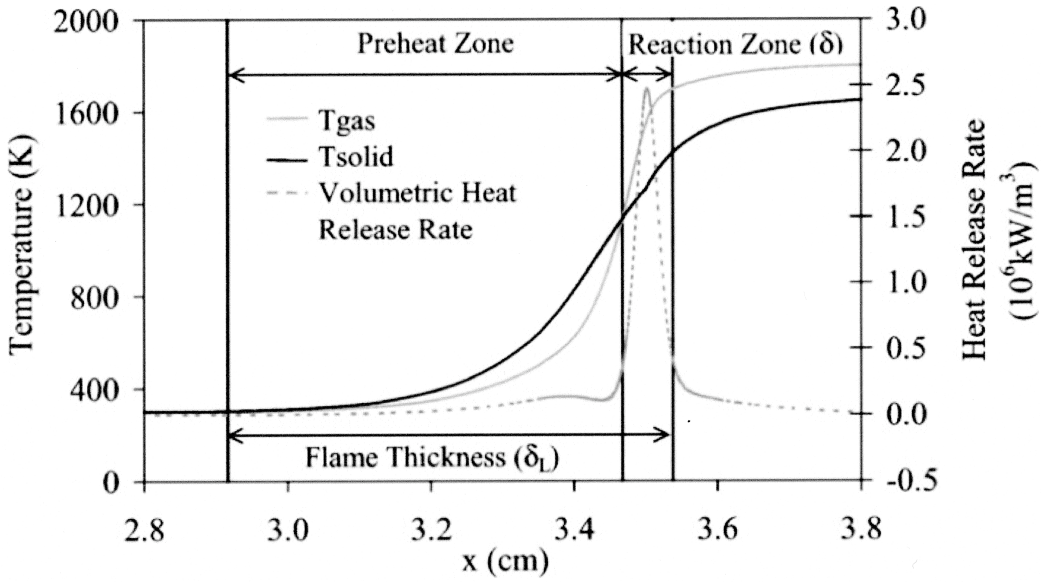

Figure 3.4 Illustration of preheating in a two-section PSZ porous burner (at ϕ = 0.65 and a flow velocity of 60 cms^{-1}) demonstrating the existence of an enlarged preheat zone (Source: Barra and Ellzey 2004).

Peak temperatures greater than the adiabatic flame temperature, as well as flame speeds higher than the associated laminar flame speed for the mixture, have been observed or predicted by several researchers (Barra and Ellzey 2004; Hanamura and Echigo 1991; Hsu, Evans and Howell 1993; Hsu, Howell and Matthews 1993; Khanna, Goel and Ellzey 1994; Kulkarni and Peck 1996; Mathis and Ellzey 2003; Vogel and Ellzey 2005).

For example, Figure 3.5 shows the predictions of Hsu, Howell and Matthews (1993) obtained using a 1-dimensional model of a PSZ burner including full chemistry, separate energy equations for the gas and solid phases, and radiative, conductive and convective heat transfer. From Figure 3.5a, which shows peak temperatures, it can be seen that super-adiabatic combustion is predicted over a wide range of equivalence ratios, with the effect becoming more pronounced for leaner mixtures. Flame speeds in excess of the laminar flame speed are also calculated (Figure 3.5b). In addition, the presence of the porous medium is predicted to extend the lean flammability limit (to ϕ = 0.36 for this particular case).

3.2.2.2 Flame stabilisation

In order to stabilise the combustion process within the porous medium a balance must be achieved between heat recirculation, heat release and heat losses, such that the effective flame speed is equal to the incoming velocity. When the flow velocity is greater than the flame speed the flame will propagate downstream and vice versa (§3.2.2.3).

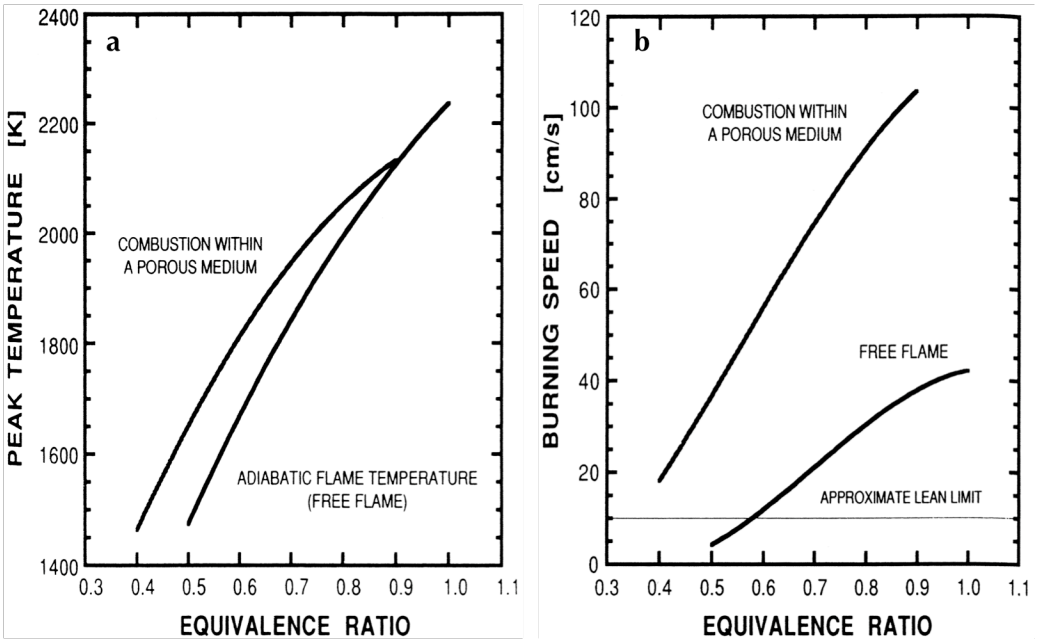

Figure 3.5 Predicted (a) peak flame temperatures and (b) burning speed and flammability limits, for combustion in a porous medium in comparison with a freely propagating, adiabatic, laminar flame (Source: Hsu, Howell and Matthews 1993).

This study is concerned only with combustion that is actually stabilised *within* the porous medium (sometimes referred to as an 'embedded' or 'submerged' flame). The related phenomenon of surface combustion, whereby the flame is stabilised at or just above the surface of a porous bed, will not be considered. This has been the subject of much previous research, for example by Golombok, Prothero and Shirvill (1991), Itaya et al. (1992) and Kawaguchi et al. (1990). The Combustion Technology group at the University of Eindhoven have also published a useful series of studies on this topic (Bouma and de Goey 1996, 1999; Bouma, Eggels and de Goey 1995; Bouma et al. 1995a,b; Schreel, van den Tillaart and de Goey 2005). More recently, Marbach, Sadasivuni and Agrawal (2007) studied surface combustion in a meso-scale system.

It is difficult to predict a priori whether or not stable combustion will be achieved in a particular porous burner for a given fuel/air mixture, and, moreover, if stable combustion is achieved, at what position in the porous bed the flame will actually be located. Nonetheless, an intuitive explanation of the flame stabilisation process in general terms is offered by Buckmaster and Takeno (1981): When a change occurs in the inlet conditions such that the flame moves downstream, for example if the flow velocity is increased, then if this movement causes an increase in the flame speed, the flame will eventually reach a location where the flame speed again matches the flow velocity, and it will stabilise in that new location. In other words, on a plot of flame speed against flame location, the flame can be stabilised at those locations where there is a positive gradient.

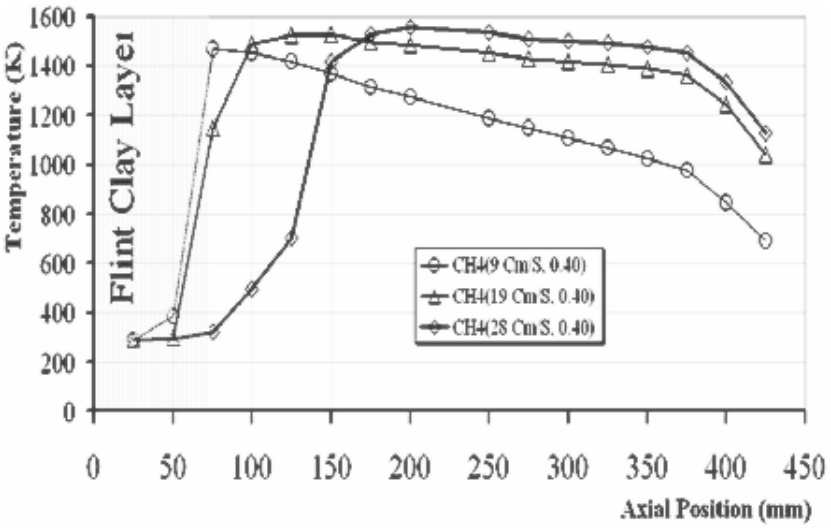

Figure 3.6 Temperature profiles for a range of flow velocities at ϕ = 0.4 (Source: Afsharvahid, Dally and Christo 2003b).

The requisite increase in flame speed will occur due to the incoming gases being preheated more effectively. As a general rule, in the upstream region of the porous bed the amount of preheating will increase as the flame moves downstream (as less heat will be lost from the upstream end of the burner). It would therefore be expected that stable combustion is likely to occur in this region.

This behaviour is predicted by a number of modelling studies (Afsharvahid, Dally and Christo 2003a; Sathe, Peck and Tong 1990; Takeno and Sato 1979) and has been confirmed experimentally in investigations using a variety of burner configurations (Afsharvahid, Dally and Christo 2003b; Hsu, Evans and Howell 1993; Kotani, Behbahani and Takeno 1984; Mathis and Ellzey 2003; Min and Shin 1991; Mital, Gore and Viskanta 1997; Sathe et al. 1990; Smucker and Ellzey 2004). To give an example, Figure 3.6 shows the results obtained by Afsharvahid, Dally and Christo (2003b) using a burner with a porous bed of alumina (Al_2O_3) spheres for a series of flow velocities at an equivalence ratio of 0.4.

Likewise, a decrease in fuel concentration is predicted to cause the flame to move downstream (Afsharvahid, Dally and Christo 2003a; Malico and Pereira 1999). Decreasing the equivalence ratio will result in a corresponding decrease in the flame speed. The flame must move to a new downstream location in order for the flame speed to increase so that it once more matches the flow velocity. Again, this prediction is supported by a number of experimental studies (Kotani, Behbahani and Takeno 1984; Kulkarni and Peck 1996; Afsharvahid, Dally and Christo 2003b).

In this way, the large heat capacity of the porous bed means that it is possible to stabilise combustion over a range of flow rates and fuel concentrations. Consequently,

porous burners are characterised by extended operating ranges and large turndown ratios. As an additional means of stabilising the flame, over a still wider range of conditions, a number of porous burners employ a two-section design. Different porous materials are used in the upstream and downstream regions of the burner—a small-pored material in the upstream, and a large-pored material in the downstream section—with the flame stabilising in the downstream section at or near the interface. This concept is examined in more detail in §3.4.2.

By the same principles, it might be expected that the combustion process would be stable against *short-term* fluctuations in the flow and concentration. This was recognised in the analysis of Takeno and Sato (1979): if the flow rate increases momentarily, the flame will move downstream; the resulting increase in preheating will increase the flame speed and bring it back to its original position. This is a topic that has not yet been explored fully: most studies, both experimental and numerical, investigate only steady-state behaviour.

Henneke and Ellzey (1997) did however examine the response of porous burners to changes in fuel flow rate. Specifically, they investigated the behaviour of the burner when the fuel supply was completely interrupted (although cold air continued to flow through the hot bed) and then re-introduced, to determine if the mixture would reignite. They used a 1-dimensional model including full chemistry plus conductive, radiative and convective heat transfer and performed transient simulations at an equivalence ratio of 0.7. They found that there is a 'critical cooling time' which is the longest time for which reignition is still possible. If the fuel is reintroduced within this time the mixture will reignite at the downstream end of the porous bed and the flame will then propagate upstream. Their simulations predicted a wide variation in critical cooling times ranging from approximately 10 to as much as 850 times the residence time of the gas in the porous bed (between 1 and 69 seconds for the system considered): it was found that porous materials with lower porosities and higher heat capacities allowed the fuel supply to be interrupted for longer.

3.2.2.3 Transient combustion

This review is concerned primarily with stationary combustion systems, where for a given set of conditions (flow velocity and equivalence ratio) the flame is stabilised within the porous medium, as described above. However, transient combustion (also commonly referred to as 'filtration' combustion) systems, based on a combustion wave propagating through the porous medium, have also been examined in numerous studies (Aldushin 1993; Babkin et al. 1983; Babkin, Korzhavin and Bunev 1991; Bingue et al. 2002c; Contarin et al. 2003, 2005; Chumakov and Knyazeva 2009; di Mare et al. 2000; Dobrego, Kozlov and Bubnovich 2003; Dobrego et al. 2005, 2008a; Du and Xie

2006; Fouteko et al. 1996; Hanamura, Echigo and Zhdanok 1993; Henneke and Ellzey 1999; Hoffmann et al. 1997; Jugjai and Chuenchit 2001; Jugjai and Nungniyom 2009; Kakutkina, Korzhavin and Mbarawa 2006; Kennedy et al. 2000, 2002; Kennedy, Fridman and Saveliev 1995; Korzhavin et al. 1982; Mbarawa, Kakutkina and Korzhavin 2007; Xie et al. 2009; Yang et al. 2009; Zhang et al. 2006; Zhdanok, Kennedy and Koester 1995). A great deal of research in this area was also carried out in Russia during the 1970s and 80s, and a selection of this early work is reviewed by Babkin and colleagues (Babkin 1993; Babkin and Laevskii 1987).

Researchers in the field of filtration combustion have identified a number of distinct combustion regimes based on the speed at which the combustion wave propagates through the porous medium. Of interest here is what is classified as the low-velocity regime, where the velocity of the combustion wave is typically under 1 mms^{-1}: it is only for this case that there is significant heat transfer between the gas and solid (Babkin 1993).

As with a stable flame, this heat transfer will lead to heat being recirculated from the hot combustion products back to the cold reactants via the solid, resulting in super-adiabatic combustion. However, in transient combustion systems there is additional complexity, because the displacement of the combustion zone relative to the solid means that the super-adiabatic effect can be either enhanced or inhibited, depending on whether the combustion wave is travelling with ('co-flow') or against ('counter-flow') the flow of the incoming gas: in the case of co-flow, there will be additional heat transfer from solid to gas upstream of the reaction zone, and the super-adiabatic effect will be enhanced (Babkin and Laevskii 1987).

The direction of propagation of the combustion wave in a given system depends on both the flow velocity and the equivalence ratio. Under ultra-lean conditions, co-flow of the combustion wave is observed, leading to a pronounced super-adiabatic effect. For higher equivalence ratios approaching the normal lean limit ($\phi = 0.5$), co-flow occurs at low flow velocities; as the flow velocity is increased the velocity of the combustion wave also increases through a maximum before falling to zero—in other words the flame is stabilised—and finally reverses direction and propagates against the flow of the incoming gas (Babkin and Laevskii 1987; Henneke and Ellzey 1999; Laevskii and Babkin 2008; Mbarawa, Kakutkina and Korzhavin 2007; Yang et al. 2009).

Transient combustion is significant for many lean-burn applications and in particular offers advantages where the energy content of the fuel is extremely low. As the transient regime can potentially provide more effective heat recirculation than a stabilised flame, a greater extension of the lean flammability limit should be possible.

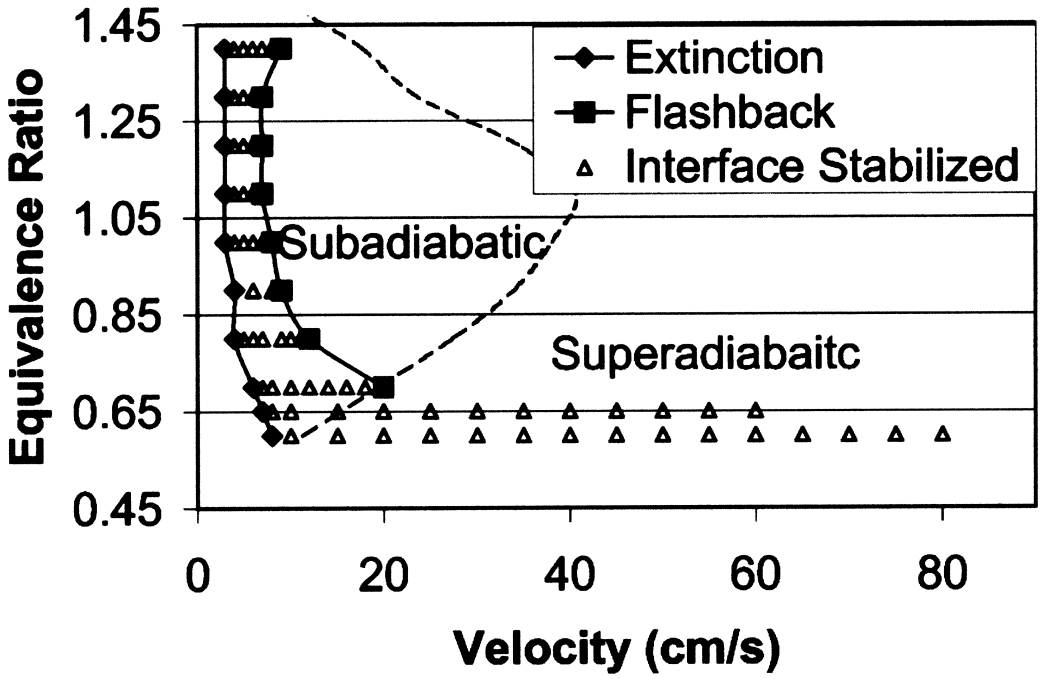

Figure 3.7 Stable operating range for a two-section FeCrAlY burner showing the existence of both sub- and super-adiabatic modes of operation (Source: Vogel and Ellzey 2005).

The challenge lies in exploiting the desirable features of transient combustion in a practical system where the combustion wave must be restricted to within the confines of a burner.

3.2.2.4 Sub-adiabatic combustion

So far, excess enthalpy or super-adiabatic combustion in a porous medium has been considered, as this is the means by which the lean flammability limit may be extended and ultra-lean combustion achieved. However, if the balance between heat release, recirculation and loss is altered such that the contribution of the recirculation component is decreased (and by implication that of heat loss increased), then a sub-adiabatic combustion regime may be observed. Heat 'lost' in this context means heat that is not recirculated to preheat the incoming reactants: in a practical burner this heat may actually be usefully recovered from the system to heat some load, either via the thermal energy of the exhaust gases or radiant heating from the porous solid (§3.4.4).

It was shown previously that a flame might be expected to stabilise within the upstream half of a porous burner. However at low velocities below the laminar flame speed, a second stable burning region at or near the downstream surface of the burner is also predicted (Min and Shin 1991; Hanamura and Echigo 1991). The regime that is observed will be strongly dependent on burner design. Most studies examine either one or the other of the sub- or super-adiabatic flame speed regimes. As a general observation, porous radiant burners, being designed to maximise radiant heating (that is heat 'loss')

from the downstream surface, typically have a relatively thin porous bed of only a few centimetres in depth, operate on fuel/air mixtures closer to stoichiometric (high temperatures being required to increase radiant output), and are characterised by sub-adiabatic flame speeds (Mital, Gore and Viskanta 1997; Rumminger et al. 1996; Viskanta and Gore 2000).

However, it is also possible to observe both super- and sub-adiabatic flame speeds in a single burner. Vogel and Ellzey (2005) investigated a two-section burner made of FeCrAlY metal foam. At equivalence ratios of 0.65 and below, stable combustion both above and below the laminar flame speed was observed; at higher equivalence ratios the burner could be operated in the sub-adiabatic mode only, as illustrated by Figure 3.7.

In the case of transient systems, sub-adiabatic combustion is obtained when the combustion wave propagates against the direction of flow (Henneke and Ellzey 1999).

3.2.2.5 Emissions

A further consequence of the recirculation of heat away from the hot combustion products is that the subsequent decrease in temperature in this region inhibits the formation of NO_X. NO_X may be formed either by the thermal ('Zeldovich') or prompt ('Fenimore') mechanism (Miller and Bowman 1989). For conditions typical of porous burners, NO formed via the thermal route, which is highly temperature dependent, constitutes the majority of NO_X emissions (Lim and Matthews 1993). Because NO_X formation is dependent on the peak temperature, NO_X emissions are observed to decrease with decreasing equivalence ratio (Delalic, Mulahasanovic and Ganic 2004; Durst and Trimis 2002; Khanna, Goel and Ellzey 1994; Mathis and Ellzey 2003; Mital, Gore and Viskanta 1997; Smucker and Ellzey 2004). The effect of flow velocity on NO_X emissions is less clear, but Durst and Trimis (2002) and Khanna, Goel and Ellzey (1994) found that NO_X emissions are relatively insensitive to flow rate. This is attributed to the fact that although reducing the flow velocity reduces the peak temperature, this is compensated for by an increased residence time in the flame zone. It should be mentioned that because emissions are typically very low (less than 30 ppm), any variations are likely to be within the calculated error of the measurements (Smucker and Ellzey 2004), making the identification of clear trends difficult.

Conversely, reduced temperatures in the combustion zone might be predicted to lead to increased emissions of the products of incomplete combustion: carbon monoxide (CO) and unburned hydrocarbons (UHC). The use of lean mixtures, however, means that this is not the case. A number of investigations find that CO emissions tend to be very low (less than 40 ppm) and that they decrease with decreasing equivalence ratio but increase with increasing flow velocity (as there will be less time for the CO formed in

the reaction zone to be oxidised to carbon dioxide (CO_2) before exiting from the burner) (Khanna, Goel and Ellzey 1994; Mathis and Ellzey 2003; Mital, Gore and Viskanta 1997; Smucker and Ellzey 2004). Khanna, Goel and Ellzey (1994) also observed that for very low flow velocities, at equivalence ratios of 0.65 or less, there is an increase in CO emissions. This is due to the low temperatures obtained under these conditions suppressing the oxidation of CO to CO_2.

Emissions of UHC from porous burners also tend to be negligible (less than 5 ppm) and, in so much as any dependencies on flow rate and fuel concentrations can be reliably identified, they follow the same trends as for CO (Mathis and Ellzey 2003; Mital, Gore and Viskanta 1997; Smucker and Ellzey 2004).

Finally, in order to minimise emissions, a homogeneous temperature distribution within the burner is desirable. Hot spots in the porous matrix can lead to an increase in the formation of NO_X, whereas cold spots might result in incomplete combustion and a subsequent increase in CO and UHC emissions (Durst and Trimis 2002).

3.3 Examples of burner performance

Much of the early experimental work on porous burners focused on their use as radiant burners, (typically operating in the sub-adiabatic combustion regime), and consequently on measuring and optimising radiant output and efficiency. Howell, Hall and Ellzey (1996) review some of this work; see also Khanna, Goel and Ellzey (1994), Mital, Gore and Viskanta (1997), Qiu and Hayden (2006) and Rumminger (1996) for some recent examples. Radiant efficiencies reported cover a wide range of values up to 40%. It is likely that the large variation in the reported efficiencies is due to the lack of a standard procedure for measuring radiant output (Leonardi, Viskanta and Gore 2002; Mital, Gore and Viskanta 1998) as well as to differences in burner design and operating conditions.

Of more concern here are those studies that tell us something about the burner's stable operating range. That is, over what range of flow rates and fuel concentrations can stable and complete combustion can be sustained? And in particular, what are the conditions, and how does the burner behave, at or near the lean limit?

Outside of the stable operating range the flame will experience either *blowoff* (the flame propagates downstream because the inlet velocity is greater than the flame speed and eventually 'blows off' the top of the burner), *flashback* (essentially the opposite situation), or, in the case of very lean mixtures, *extinction* (because the temperature in the burner is not sufficient for the flame to sustain itself). In practice, some of these concepts are not so clearly defined: For example, blowoff can occur gradually, with the flame starting to blow off at one location on the burner surface while still being

stabilised at other locations (Smucker and Ellzey 2004; Wharton, Ellzey and Bogard 2005). Or, where multi-section burner designs (§3.4.2) are used, with a 'preheating' section upstream of the main combustion section, the undesirable occurrence of the flame stabilising within the preheating section (rather than leaving the burner altogether) is often considered to be flashback.

Commonly the operating range of a porous burner is illustrated by a 'stability diagram' or 'burner map' (e.g. Figure 3.7), which plots either firing rate or velocity against equivalence ratio. These show the stable burning region, as well as indicating those regions where blowoff, flashback or extinction occur. Alternatively, the burner's performance may be more simply specified in terms of its thermal power or load (kW), firing rate (kWm^{-2}) or power density (kWm^{-3}).

As far as exploring burner operating range under lean conditions is concerned, there are two main bodies of work of interest: that carried out by Ellzey and colleagues at the University of Texas at Austin (Chaffin et al. 1991; Ellzey and Goel 1995; Khanna, Goel and Ellzey 1994; Mathis and Ellzey 2003; Smucker and Ellzey 2004; Vogel and Ellzey 2005), and that undertaken by the combustion technology group at the University of Erlangen-Nuremburg (see Durst and Trimis (2002) and Trimis and Durst (1996) for an overview). The burners used by the Austin group have tended to be fairly similar, in that they use a two-section design, combustion chambers of diameter 5–10 cm and reticulated ceramic (or more recently metallic) foams as the porous material. Those developed by the Erlangen group have tested a wider variety of porous materials including packed beds and lamella structures (§3.4.1.2) and have been integrated with heat exchangers for energy recovery.

The performance of both sets of burner is fairly similar however, and can be summarised as:

- Stable equivalence ratios ranging from 0.5 to fuel rich.
- Flow velocities of up to 2 ms^{-1}.
- Firing rates of up to 4000 kWm^{-2}, but typically no more than 3000 kWm^{-2}. (Often the maximum firing rate may be determined not by the limitations of the burner itself, but by the practicalities of what can be measured in a laboratory environment: for example, heating may become so great that it becomes a hazard (Mathis and Ellzey 2003).
- Emissions of NO_X, CO, and UHC of less than 40 ppm (for lean mixtures).
- Maximum pressure drops of 0.1 $bar \cdot m^{-1}$ (Smucker and Ellzey 2004) (although this is not usually reported, and will be highly dependent on the porous material used).

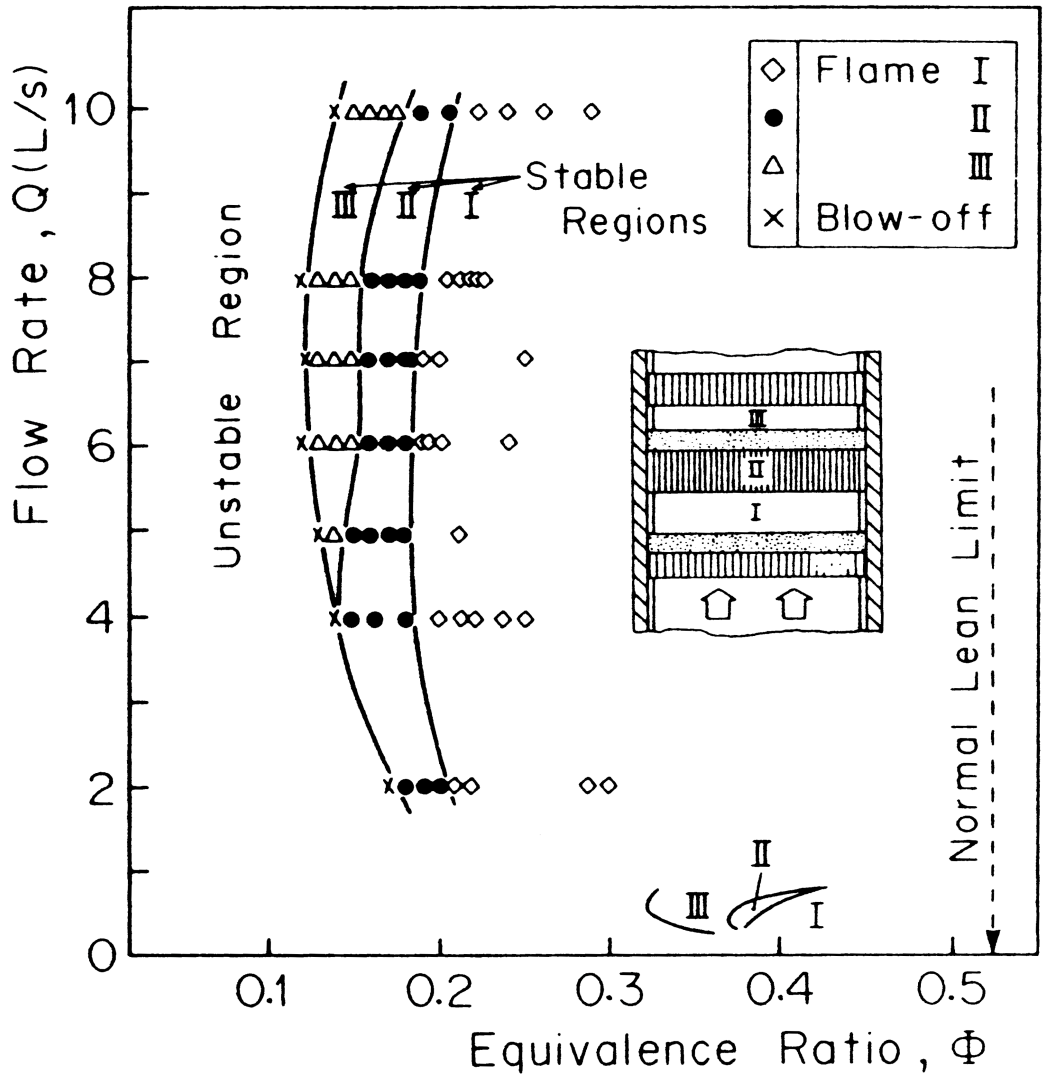

Figure 3.8 Stability diagram for combustion in a porous burner using a bundle of Al_2O_3 tubes; flame type II represents combustion actually within the porous medium (Source: Kotani, Behbahani and Takeno 1984).

3.3.1 Examples of ultra-lean burner performance

Investigations involving ultra-lean combustion (below the lean flammability limit of $\phi = 0.5$) are not at all common.

The early experimental work on combustion in a porous medium by Kotani and Takeno (1982) and Kotani, Behbahani and Takeno (1984) resulted in combustion being maintained at equivalence ratios of about 0.2, as shown by the burner map in Figure 3.8. The burner used in this work combined the porous medium—in this case a bundle of Al_2O_3 tubes of inner diameter 0.6–0.8 mm—with an external heat exchanger surrounding the combustion chamber.

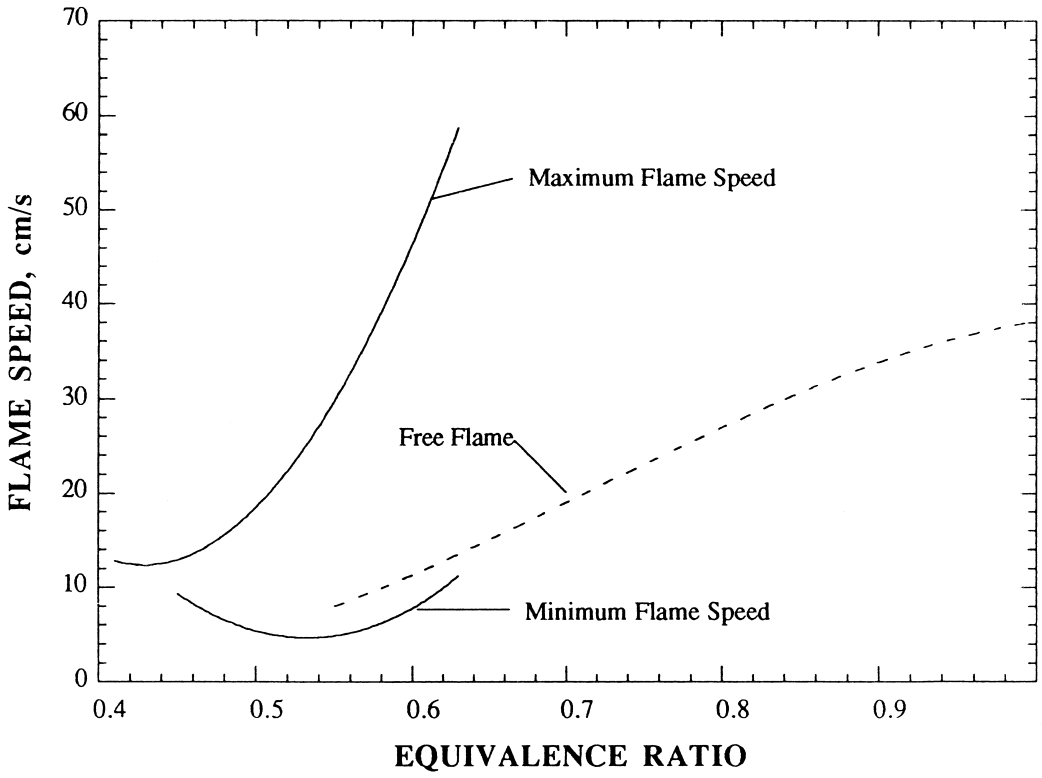

Figure 3.9 Stability diagram for a two-section PSZ burner (Source: Hsu, Evans and Howell 1993).

In later work, Hsu, Evans and Howell (1993) carried out an experimental study on a two-section burner design (§3.4.2) consisting of two reticulated ceramic PSZ cylinders. The cylinders were each 5.1 cm in both diameter and length, and insulated circumferentially. The preheating section had a pore density of 25 ppcm and the combustion section 4 ppcm. Figure 3.9 shows the stability diagram obtained for this burner. It can be seen that there was a modest extension of the lean limit to $\phi = 0.41$ and that above this limit stable combustion was possible over a wide range of velocities at any given equivalence ratio. These findings were corroborated by a numerical analysis of the same burner, which predicted the lean limit to occur at $\phi = 0.43$.

More recently, Christo and colleagues at the University of Adelaide (Afsharvahid, Dally and Christo 2003b; Afsharvahid et al. 2002; Christo et al. 2002) investigated the performance of a larger burner consisting of an insulated cylinder of 15.4 cm diameter and 60 cm in length filled with 6 mm diameter Al_2O_3 spheres plus a thin layer of flint clay beads at the base of the combustion chamber to act as a flashback arrestor. Only a limited selection of preliminary results were reported but these indicated that it was possible to maintain combustion at $\phi = 0.1$ at a firing rate of 90 kWm^{-2} (Christo et al. 2002), as demonstrated by the steady-state temperature profiles shown in Figure 3.10. However it can be seen that these temperature profiles are somewhat erratic, and as a complete set of results has not been published this finding should perhaps be treated

with some scepticism as regards the stability and completeness of the combustion process: quite possibly this is actually an example of transient combustion, with the flame propagating extremely slowly, at less than 1 mms^{-1}, up the porous bed (§3.2.2.3).

Nevertheless, emissions of CO and NO_X were measured at equivalence ratios of 0.35 and 0.4 and were found to be in the range 0–5 ppm in each case (Afsharvahid, Dally and Christo 2003b), indicating that at these slightly higher fuel concentrations at least, combustion was complete.

Finally, a number of studies on transient combustion systems have shown unequivocally that it is possible to achieve a significant extension of the lean limit into the ultra-lean regime. For example, Bingue et al. (2002c), using a 45 cm long, 3.8 cm diameter combustion chamber filled with 3 mm Al_2O_3 spheres, obtained combustion at equivalence ratios down to 0.25. At this equivalence ratio, and at a flow velocity of 0.12 ms^{-1}, the combustion wave propagated downstream with a velocity of 0.4 mms^{-1}. Kennedy et al. (2000) operated a burner of the same design at a higher flow velocity of 0.25 ms^{-1} and were able to extend the lean limit to $\phi = 0.2$.

So, from what has been reported in the literature, it can be concluded that stable ultra-lean combustion in porous burners is possible, but that there is a lack of reliable data relating specifically to this phenomenon.

In part this is because the majority of researchers have hitherto been more concerned with other aspects of burner performance, such as radiant output, as previously discussed.

It is also indicative of a more general lack of reliable measurements from porous burners; such data being inherently difficult to obtain due to the restrictive presence of the porous solid. It might be expected that accurate in-pore measurements of temperature, species concentration, gas velocity, turbulence intensity and so on would greatly enhance our understanding of the processes at work.

3.4 Burner design considerations

As previously discussed, combustion in a porous burner involves stabilising a flame within the pores of a solid matrix, and entails an intimate coupling of combustion, heat transfer and fluid dynamics. Despite an incomplete understanding of all the processes at work, an attempt can still be made to exploit the resulting desirable performance characteristics—namely extended flammability limits, high flame speeds and low emissions—in the design of practical burners for lean-burn applications.

Selection of a porous material with the correct thermo-physical properties is likely to be the single most important design decision.

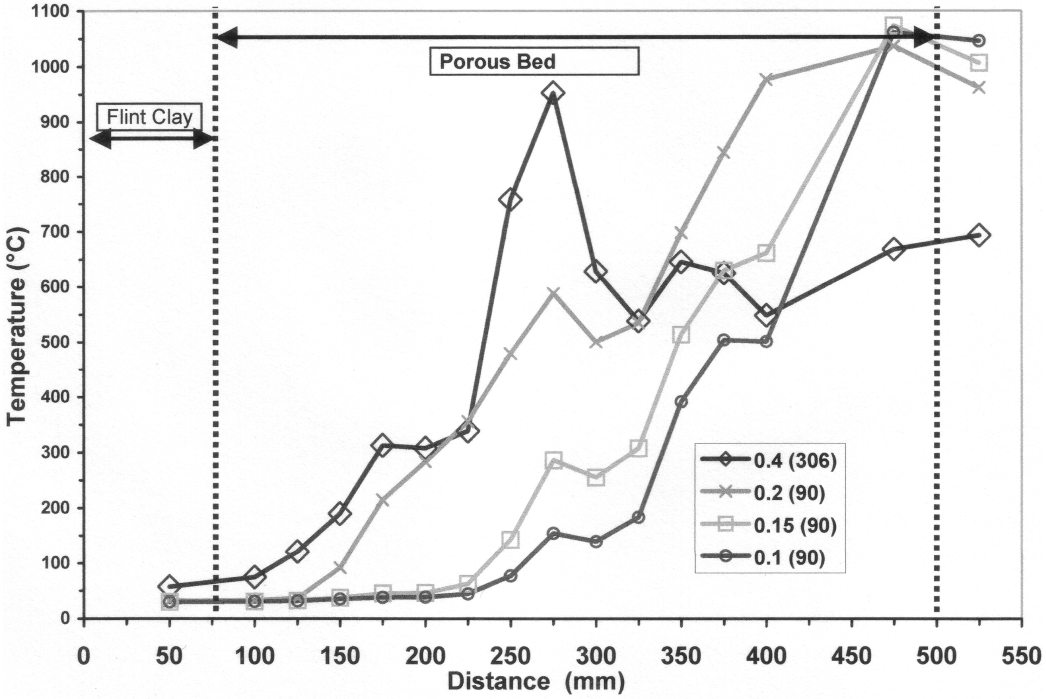

Figure 3.10 Temperature profiles within a porous bed of Al_2O_3 spheres for various equivalence ratios and firing rates (indicated by the number in brackets; in kWm^{-2}) (Source: Christo et al. 2002).

Other factors to consider include: the length of the porous bed; the use of multi-section designs; the shape and orientation of the combustion chamber; the integration of the burner with some form of external heat recirculation to provide additional preheating of the incoming fuel/air mixture; and if (and how) useful energy is to be extracted from the system.

3.4.1 Porous material selection

The principle of heat recirculation via a porous solid is fundamental to porous burner operation: choosing a porous material with heat transfer properties that allow this recirculation to proceed effectively is of primary importance. Conductive, convective and radiative heat transfer all contribute to the heat recirculation process, and so the thermal conductivity, convective heat transfer coefficient, emissivity and optical thickness (or its inverse, the radiative extinction coefficient) of a material must be considered (Fend et al. 2005).

A number of studies have used models of varying degrees of complexity to investigate the influence of these heat transfer parameters on burner performance. They confirm that increasing the thermal conductivity or convective heat transfer coefficient increases the degree of heat recirculation (Hsu, Howell and Matthews 1993; Lim and Matthews 1993; Barra et al. 2003; Fu, Viskanta and Gore 1998).

For example, Barra et al. (2003) used a 1-dimensional model incorporating a detailed chemical mechanism and separate energy equations for the gas and solid phases to investigate the influence of the thermal conductivity, convective heat transfer coefficient and radiative extinction coefficient on the stable range of flow velocities for an equivalence ratio of 0.65. They found that a high thermal conductivity and heat transfer coefficient result in both the largest stable operating range and the highest maximum velocity. Additionally, they discovered that there is an optimum value for the radiative extinction coefficient. They explained this finding as follows: If the extinction coefficient is too large then radiation takes place over too small a distance; conversely, if the extinction coefficient is too small then the radiation will be spread over too large an area; in either case the incoming gases will not be preheated effectively.

All of the relevant studies to date have investigated the effect of changing the various heat transfer parameters at a single equivalence ratio. A parametric study on the effect of each of these parameters on the achievable lean limit has not been reported.

Another important consideration when selecting a porous material is the pore size (or its inverse, the pore density). This will influence the combustion process via its effect on heat transport. Typically, small pored materials exhibit good conductive (more solid contact surfaces) and convective (larger internal surface area), but poor radiative (low optical thickness), heat transfer, and vice versa. There is clearly a trade-off between the three different modes of heat transfer suggesting that for any given system there will be an optimum pore size. Furthermore, additional heat transfer may occur due to thermal dispersion effects, that is, enhanced heat transfer due to hydrodynamic mixing of the gas within the pores, and these will also be strongly influenced by pore size and geometry (Fend et al. 2005).

Hsu, Evans and Howell (1993) investigated the effect of pore size on the stable operating range of a two-section burner consisting of reticulated foam cylinders made of PSZ. Foams of three different pore densities (4, 12 and 18 ppcm) were tested in the combustion zone. The 4 ppcm foam—the largest pore size—was found to be the most effective of the three at extending the lean limit, although clearly whether or not the actual optimum pore size is larger or smaller than this was not revealed by this experiment.

The volumetric porosity of the material is also important. A high porosity and permeability are desirable in order to minimise the pressure drop across the burner, as well as to decrease the time required to preheat the porous bed during the start-up phase (Mößbauer, Pickenäcker and Trimis 1999).

The durability of the material must also be considered. There are certain obvious constraints that any material must satisfy, namely an application temperature above the

burner operating temperature and resistance to oxidative or reductive atmospheres. The importance of a material's ability to withstand the high temperature gradients expected during burner operation, particularly during start-up and shut-down, has also been noted (Durst and Trimis 2002; Howell, Hall and Ellzey 1996): a low thermal expansion and high resistance to thermal shock are therefore desirable attributes.

Other general considerations include the tribological (erosion and wear resistance) performance of the material, its cost and availability, the convenience with which it can be employed and the ability to manufacture it in the desired geometry.

The overall performance of a porous material will depend on its particular combination of base material and porous structure. The solid material chosen will influence the overall properties of the porous matrix via its thermal conductivity, emissivity, temperature and corrosion resistance, thermal expansion, and mechanical strength at high temperatures. The geometrical structure employed will affect the radiative heat transport via its optical thickness, the conductive heat transport via the existence and extent of contact surfaces or solid material bridges, and the convective heat transport via the porosity and pore size and the resultant internal surface area and flow patterns. The porous structure will also determine the pressure drop and have a deciding influence on the strength and thermal shock resistance of the final material.

A wide variety of porous media have been used or suggested for porous burner applications. Useful reviews on this topic have been published by the combustion technology group at the University of Erlangen-Nuremburg (Durst and Trimis 2002; Mößbauer, Pickenäcker and Trimis 1999; Pickenäcker et al. 1999a,b), as well as by Howell, Hall and Ellzey (1996), who concentrate on ceramic foams. See also Greil (2002), who gives a more general overview of advanced engineering ceramics, including foams. The main base materials used are ceramics, such as Al_2O_3, silicon carbide (SiC) and zirconia (ZrO_2), and high temperature metal alloys. Possible geometrical structures include reticulated foams, packed beds and lamella structures.

3.4.1.1 Base materials

Ceramics. Ceramics are suitable for porous burner applications because of their high usage temperatures, chemical stability and resistance to erosion and wear (Bowen 1980). The most commonly used high temperature ceramics are Al_2O_3, SiC and ZrO_2, the relevant properties of which are summarised in Table 3.1.

Al_2O_3 is the most popular, employed either in a packed bed (Afsharvahid, Dally and Christo 2003b; Christo et al. 2002; Trimis and Durst 1996; Xiong, Khinkis and Fish 1995) or as a lamella structure (Al-Hamamre et al. 2006; Brenner et al. 2000; Bubnovich et al. 2010; Delalic, Mulahasanovic and Ganic 2004; Kamal and Mohamad 2006b; Pickenäcker and Trimis 2001). It has a high application temperature and is resistant to wear and

corrosion, as well as being economical. It has a moderate thermal conductivity and emissivity, but a large coefficient of thermal expansion and poor thermal shock resistance (ASM International 1995; Mößbauer, Pickenäcker and Trimis 1999; Pickenäcker et al. 1999a). The properties of any alumina-based ceramic depend on the actual Al_2O_3 content: ceramics with higher silica contents will typically have lower maximum usage temperatures and thermal conductivities (Pickenäcker et al. 1999a).

SiC and SiSiC ceramics oxidise at around 900K (Pickenäcker et al. 1999a), but as long as the resulting surface layer of silica remains stable, can be used up to reasonably high temperatures. Compared with Al_2O_3, they have the benefits of a high thermal conductivity and emissivity, a lower coefficient of thermal expansion and very good thermal shock resistance (ASM International 1995; Mößbauer, Pickenäcker and Trimis 1999; Pickenäcker et al. 1999a). They are most commonly used as reticulated foams (Afsharvahid, Ashman and Dally 2008; Alavandi and Agrawal 2008; Al-Hamamre et al. 2006; Delalic, Mulahasanovic and Ganic 2004; Kamal and Mohamad 2005; Kaplan and Hall 1995; Kesting et al. 2001; Mach et al. 2007; Pickenäcker and Trimis 2001; Schmidt et al. 2005a; Trimis and Durst 1996; Voß, Al-Hamamre and Trimis 2007b), but have also been employed in packed beds (Xiong, Khinkis and Fish 1995) and as static mixer structures (Brenner et al. 2000; Schmidt et al. 2007).

ZrO_2 based ceramics generally have a very high application temperature but a low thermal conductivity, high coefficient of thermal expansion, and moderate thermal shock resistance and emissivity (ASM International 1995; Mößbauer, Pickenäcker and Trimis 1999; Pickenäcker et al. 1999a). Pure ZrO_2 undergoes a destructive phase change from tetragonal to monoclinic when cooled from the sintering temperature, and must be stabilised against this by the use of additives such as magnesia, yttria, calcium oxide or ceria. The resulting stabilised or partially stabilised zirconia will typically have a lower application temperature—around 2100K—than the pure solid (Cannon et al. 2000; DePoorter, Brog and Readey 1992; Gómez et al. 2009; Pickenäcker et al. 1999a).

Table 3.1 Properties of some common ceramics.

Property	Al_2O_3	SiC	ZrO_2
Maximum usage temperature in air (K)	2200	1900	2600
Thermal conductivity at 1300K ($Wm^{-1}K^{-1}$)	5–6	20–50	2–4
Total emissivity at 2000K	0.28	0.9	0.31
Coefficient of linear thermal expansion 300–1300K ($10^{-6}K^{-1}$)	8	4–5	10–13
Resistance to mild thermal shock ($10^{-3}W^{-1}$)	3	23	1

Source: Pickenäcker et al. (1999a).

Although the heat transfer properties of ZrO_2 do not seem particularly favourable, various researchers have used ZrO_2 based ceramic foams in porous burners. Examples include PSZ with magnesia as the binder (Hsu, Evans and Howell 1993; Khanna, Goel and Ellzey 1994), yttria- and magnesia-stabilised zirconia (Kaplan and Hall 1995), and a yttria-stabilised zirconia/alumina composite (YZA) (Mathis and Ellzey 2003; Smucker and Ellzey 2004). The use of zirconia-toughened ceramics such as zirconia-toughened mullite (ZTM) (Mathis and Ellzey 2003) has also been reported; another such possibility might be zirconia-toughened alumina (ZTA) (DePoorter, Brog and Readey 1992).

Other high temperature ceramics previously employed in porous burners include lithium aluminium silicate (LAS) (Sathe et al. 1990), cordierite (Mital, Gore and Viskanta 1997) and mullite (Meng et al. 1991). It has also been suggested (Zhdanok, Dobrego and Futko 2000) that semi-transparent materials, for example quartz spheres or yttria-based ceramics, be considered as a means of increasing radiant heat transfer.

Metals. Surface burners, where the flame is stabilised at the downstream surface of the porous bed, rather than within the porous matrix itself, commonly use a mat composed of woven metal fibres as the porous material. In the past stainless steel was usually used (e.g. Kawaguchi et al. 1990) and more recently high temperature alloys such as FeCrAlY have been employed (Leonardi, Gore and Viskanta 2001; Leonardi, Viskanta and Gore 2002). Howell, Hall and Ellzey (1996) suggest that wire meshes are unsuitable for use in burners where the flame is actually located within the porous matrix, as the temperatures encountered could lead to the rapid degradation of such fine metal structures. Having said this, Huang et al. (2002) reported stable combustion within a porous bed composed of bundles of stainless steel wire mesh, and more recently Bakry (2008) used a nickel-chromium-steel alloy mesh made of 1.2 mm wire; no mention was made of the long-term durability of these burners.

The development of high temperature alloys, combined with the ability to produce them in reticulated foam structures (Porvair n.d.), suggests that metals may become an increasingly valid and attractive alternative to ceramics for porous burner applications. Alloys such as FeCrAlY are designed for oxidation resistance and high temperature use, up to 1700K (Lai 1992; MatWeb n.d.). To date there are limited examples (Cookson and Floyd 2007; Vogel and Ellzey 2005) of the use of FeCrAlY foam in porous burners, so it is difficult to judge the performance of this material compared with its ceramic counterparts.

Carbon-carbon composites. Carbon-carbon (C-C) composite materials (carbon fibre reinforcement in a graphite matrix) are another alternative. C-C composites have excellent thermal shock resistance and thermal conductivity, however because they oxidise readily at temperatures above 800K, a protective coating, for example SiC, rhenium, hafnium or iridium, must be applied. A porous burner composed of a C-C

composite foam coated in SiC has recently been developed (Marbach and Agrawal 2005).

3.4.1.2 Porous structures

Foams. Reticulated ceramic or metallic foams have an open-pore structure made up of an interconnected network of dodecahedral-like cells, with solid struts forming the cell edges (Gibson and Ashby 1997), as shown in Figure 3.11a. The literature contains numerous studies of porous burners made of reticulated ceramic foams, as documented above; the use of metallic foams is less common.

Reticulated foams are usually described in terms of a volumetric porosity plus linear pore density (number of pores per centimetre (ppcm)). Foams used in porous burners typically have porosities in the range 70–90%, and pore densities in the range 2–25 ppcm, equating to nominal pore sizes (1/ppcm) in the range 0.4–5 mm. Actual pore sizes, when measured, are generally smaller; half the nominal size in some cases (Howell, Hall and Ellzey 1996).

Foams typically exhibit good convective heat transport due to their large internal surface area. Radiative and conductive heat transport are also generally good, with the optical thickness typically of the order of 10 pore diameters. Their high porosity means that the pressure drop will be relatively low. They are also low in weight. Foams have the additional advantage of being manufacturable in a variety of complex shapes, and their rigid structure leads to flexibility in the angle at which the burner can be operated (Durst and Trimis 2002; Howell, Hall and Ellzey 1996; Pickenäcker et al. 1999b).

However, this rigidity also leads to concerns about the durability of reticulated foams in a burner environment. Ceramic foams exhibit poor thermal shock resistance and low fracture toughness. Hsu, Evans and Howell (1993) and Wharton, Ellzey and Bogard (2005) described the deterioration of burners made of PSZ and YZA foams respectively: the propagation of cracks though the foam eventually disturbed the uniformity of the flow causing the flame to tilt.

Elverum, Ellzey and Kovar (2005) investigated the durability of YZA foams in a porous burner. They performed compression tests on foam samples before and after testing in a typical burner environment. Degradation in compressive strength as a result of the burner tests was observed, with most of the damage found to occur due to the high thermal gradients present during the burner start-up phase. A scanning electron microscope (SEM) analysis revealed that failure involved the propagation of cracks from intrastrut pores—defects resulting from the manufacturing process. Comparable tests were recently carried out by Oliveira (2008) using mullite foams, with similar findings.

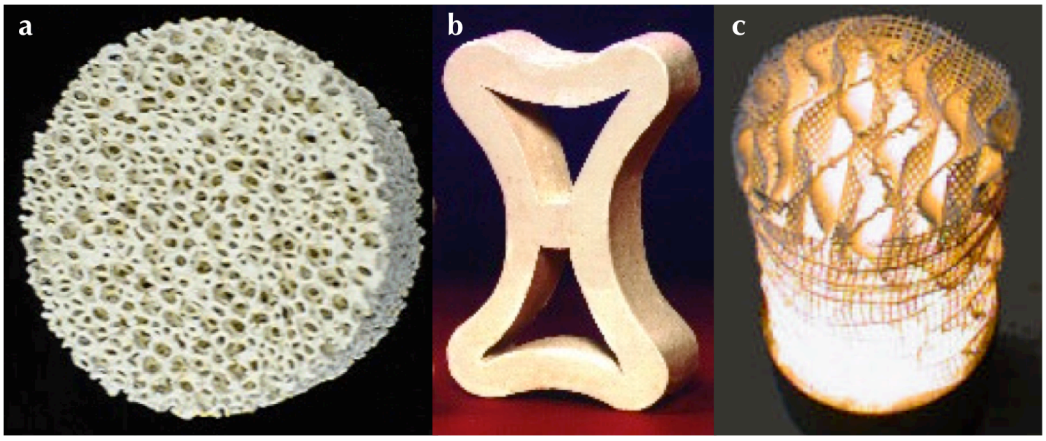

Figure 3.11 Examples of porous structures: (a) Reticulated foam made of ZrO_2 (Source: Durst 2006). (b) Random packing shape for use in regenerative thermal oxidisers (Source: San-Gobain NorPro n.d.). (c) Lamella structure made of Al_2O_3 fibres (Source: Mößbauer, Pickenäcker and Trimis 1999).

Schmidt et al. (2005a,b) also performed durability tests, in this case on SiSiC foams. They found that the silica layer that forms on the surface, and inside the intrastrut pores, of such foams, whilst stable under steady-state conditions, is quickly destroyed under thermal cycling (in other words after repeated start-up and shut-down). The formation of cracks in the foams can be attributed to tensile stresses resulting from a thermal mismatch between the SiSiC foam itself and the silica coating (Jacobson 1993). Attempts to improve the durability of the foams by applying a cordierite based coating to protect against corrosion were unsuccessful.

The use of multiple foam slices rather than a single large piece of foam is one way of combating durability issues (Voß 2008). The quality of thin slices tends to be higher, as manufacturing difficulties are reduced. Additionally, each individual piece would be exposed to a smaller thermal gradient than the burner as a whole. Furthermore, if failure were to occur, it would only be necessary to substitute the damaged piece, rather than replacing the entire porous bed.

Material durability is especially important if porous burners are to be successfully commercialised. To this end, researchers at the University of Erlangen-Nuremburg have instigated a project involving long-term (up to 3000 hours of thermal cycling) durability tests, which aims to determine the likely performance of a number of different ceramic foams over a burner's lifetime; this work is ongoing (Mach et al. 2005).

Packed beds. Packed beds of discrete particles are a commonly used alternative to foams. They have the advantage of increased durability as the particles are small robust shapes, and are not constrained in a rigid matrix. Packed beds of ceramic spheres, typically Al_2O_3 and of diameter 5–20 mm, are commonly used in porous burners (§3.4.1.1). However, packed beds of spheres are characterised by relatively low porosities—in the range 30–50% depending on bead size (Howell, Hall and Ellzey

1996)—and the ensuing disadvantages. The porosity can be increased by using an irregular packing shape such as a Raschig ring or saddle. Using a packed bed of saddles, for example, can increase the porosity to 90% or above (Perry and Green 1997). Various bespoke packing shapes (see for example Figure 3.11b) intended for VOC destruction in regenerative thermal oxidisers are also available (San-Gobain NorPro n.d.). These have been designed in a shape that provides optimal heat transfer, so should be suitable for use in porous burners. Xiong, Khinkis and Fish (1995) studied a burner comprising a packed bed of 'irregularly shaped' SiC particles; otherwise the use of packing shapes other than spheres has not been explored to any great extent.

Lamella structures. Structures, such as those found in static mixers, composed of several perforated ceramic lamellas arranged side by side and twisted with respect to one another (Figure 3.11c) are another alternative; the use of lamellas made out of Al_2O_3 fibres has been reported (Brenner et al. 2000; Kamal and Mohamad 2006b; Pickenäcker and Trimis 2001). These structures have a very high porosity of over 95%, and consequently a very low pressure drop and short start-up phase. They have a high internal surface area and so good convective heat transfer. The open structure means that radiative heat transfer is very high, although the conductive heat transport is negligible. They also reportedly exhibit good mechanical stability and thermal shock resistance (Mößbauer, Pickenäcker and Trimis 1999; Pickenäcker et al. 1999b).

Micro-fibrous media. Recently, Yang et al. (2009) studied transient combustion in a highly porous (95%) micro-fibrous ceramic composed of 4 μm silica/alumina fibres. The durability of such materials is questionable however, due to their fine structure.

3.4.1.3 Porous material selection for lean-burn applications

The most appropriate porous material will depend on the application for which the burner is intended. With respect to ultra-lean CH_4 combustion, maximising the heat recirculation assumes primary importance. It has been shown that at lower equivalence ratios conduction rather than radiation becomes the dominant mode of heat transport (Barra and Ellzey 2004), so a material with a superior thermal conductivity would be favourable. Furthermore, when operating on very lean mixtures, maximum burner temperatures will be fairly low at around 1500K or less (Christo et al. 2002): this means the choice of porous material is extended to include materials with only a moderate maximum usage temperature. Given all of the above, foams made of either SiC or a metal alloy seem most promising.

Also, in order to improve heat recirculation, maximising the *axial* heat transfer, against the direction of flow, is of particular interest. With the exception of lamella structures, which are probably not suitable for lean-burn applications due to their low thermal conductivity, the materials discussed so far have been homogeneous, transporting heat

uniformly in all directions. However materials capable of transferring heat preferentially in the desired direction could potentially be superior: for example, the bundle of Al_2O_3 tubes used in the experiments of Kotani and Takeno (1982) and Kotani, Behbahani and Takeno (1984), or the honeycomb structure employed by Min and Shin (1991). This is certainly an area that warrants further research.

As previously described, a number of modelling studies have investigated the effect of altering each of the various heat transfer parameters on burner operation. In a real material the effects of the different parameters cannot be isolated in this way (for example decreasing the pore size might increase conduction but it will also decrease radiation). Also, the relevant thermo-physical properties of many common materials, particularly reticulated foams, are poorly characterised. This hinders the development of accurate models, as some of the most important parameters will not be reliably known. It is consequently difficult to carry out modelling studies that compare actual available materials.

Moreover, there are few experimental investigations that objectively compare the performance of one or more porous material in the same burner (some studies that do attempt to do this are described below). It is difficult to analyse the performance of porous materials across different studies because the effect of the porous material cannot be isolated from other differences in burner design or experimental procedure.

Xiong, Khinkis and Fish (1995) compared the performance of a porous burner (with an integrated heat exchanger) made of a packed bed of Al_2O_3 spheres with one composed of irregularly shaped SiC particles. They observed that combustion could be stabilised over a wider range of fuel concentrations for the SiC burner, indicating that the SiC provided more effective heat recirculation. They also investigated the effect of porous material on emissions. NO_X emissions were found to be lower but CO emissions higher in the SiC bed because of the more effective cooling of the post-flame region. However, not enough information was provided about the two materials (for example particle size was not given) to be able to draw useful conclusions from this study.

Mathis and Ellzey (2003) investigated two different materials, YZA and ZTM reticulated foams, in a two-section burner, with the aim of stabilising combustion at the interface between sections. The foams were identical, other than in their use of different base materials. It was found that the YZA burner stabilised combustion over a range of firing rates at an equivalence ratio of 0.65, but that the ZTM burner did not stabilise the flame effectively: at lower firing rates the flame propagated into the upstream preheating section. Incomplete knowledge of the properties of the two different materials means it is not possible to determine precisely why this was the case.

Al-Hamamre et al. (2006) compared two different burners—each with the same dimensions—for the combustion of landfill gas (CH_4 in CO_2) and low-calorific value syngas (a mixture of CO, CH_4 and H_2 in CO_2 and N_2). The first burner was composed of Al_2O_3 lamellas and the second of SiC foam: they found that for each of the fuels investigated the SiC burner was more effective at extending the lean limit.

These studies, although limited, highlight the importance of correct material selection on burner operation, and the need for further research in this area.

3.4.2 Multi-section design

A two-section or 'bi-layered' design consisting of a small-pored upstream section in which the incoming gas mixture is preheated, and a large-pored downstream section in which the combustion process actually takes place was patented by researchers at the University of Erlangen-Nuremburg in 1993 (Durst, Trimis and Dimaczek 1993). Most of the recent literature describes porous burners constructed according to this design (Afsharvahid, Dally and Christo 2003b; Bubnovich et al. 2010; Chaffin et al. 1991; Christo et al. 2002; Delalic, Mulahasanovic and Ganic 2004; Hsu, Evans and Howell 1993; Khanna, Goel and Ellzey 1994; Mathis and Ellzey 2003; Mital, Gore and Viskanta 1997; Rumminger 1996; Smucker and Ellzey 2004; Vogel and Ellzey 2005). A two-section design performs one or both of the following roles: first, the interface between the two sections provides an additional means of stabilising the combustion process over a wide range of flow rates and second, the upstream section acts as a flashback arrestor or 'flame support layer'.

It has been suggested that the interface between the two sections acts as a 'flameholder', with the sudden change in pore size at the interface leading to local quenching of the flame (Durst and Trimis 2002). Chaffin et al. (1991) sought to enhance the role of the interface as flameholder by actually inserting a water-cooled brass ring around the circumference of the burner at that location. They asserted that this design allowed the stability range to be further extended, although no results comparing burner performance with and without the addition of this device were presented.

An alternative explanation for the role of the interface in combustion stability is suggested by Hsu, Evans and Howell (1993) based on the explanation for flame stability offered by Buckmaster and Takeno (1981) (§3.2.2.2) whereby on a plot of flame location against flame speed, the flame can be stabilised at those locations where there is a positive gradient. For a two-section design, there is a large jump in flame speed across the interface due to the increase in pore size, resulting in the ability to stabilise combustion over a larger flow range.

The upstream section can additionally serve as a flashback arrestor if the pore size in this section is chosen to be less than the minimum required for flame propagation. Materials with pore sizes of the order of 1 mm or less are typically used.

The two-section design is not always employed to optimal effect in its capacity either as flameholder or flashback arrestor. Some investigations have shown that the flame will propagate away from the interface when the flow velocity is increased or the equivalence ratio decreased, with the combustion process eventually stabilising in some downstream location (Afsharvahid, Dally and Christo 2003b; Christo et al. 2002; Mathis and Ellzey 2003). Conversely, there are reports of the flame propagating into, and sometimes stabilising within, the preheating region (Hsu, Evans and Howell 1993; Mathis and Ellzey 2003).

Previously (§3.4.1), the properties desirable in the porous material used in the main combustion region of the burner were surveyed. The sought-after properties for the material used in the preheating section will be slightly different, most obviously the requirement for a smaller pore size as already discussed. Additionally, poor heat transport properties might make for a more effective flashback arrestor. There seems to be a conflict here though, because if the flame is to be stabilised at the interface, the upstream section must also serve to preheat the incoming gases (although in practice some degree of preheating will also occur at the start of the downstream combustion section), implying that the convective heat transport properties at least should be good.

The findings of Barra et al. (2003) support the first view. They modelled the effects of the heat transport properties of the upstream section in a two-section burner at an equivalence ratio of 0.65. They found that a low thermal conductivity and convective heat transfer coefficient resulted in the largest stable operating range. They also concluded that it was the properties of the upstream section that significantly determined the minimum achievable flow velocity.

Examples of materials that have been used in the preheating section include packed beds of flint clay beads (Afsharvahid, Dally and Christo 2003b; Christo et al. 2002) and Al_2O_3 spheres (Bubnovich et al. 2010); and reticulated foams composed of PSZ (Hsu, Evans and Howell 1993; Ellzey and Goel 1995; Khanna, Goel and Ellzey 1994), YZA (Mathis and Ellzey 2003) and FeCrAlY (Vogel and Ellzey 2005).

The length of the preheating section might also be expected to influence burner performance. Mathis and Ellzey (2003) tested two different preheating sections of length 2.5 cm and 5.1 cm in a two-section YZA burner. The length of the main combustion section was 5.1 cm and the pore densities of the foam were 23.6 and 3.9 ppcm in the upstream and downstream sections respectively. They reported that the

longer upstream section allowed the minimum stable firing rate to be extended, although the effect was not found to be significant.

The use of *three*-section burner designs has also been reported. Brenner et al. (2000) used a burner comprising a preheat section made of 18 ppcm ZrO_2 foam, followed by a section of 8 ppcm ZrO_2 foam, followed by lamellas made of Al_2O_3 fibres; the benefit of using such an arrangement was not elucidated however. Hsu (1996) also reported using a three-section design, again in a ZrO_2 foam burner. In this case the three sections formed a 'sandwich' structure, with small-pored sections both upstream and downstream of the main combustion region. The third section was intended to provide both a means of redirecting radiative flux back into the combustion zone and an additional interface at which the flame could stabilise. It was shown that this three-section design supported a broader range of flow velocities, although the lowest equivalence ratio investigated was only 0.7.

Finally, it should be noted that the use of multi-section designs involving regions of porous material with smaller pores or lower porosities will increase the pressure drop across the burner, and this must be accounted for when assessing the relative merits of a given design. In order to minimise the pressure drop, Bakry (2008) successfully employed slotted refractory brick (with uniformly spaced slots of width 1.6 mm and spacing 10 mm), rather than the porous materials typically used, in the upstream section.

3.4.3 Shape and orientation of combustion chamber

The default configuration for a porous burner is a cylindrical combustion chamber oriented vertically such that the incoming fuel/air mixture flows upwards through the porous bed; the majority of reported studies use this construction. Square or rectangular cross-sectional geometries are also fairly common (e.g. Rumminger et al. 1996; Christo et al. 2002; Xiong, Khinkis and Fish 1995; Brenner et al. 2000), and more so for porous radiant burners. Trimis and Durst (1996) suggest that for larger burners, for some applications a rectangular design might be preferable, as one dimension could then be kept reasonably small. This might be desirable if the combustion chamber were surrounded by a heat exchanger for example. Mößbauer, Pickenäcker and Trimis (1999) reported a porous burner with a ring-shaped cross-section, in the centre of which a conventional premixed burner could be operated, potentially allowing a further extension of the operating range. Although certain configurations might be appropriate for particular applications, it seems unlikely that the shape of the cross-section would have much effect on the combustion process itself.

As regards the orientation of the combustion chamber, Huang, Chao and Cheng (2002) used a horizontally oriented burner.

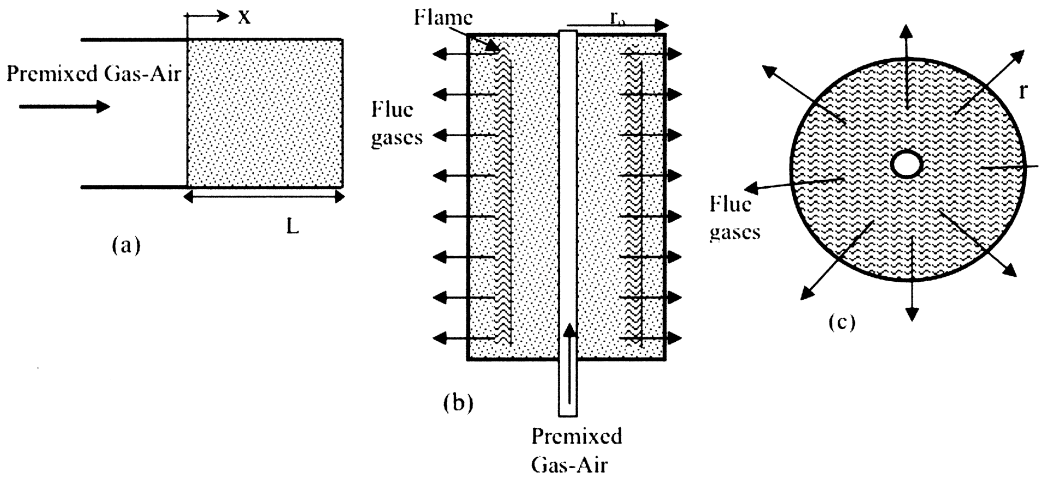

Figure 3.12 Schematic representations of (a) axial flow, (b) radial flow and (c) spherical burners (Source: Mohamad 2005).

A number of studies by the combustion technology group at the University of Erlangen-Nuremburg used a vertically oriented chamber with the gas flowing downwards. This arrangement was used because their burner incorporates heat exchanger tubes in the porous bed downstream of the combustion region; a downward-flow arrangement allows the condensed water thus produced to flow out of the base of the burner. As before, the orientation of the burner is unlikely to have a significant effect on the combustion process per se.

All the burner designs considered so far have essentially involved the flow of gas through a combustion chamber in the axial direction (Figure 3.12a). However cylindrical (Figure 3.12b) or even spherical (Figure 3.12c) geometries where the flow is in the radial direction have also been suggested.

Such geometries have been analysed numerically (Mohamad 2002, 2003, 2005; Zhdanok, Dobrego and Futko 1998) and it has been shown that, because the flow velocity is inversely proportional to radial location, they provide a natural means of stabilising the flame. A porous surface burner operating on natural gas/hydrogen mixtures using the cylindrical radial-flow arrangement was reported by Bröckerhoff and Emonts (1994). More recently Kamal and Mohamad (2006b,c) used a similar arrangement to study the enhancement of the combustion of CH_4/air mixtures by swirl imparted by rotation of the central burner tube. Otherwise there have been no practical realisations of these geometries.

Finally, an interesting modification to the normal cylindrical axial-flow burner design has been suggested: If the radius of the combustion chamber increases gradually, to form a funnel shape, then at lower firing rates only the smaller cross-sections are used, allowing a sufficiently high velocity to be maintained. The opposite is true at higher

firing rates and in this way the stable operating range of the burner can be enlarged (Durst and Trimis 2002; Voß, Al-Hamamre and Trimis 2007a).

3.4.4 Recovery of useful energy

The two main means by which useful energy can be extracted from a porous burner are the use of the burner for radiant heating or its integration with a heat exchanger to allow the recovery of thermal energy. Viskanta (1991) provides an overview and comparison of these two approaches.

Radiant heating has been the focus of much of the previous research on porous burners—see Howell, Hall and Ellzey (1996) for a review of the topic. Porous radiant burners work on the principle that if a suitably emitting porous medium is used, the energy in the fuel can be converted to radiant energy and used to heat a load. Porous radiant burners must therefore be designed such that the available radiating surface—usually the downstream end of the burner, but it could be the circumferential surface (Ellzey and Goel 1995)—is maximised, and the flame is stabilised close to this surface. These burners therefore usually have a relatively thin porous bed. Because a high temperature is required to maximise the radiant output, they are also typically run on close to stoichiometric mixtures. Qiu and Hayden (2006) suggest that porous radiant burners could also be used as a low-glare light source in an integrated heat and light system where the light is distributed through light pipes.

Recovery of thermal energy by means of an integrated heat exchanger is less well documented. However a number of investigations have looked at inserting heat exchanger tubes into the porous matrix, either within, or downstream of, the combustion zone (Delalic, Mulahasanovic and Ganic 2004; Durst and Trimis 2002; Echigo et al. 1983; Jugjai and Sawananon 2004; Liu and Hsieh 2004; Mohamad, Ramadhyani and Viskanta 1994; Mohamad, Viskanta and Ramadhyani 1994; Xiong, Khinkis and Fish 1995). The working fluid is heated by the hot combustion products as well as by radiation from the porous bed itself. The presence of cold surfaces in the flame zone is to be avoided, as this could lead to incomplete combustion and consequently increased CO and UHC emissions (Trimis and Durst 1996), so designs where the heat exchange takes place downstream of the actual combustion region are preferable. A further possibility would be to directly integrate a second reactor, in which an endothermic reaction occurs, into the porous burner; such a system could for example combine CH_4 combustion and steam reforming (Ismagilov et al. 2001).

In addition, the incorporation of porous media into the combustion chambers of gas turbines (Mößbauer, Pickenäcker and Trimis 1999) or internal combustion engines (Durst and Weclas 2001; Hanamura, Bohda and Miyairi 1997; Hanamura and Nishio 2003; Liu, Xie and Wu 2009a,b; Weclas n.d.; Zhao, Wang and Xie 2009) has been

suggested. The direct generation of electricity in thermoelectric (Hanamura, Kumano and Iida 2005) or thermophotovoltaic (Catalano 1996; Qiu and Hayden 2006, 2007) systems based around combustion in a porous medium has also been advocated.

3.4.5 Provision of supplementary external preheating

As previously described, heat exchangers can be integrated with porous burners as a means of extracting useful energy from the combustion process. However it is also possible to use an external heat exchanger to recover and recirculate heat from the exhaust gases to preheat the incoming fuel/air mixture, in order to supplement the internal heat recirculation provided by the porous bed.

This concept was demonstrated in early experimental work on porous burners carried out in the early 1980s by Takeno and colleagues (Kotani and Takeno 1982; Kotani, Behbahani and Takeno 1984). Their burner used a bundle of Al_2O_3 tubes as the porous medium and combined this with external heat recirculation as shown schematically in Figure 3.13. They were able to maintain stable combustion at equivalence ratios of 0.2 using this design.

Around the same time Echigo and co-workers (Echigo et al. 1983) at the Tokyo Institute of Technology developed a porous burner whose combustion chamber contained a ceramic plate burner followed by a layer of stainless steel mesh to facilitate heat recirculation. The steel mesh was surrounded by an arrangement of heat exchanger tubes for preheating the incoming combustion air. They operated the burner on a mixture of CH_4 and hydrogen and were able to significantly extend the lean limit (from $\phi = 0.284$ to 0.1).

More recently, Christo et al. (2002) used a pilot-scale burner incorporating preheating of the incoming reactants by the exhaust gases in an external heat exchanger to demonstrate the concept of ultra-lean combustion of LPG, however not much information about the configuration of this burner was provided.

The concept of providing supplementary external preheating in this way has not been extensively investigated. Given that in each of the above examples the lean flammability limit was extended, this seems a highly promising area for further research.

In order to reduce the lean flammability limit further it would be necessary to provide additional preheating of the reactants or porous bed from an auxiliary source such as an electric heater. This possibility was examined theoretically by Berlin et al. (2006) and Gnesdilov et al. (2006), and realised practically by Contarin et al. (2005) and Cunill, van de Beld and Westerterp (1997) who used an electric heater embedded in the porous matrix.

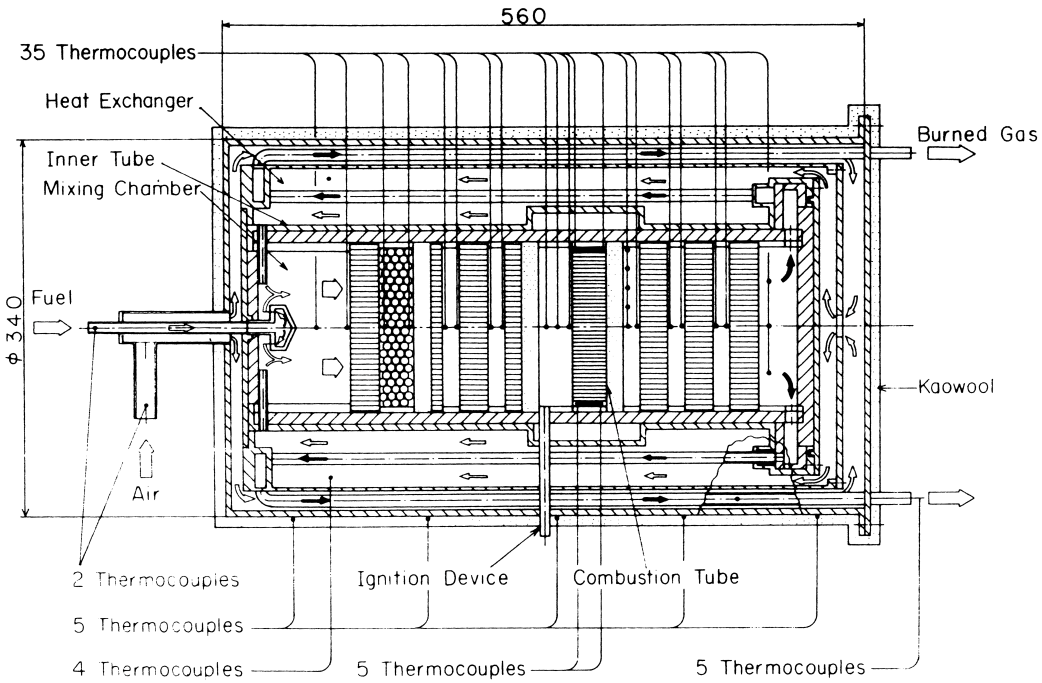

Figure 3.13 Design of a porous burner incorporating external preheating (Source: Kotani, Behbahani and Takeno 1982).

Such an arrangement could also be used to warm up the porous bed during the start-up phase.

3.4.6 Reciprocal flow operation

Previously (§3.2.2.3), the advantages of transient combustion for ultra-lean applications were discussed. It was mentioned that the main challenge associated with developing a practical transient combustion system was finding a way to confine a propagating flame within the limits of a stationary burner. One way of doing this is to use a burner design featuring reciprocal flow operation.

In a reciprocal flow burner, the direction of flow is periodically reversed by means of flow switching values at either end of the combustion chamber. For a combustion wave propagating in the same direction as the incoming gas, if the length of each half-cycle is controlled so that it is greater than the residence time of the gas, but less than that of the combustion wave, then the combustion wave can be restricted to within the limits of the burner. Each time the flow direction is switched, the incoming gas is preheated as it passes through the hot region of the porous bed where the combustion and post-combustion zones were located in the previous half-cycle (Kennedy et al. 1995).

In theory, reciprocal flow operation will result in a trapezoidal temperature profile (Hanamura, Echigo and Zhdanok 1993).

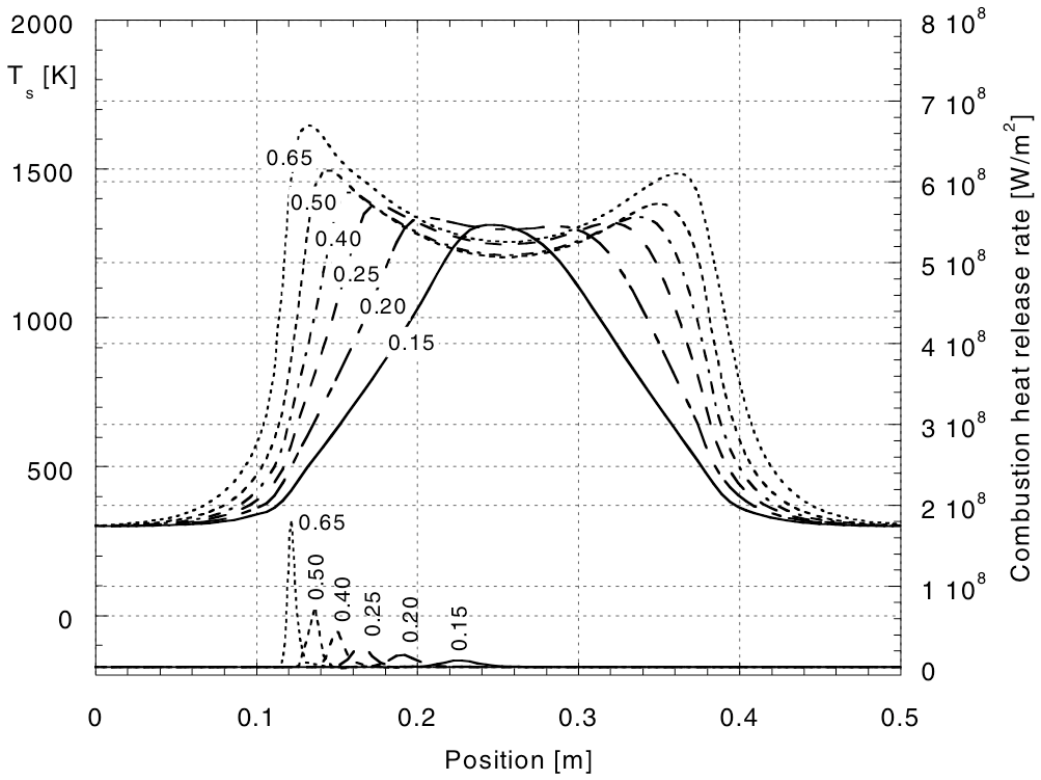

Figure 3.14 Temperature profiles in a reciprocal flow burner for various equivalence ratios at a flow velocity of 20 cms^{-1} (Source: Contarin et al. 2003).

In practice, due to radial heat losses, an M-shaped profile is likely to be observed (Contarin et al. 2003, 2005; Du and Xie 2006; Hoffmann et al. 1997; Kushwaha et al. 2004, 2005; Jugjai and Nungniyom 2009, Xie et al. 2009), as illustrated in Figure 3.14. It can be seen that at lower equivalence ratios, the two temperature peaks are closer together, with the profile eventually taking on a triangular shape at the lean limit.

As with those operating with a stable flame, reciprocal flow burners may be integrated with heat exchangers—either embedded in the terminal sections of the combustion chamber (Contarin et al. 2003, 2005), or surrounding it (Jugjai and Chuenchit 2001)—in order to extract energy or to provide supplementary preheating to the incoming combustion air.

One of the main disadvantages of the reciprocal flow burner design is the need to maintain reliable operation of the mechanical flow switching values (Dobrego et al. 2005). In addition, a more complex burner control strategy is required.

3.4.7 Other design considerations

Depth of porous bed. The required depth of the porous bed also needs to be considered. As has previously been discussed, the balance between heat release, heat recirculation and heat losses will determine the position at which the flame stabilises within the

porous bed. Changes in flow rate or fuel concentration may cause the flame to propagate up- or downstream before stabilising at a new location. However it is difficult both to predict a priori at what location the flame will stabilise for a given burner, and to determine what the effect of changing the depth of the porous bed on burner performance will be.

Active flame stabilisation. The incorporation of some form of what can be described as 'active flame stabilisation' (Duran and Rost 2005; Martin, Stilger and Holst 1991) into the burner design—and operating procedure—as a means of stabilising and maintaining the flame at a desired location in the porous bed might also be considered. Essentially this involves monitoring the bed temperature and using a programmable control system to automatically adjust the flow rate and composition of the incoming fuel air mixture—either by adding supplementary fuel or additional dilution air—to counteract any changes observed in the temperature profile. This capability could be especially valuable in ultra-lean combustion systems, as many low-grade fuels—such as CH_4 emissions—are subject to unplanned fluctuations in both flow rate and energy content.

Insulation. In order for heat to be recirculated efficiently, radial heat losses should be minimised. Typically the combustion chamber will be encased in an insulating sleeve made of fibrous Al_2O_3 or some similar material. Another possibility would be to surround the burner with an evacuated jacket (Cunill, van de Beld and Westerterp 1997).

Flow distribution. For effective operation, a uniform flow distribution is required, as well as thorough mixing of the fuel and air feeds (if they are not premixed). The design of the burner inlet will determine whether or not this is the case, so the provision of a flow-straightening device such as a perforated plate or a honeycomb grate (Liu and Hsieh 2004) might be considered.

Non-premixed operation. The operation of porous burners with non-premixed flames is also possible (Kamal and Mohamad 2005; Meng et al. 1991). However, because the presence of the porous material inhibits mixing of the fuel and air—increasing the likelihood of incomplete combustion—it is desirable in this case to stabilise the flame just ahead of the porous matrix. This allows the fuel and air to mix before actually entering the solid, although the reaction zone may extend into the porous region itself and there will of course still be heat transfer between the burnt gases and the solid matrix.

High-pressure operation. For applications where a high throughput is required, operating the burner at elevated pressures might be an option. Mößbauer, Pickenäcker and Trimis (1999) reported that a high-pressure porous burner chamber had been developed for

use in a gas turbine, but no results were presented. Noordally et al. (2004) developed a burner—also intended for gas turbine applications—with a nominal maximum operating pressure of 18 bar, although the practical maximum operating pressure (at ϕ = 0.6) was found to be around 12 bar, above which increasing temperatures in the inlet lead to concerns over flashback. More recently, Altendorfner et al. (2007) designed a burner intended to operate at elevated pressures of 10–15 bar, however so far only experiments under atmospheric conditions have been reported. This is an area that needs further investigation.

EGR and staged operation. Other burner design features reported in the literature include the use of exhaust gas recirculation (EGR) (Mößbauer, Grüber and Trimis 2001) and the staged addition of the reactants (Bell, Chaffin and Koeroghlian 1992; Ellzey and Goel 1995; Pickenäcker and Trimis 2001), however neither of these is particularly relevant to lean-burn applications.

3.5 Conclusions and recommendations for further research

Porous burners operate on the principle that when a premixed fuel/air mixture burns within the cavities of a solid porous matrix, the solid serves as a means of recirculating heat from the hot combustion products to the incoming reactants, leading to excess enthalpy burning. Combustion in a porous medium is characterised by increased flame speeds, extended flammability limits, stability across a wide range of conditions, and low emissions.

There is an extensive body of research relating to porous burners comprising both experimental and numerical investigations. Despite this, some of the fundamental processes involved are still not well understood, due both to the difficulties involved in obtaining accurate experimental measurements from within the solid matrix and because some of the relevant properties of the most commonly used porous materials are not reliably known. This presents problems both for the development of accurate models, and for the design of burners to meet the particular requirements of a given lean-burn application.

A number of specific topics have been identified that have not been explored fully to date and where further research would therefore be beneficial. These include:

- The effect of the heat transfer properties of the porous material on burner operating range.
- The use of novel porous materials including alternative packing shapes, metal foams, and materials capable of transporting heat preferentially in one direction.
- A better characterisation of commonly used porous materials.

- An objective and comprehensive comparison of materials and their effect on burner performance.
- The effect of porous bed depth on burner operating range.
- The effect of operating the burner at elevated pressures.
- The effect of the use of supplementary external preheating of the incoming fuel/air mixture.

With respect to ultra-lean combustion in particular, although the phenomenon has been observed in a handful of experimental studies, there is a lack of research focused specifically on this topic. Further work, both experimental and modelling, is required in this area generally, and particularly as regards the optimisation of burner designs for lean-burn applications such as the mitigation of CH_4 emissions.

Additionally, there has been little attention paid thus far to issues regarding scale-up and how the technology might be practically applied outside of the laboratory: this merits further consideration.

The remainder of this thesis aims to address some of these issues. Part 2 discusses a pilot-scale demonstration of a novel porous burner system for ultra-lean combustion that incorporates supplementary external preheating. Part 3 concerns the development of a computational fluid dynamics (CFD) model of the burner capable of exploring the topics listed above.

Part 2

PILOT-SCALE DEMONSTRATION

Chapter 4

BURNER DESIGN AND CONSTRUCTION

4.1 Introduction

Part 2 of this thesis concerns a pilot-scale demonstration of an experimental porous burner system for ultra-lean methane (CH_4) combustion. This chapter describes the design and construction of the system.

As previously discussed (§3.4), a number of burner design considerations are relevant to the optimisation of burner performance for ultra-lean applications, including: selection of an appropriate material for the porous matrix; the use of 'multi-section' designs where different porous materials are used in each section; the depth of the porous bed; and the incorporation of external heat exchangers to supplement the heat recirculation provided by the porous matrix. All of these issues will be addressed here.

In the following sections the various phases in the design procedure—including the initial process design, the design of the main items of equipment, and the selection of a suitable porous matrix for the burner—will be discussed. Details of a computational fluid dynamics (CFD) model developed as part of the design process will also be presented. Finally, the construction of the burner and commissioning of the system will be described.

4.2 Process design

In its simplest form a porous burner system would consist of a premixed CH_4/air feed entering the burner, complete and stable combustion occurring within it, and the exhaust gas (composed of air, water and carbon dioxide (CO_2)) exiting the burner and being discharged to the atmosphere. In a practical system some means of extracting useful energy from the system would also be included, either by using the burner for radiant heating, or by incorporating a heat exchanger into the system to allow for the recovery of thermal energy (§3.4.4).

However, the current design is intended for the combustion of ultra-lean CH_4/air mixtures. The intention is therefore to recover heat from the burner, not to extract useful energy from the system, but to recirculate that heat to preheat the incoming CH_4/air mixture (in order to supplement the internal heat recirculation provided by the porous bed) (§3.4.5).

The process flow diagram (PFD) of the system is shown in Figure 4.1. It can be seen that two heat exchangers have been incorporated into the process. A primary heat exchanger (HX1) is positioned at the outlet of the porous burner, allowing the incoming CH_4/air mixture to be heated both by the hot exhaust gases exiting from the burner, and via radiant heating from the porous matrix.

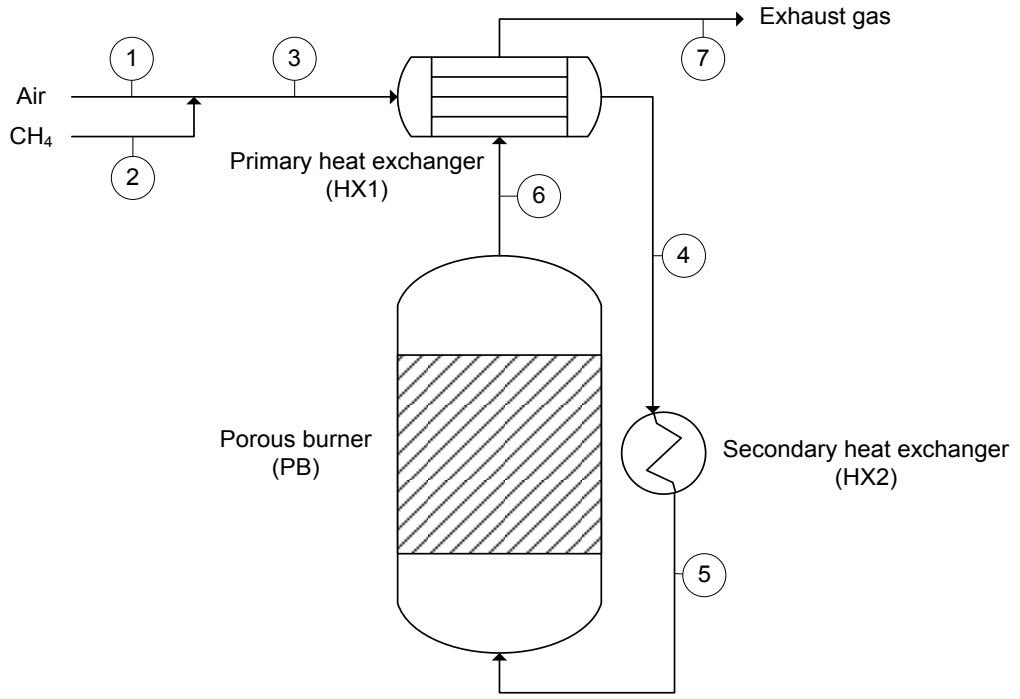

Flows (kgh^{-1})

Line no.	1	2	3	4	5	6	7
Stream / Component	Air feed	CH_4 feed	HX1 feed	HX1 outlet	HX2 outlet	PB outlet	Exhaust
Air	129.0	—	129.0	129.0	129.0	—	—
CH_4	—	0.4	0.4	0.4	0.4	—	—
Exhaust gas	—	—	—	—	—	129.4	129.4
Total	129.0	129.4	129.4	129.4	129.4	129.4	129.4
Temperature (K)	300	300	300	1000	1024	786	426

Figure 4.1 Process flow diagram (PFD) of the porous burner system.

A secondary heat exchanger (HX2) is also shown. It is intended that this be designed such that it can recuperate some of the heat lost by conduction through the burner walls, in order to further preheat the incoming mixture.

A mass and energy balance of the system was performed according to the methodology described by Sinnott (1999). The calculations were performed at the system's design capacity of 130 kgh^{-1} total throughput, and at a CH_4 concentration of 0.5 vol% (typical of actual lean-burn applications, such as the combustion of mine ventilation air (MVA)).

Assumptions and approximations used in the calculations included:

- CH_4 and air feeds are both at room temperature (300K).
- The air feed is dry and composed of 78% nitrogen (N_2) and 22% oxygen (O_2).
- Complete and stable combustion occurs in the burner according to the reaction

$$CH_4 + 2O_2 = 2H_2O + CO_2$$

- Heat loss by radiation to HX1 comprises 40% of burner output (see §3.3).
- Heat loss by conduction to HX2 comprises 3% of burner output.
- Heat losses from the system comprise 1% of burner output.
- The gas leaving HX1 (stream 4) is heated to 1000K (based on past experience).

The resulting stream properties are given in the PFD (Figure 4.1).

4.3 Equipment design

Based on the process described above, the design of the main items of equipment (the porous burner and associated heat exchange system) was undertaken. The design is based on engineering judgement derived from practical experience of similar systems (Christo et al. 2002), and follows recent trends in porous burner design (§3.4). The design work was carried out using AutoCAD 2002 (Autodesk n.d.).

In the previous section, it was assumed that the CH_4 and air feeds would be premixed, as would be the case for most real-world lean-burn applications. In designing the equipment, a second scenario—where the feeds are separate, with mixing only occurring immediately prior to the gas entering the combustion chamber—was also considered. This might be the case in certain applications, but such a design would also provide a means for the gas mixture to be 'boosted' with extra CH_4 either during start-up or if fluctuations in the main feed caused the CH_4 concentration to fall below the combustible limit. Two alternative design configurations were therefore produced.

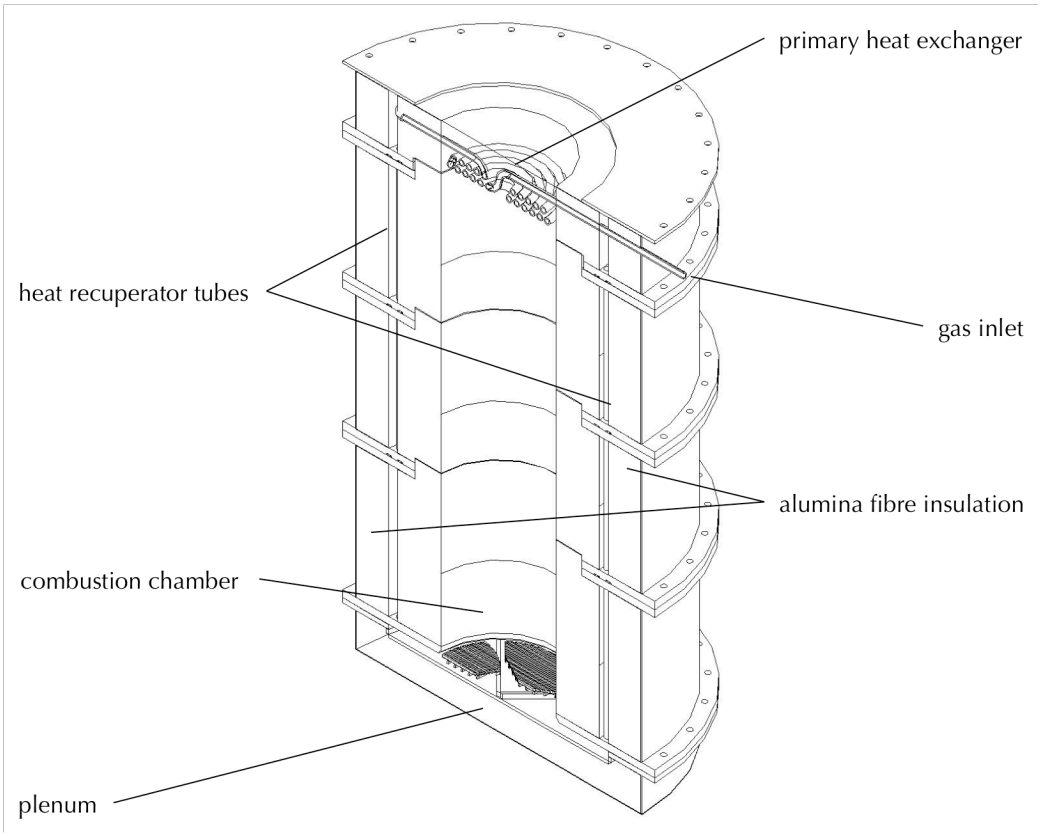

Figure 4.2 Design of the porous burner system (configuration 1).

Henceforth these shall be referred to as configuration 1, where the CH_4 and air feeds are premixed, and configuration 2, where they are separate.

Configuration 1 is shown in Figure 4.2, and configuration 2 in Figure 4.3. The main features of the burner design are the same in each case. The central combustion chamber of the burner—which is filled with the porous matrix—is a cylinder of 26 cm diameter. The combustion chamber is oriented vertically such that the incoming CH_4/air mixture flows upwards through the porous bed. The maximum depth of the porous bed is 90 cm. However, because it is not known *a priori* at what position in the bed the flame will stabilize, the combustion chamber has been designed in a modular way, enabling the depth of the bed to be adjusted as required; this arrangement will also allow the effect of bed height on burner performance to be investigated.

The three modules of the main chamber are combined with an arrangement of external heat exchanger tubes for preheating either the incoming CH_4/air mixture (in the case of configuration 1) or just the air (in the case of configuration 2). The cold gas flows into the primary heat exchanger comprising 12 layers (only two of which are shown in Figures 4.2 and 4.3) of staggered spirals sitting above the porous bed. Here it is heated by a combination of the burner exhaust gases entering from below plus radiation from the hot porous bed itself.

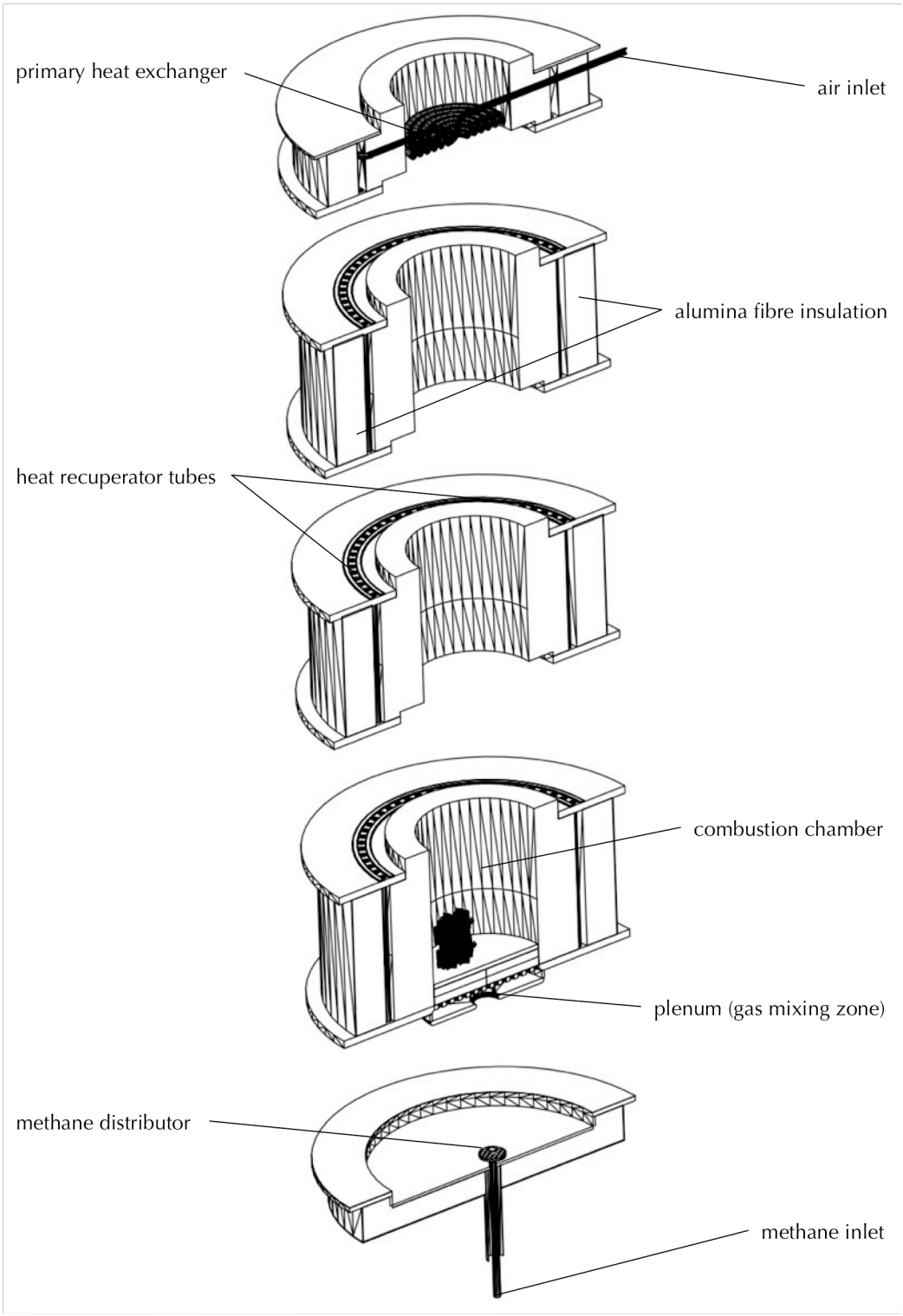

Figure 4.3 Design of the porous burner system (exploded view) (configuration 2).

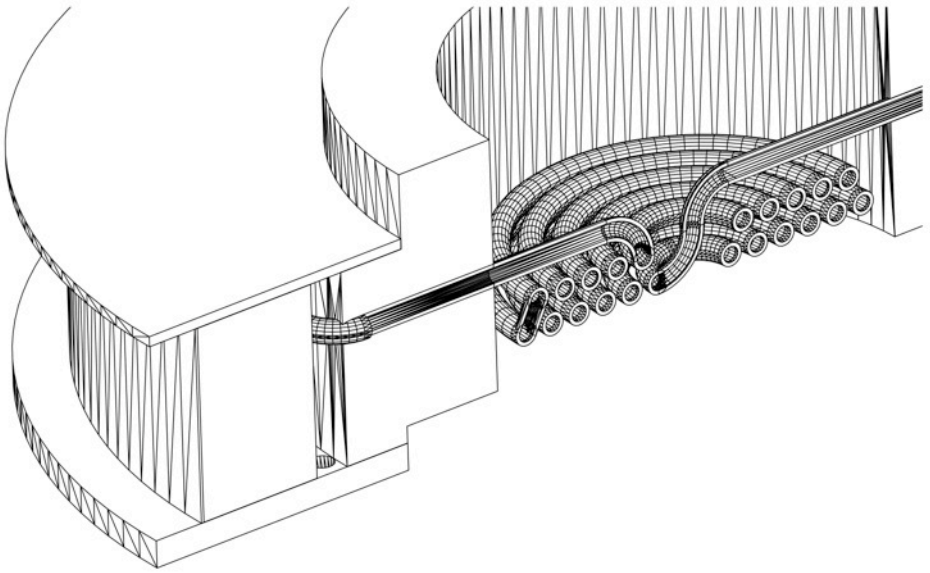

Figure 4.4 Magnified view of the primary heat exchanger. For simplicity only two of the 12 layers of spirals are shown.

A magnified view of the primary heat exchanger is shown in Figure 4.4.

The preheated gas then flows down through a series of circumferential heat recuperator tubes (the secondary heat exchanger) surrounding the combustion chamber to a plenum at the base of the burner. In configuration 1 (Figure 4.5), this preheated gas then enters the porous bed directly. In configuration 2 (Figure 4.6), the preheated air is mixed with the incoming CH_4 before flowing upward into the porous bed.

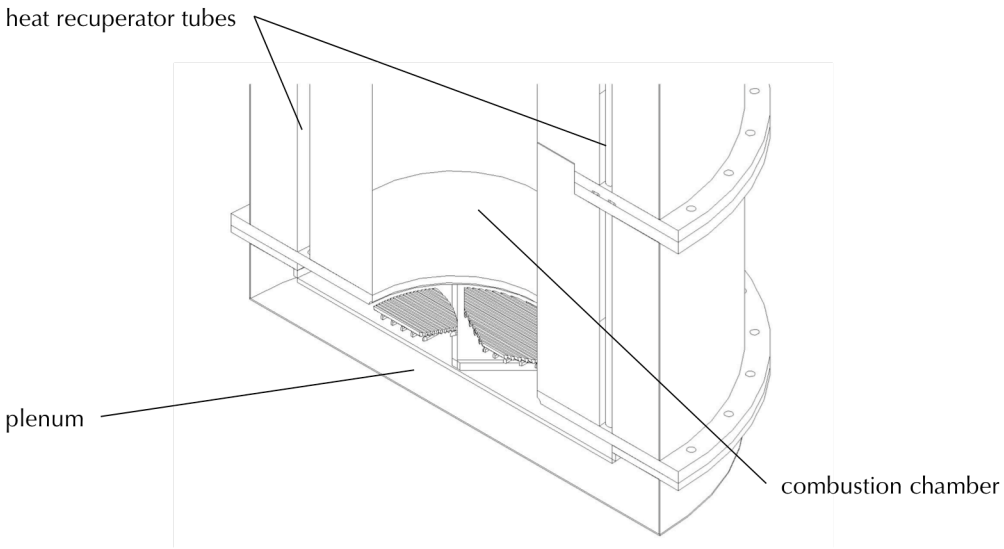

Figure 4.5 Magnified view of the base of the burner (configuration 1).

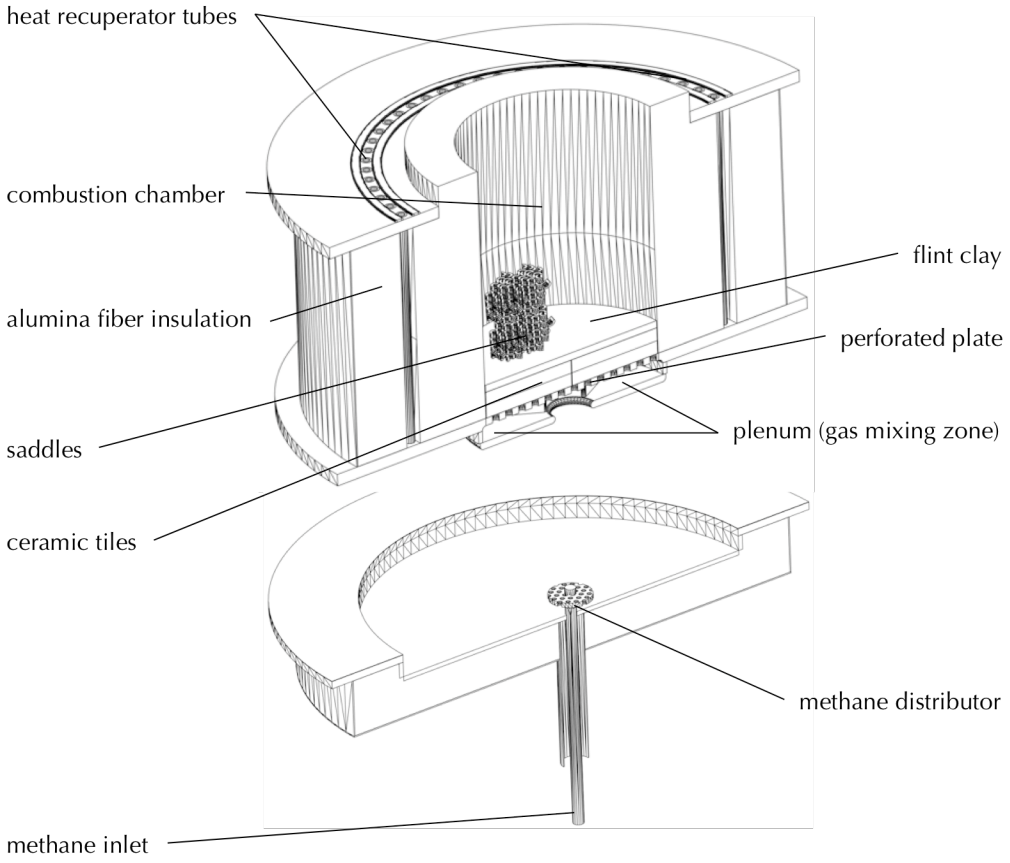

Figure 4.6 Magnified view of the base of the burner (configuration 2) showing the CH_4 inlet and distributor.

As previously discussed, although a number of past studies have examined integrating heat exchangers with porous burners as a means of extracting useful energy from the system, the concept of using an external heat exchanger to recover and recirculate heat from the combustion process—to supplement the internal heat recirculation provided by the porous bed—has not been extensively investigated; the current design is innovative in this regard. With respect to ultra-lean combustion, maximizing heat recirculation is of primary importance; so, if effective, this enhancement could offer a significant advantage.

To minimize radial heat losses, the entire assembly is surrounded by alumina (Al_2O_3) fibre insulation, as illustrated in Figures 4.2 and 4.3.

4.4 Porous material selection

The complex interaction between combustion, heat transfer and fluid mechanics processes that occurs in a porous burner means that selection of a porous material with suitable thermophysical properties is essential to achieving stable operation.

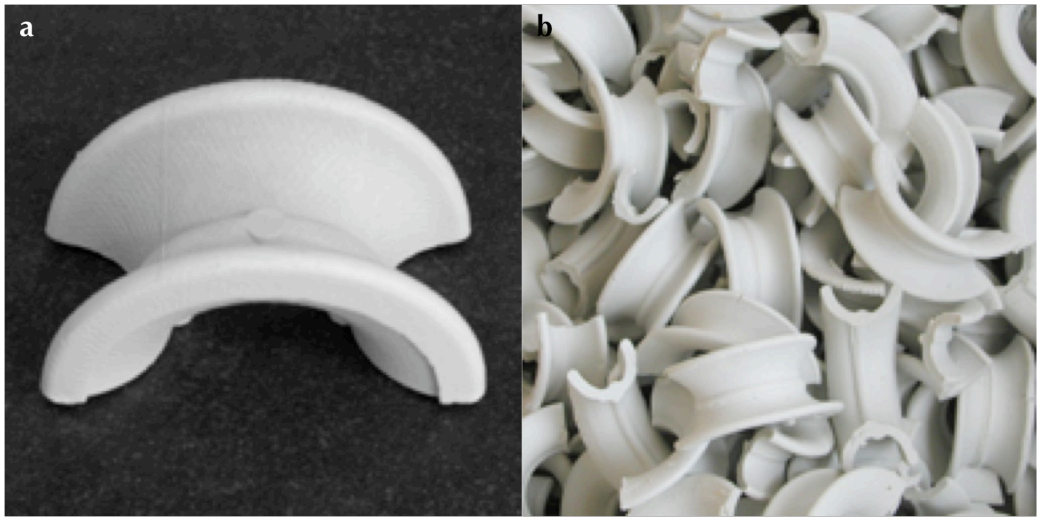

Figure 4.7 (a) An example of a ½″ ceramic saddle. (b) A packed bed of saddles as used in the main porous bed.

The overall performance of a porous material will depend on its particular combination of base material and porous structure. Commonly used materials include ceramics (such as Al_2O_3, silicon carbide (SiC) and zirconia (ZrO_2)) or high temperature metal alloys. Possible structures are reticulated foams, packed beds, and lamella structures (§3.4.1). The burner's intended application will determine the porous material selected: for ultra-lean combustion, the maximum operating temperature is likely to be less than 1500K, so materials with relatively modest maximum usage temperatures can be considered. Additionally, since conduction rather than radiation is the dominant mode of heat transport under these conditions, using a material with a higher thermal conductivity should assist in maximizing heat recirculation (§3.4.1.3).

In the present design the main combustion chamber is filled with a porous bed of 60% Al_2O_3, ½″ ceramic saddles (Figure 4.7). Al_2O_3 is a popular choice for porous burner applications—despite the superior heat transfer properties of alternatives such as SiC—because it has a higher maximum usage temperature (2200K in air), is chemically stable (SiC oxidizes at around 1000K), is resistant to erosion and wear, and is economical (§3.4.1.1). A packed bed of discrete particles was selected over an alternative rigid structure—such as a reticulated foam—due to its superior durability; the particles are small robust shapes and are not constrained in a rigid matrix (which could be subject to cracking). Packed beds of spheres are commonly used in porous burners, including for lean-burn applications (Christo et al. 2002), however the current design is novel in using a random packing of saddles. The use of an irregular packing shape allows a higher porosity to be achieved—66% in the case of the ½″ saddles used here (RVT Process Equipment n.d.). This should in turn minimize the pressure drop across the burner. It

should also increase the turbulence intensity of the flow, further enhancing heat transfer.

Below the main porous bed is a 1 cm deep layer of 3 mm flint clay beads. This has a lower porosity (48%), and worse heat transport properties, than the main porous bed (Lynch 2001); it is intended to improve the flow distribution at the entrance to the combustion chamber (see later), and to act as a flashback arrestor.

Below the flint clay layer is a 2.6 cm deep layer of cordierite tiles that act as burner blocks, supporting the packed bed above, and acting as an additional flashback arrestor.

4.5 CFD Model

In order to investigate ultra-lean combustion, it will be necessary to run the burner at the limits of its operating range. An even flow distribution—and, in the case of configuration 2, thorough mixing of the CH_4 and air feeds—is essential under these conditions, as, for example, local cold spots in the burner could cause the flame to be extinguished. A CFD model was therefore developed to describe the flow pattern of the fluid entering the combustion chamber, in order to verify the suitability of the design in this regard.

4.5.1 CFD methodology

The CFD analysis was performed using the general-purpose commercial CFD code ANSYS CFX 10.0 (ANSYS n.d.). All simulations were performed on an HP xw8400 workstation running Microsoft Windows XP with an available RAM of 3.25 GB.

4.5.1.1 Geometry and mesh

The CAD geometry previously developed in AutoCAD (Figures 4.2–4.6) was simplified and modified using ANSYS DesignModeler (ANSYS n.d.) to prepare it for use in the CFD analysis.

For configuration 1, the components of the burner relevant to the CFD model are illustrated in Figure 4.8, with Figure 4.9 showing the corresponding model domain. Similarly, for configuration 2, the burner components and model domain are shown in Figures 4.10 and 4.11 respectively.

For configuration 1, the model domain is composed of two major regions: a fluid region encompassing the plenum plus the adjoining ends of the heat recuperator tubes, and a porous region representing the three modules of the combustion chamber filled with its packed bed of saddles. An additional porous region, corresponding to the thin layer of flint clay between the plenum and combustion chamber, is also shown, and will be discussed later.

For configuration 2, the model domain comprises a fluid region encompassing the plenum; the ends of the heat recuperator tubes and the CH_4 inlet; and porous regions representing the flint clay layer and an additional layer of cordierite tiles beneath it (see later).

The meshes that were generated from these model domains are shown in Figures 4.12 and 4.13 for configurations 1 and 2 respectively. A mesh composed of 1.4×10^6 elements in total was used for configuration 1 and 1.9×10^6 elements in total for configuration 2. In each case the mesh comprised tetrahedral elements throughout the bulk of the flow, with a thin layer of prismatic elements adjacent to the walls to capture boundary layers.

4.5.1.2 Governing equations

The conservation equations for mass, momentum and energy are given by

Continuity equation:

$$\frac{\partial \rho_g}{\partial t} + \nabla \cdot (\rho_g \mathbf{u}) = 0 \tag{4.1}$$

Momentum equation:

$$\frac{\partial \rho_g \mathbf{u}}{\partial t} + \nabla \cdot (\rho_g \mathbf{u} \otimes \mathbf{u}) = -\nabla p + \nabla \cdot ((\mu + \mu_t)\nabla \mathbf{u}) + \mathbf{S}_m \tag{4.2}$$

Energy equation:

$$\frac{\partial \rho_g E_g}{\partial t} + \nabla \cdot (\rho_g \mathbf{u} E_g) = \nabla \cdot ((k_g + c_p \mu_t / \sigma_t)\nabla T_g) + S_E \tag{4.3}$$

CFX solves the conservation equations using a finite volume method.

4.5.1.3 Physical models and fluid properties

For configuration 1, the fluid was modelled as an isothermal, fixed composition, ideal gas mixture composed of air and CH_4. For configuration 2, the fluid was modelled as a variable composition ideal gas mixture composed of air and CH_4; a heat transfer model that accounted for the transport of thermal energy but not for kinetic energy effects was employed. In each case buoyancy was neglected, turbulence was accounted for using a k-ε model (Launder and Spalding 1974), adiabatic and no-slip conditions were applied at the walls, and a reference pressure of 1 atm was used. The combustion reaction was not considered.

Flow through the porous regions was modelled using an isotropic momentum loss model based on Darcy's law. Table 4.1 gives the properties of each porous region.

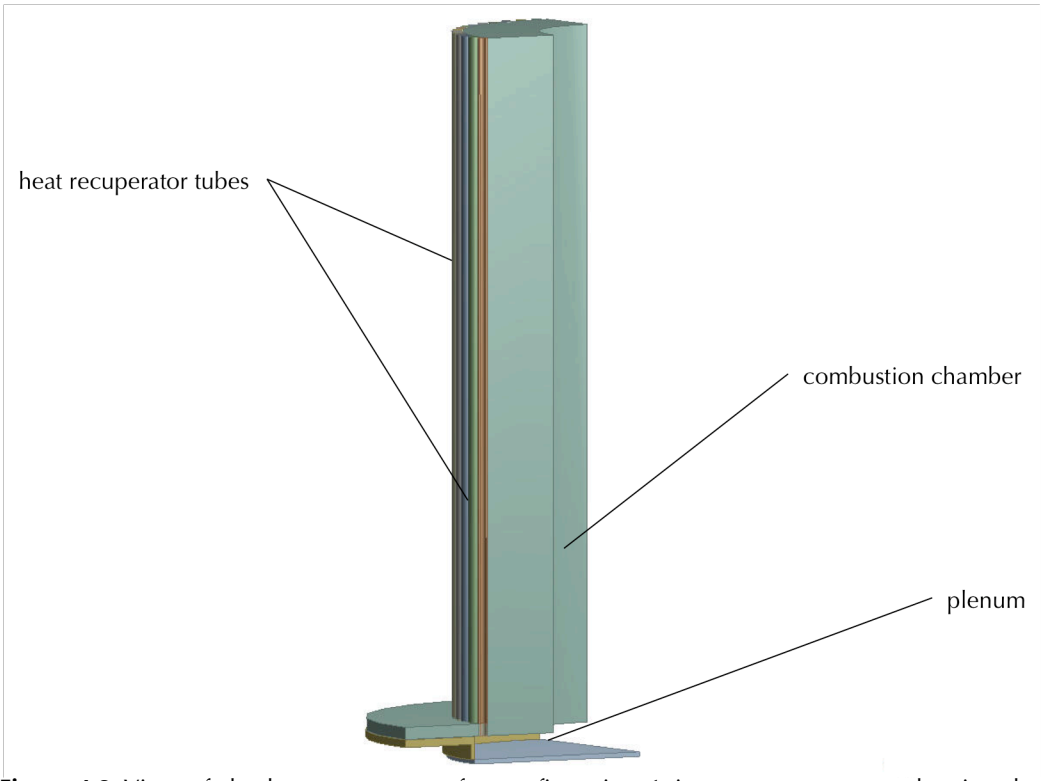

Figure 4.8 View of the burner geometry for configuration 1 in quarter symmetry showing the components to be modelled.

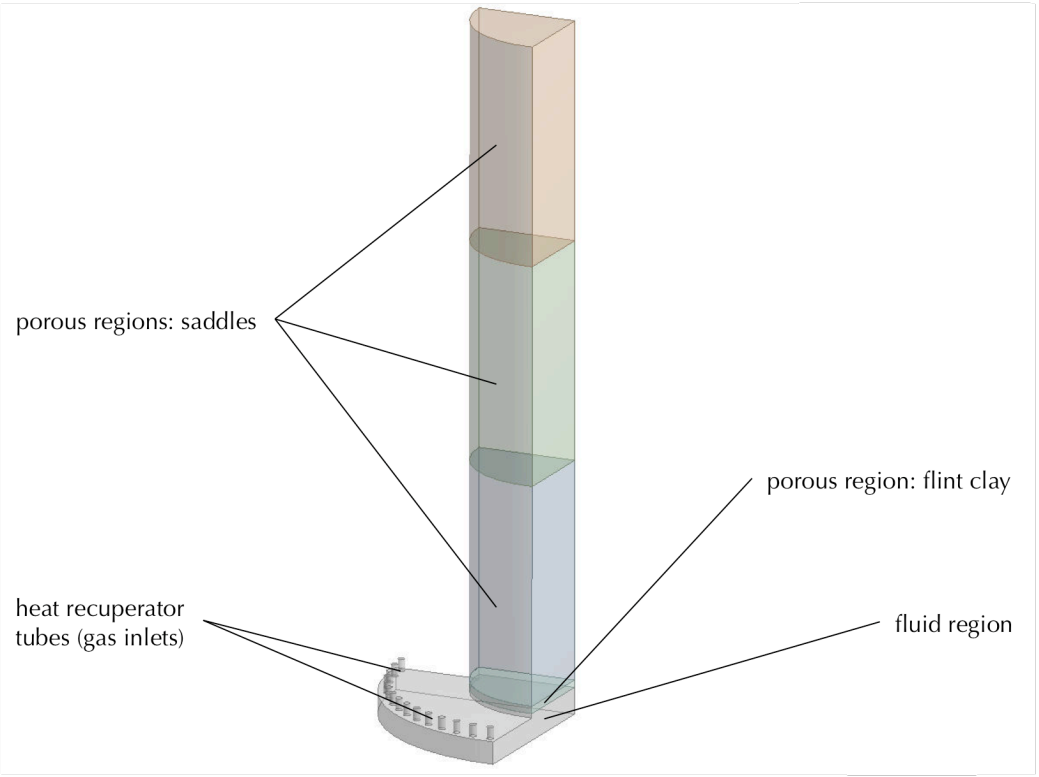

Figure 4.9 View of the burner geometry for configuration 1 in quarter symmetry showing the model domain.

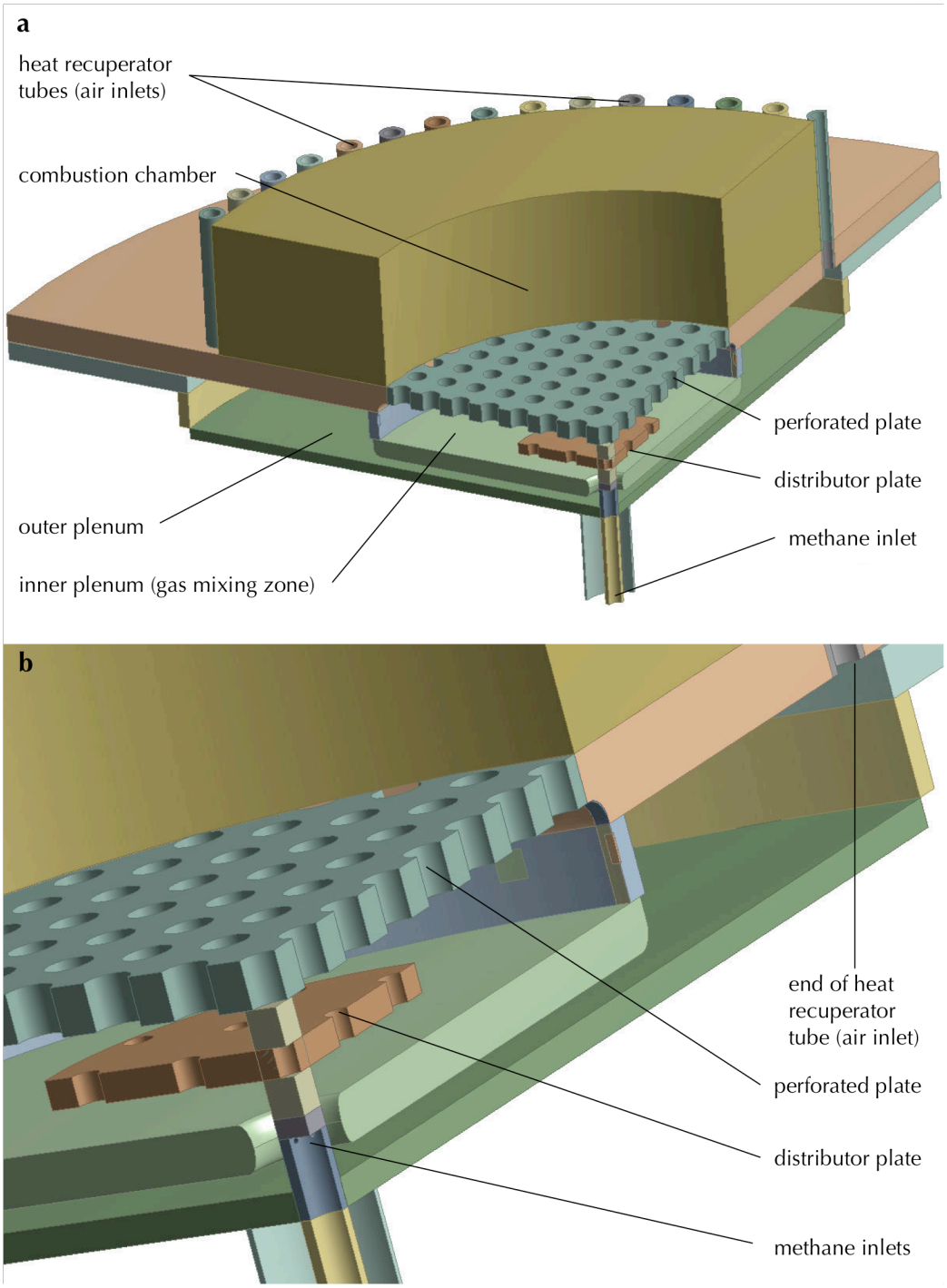

Figure 4.10 View of the burner geometry for configuration 2 in quarter symmetry showing (a) the components to be modelled and (b) a magnified view of the CH_4 inlet and mixing zone.

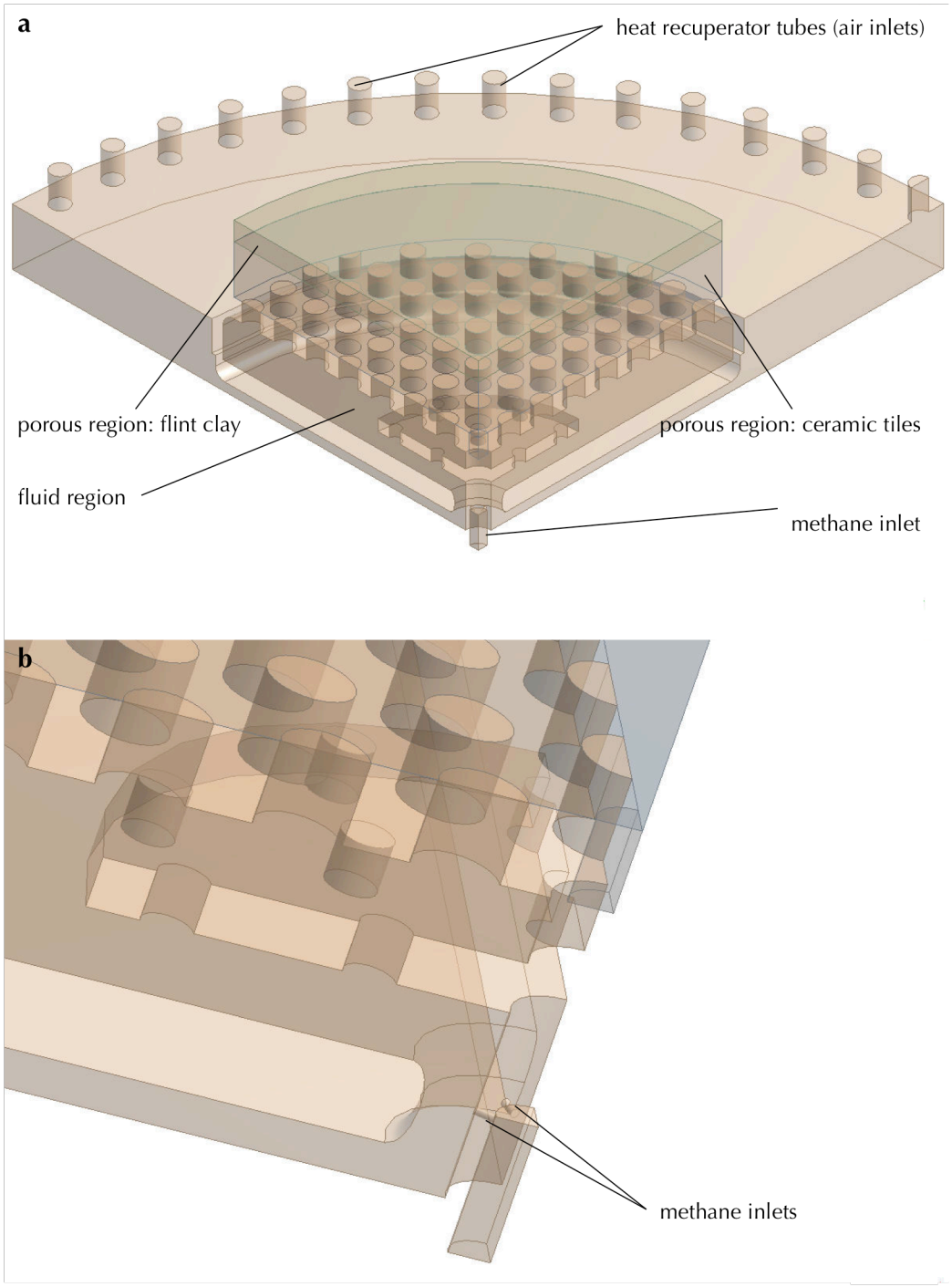

Figure 4.11 View of the burner geometry for configuration 2 in quarter symmetry showing (a) the entire model domain and (b) a magnified view of the CH_4 inlet and mixing zone.

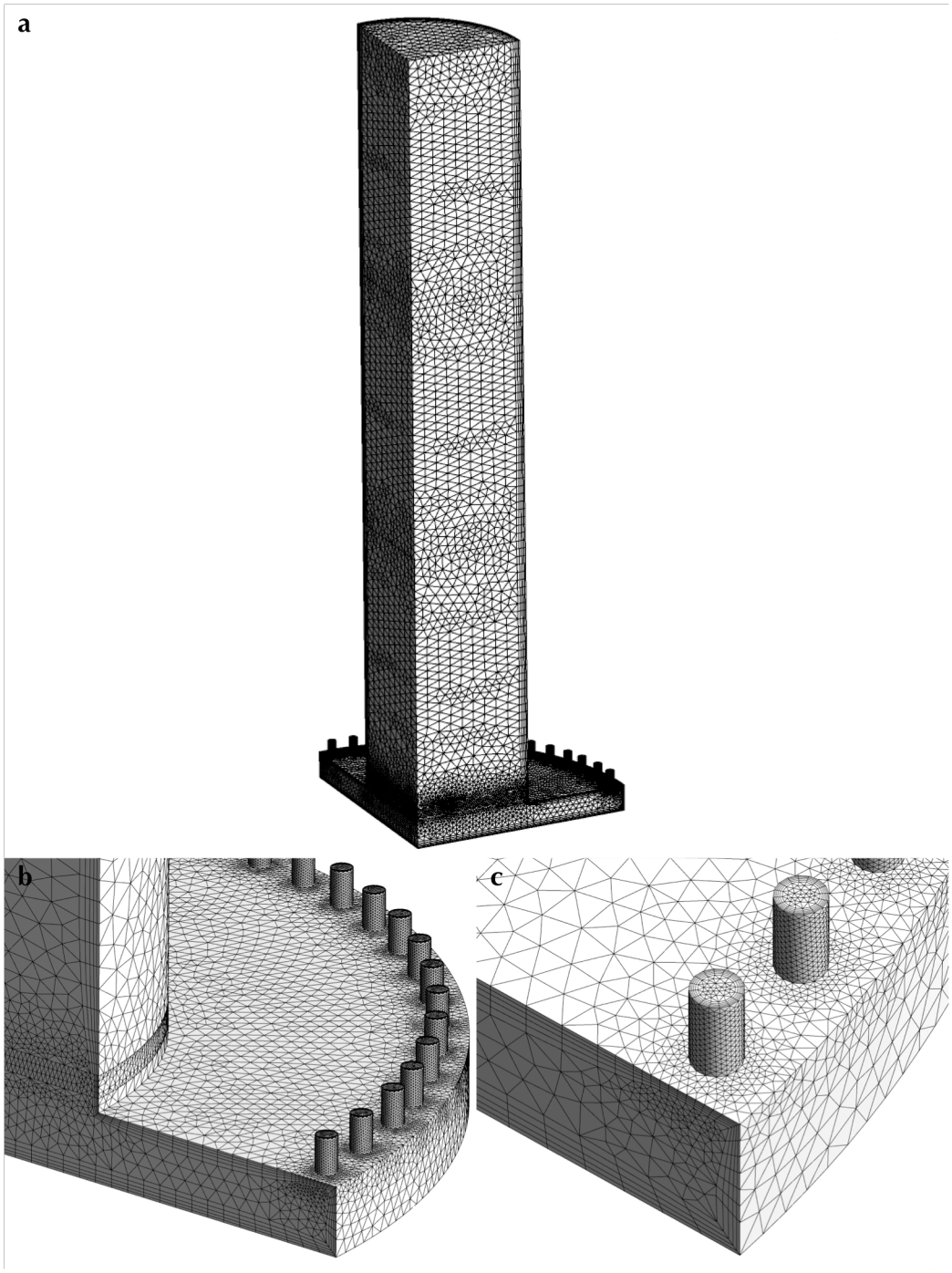

Figure 4.12 View of the mesh for configuration 1 showing (a) the whole mesh and (b) and (c) magnified views of the plenum plus the adjoining ends of the heat recuperator tubes illustrating the dense meshing that was applied in these regions.

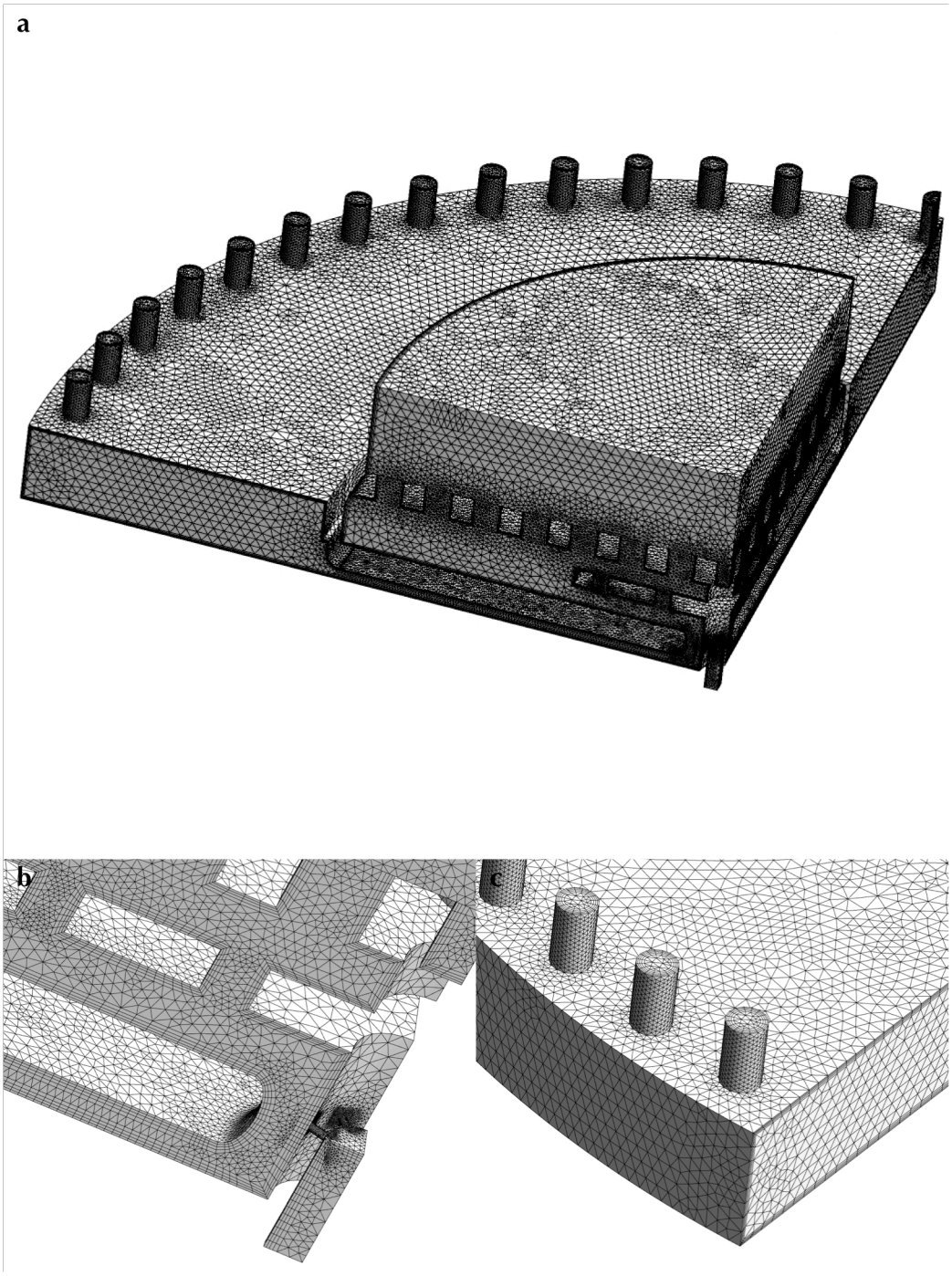

Figure 4.13 View of the mesh for configuration 2 showing (a) the whole mesh and magnified views of (b) the CH_4 inlet and mixing zone and (c) the ends of the heat recuperator tubes, illustrating the dense meshing that was applied in these regions.

Table 4.1 Properties of the porous regions.

Porous material	Porosity Φ (%)[a]	Permeability κ (m^2)[b]
½″ saddles	66	2×10^{-6}
3 mm flint clay beads	48	1×10^{-8}
Cordierite tiles	70	2×10^{-9}

[a] The porosity values are as specified by the manufacturer (RVT Process Equipment n.d.) in the case of the saddles, as previously measured (Lynch 2001) for the flint clay, and as given by García, Miranzo and Osendi (2003) for the cordierite tiles.

[b] The permeabilities were calculated using Darcy's law combined with the Ergun equation for turbulent flow through a packed bed of non-spherical particles, in the manner described by Kay and Nedderman (1985). See appendix B for details.

4.5.1.4 Simulation conditions

Configuration 1. Steady state simulations were performed for a series of cases corresponding to expected burner operating conditions ranging from start-up to ultra-lean, in order to determine the effects of flow rate, CH_4/air ratio and preheat temperature (in other words the preheating provided by the arrangement of external heat exchanger tubes) on the flow distribution. A representative subset of the cases studied is given in Table 4.2.

Configuration 2. Steady state simulations were performed for a limited number of cases, two of which—corresponding to ultra-lean (case A) and start-up (case B) operating conditions—are shown in Table 4.3.

Table 4.2 Summary of cases used to investigate the flow distribution for configuration 1.

Case	CH_4 concentration (vol%)	Mass flow rate (kgh^{-1})[a]	Preheat temperature (K)
A	0.5	30	1000
B	0.5	70	1000
C	0.5	110	1000
D	0.5	150	1000
E	0.1	110	1000
F	1	110	1000
G	5.5	110	1000
H	0.5	110	300
I	0.5	110	650
J	0.5	110	1350

[a] The mass flow rates shown are the total (air plus CH_4) flow rates for the complete burner.

Table 4.3 Summary of cases used to investigate the flow and CH_4 distribution for configuration 2.

Case	CH_4 concentration (vol%)	CH_4 mass flow rate (kgh^{-1})[a]	Air mass flow rate (kgh^{-1})[a]	Air preheat temperature (K)
A	0.5	0.3	114	1000
B	5.5	1	30	1000

[a] The mass flow rates shown are for the complete burner.

As previously discussed, in configuration 2 the CH_4 and air feeds are separate, with mixing of the two only occurring in the plenum immediately below the combustion chamber. The main aim of these simulations was therefore to ensure that complete mixing of the CH_4 and air has occurred before they enter the main porous bed.

4.5.2 CFD results and analysis

4.5.2.1 Configuration 1

The effect of mass flow rate on the flow distribution is demonstrated in Figure 4.14, which shows velocity profiles for a range of flow rates on a horizontal plane 1 cm into the porous bed (in other words just above the entrance to the combustion chamber). To enable comparison between cases, the velocity is expressed in terms of the ratio of the actual velocity to a superficial velocity based on the mass flow rate. It can be seen that in each case the flow pattern produced was uneven, becoming more so as the flow rate increases. Even at the lowest flow rate investigated, where the profile is most uniform, the variation in velocity would be unacceptable for lean burn operation.

For the range of CH_4 concentrations considered, the CH_4/air ratio was not found to have a significant effect on the final flow distribution, as illustrated by Figure 4.15. As before however, an unacceptably poor flow distribution was observed for each of the cases studied.

Figure 4.16 shows the effect of preheat temperature on the flow distribution. Again, an uneven flow distribution was observed for each of the cases investigated (note the difference in scale here as compared with the previous two figures). However, it was found that the preheat temperature had no pronounced effect on the flow distribution, except when there is negligible preheating, as seen in Figure 4.16a (case H in Table 4.2). The unexpected velocity profile obtained for this case is due to the presence of a recirculation zone at the entrance to the combustion chamber. This is demonstrated by Figure 4.17b, which shows a number of streamlines (paths taken by individual fluid particles) initiating from the heat recuperator tubes and flowing through the model domain. For comparison, Figure 4.17a shows an example (case C in Table 4.2) of the streamlines that would otherwise be expected, with the recirculation zone absent.

Previous experience has shown that the addition of a thin layer of a less permeable porous material before the main porous bed serves to even out the velocity profile. Hence an extra porous region, positioned between the plenum and combustion chamber, was added to the model, as shown earlier in Figure 4.9. When the properties of this layer were set to represent a 1 cm thick layer of 3 mm flint clay beads (see Table 4.1), a uniform velocity profile was achieved across the range of conditions studied. This is illustrated by Figures 4.18 and 4.19, which show the velocity profiles (this time on a vertical plane through the first module of the combustion chamber) for cases D and H in Table 4.2 respectively; in other words, under conditions where particularly poor flow profiles were previously obtained. The inclusion of the flint clay was not found to have a significant effect on the overall pressure drop across the burner.

4.5.2.2 Configuration 2

Figure 4.20 shows CH_4 mass fraction profiles on a horizontal plane through the combustion chamber at the exit of the flint clay layer (in other words at the start of the main porous bed of saddles). It can be seen that under start up conditions (Figure 4.20b) the profile is relatively even, with an overall variation in mass fraction of less than 15%. However, under typical ultra-lean conditions (Figure 4.20a) the overall variation is about 30%, which is unacceptably high. Furthermore, referring back to Figure 4.10, which shows the burner geometry, it is apparent that the CH_4 concentration is higher in those areas immediately above the CH_4 inlet pipes. Clearly, the design of the CH_4 distribution system and mixing zone is suboptimal, and would have to be modified if this configuration were to be developed into a working system. Possible modifications might include changing the number and location of the CH_4 inlets, altering the size and vertical location of the distributor plate, modifying the size and arrangement of holes in both the distributor and larger perforated plate, and adjusting the geometry of the inner plenum.

On the other hand, a relatively uniform velocity distribution was obtained for each of the cases studied, as illustrated by Figure 4.21, which shows the velocity profiles on a horizontal plane through the combustion chamber at the exit of the flint clay layer. This would of course be expected, as the model of configuration 2 included not only a 1 cm thick layer of 3 mm flint clay beads, but also an additional porous region representing a layer of cordierite tiles below it.

Figure 4.22 shows both CH_4 and air streamlines and hence demonstrates the flow pattern of both gases through and around the distributor and throughout the mixing zone. This helps to explain the effect of the mixing zone geometry on the final CH_4 distribution and would be useful in optimising the design.

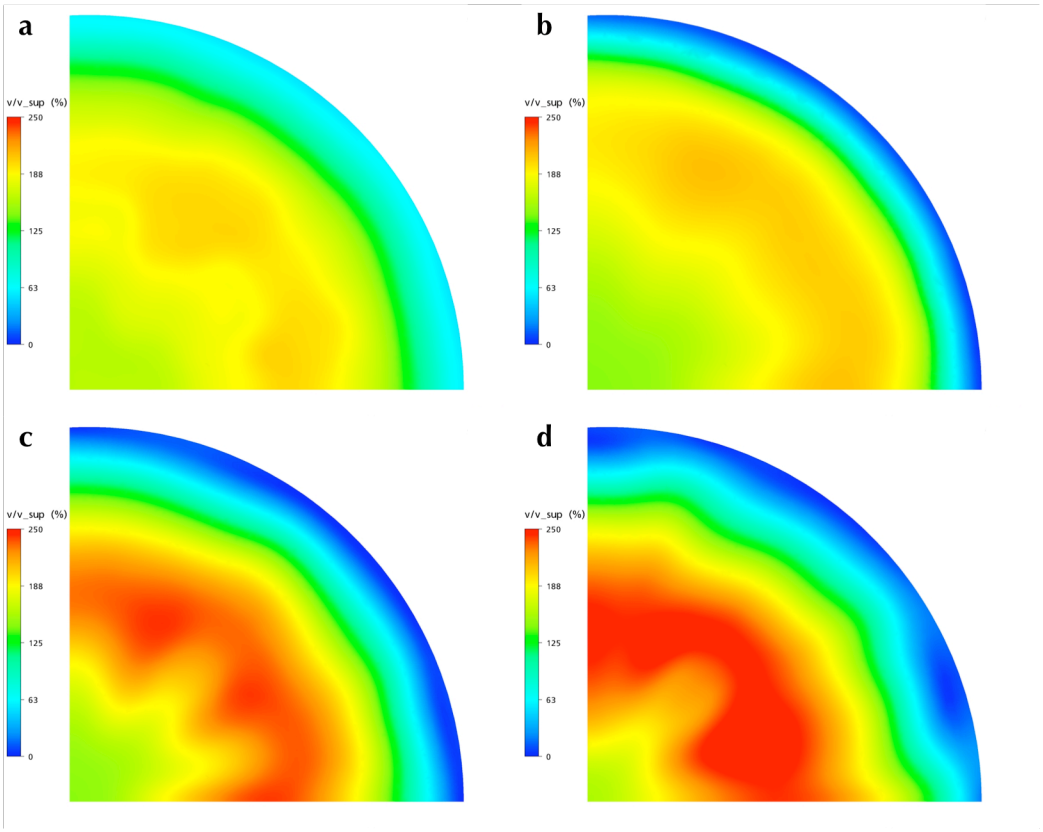

Figure 4.14 Effect of mass flow rate: Velocity profiles (expressed in terms of the ratio of velocity to a superficial velocity based on the mass flow rate) on the horizontal plane 1 cm into the combustion chamber at a CH_4 concentration of 0.5 vol%, preheat temperature of 1000K, and total mass flow rates of (a) 30 kgh^{-1} (b) 70 kgh^{-1} (c) 110 kgh^{-1} and (d) 150 kgh^{-1}. The scale ranges from 0 (blue) to 250% (red).

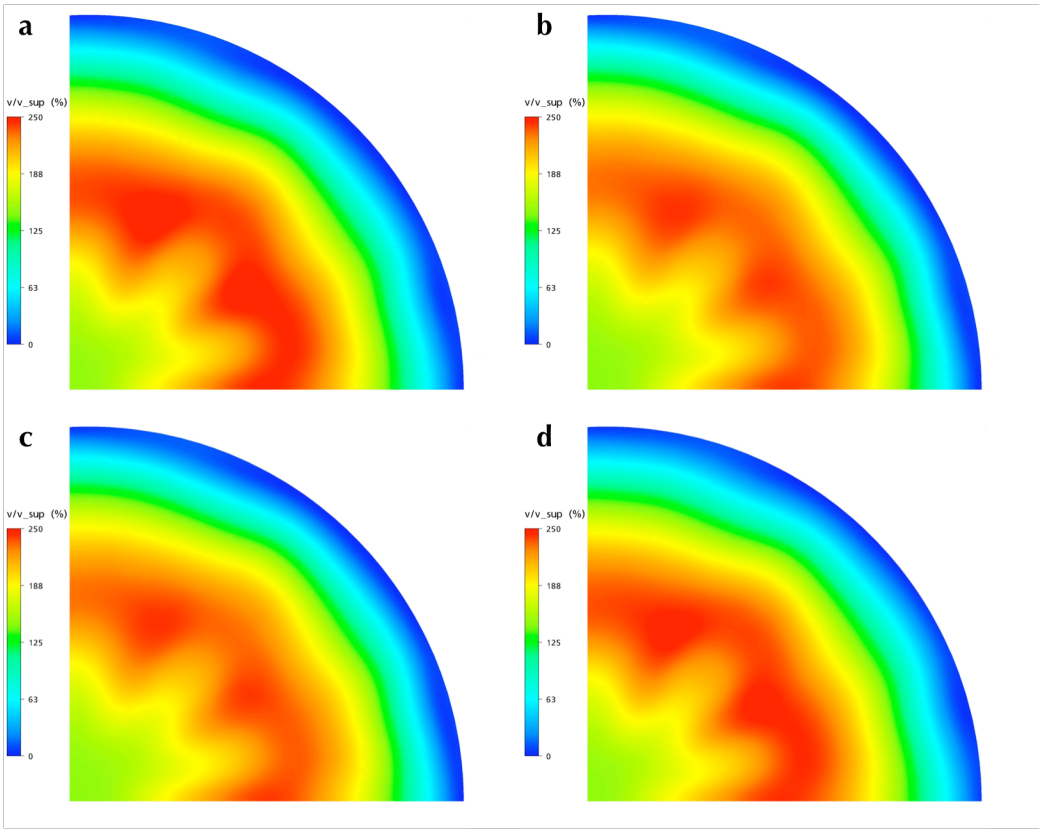

Figure 4.15 Effect of CH_4 concentration: Velocity profiles (expressed in terms of the ratio of velocity to a superficial velocity based on the mass flow rate) on the horizontal plane 1 cm into the combustion chamber at a total mass flow rate of 110 kgh^{-1}, preheat temperature of 1000K, and CH_4 concentrations of (a) 0.1 vol% (b) 0.5 vol% (c) 1 vol% and (d) 5.5 vol%. The scale ranges from 0 (blue) to 250% (red).

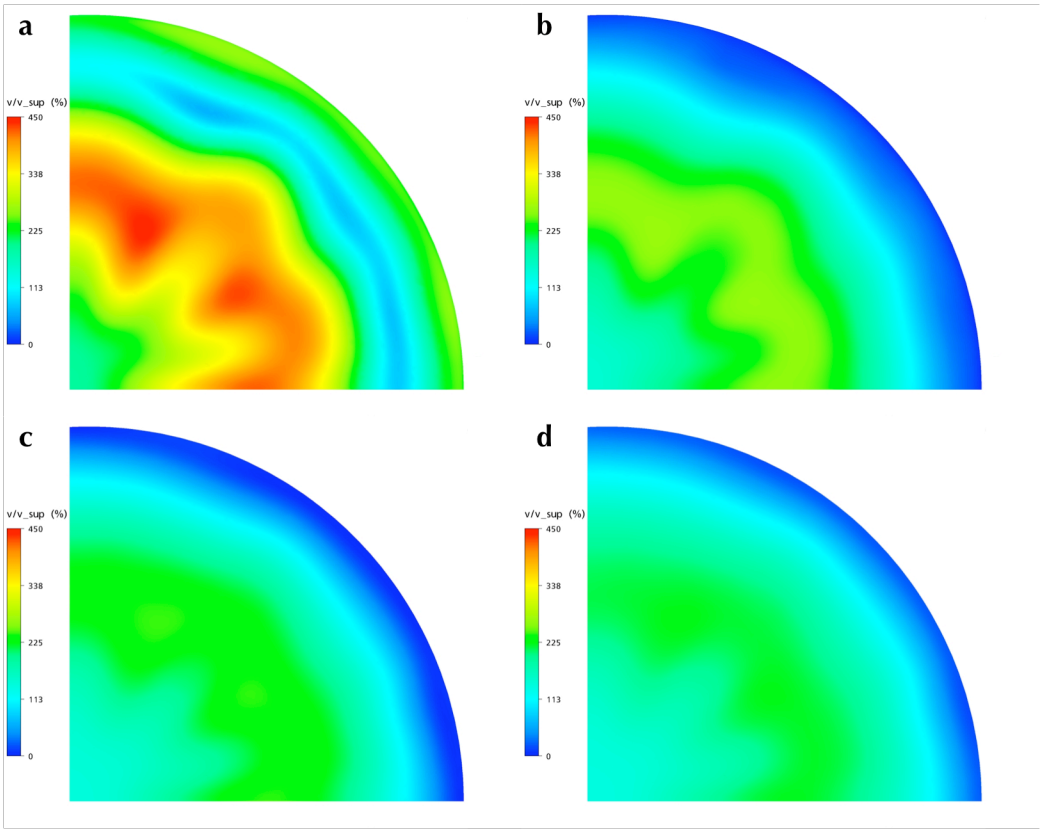

Figure 4.16 Effect of preheat temperature: Velocity profiles (expressed in terms of the ratio of velocity to a superficial velocity based on the mass flow rate) on the horizontal plane 1 cm into the combustion chamber at a total mass flow rate of 110 kgh^{-1}, CH_4 concentration of 0.5 vol%, and preheat temperatures of (a) 300K (b) 650K (c) 1000K and (d) 1350K. The scale ranges from 0 (blue) to 450% (red).

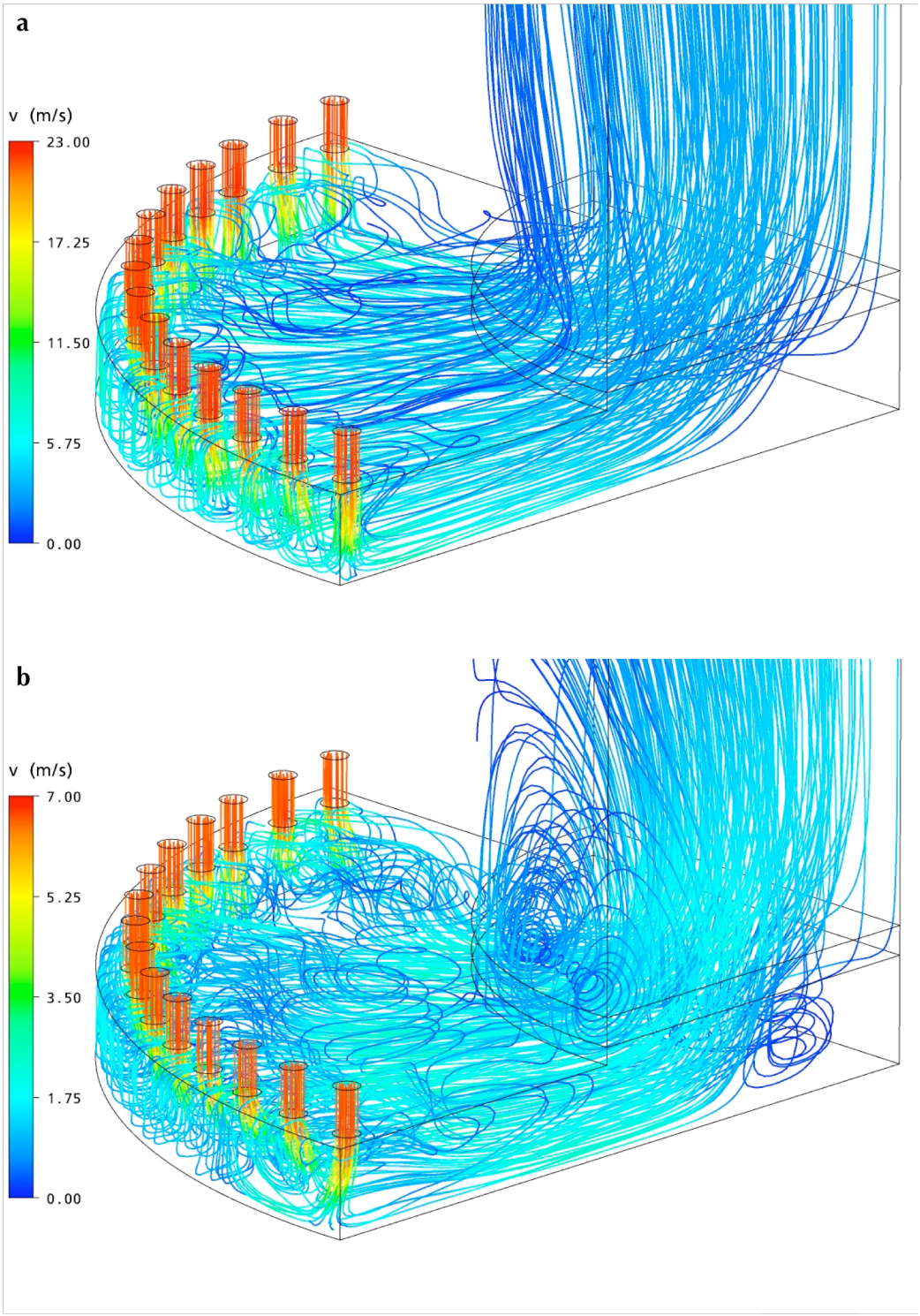

Figure 4.17 Streamlines (paths that fluid particles would take through the model domain) initiating from the heat recuperator tubes for (a) case C and (b) case H in Table 4.2.

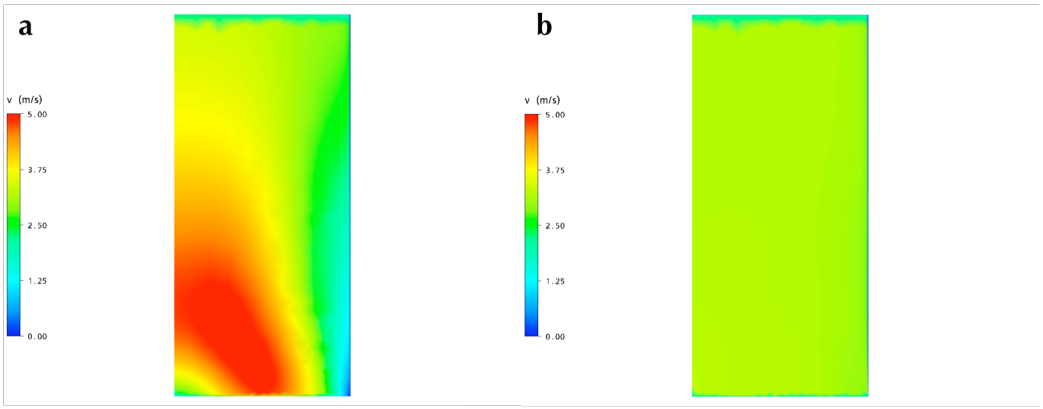

Figure 4.18 Effect of flint clay layer: Velocity profiles for case D in Table 4.2 on the vertical plane of module 1 of the combustion chamber (a) without and (b) with the addition of a 1 cm layer of flint clay. The scale ranges from 0 (blue) to 5 ms^{-1} (red).

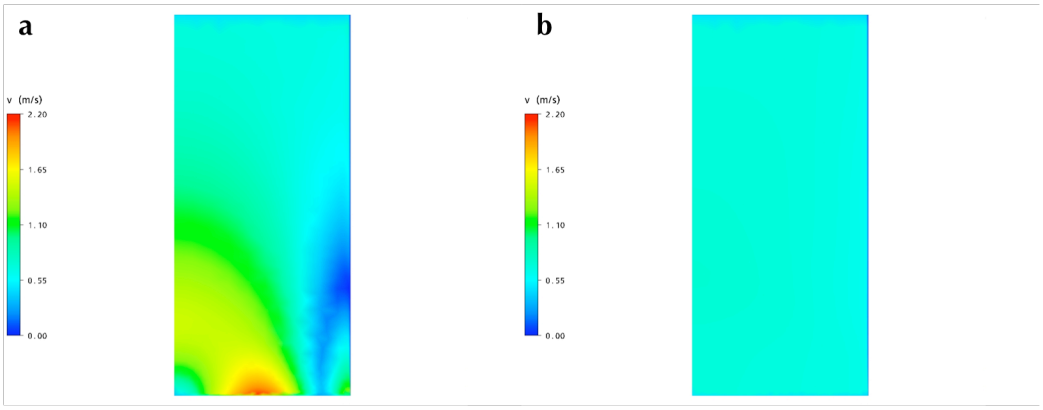

Figure 4.19 Effect of flint clay layer: Velocity profiles for case H on the vertical plane of module 1 of the combustion chamber (a) without and (b) with the addition of a 1 cm layer of flint clay. The scale ranges from 0 (blue) to 2.2 ms^{-1} (red).

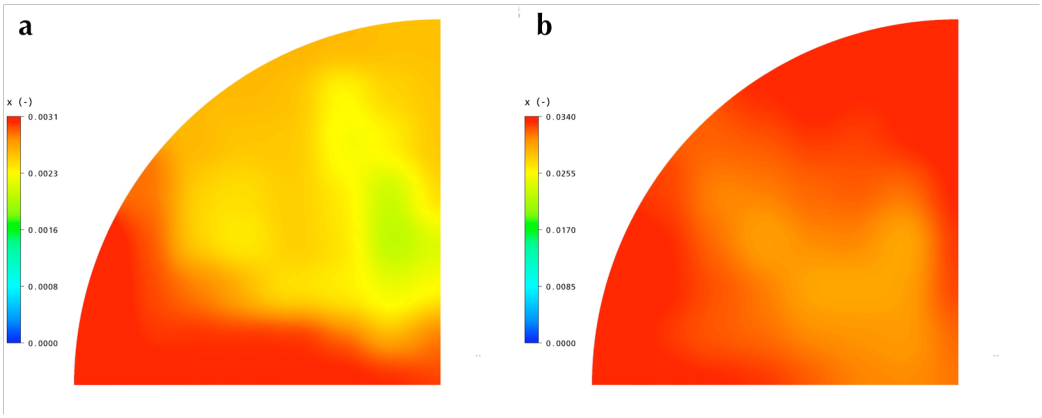

Figure 4.20 CH_4 mass fraction profiles on the horizontal plane at the exit of the flint clay layer for (a) case A (b) case B in Table 4.3. The scale ranges from 0 (blue) to (a) 0.0031 and (b) 0.034 (red).

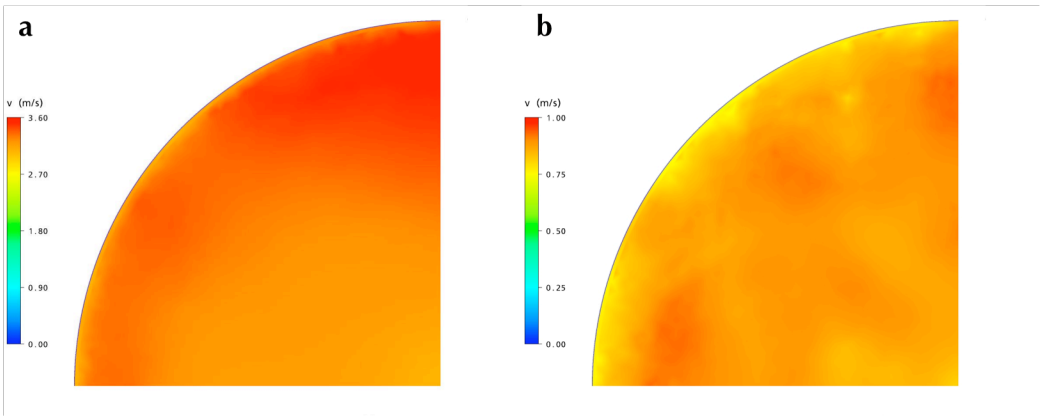

Figure 4.21 Velocity profiles on the horizontal plane at the exit of the flint clay layer for (a) case A (b) case B in Table 4.3. The scale ranges from 0 (blue) to (a) 3.6 ms^{-1} and (b) 1 ms^{-1} (red).

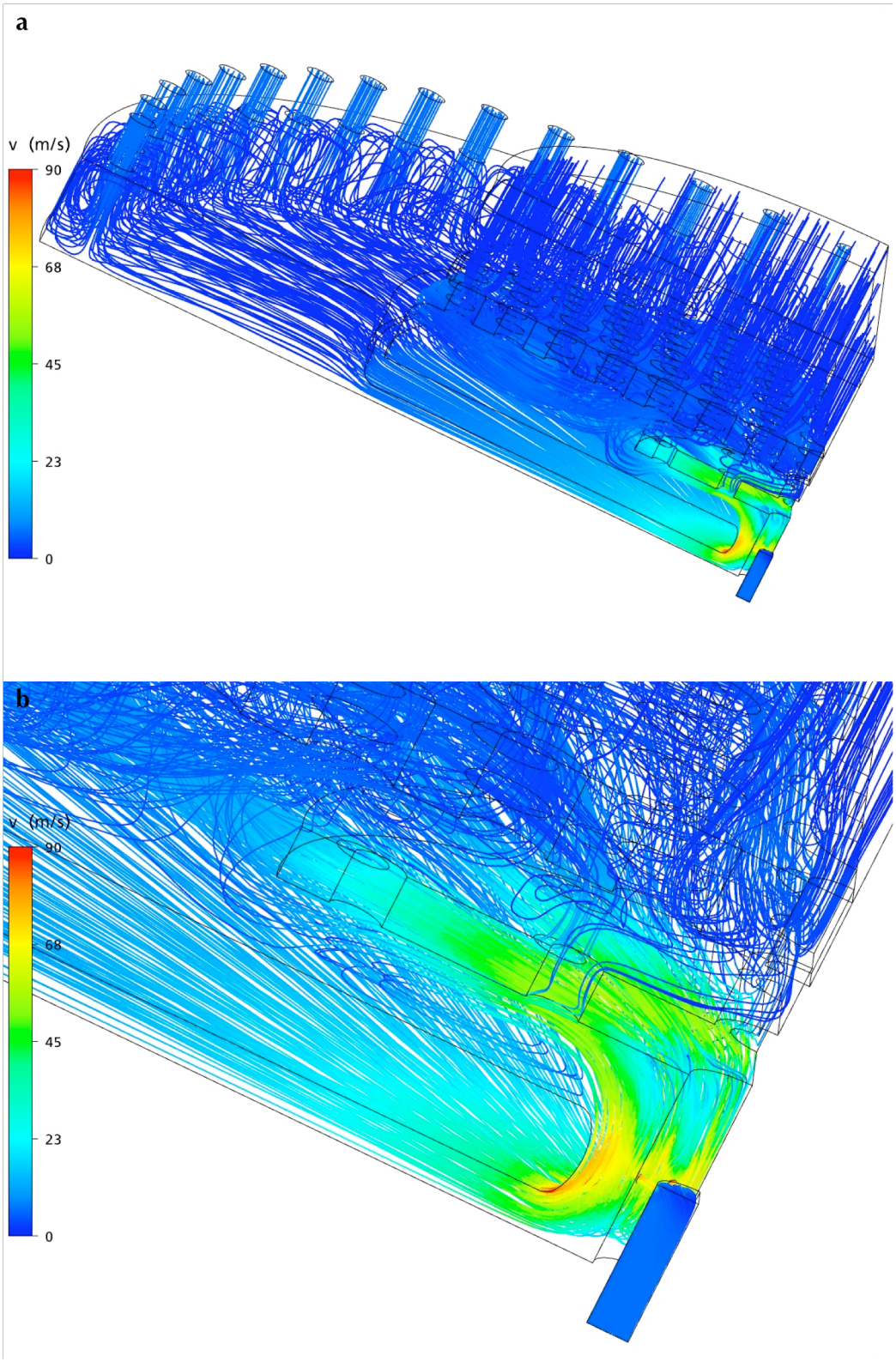

Figure 4.22 Streamlines (paths that fluid particles would take through the model domain) initiating from the heat recuperator tubes and CH_4 inlets for case A (a) over the whole model domain and (b) a magnified view of the CH_4 inlets and mixing zone.

4.6 Construction and commissioning[†]

The burner was constructed in configuration 1, in other words with the CH_4 and air feeds premixed, the rational being that this would in reality be the case for most ultra-lean applications. Should it later become necessary to have an additional CH_4 feed, as per configuration 2, the modular design of the burner means that it would be relatively straightforward to replace the plenum section at the base of the burner with a new section in the alternative, more complex, configuration.

Some images of the burner under construction are shown in Figure 4.23. Figure 4.23a shows the 12 layers of spirals comprising the primary heat exchanger sitting above the combustion chamber. Figure 4.23b shows all three modules of the combustion chamber surrounded by the circumferential tubes of the secondary heat exchanger.

The combustion chamber was manufactured from a standard castable refractory material. The circumferential heat recuperator tubes and the bottom three layers of spirals in the primary heat exchanger—those closest to the heat source—were fabricated from Inconel; stainless steel was used for the remaining heat exchanger spirals.

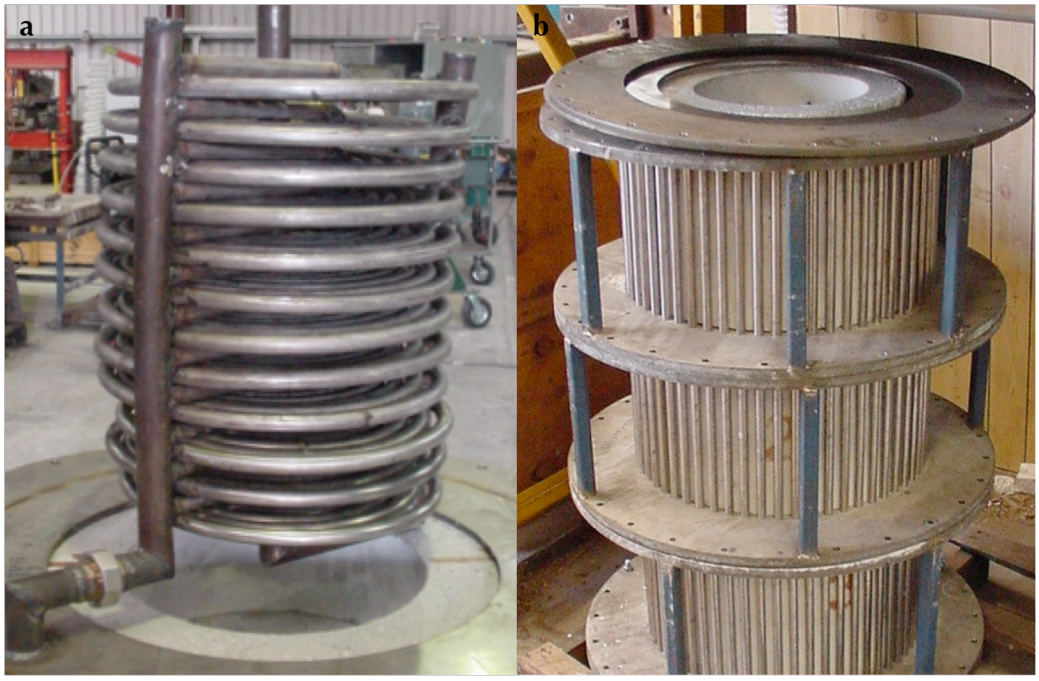

Figure 4.23 The burner under construction: (a) Primary heat exchanger. (b) Secondary heat exchanger (heat recuperator tubes).

[†] Construction of the burner, as well as cold and hot commissioning of the system, was carried out by BEST Energies Australia Pty Ltd (http://www.bestenergies.com).

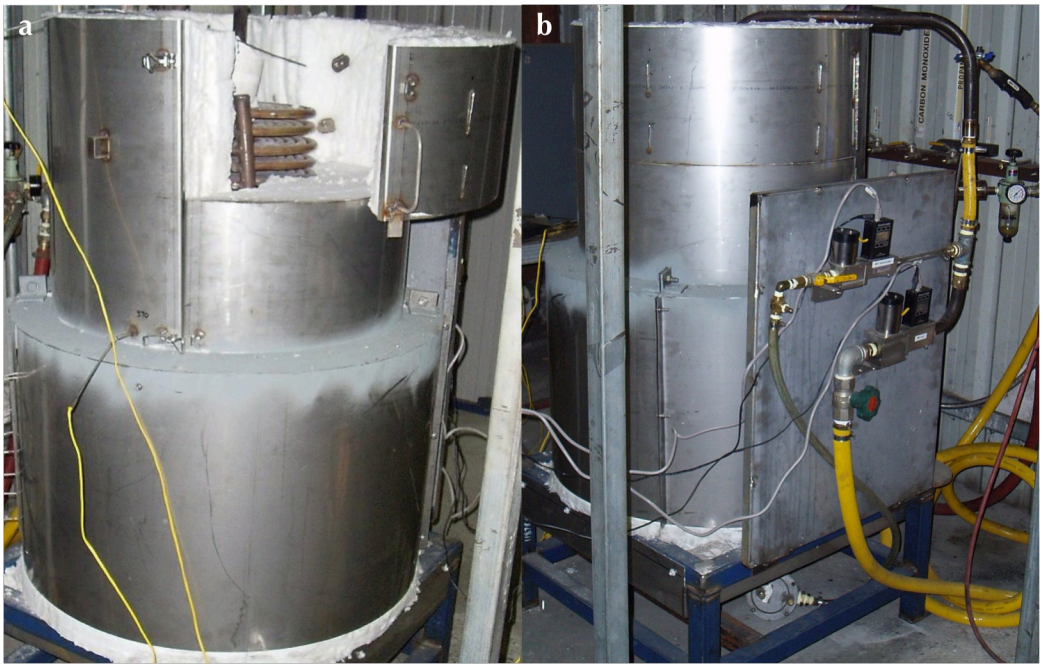

Figure 4.24 The completed burner (a) open to show the primary heat exchanger and (b) in operation.

The completed burner is shown in Figure 4.24. In Figure 4.24a the top of the burner has been opened so that the primary heat exchanger is visible; the alumina fibre insulation that surrounds the burner assembly can also be seen. Figure 4.24b shows the burner in operation.

The valve train, which has been mounted to the front of the burner, can also be seen: this, along with other aspects of the experimental set-up including the ignition, control, instrumentation and data acquisition systems, will be discussed in the following chapter.

Chapter 5

EXPERIMENTAL SET-UP AND PROCEDURE

5.1 Introduction

This chapter describes the experimental set-up for the pilot-scale demonstration of the porous burner system. This includes details of the equipment used for flow measurement and control, temperature measurement, data acquisition, and exhaust gas analysis. The burner operating procedure is also outlined.

5.2 Experimental set-up

The piping and instrumentation diagram (P&ID) of the system is shown in Figure 5.1. Natural gas (NG) is used as the fuel, in place of pure methane (CH_4), both to reduce costs and because real fuels—such as CH_4 emissions—are typically not pure hydrocarbons in any case. The NG feed, which is taken from the mains supply, is mixed with the compressed air feed prior to entering the primary heat exchanger (HX1). Both feeds are filtered to remove moisture. It can also be seen that some NG is drawn from the main line to power a pilot burner. This sits directly above the porous bed of the main burner, as shown in Figure 5.2, and is used to ignite it (see later).

As described in the previous chapter (§4.3), the NG/air mixture flows through HX1, where it is heated by the burner exhaust gases entering from below, as well as via radiation from the porous bed. The preheated gas mixture then proceeds through the secondary heat exchanger (HX2), where it is further heated via convection from the burner walls, before entering the porous burner.

The combustion chamber of the porous burner itself is filled with three layers of porous materials, as described previously (§4.4, and see Figure 5.3): 2.6 cm of burner blocks (cordierite tiles) at the base of the combustion chamber that act as a flashback arrestor, a 1 cm deep packed bed of 3 mm flint clay beads, and an 85 cm deep packed bed of 60% alumina (Al_2O_3) ½" saddles.

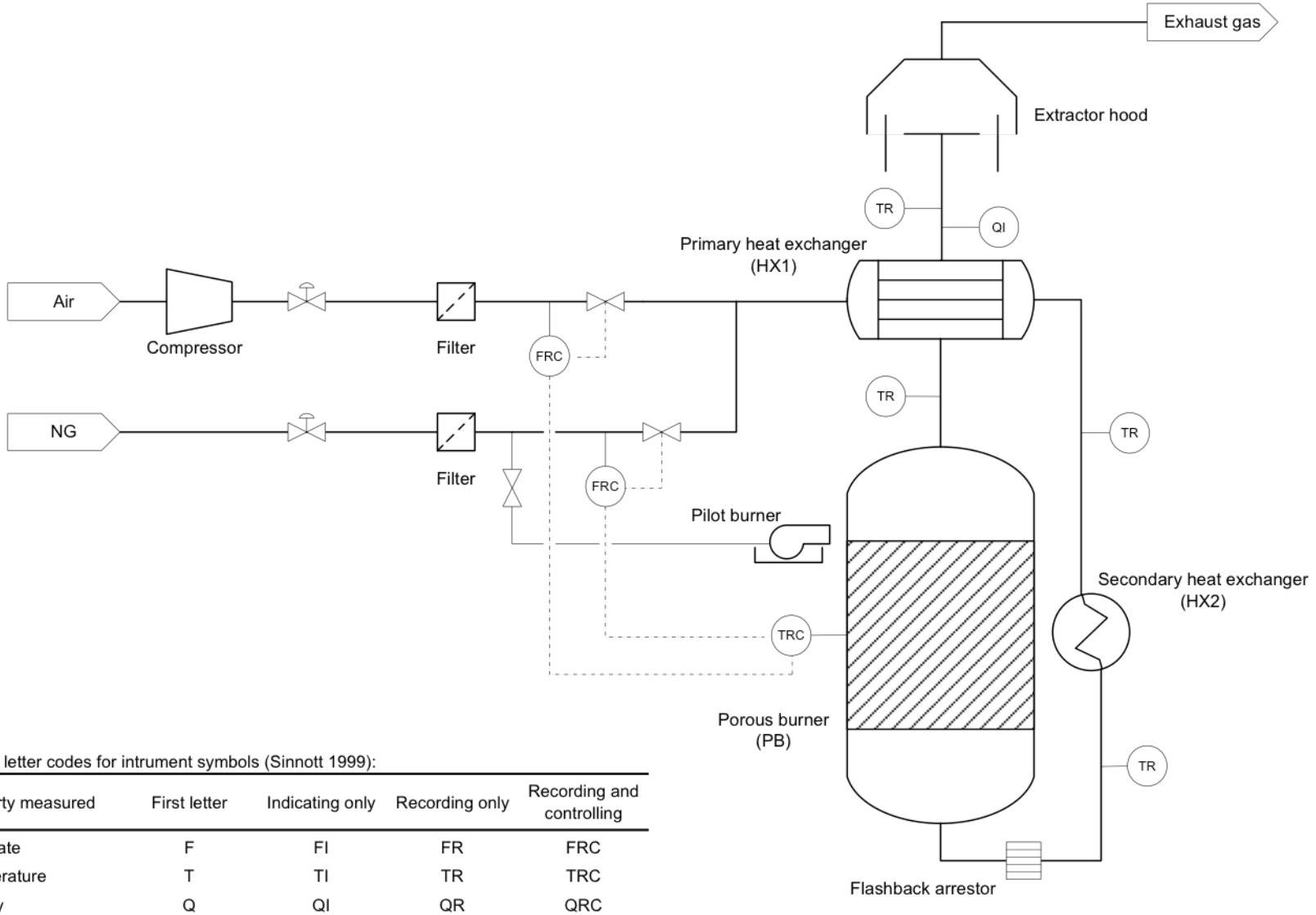

Key to letter codes for intrument symbols (Sinnott 1999):

Property measured	First letter	Indicating only	Recording only	Recording and controlling
Flow rate	F	FI	FR	FRC
Temperature	T	TI	TR	TRC
Quality	Q	QI	QR	QRC

Figure 5.1 Piping and instrumentation diagram (P&ID) of the porous burner system.

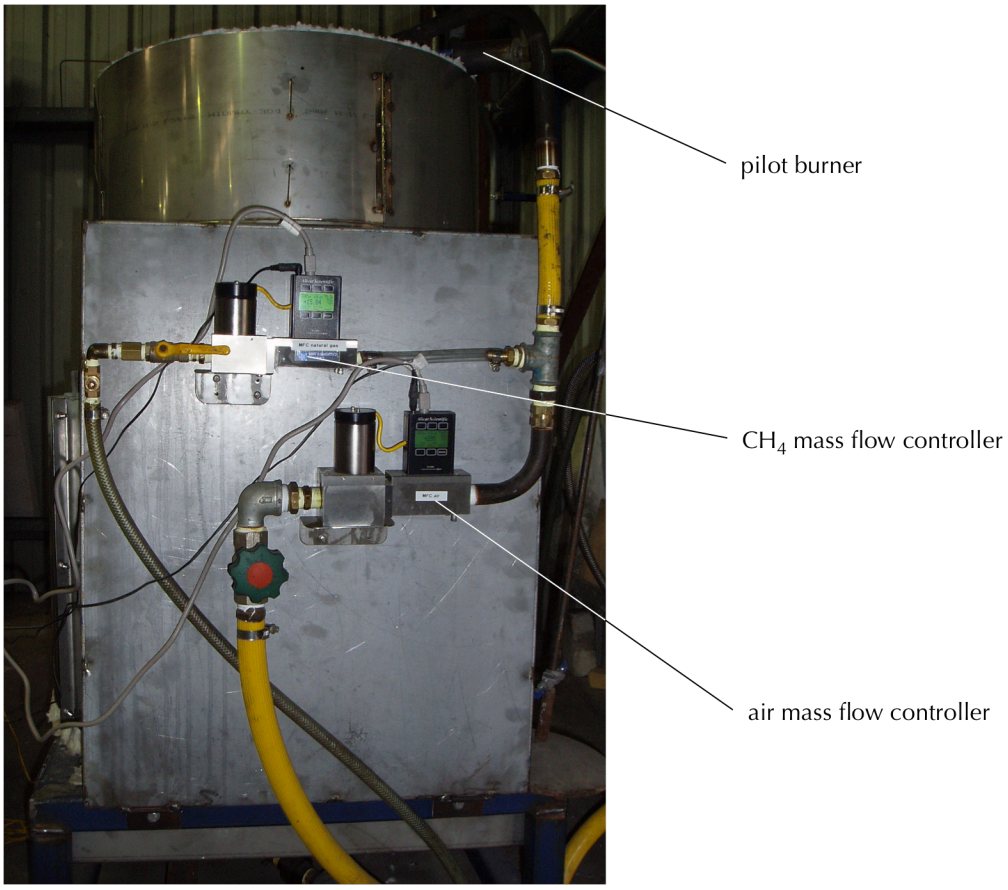

Figure 5.2 The porous burner system, showing the valve train and pilot burner.

The entire assembly is surrounded by Al_2O_3 fibre insulation.

The exhaust gas from the burner passes through HX1, before being released to the atmosphere via an extractor hood.

5.2.1 Flow measurement and control

The air and NG flow rates are each measured and controlled independently via separate mass flow controllers (MFCs), and in addition there are manual shut-off valves on each gas line. Both MFCs are Alicat Scientific MC series devices (Alicat n.d.), which use differential pressure measurements within a laminar flow region to determine the flow rate. The air MFC has a range of 0–1500 slpm—although the practical upper limit in the current system is ~1200 slpm due to the limitations of the air compressor—and the NG MFC a range of 0–50 slpm. The MFCs have an uncertainty of ±0.8% of the reading or ±0.2% of the full range (whichever is the larger). Although NG is being used, the MFC is calibrated for CH_4, so the measured flow rate must be corrected to give the NG flow rate using the formula

$$Q_{NG} = \frac{Q_{CH_4(measured)}\mu_{CH_4}}{\mu_{NG}} \quad (5.1)$$

The flow rates are monitored, logged and controlled using Flow Vision (Alicat's bespoke software package) running on a PC.

5.2.2 Temperature measurement

The temperature throughout the system is measured using an arrangement of thermocouples, the locations of which are shown in Figure 5.3. A series of 14 thermocouples measure the temperature profile along the central axis of the main porous bed, from just above the flint clay layer (TPB01) to the exit of the bed (TPB14). Additional thermocouples (THX1 and THX2) measure the temperature of the gas at the outlets of each heat exchanger, and the temperature of the exhaust gas (TE).

Although not shown in Figure 5.3, the external (outside of the Al_2O_3 fibre insulation) wall temperature (TW) is also measured to determine the extent of heat losses from the system.

Temperatures above 1500K are not expected in the current system; therefore, Inconel 600 mineral-insulated metal-sheathed (MIMS) K-type thermocouples of 3 mm diameter, 550 mm length and each with 3 m of PVC extension cable are used (Temperature Controls n.d.). Thermocouples are suitable for measuring temperatures in porous burners as they are rugged and inexpensive, and capable of being inserted into the porous bed. K-type (chromel versus alumel) thermocouples are a widely used low cost general-purpose thermocouple suitable for measurements in the range 0–1530K, whilst the high nickel alloy Inconel 600 is ideal for use in combustion environments as it has a maximum operating temperature of 1420K (continuous) or 1640K (intermittent) and resists oxidation (ASTM 1993). Magnesium oxide is used as the insulator due to its compatibility with the thermocouple elements and the sheath material, its low cost and its availability. As well as shielding the thermocouple wires from the environment, the MIMS arrangement also protects the thermocouple against possible mechanical damage from the packed bed.

A DataTaker DT600 (DataTaker n.d.), a self-contained data acquisition unit, is used to record the temperature measurements. The DataTaker has an internal temperature sensor, and automatically applies cold junction compensation. The temperatures are monitored and logged using DeLogger (DataTaker's bespoke software package) running on a PC. All temperature measurements are recorded every 30 seconds and the temperature profile in the bed is used to determine when and how to adjust the gas flow rates. In addition, the temperature measured by THX2 is recorded every 5 seconds and monitored to warn of the possibility of flash back.

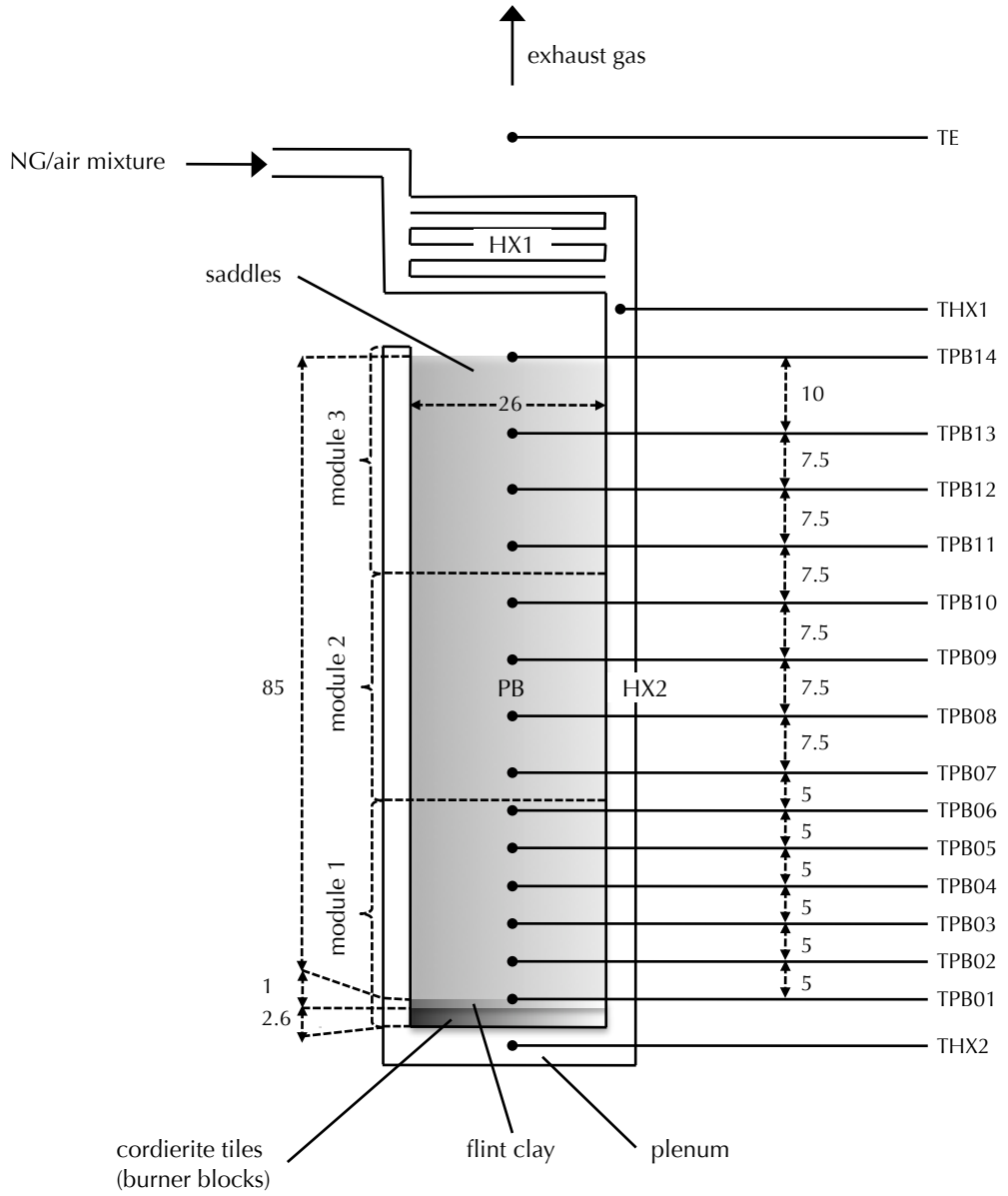

Figure 5.3 Schematic of the porous burner showing selected dimensions, porous materials, and thermocouple locations. All dimensions are given in cm.

K-type thermocouples have a resolution of 0.1K in the temperature range of interest (ASTM 1993). However, the intrinsic uncertainty for MIMS type thermocouples is ±2.2K or 0.75% of the reading (whichever is larger) when new (Jones 2002), and may decline over time (as thermocouples suffer from ageing, especially after prolonged exposure to temperatures at the extremes of their useful operating range). In addition, the uncertainty in the cold junction compensation is ±1.5K (DataTaker n.d.).

These uncertainties are relatively small however, and experimental errors associated with the thermocouple installation are likely to dominate (Nakos 2002). At high

temperatures thermocouples lose heat through convection and radiation, causing the measured temperature to be lower than the true gas temperature. The effect of this can be significant, and if accurate values are required the measured readings must be corrected for these losses. The magnitude of the necessary corrections generally increases as the diameter of the thermocouple, and the velocity of the gas, increases (Sato et al. 1975). Measurements in porous burners have the additional complication of radiant flux *to* the thermocouple from the porous matrix. A comprehensive uncertainty analysis would therefore involve performing an energy balance at the thermocouple tip that accounted for all possible heat losses *and* gains (Jones 2002). It should also be noted that the stated thermocouple locations might not be entirely accurate as the thermocouples may be dislodged from their original positions by the addition of the porous material.

For the current study, the measured temperature profile will be used only as a means of determining if, and where, in the porous bed the flame stabilises. Accurate absolute values for the temperature are not required for this purpose, so no attempt was made to perform the corrections described above, and a full uncertainty analysis is not carried out. It is nevertheless necessary, when analysing the results, to recognise that a large degree of uncertainty in the temperature exists.

5.2.3 Exhaust gas analysis

Analysis of the exhaust gas was carried out using a Scout portable multi-gas monitor (Scott n.d.), which uses electrochemical sensors to measure carbon monoxide (CO) and unburned hydrocarbon (UHC) concentrations. An exhaust gas sample is drawn from a position above HX1 and in line with the central axis of the porous burner, using the sample probe and line provided with the monitor. CO and UHC are the products of incomplete combustion, and are therefore monitored in order to ensure that the combustion process in the porous burner is complete. Significant nitrogen oxide (NO_X) formation is not expected when operating the burner under ultra-lean conditions (§3.2.2.5), and so NO_X levels are not measured. The emissions measurements are corrected to 6% oxygen (O_2) according to the method described by Baukal (2001), to allow for comparison with other systems.

5.3 Experimental procedure

The procedure outlined here was developed via trial and error during commissioning of the burner and found to be effective. A comprehensive step-by-step procedure can be found in Appendix C.

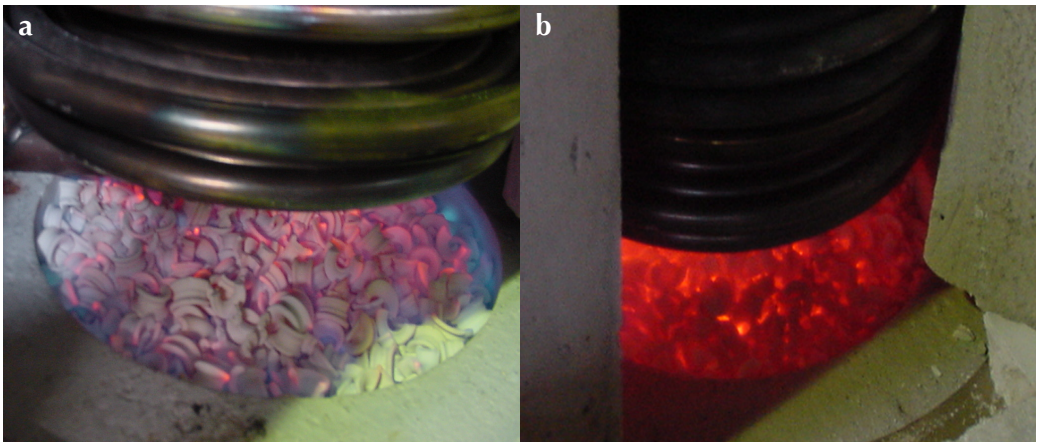

Figure 5.4 The porous bed (a) just after ignition, with a blue flame still visible above the bed and (b) during normal operation.

5.3.2 Ignition

As previously discussed, a small NG-fired pilot burner sits above the porous bed of the main burner. In order to ignite the porous burner, the air and NG flows are set to suitable ignition conditions (Table 5.1) and the pilot burner is switched on.

The gas mixture ignites on top of the porous bed; when the burner casing is opened, a blue flame is visible above the bed (Figure 5.4a). By observing the temperature profile within the porous bed it can be seen that the flame immediately propagates down the combustion chamber and stabilises within the porous bed of saddles, just above the flint clay layer. The temperature at this location (TPB01) is monitored, and once it reaches approximately 1200K, ignition is considered complete and the pilot burner is switched off. The ignition process takes 2–3 minutes.

5.3.2 Warm-up

Once ignition is complete the air and NG flows are set to the warm-up conditions given in Table 5.1. The temperature profile of the porous bed is monitored until the burner has reached the desired operating temperature, which is dependent on the requirements of the particular experiment to be performed.

Table 5.1 Burner operating conditions.

Operating phase	NG concentration (vol%)	Firing rate (kWm^{-2})
Ignition	10.6	500
Warm-up	5.6	500
Normal operation	0.8–4.6	50–300

This process can take up to 2–3 hours (depending on the initial temperature of the bed and the required operating temperature), due to the large thermal mass of the porous bed. At this stage the blue flame is no longer visible above the bed, and the saddles can be seen to glow red-hot (Figure 5.4b).

5.3.3 Normal operation

Once warm-up is complete the air and NG flows are set to the required experimental conditions. The temperature profile of the porous bed is monitored and recorded until it reaches steady-state, or, if the combustion process is not stable (for a given set of conditions), the flame either extinguishes or blows off the top of the porous bed. The range of operating conditions investigated is given in Table 5.1. The behaviour of the porous burner system under these conditions is described in the following chapter.

Chapter 6

EXPERIMENTAL RESULTS AND ANALYSIS

6.1 Introduction

In this chapter results illustrating the behaviour and performance of the pilot-scale porous burner system are presented and discussed.

A series of experiments was undertaken in which burner operating conditions were systematically varied over the range given in the previous chapter (§5.3.3). For each set of conditions, the temperature profile in the porous bed was measured to determine if, and where in the bed, the flame stabilised, and the exhaust gas was analysed to confirm that combustion was complete. It is worth noting here that operating parameters are presented throughout in terms of the natural gas (NG) concentration (vol%) and firing rate (kWm^{-2})[†], which together give a complete description of burner operating conditions.

In the next section the bed temperature profiles are used to demonstrate the behaviour of the burner under different experimental conditions. Burner performance will then be analysed by considering the operating range, thermal performance and emissions profile. The effectiveness of the heat exchanger system will also discussed.

6.2 Temperature profiles

Figure 6.1 illustrates a typical temperature profile (in this case for a firing rate of 300 kWm^{-2} and NG concentration of 2.9 vol%). The complete axial temperature profile for the system is shown: The start of the horizontal axis (-5 cm) corresponds to the temperature of the preheated reactants at the centre of the plenum (thermocouple THX2 in Figure 5.3), and the end of the axis to the temperature of the exhaust gas *after* it has passed through HX1 (thermocouple TE).

[†] All firing rates are based on the lower heating value (LHV) of NG.

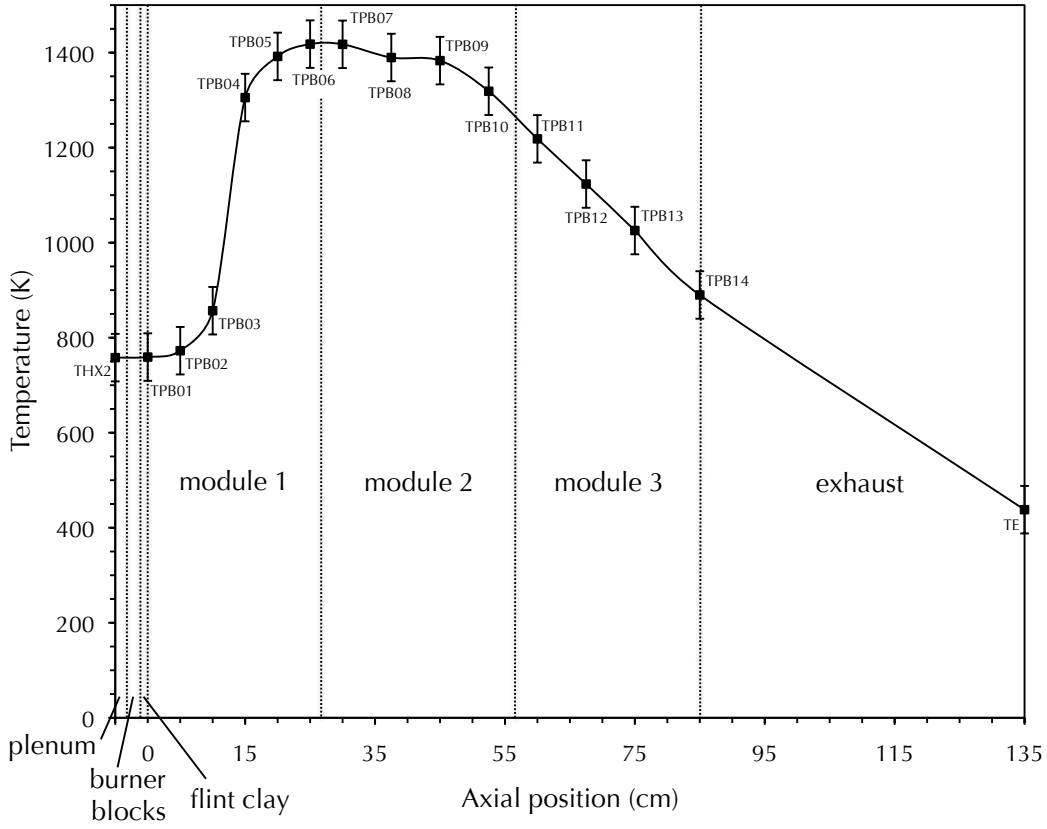

Figure 6.1 Typical temperature profile: Temperature profile with error bars for a firing rate of 300 kWm^{-2}, NG concentration of 2.9 vol% and bed depth of 85 cm (modules 1 to 3).

The locations of the three modules of the combustion chamber are also indicated; note that 0 cm on the horizontal axis corresponds to the start of the main porous bed of saddles (thermocouple TPB01).

The uncertainty in the temperature measurements was estimated to be ±50K based on the accuracy of the equipment (§5.2.2) and the repeatability of the results. The corresponding error bars are shown in Figure 6.1, but for the sake of clarity will henceforth not be included.

It can also be seen from Figure 6.1 that when the flame stabilises downstream from the base of the porous bed (which, as will become clear in the following sections, is the case for the ultra-lean conditions of interest to this study), the temperature measured by THX2 is the same—to within the margin of error for the temperature measurements—as that measured by TPB01. Therefore, again in the interest of clarity, the remaining temperature profiles will include only those measurements taken within the main porous bed itself (thermocouples TPB01 to TPB14).

6.2.1 Stable combustion

The current porous burner system has been designed as a stationary combustion system. This study is therefore concerned primarily with stable combustion, where for a given set of operating conditions the flame is stabilised within the porous bed.

In order to stabilise the combustion process a balance must be achieved between heat recirculation, heat release and heat losses, such that the effective flame speed is equal to the incoming velocity. When the flow velocity is greater than the flame speed the flame will propagate downstream and vice versa.

As previously discussed (§3.2.2.2), when a change occurs in the inlet conditions such that the flame moves downstream, then, if this movement causes an increase in the flame speed, the flame will eventually reach a location where the flame speed again matches the flow velocity, and it will stabilise in that new location.

The requisite increase in flame speed will occur due to the incoming gases being preheated more effectively. As a general rule, in the upstream region of the porous bed the amount of preheating will increase as the flame moves downstream (as less heat will be lost from the upstream end of the burner). It would therefore be expected that stable combustion is likely to occur in this region. In the downstream region by contrast, as the flame moves further downstream the increase in preheating will be offset by increased heat losses from the downstream end of the burner.

The situation is more complex in the current system due to the presence of the external heat exchangers (HX1 and HX2 in Figure 5.1). These recover heat from the burner to supplement the preheating provided by the internal heat recirculation within the porous bed. Depending on the effectiveness of the heat exchanger arrangement, heat 'losses' from the porous bed are not necessarily heat losses from the system.

The following sections examine how burner configuration (the number of modules present) and operating parameters affect the temperature profiles. All profiles are for stable combustion and were recorded once the temperature in the porous bed had reached a steady-state condition.

6.2.1.1 Effect of bed depth

Figure 6.2 illustrates the effect of the depth of the porous bed on the temperature profile. Temperature profiles for the burner with a single module (a bed depth of 25 cm) and all three modules (a bed depth of 85 cm) in place are compared. A firing rate of 300 kWm^{-2} and NG concentration of 4.6 vol% were used in both cases.

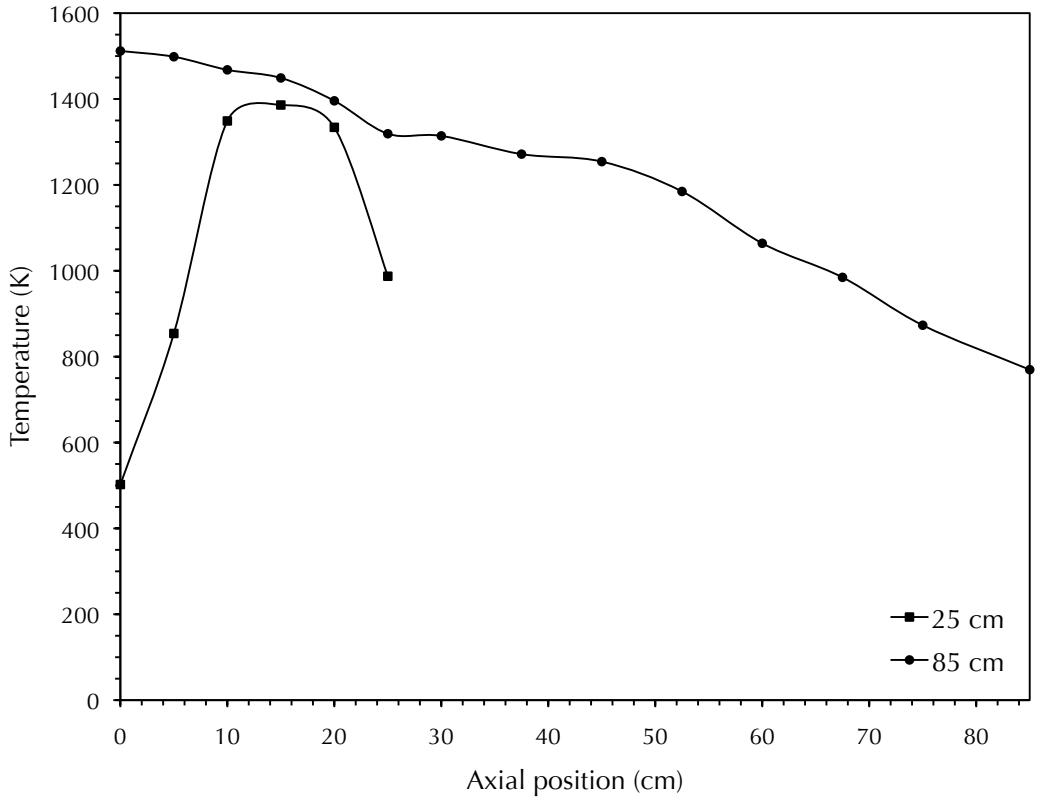

Figure 6.2 Effect of bed depth: Temperature profiles for bed depths of 25 and 85 cm (corresponding to module 1 only and modules 1 to 3 respectively), at a firing rate of 300 kWm^{-2} and NG concentration of 4.6 vol%.

For the deeper bed, for these operating conditions, it can be seen that the flame stabilises at the base of the bed (at the interface between the flint clay and saddles)[†]. Under the same conditions, with the shallower bed depth, the flame stabilises further downstream, near the middle of module 1, and the maximum temperature is lower.

It became clear after initial experiments that it was difficult to stabilise ultra-lean mixtures with only a single module present: the lowest NG concentration at which stable combustion could be obtained was 3.5 vol%, only a modest extension of the lean limit. As this study is primarily concerned with the ultra-lean region, it was decided that experimental effort would focus on the burner in the three-module configuration. Consequently, only limited experiments were carried out using a single module.

[†] The material properties—particularly the small pore size—of the flint clay (§4.4), the fact that no indications of flashback were observed in the course of the experiments, and previous observations of interface-stabilised flames by other researchers (§3.4.2), suggest that the flame stabilises at the interface between the flint clay and the saddles. However, as the temperature within the flint clay was not measured, it is impossible to state conclusively that this is the case. It is possible that the flame actually stabilises—or at least that significant preheating occurs—within the flint clay layer itself.

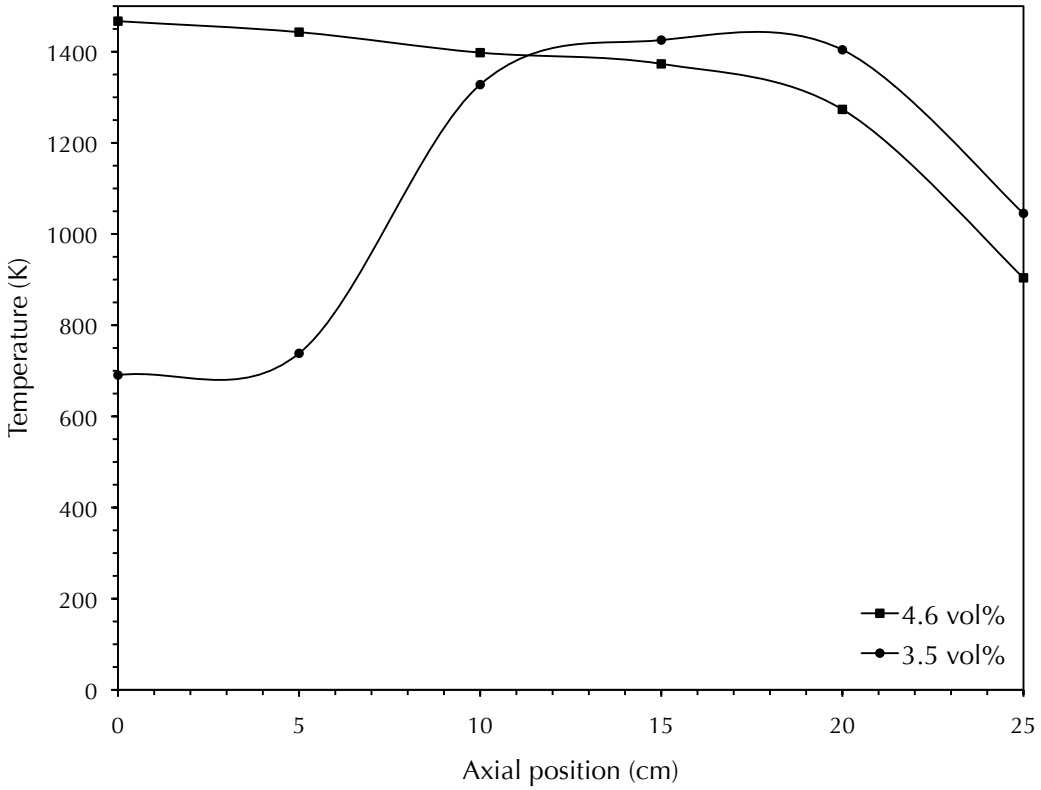

Figure 6.3 Effect of NG concentration: Temperature profiles for NG concentrations of 4.6 and 3.5 vol%, at a firing rate of 250 kWm^{-2} and bed depth of 25 cm (module 1 only).

6.2.1.2 Effect of natural gas concentration

In order to determine the effect of NG concentration on burner behaviour, the concentration was varied whilst keeping the firing rate constant. Figures 6.3 and 6.4 provide examples of the results thus obtained.

Figure 6.3 compares the temperature profiles at NG concentrations of 4.6 and 3.5 vol% for a firing rate of 250 kWm^{-2} with only a single module present. It can be seen that at a concentration of 4.6 vol% the flame stabilises at the base of the main porous bed (for this firing rate). At the lower concentration the combustion zone was observed to migrate downstream, eventually stabilising around the centre of the bed, as shown by the temperature profile. The maximum temperature is approximately 50K lower at 3.5 vol%, although this is within the margin of error for the temperature measurements.

Similarly, Figure 6.4 compares the temperature profiles when all three modules are in place and at a higher firing rate of 300 kWm^{-2} for NG concentrations between 2.9 and 4.6 vol%. Again, it can be seen that the flame is located at the base of the porous bed at 4.6 vol%. On reducing the concentration to 3.5 vol% the flame moves away from the base of the bed slightly and stabilises approximately 5 cm downstream.

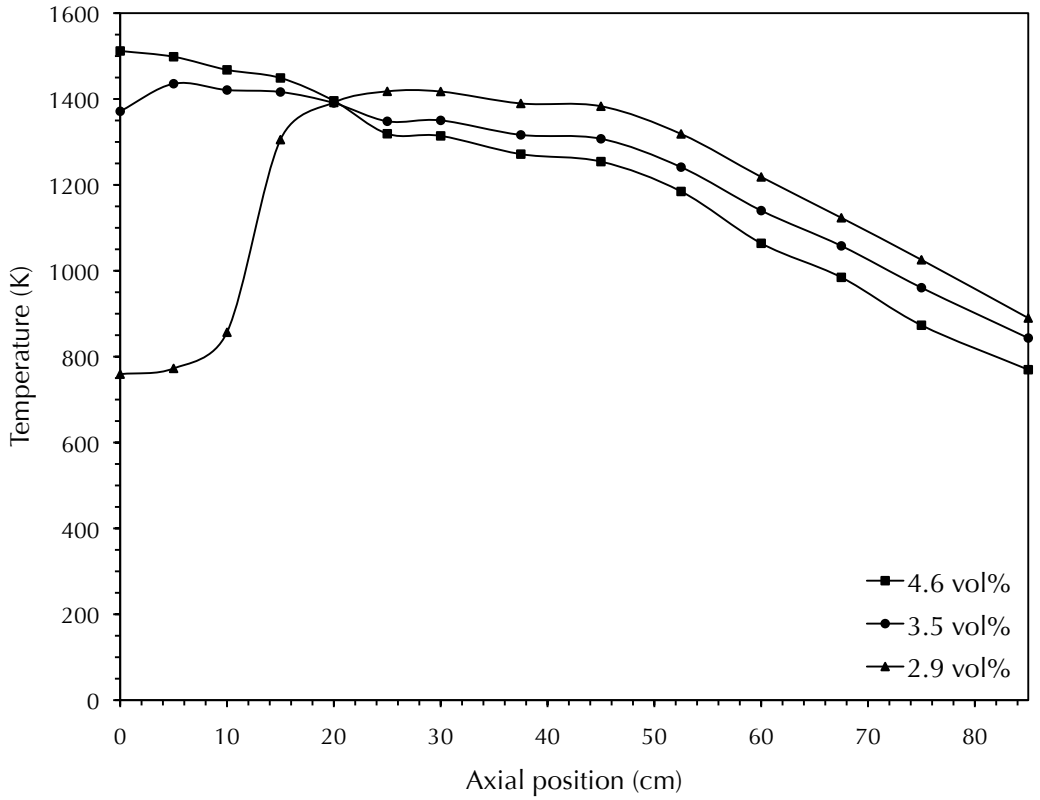

Figure 6.4 Effect of NG concentration: Temperature profiles for NG concentrations of 4.6, 3.5 and 2.9 vol%, at a firing rate of 300 kWm^{-2} and bed depth of 85 cm (modules 1 to 3).

On lowering the concentration further, to 2.9 vol%, there is a more significant movement downstream to a new stable location near the end of module 1.

There is also a reduction in the maximum temperature (of approximately 100K over the full range of concentrations shown) as the concentration is reduced. These results are typical of the behaviour observed on reducing the NG concentration: as a general rule, a decrease in NG concentration causes the flame to stabilise further downstream.

According to the description of the flame stabilisation process given above, because a decrease in NG concentration results in a corresponding decrease in flame speed, the flame must move downstream in order for the flame speed to increase (due to more effective preheating) so that it once again matches the flow velocity. This behaviour matches that observed in a number of other experimental studies (as discussed in §3.2.2.2).

The lowest NG concentrations for which combustion could be stabilised were 3.5 vol% and 2.3 vol% for bed lengths of 25 and 85 cm respectively.

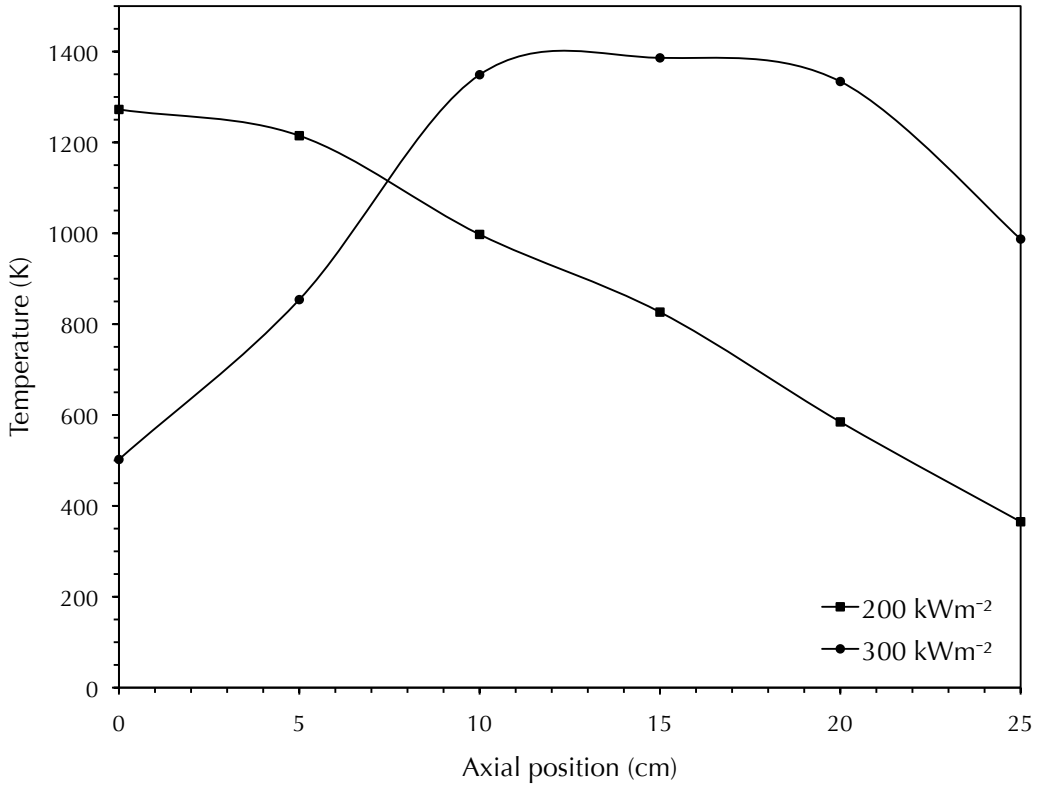

Figure 6.5 Effect of firing rate: Temperature profiles for firing rates of 200 and 300 kWm^{-2}, at a NG concentration of 4.6 vol% and bed depth of 25 cm (module 1 only).

6.2.1.3 Effect of firing rate

To determine the effect of firing rate on burner behaviour, the firing rate was varied whilst keeping the NG concentration constant. A selection of the results obtained is given in Figures 6.5 and 6.6.

Figure 6.5 compares the temperature profiles at firing rates of 200 and 300 kWm^{-2} at a NG concentration of 4.6 vol% for a single module. It can be seen that at the lower firing rate the flame stabilises at the base of the main porous bed (at this concentration). As the firing rate is increased the flame moves downstream, eventually stabilising near the centre of the bed.

Likewise, Figure 6.6 compares temperature profiles with all three modules present, at a NG concentration of 3.5 vol%, for firing rates of 150 and 300 kWm^{-2}. It can be seen that at a firing rate of 150 kWm^{-2} the combustion zone is located at the base of the porous bed. On increasing the firing rate to 300 kWm^{-2} the flame moves away from the base of the bed and stabilises around 8 cm downstream.

In general, it was observed that an increase in firing rate causes the flame to stabilise at a location further downstream of the inlet.

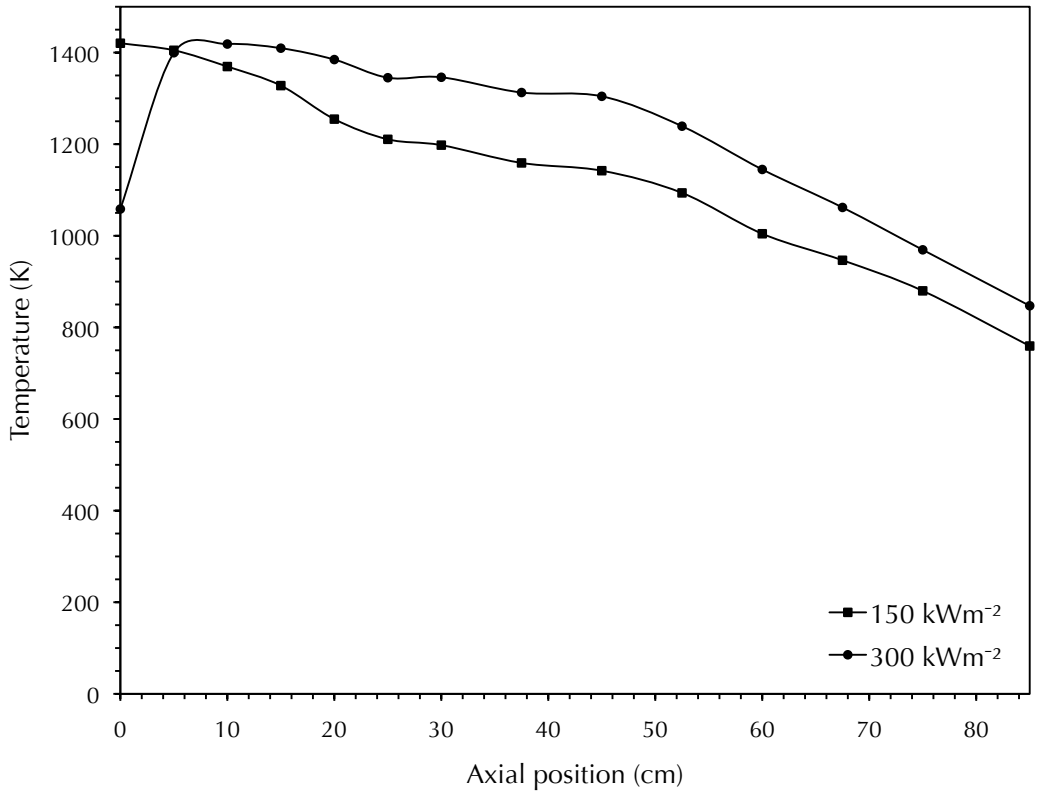

Figure 6.6 Effect of firing rate: Temperature profiles for firing rates of 150 and 300 kWm^{-2}, at a NG concentration of 3.5 vol% and bed depth of 85 cm (modules 1 to 3).

When the firing rate is increased while keeping the NG concentration constant, the flow velocity must by definition increase. The flame therefore moves downstream in order for the amount of preheating—and hence flame speed—to increase, until it reaches a location where the flame speed is again equal to the flow velocity. Again, this behaviour concurs with that observed by other researchers (§3.2.2.2).

6.2.2 Transient combustion

It was shown in the previous section that reducing the NG concentration causes the flame to stabilise at a location further downstream of the inlet. If the NG concentration is decreased further, a point will be reached beyond which the flame will not stabilise, and steady-state will never be reached. The combustion zone will continue to propagate downstream and eventually blow off the top of the porous bed. This is known as the transient ('filtration') combustion regime.

Figure 6.7 illustrates transient combustion. It shows a sequence of temperature profiles recorded over a period of 5 hours for a firing rate of 100 kWm^{-2} on reducing the concentration to 2.3 vol%. It can be seen that the combustion zone slowly migrates downstream.

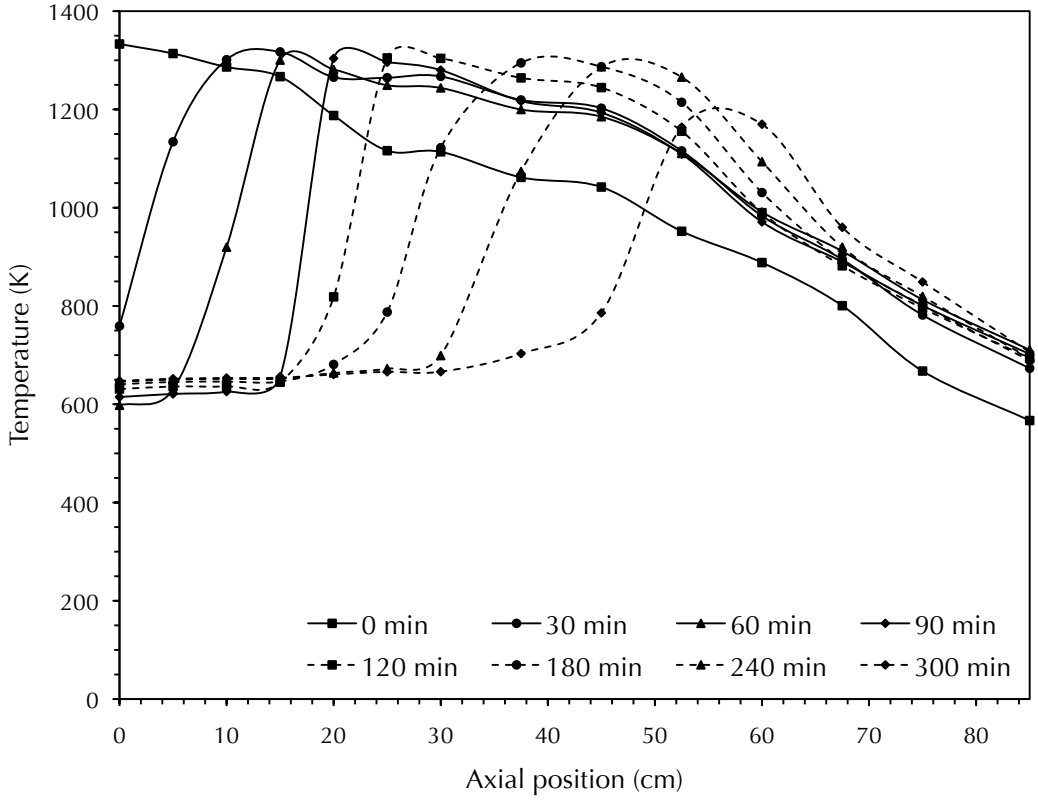

Figure 6.7 An example of transient combustion: Variation in temperature profile over time for a firing rate of 100 kWm^{-2}, NG concentration of 2.3 vol% and bed depth of 85 cm (modules 1 to 3).

Once it reaches the third module of the combustion chamber the temperature in the flame zone starts to drop due to heat losses from the downstream end of the porous bed. After this point the velocity of the combustion wave increases and soon afterwards blowoff occurs.

The velocity of the combustion wave in the above example is approximately 0.05 mms^{-1}, and across all the conditions investigated was in the range 0.04 to 0.1 mms^{-1}. This places it in what is commonly identified as the low-velocity filtration combustion regime (defined as where the combustion wave velocity is under 1 mms^{-1}), as would be expected for the current case where there is significant heat transfer between gas and solid. The combustion wave velocity was observed to increase with increasing firing rate or decreasing NG concentration. In all cases the combustion wave travelled with ('co-flow') the flow of the incoming gas: this is in agreement with what has been observed in previous studies under ultra-lean conditions (§3.2.2.3).

It is worth noting that the pattern of migration of the flame zone seen in Figure 6.7 is the same as that observed for those cases of stable combustion where the flame stabilises away from the base of the porous bed. The difference being that instead of blowing off, the combustion wave eventually reached a location at which it was stable

and came to a halt. Indeed, the slow response time of the burner to changes in operating parameters, and the low velocity of the combustion wave, as shown in Figure 6.7, made it difficult in practice to determine the boundary between the stable and transient regimes. A period of 3–5 hours was typically required to determine whether or not the flame would eventually stabilise under a particular set of conditions. A beneficial outcome of this same behaviour is that the process appears stable against short-term fluctuations in the firing rate or NG concentration, although this was not investigated systematically.

6.2.3 Path-dependency of temperature profiles

Another interesting feature of the system is the apparent path-dependency of the flame location. This is most easily illustrated by means of an example. Both Figures 6.4 and 6.6 show temperature profiles along the porous burner for the same set of experimental conditions: bed depth of 85 cm, firing rate of 300 kWm^{-2} and NG concentration of 3.5 vol%. In Figure 6.4, the temperature profile is that obtained on reducing the NG concentration from 4.6 vol% to 3.5 vol% whilst keeping the firing rate constant, whereas in Figure 6.6, the temperature profile is that measured on increasing the firing rate from 150 kWm^{-2} to 300 kWm^{-2} whilst keeping the NG concentration constant. It can be seen that the two profiles are different: In Figure 6.4 the flame is located approximately 5 cm into the porous bed, whereas in Figure 6.6 it is located another 3 cm downstream.

The behaviour illustrated by this example was found to be typical of burner operation. It appears that the flame location cannot be predicted solely from the current experimental conditions, and that for a given set of conditions there can be more than one steady-state flame location. It is conjectured that the temperature profile obtained under a given set of conditions is dependent not only on the *current* conditions, but also on the history of the system and the *path* by which those conditions are approached. That is, in order to predict the current flame location, it is also necessary to know the *previous* state of the system (experimental conditions and flame location) and, by inference, which parameter (NG concentration or firing rate or both) is being altered, and whether or not that parameter is increasing or decreasing. This path-dependency—or hysteresis—of the system is an interesting topic that certainly warrants further research.

6.3 Burner performance

Burner performance is typically characterised in terms of operating range, thermal performance and emissions profile. This study is primarily interested in the stable operating range of the system, and in particular the amount by which the lean flammability limit can be extended.

6.3.1 Operating range

The stable operating range of a burner is defined as the range of firing rates and NG concentrations over which stable and complete combustion can be achieved. This is most clearly illustrated by means of a burner map, as shown in Figure 6.8 for the current system. The region of interest, the stable ultra-lean combustion regime, is highlighted.

The transient combustion/blowoff regime is also labelled. In the case of very lean mixtures and at low firing rates the temperature in the burner is not sufficient for the flame to sustain itself and extinction occurs, and this is also indicated on the burner map. In previous studies the phenomenon of flashback was also observed. This is essentially the opposite behaviour to blowoff, with the flame leaving the porous bed via the upstream end. Probably due to the use of ultra-lean mixtures, flashback was not encountered in the current system.

From the experimental data points marked on the burner map, it can be seen that this is by no means a comprehensive description of the burner. As well as the intrinsic stability limits of the combustion process, there were constraints imposed on what data could be collected by the experimental design and set-up. First, as the current investigation is concerned with ultra-lean combustion, only limited experiments were carried out above the lean flammability limit, and stoichiometric and rich conditions were not considered. Second, data were not obtained at high NG concentrations and firing rates (the top right hand corner of the burner map) due to concerns about the integrity of the burner blocks and the subsequent risk of flashback at the elevated temperatures that would be obtained under these conditions. Also, the maximum operating temperature of the K-type thermocouples is 1640K. Finally, experiments could not be run at low concentrations and high firing rates due to the limited capacity of the air compressor.

Figure 6.9 provides an alternative version of the burner map, with the total (air plus NG) flow velocity plotted as a function of NG equivalence ratio (ϕ). This is a common method of describing burner operation by researchers in certain disciplines, and is included so that the reader may easily compare the performance of the current system with that of other porous burners described in the literature.

It can be seen from Figures 6.8 and 6.9 that the stable lean flammability limit for the porous burner system is 2.3 vol% (ϕ = 0.24). This is a considerable extension of the conventional lean limit of a free flame for NG of 4.3 vol%. Operating in the transient combustion regime allows the lean limit to be reduced further still, to 1.1 vol% (ϕ = 0.11).

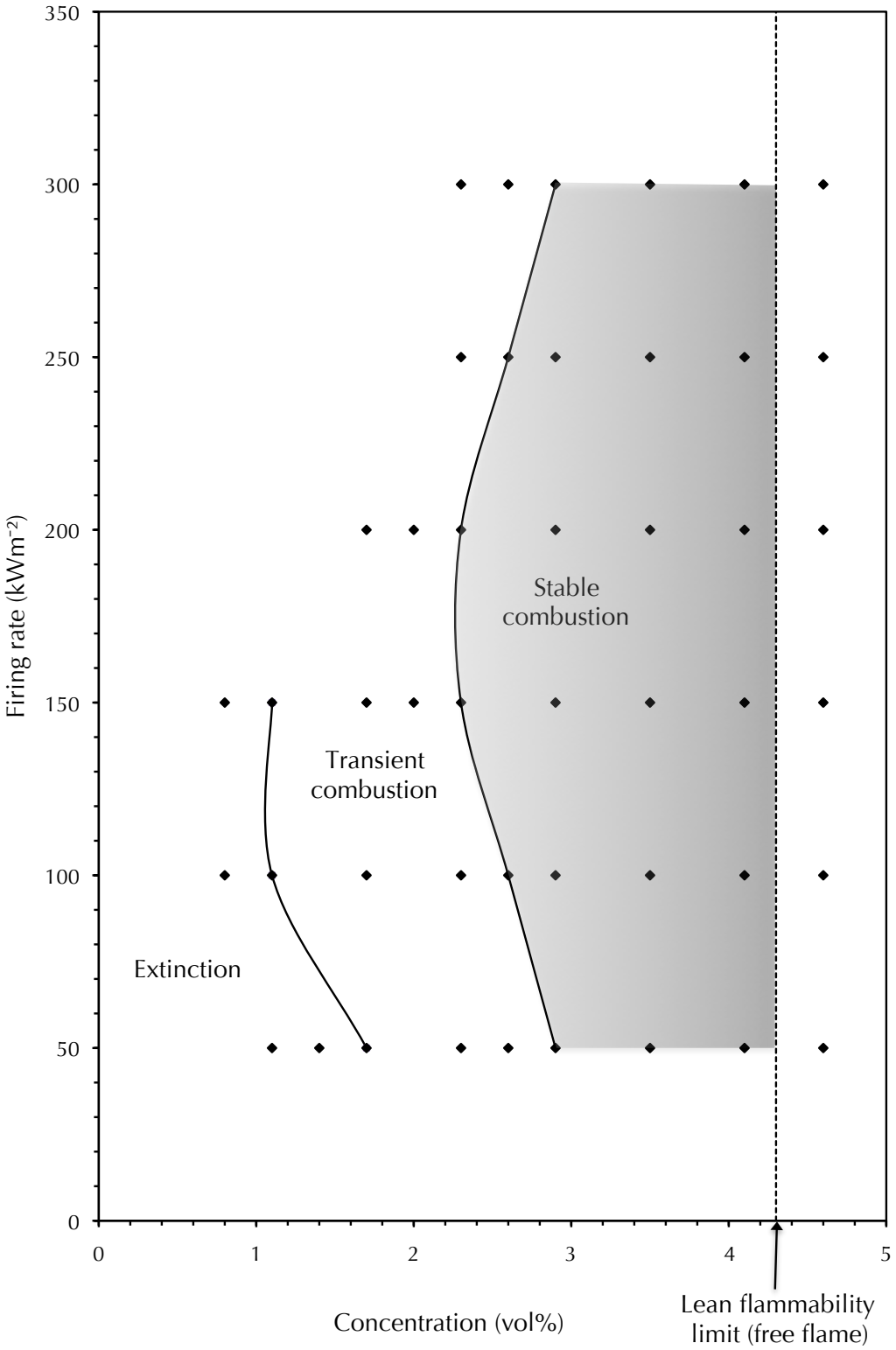

Figure 6.8 Burner map of the porous burner system presented in terms of NG concentration and firing rate. Data points are marked and the stable ultra-lean combustion region is highlighted.

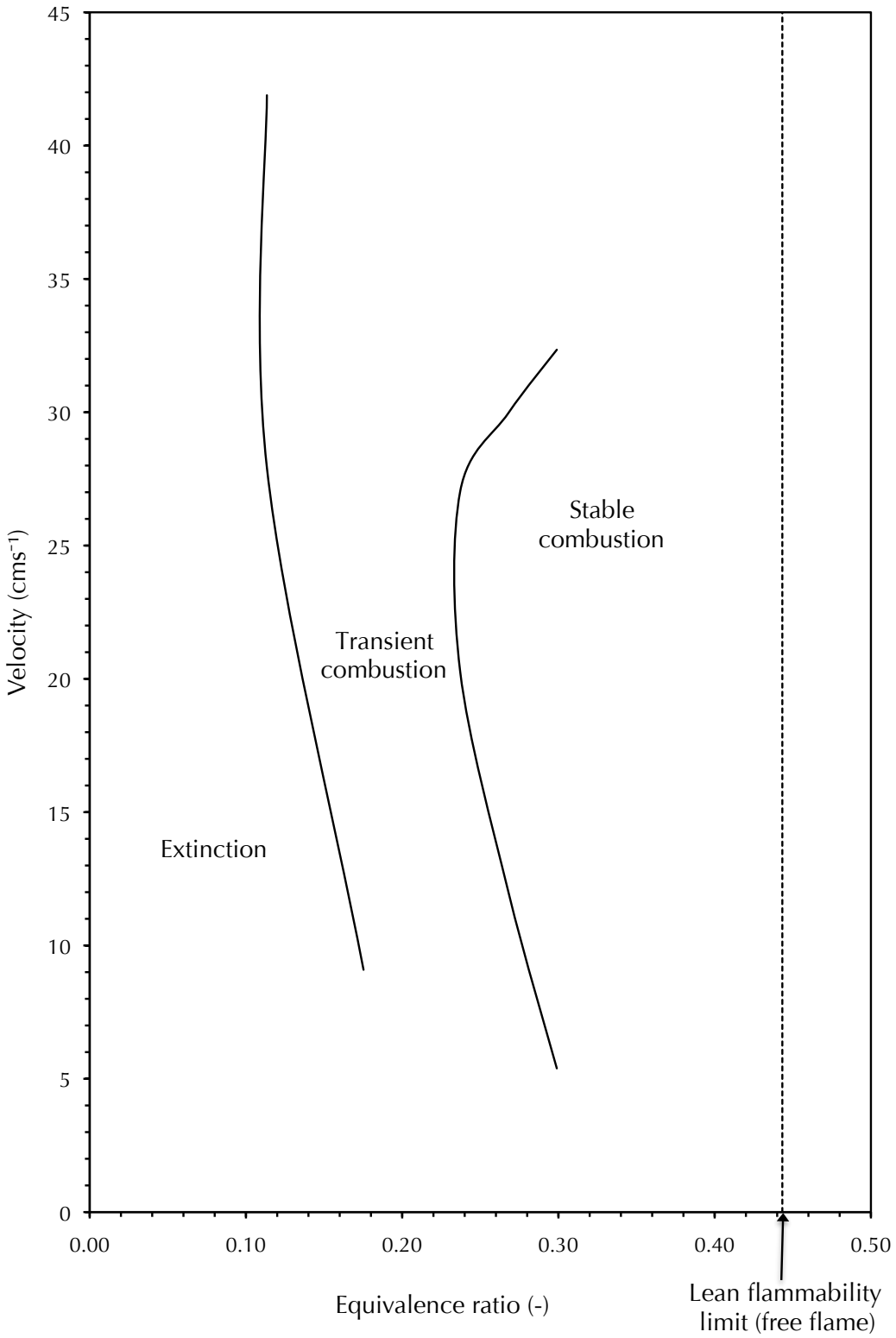

Figure 6.9 Burner map of the porous burner presented in terms of NG equivalence ratio and total (air plus NG) flow velocity.

It is also worth noting that although, as previously discussed (§6.2.3), the system was observed to exhibit path-dependency in terms of the temperature profile obtained for a given set of experimental conditions, for the range of conditions studied the actual lean limit that could be achieved was *not* found to be path-dependent.

It is also important to realise the significance of using NG rather than methane (CH_4) as the fuel in the context of burner performance. The composition of NG is given in Table 6.1. Although composed principally of CH_4, the presence of the higher alkanes alters its combustion characteristics. This is illustrated by Table 6.2, which compares the key combustion properties of CH_4 with those of a typical NG mixture. It should also be appreciated that the composition of NG can vary significantly between different sources (as demonstrated by the wide concentration ranges given in Table 6.1), and that even subtle differences in fuel composition can result in large changes in burner performance.

Crucially—from the perspective of the current study—the lean flammability limit of NG (4.3 vol%) is already lower than that of CH_4 (5 vol%). Le Chatelier's law (Le Chatelier 1891), which governs the flammability limits of gaseous mixtures, has been shown to successfully predict the lean limits of mixtures of combustible gases from the lean limits of their constituents (Coward and Jones 1952). However, whilst applicable to the conventional flammability limits of free flames, this method is not necessarily valid for the current system. Nor is it theoretically possible to determine the lean limit of a single component (in this case CH_4) from the lean limit of the mixture (NG).

Table 6.1 Composition of NG.

Component	Concentration range (vol%)
Methane (CH_4)	86.3–95.2
Ethane (C_2H_6)	2.5–8.1
Propane (C_3H_8)	0.6–2.8
Butanes (C_4H_{10})	0.13–0.66
Pentanes (C_5H_{12})	0–0.44
Hexanes (C_6H_{14}) plus	0–0.09
Carbon dioxide (CO_2)	0–1.1
Nitrogen (N_2)	0.31–2.47
Helium (He)	0.01–0.06

Source: Perry and Green (1997).

Therefore, it must suffice to say that the difference in flammability limits should be considered when evaluating burner performance with respect to potential applications where CH_4, rather than NG, is to be used as the fuel, as the stable operating range of the system is likely to be narrower than that measured here.

6.3.2 Thermal performance

The system can also be characterised in terms of its thermal performance: For ultra-lean operation the thermal power of the porous burner is 16.3 kW, which corresponds to a power density of approximately 500 kWm^{-3}. The power modulation range (turndown ratio) is 6:1.

6.3.3 Emissions profile

The exhaust gas was monitored throughout burner operation for the products of incomplete combustion—carbon monoxide (CO) and unburned hydrocarbons (UHC)—as described in the previous chapter.

Levels of UHC up to a maximum of 20 ppm, and for the most part less than 10 ppm, were recorded over the range of conditions studied throughout both the stable and transient combustion regimes. Rapid rises in UHC levels were of course observed when the flame extinguished.

Emissions of CO were typically less than 40 ppm over the stable operating range of the burner.

Table 6.2 Combustion characteristics of CH_4 and NG.[a]

Property	CH_4	NG
Flammability limits (vol%)[b]	5–15	4.3–15
Auto-ignition temperature (K)[c]	905	810–905
Adiabatic flame temperature at stoichiometry (K)[d]	2226	2214
Maximum flame speed (cms^{-1})[b]	45	30
Lower heating value LHV ($MJkg^{-1}$)[e]	50.1	49.8
Higher heating value HHV ($MJkg^{-1}$)[e]	55.5	54.2

[a] For combustion in air at standard temperature and pressure.
[b] From Perry and Green (1997).
[c] From Glassman (1996).
[d] From Dunn-Rankin (2008).
[e] From Borman and Ragland (1998).

A rise in CO emissions to a maximum of 100 ppm was observed during transient combustion when the combustion zone was located near the downstream end of the burner (just prior to blowoff occurring). This could be due to there being less time for the CO formed in the reaction zone to be oxidised to CO_2 before exiting the burner. Alternatively, it could be the case that the low combustion temperatures produced at these extremely low NG concentrations suppressed the oxidation of CO to CO_2.

Overall, negligible emissions of both UHC and CO indicate that the combustion process in the burner was complete.

6.3.4 Heat exchanger performance

The gas temperatures at the outlets of each heat exchanger, as well as the temperature of the exhaust gas (thermocouples THX1, THX2 and TE respectively in Figure 5.3), were measured throughout burner operation in order to assess the effectiveness of the heat exchanger arrangement.

Temperatures measured by THX1 ranged from 500 to 800K over the range of operating conditions considered, but were typically between 700 and 750K, with the temperature of the exhaust gas (TE) ranging from 300 and 400K. This demonstrates that the primary heat exchanger (HX1, the spiral positioned at the exit of the porous bed) was effective in preheating the incoming NG/air mixture. Because in most cases the flame stabilised in the *upstream* half of the porous burner, it is likely that this preheating occurred primarily via convection from the hot combustion products leaving the porous bed, rather than radiation from the downstream end of the bed itself.

The temperature differences between THX1 and THX2 were within the margin of error for the temperature measurements. Hence the secondary heat exchanger (HX2, the circumferential heat recuperator tubes) was shown to be effective in maintaining the preheated gas at an elevated temperature, but not in providing any additional preheating.

It should also be mentioned here that the maximum preheat temperature obtained over the range of operating conditions considered was less than the auto-ignition temperature of NG (see Table 6.2), so there was no possibility of the mixture actually igniting in the heat exchanger system before entering the porous bed.

As previously shown, changes in the firing rate and NG concentration influence both the maximum temperature and flame location. It would be reasonable to assume that these two factors, along with heat losses from the system, should combine to influence the extent of preheating. However in practice it was not possible to reliably identify any relationship between the amount of preheating and individual burner operating parameters.

It was previously stated that stable combustion occurs when a balance is achieved among heat recirculation, heat release, and heat losses (such that the effective flame speed is equal to the incoming velocity), but that the presence of the heat exchangers further complicates the situation in the current system (as heat 'losses' from the porous bed are not necessarily heat losses from the system). The could explain the apparently contradictory phenomenon observed on the burner maps (Figures 6.8 and 6.9) whereby at certain NG concentrations stable combustion occurs at 'intermediate' firing rates, with transient combustion at both higher and lower firing rates; without the presence of the heat exchangers, increasing the firing rate at a given NG concentration would logically cause a move from the stable to the transient combustion regime.

Heat losses from the system were estimated by measuring the external (outside of the alumina fibre insulation) wall temperature (TW). The maximum (at the vertical position on the wall corresponding to the flame location) external temperatures were found to be as high as 600K, indicating extensive heat loss. This is of concern since for increasingly ultra-lean mixtures heat losses from the system will ultimately become controlling, determining the lean limit that can be achieved (§3.2.1).

From the temperatures measured throughout the system, it is estimated that radial heat losses actually account for approximately 10% of burner output, and that the heat exchanger system was achieving efficiencies of around 60–70%. The temperatures measured for the exhaust gas (TE) indicate that there is also still potential for recovering additional energy downstream of the porous bed.

The next part of this thesis concerns the development of a computational fluid dynamics (CFD) model of a porous burner. This will allow an idealised version of the pilot-scale system described in this chapter to be studied, without the limitations of excessive heat losses and other experimental restrictions encountered here.

Part 3

COMPUTATIONAL FLUID DYNAMICS MODEL

Chapter 7

DEVELOPMENT OF A KINETIC MECHANISM

7.1 Introduction

Part 3 of this thesis concerns the development of a computational fluid dynamics (CFD) model of a porous burner. The full CFD model will be described in Chapter 8. This chapter concerns the development of the skeletal kinetic mechanism for methane (CH_4) combustion that will be used in the model.

As previously discussed, combustion in a porous burner involves stabilising a flame within the pores of a solid matrix, and thus entails an intimate coupling of combustion, heat transfer and fluid dynamics (§3.2.2). In order to accurately describe combustion behaviour in a porous burner, it is necessary to use a relatively detailed multi-step chemical kinetic mechanism (Hsu and Matthews 1993; Zhou and Pereira 1998).

The combustion of CH_4 can be summarised by the simple single-step reaction

$$CH_4 + 2O_2 = 2H_2O + CO_2$$

but in reality proceeds through a large number of elementary steps. The chemistry of CH_4 combustion has been thoroughly investigated, and a number of reviews on the chemical kinetic modelling of combustion—including that of CH_4—are available (Cathonnet 1994; Miller and Kee 1990; Simme 2003; Westbrook and Dryer 1984).

The development of detailed chemical kinetic mechanisms involves the identification of reaction pathways and the accurate determination of the kinetic constants of the associated reactions. A number of detailed mechanisms describing CH_4 combustion are available in the literature or online (Bendtsen, Glarborg and Dam-Johansen 2000; Bromly et al. 1996; Chevalier 1993; Glarborg et al. 1998; Hughes et al. 2001; Karim, Hanafi and Zhou 1993; Konnov 2000; Miller and Bowman 1989; Smith et al. 1999). These comprehensive mechanisms typically comprise several hundred elementary reactions, and involve dozens of chemical species. They are based on large experimental datasets, and describe the combustion of CH_4 over a wide range of conditions (temperature,

pressure and concentration), and for a number of reactor geometries (for example flow reactors, shock tubes and burner stabilised flames).

For this thesis, a computational fluid dynamics (CFD) model of a porous burner was developed (and is described in the next chapter). Although there is no theoretical limitation preventing the use of a comprehensive kinetic mechanism in a CFD code, such an approach would be prohibitively computationally expensive.

In a CFD model, the evolution of the system is governed by a set of differential equations that evolve according to several different timescales; *stiffness* in the numerical system arises when the integration must be performed over a wide range of timescales. In order to accurately predict combustion in a porous burner, the chemistry must be solved in conjunction with the fluid flow and heat transfer processes. This introduces a stiffness problem, as the chemistry timescales are several orders of magnitude faster than the physical timescales associated with the flow. Within a large mechanism, there will also be significant variation in the timescales for the different species and reactions, due principally to fast depleting radicals that quickly reach quasi-steady state (QSS), and fast reversible reactions in partial equilibrium (PE). In addition, the conservation equations for each species are strongly coupled to the energy equation, as the reaction rates are highly temperature dependent.

The large size of the numerical system, its highly coupled nature, and the stiffness introduced by the fast chemical timescales, are all major factors that prevent the use of detailed kinetic mechanisms in CFD simulations of practical combustion systems. In order to reduce computational demand, and thus allow the implementation of chemical kinetics in CFD models, reduction of the detailed mechanism to a more manageable form is required.

Mechanism reduction approaches can generally be categorised as lumping, whereby similar species and reaction pathways are combined such that the number of variables is reduced; timescale analysis based methods, which involve making assumptions regarding QSS and PE to create a small set of global reactions; and reduction to a so-called skeletal mechanism containing fewer elementary reactions. Various novel approaches have also been developed, involving techniques such as artificial neural networks and tabulation. A number of useful reviews covering the various mechanism reduction techniques are available (Griffiths 1995; Ho 2008; Law et al. 2003; Lu and Law 2009; Tomlin, Turányi and Pilling 1997; Turányi 1990b).

Skeletal mechanisms comprise a subset of the elementary reactions from the full mechanism, and meet the conflicting requirements of computational feasibility and chemical comprehensiveness. They are capable of accurately reproducing the predictions of the full detailed mechanism, but for a more limited set of conditions. The

feasibility of implementing a skeletal kinetic mechanism in a CFD model has previously been demonstrated (Jazbec, Fletcher and Haynes 2000), and this approach will be used here.

Further reduction of the mechanism could be performed by identifying QSS species and PE reactions, however the resulting equations would be a set of non-linear coupled algebraic equations requiring solution via an iterative method. This would impose a significant additional computational cost, so will not be undertaken here.

A number of skeletal mechanisms for CH_4 combustion are described in the literature (for example Bilger and Stårner 1990; Gokulakrishnan et al. 2005; Jazbec, Fletcher and Haynes 2000; Li and Williams 2002; Mendiara et al. 2004; Romero 1998), however it was not possible to obtain an up-to-date skeletal mechanism relevant to the ultra-lean conditions of interest. It was therefore necessary to carry out a new mechanism reduction to obtain a suitable skeletal mechanism for use in the porous burner CFD model.

The remainder of this chapter describes the reduction of a comprehensive detailed CH_4 oxidation chemistry to a skeletal mechanism for ultra-lean combustion. In the following section, the selection of a suitable detailed mechanism to act as the starting point for the reduction will be discussed. The mechanism reduction methodology will then be explained and the skeletal mechanism thus developed will be presented. Finally, the validation of the skeletal mechanism over a range of conditions of interest will be described.

7.2 Selection of detailed mechanism

The first step in the reduction of a kinetic mechanism is the selection of an appropriate detailed mechanism to act as the starting point for the reduction. A number of potentially suitable detailed mechanisms were identified. These include the widely used GRI-Mech mechanism for natural gas combustion (Smith et al. 1999); Alexander Konnov's mechanism for the combustion of small hydrocarbons (Konnov 2000); the Leeds methane oxidation mechanism (Hughes et al. 2001); and two mechanisms developed specifically to describe ultra-lean methane combustion at low temperatures (Bendtsen, Glarborg and Dam-Johansen 2000; Bromly et al. 1996).

The performance of these five detailed mechanisms was evaluated using the commercial kinetic modelling software package CHEMKIN 4 (Kee et al. 2005).

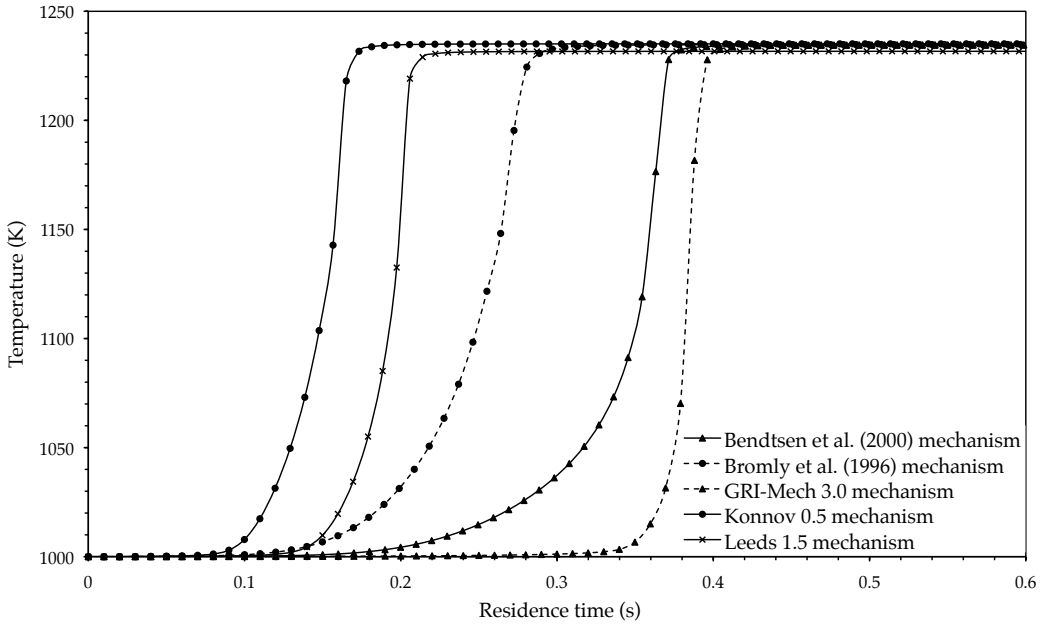

Figure 7.1 Comparison of temperature profiles predicted by five different detailed kinetic mechanisms for CH_4 combustion in an adiabatic PFR at atmospheric pressure, for an initial methane concentration of 1 vol%, and inlet temperature of 1000K.

Simulations were carried out for an adiabatic plug flow reactor (PFR)[†] at atmospheric pressure, over a range of conditions of interest to ultra-lean porous burner operation: CH_4 concentrations from 0.1 to 2 vol%, and inlet temperatures from 800 to 1200K.

Figures 7.1 and 7.2 are illustrative of the results obtained. Figure 7.1 shows the temperature profiles predicted by each mechanism, for a methane concentration of 1 vol% and initial temperature of 1000K. Figure 7.2 shows the carbon monoxide (CO) concentration profiles derived for the same conditions.

It can be seen that for the ultra-lean, low-temperature conditions considered, there are significant differences in the combustion behaviour predicted by each of the mechanisms. The variation in the prediction of the onset of combustion is particularly pronounced. Additionally, from the CO peaks shown in Figure 7.2, it can be seen that a broader combustion zone is predicted by the two dedicated low-temperature mechanisms (Bendtsen, Glarborg and Dam-Johansen 2000; Bromly et al. 1996).

It was found that these differences are particularly pronounced at lower temperatures, and for leaner mixtures.

[†] Gases passing through packed beds approximate plug flow (Levenspiel 1999). Therefore, the simple case of an adiabatic PFR, with inlet temperatures corresponding to preheat temperature obtained via heat recirculation in the porous burner, will be used throughout this chapter for the reduction and validation of the mechanism.

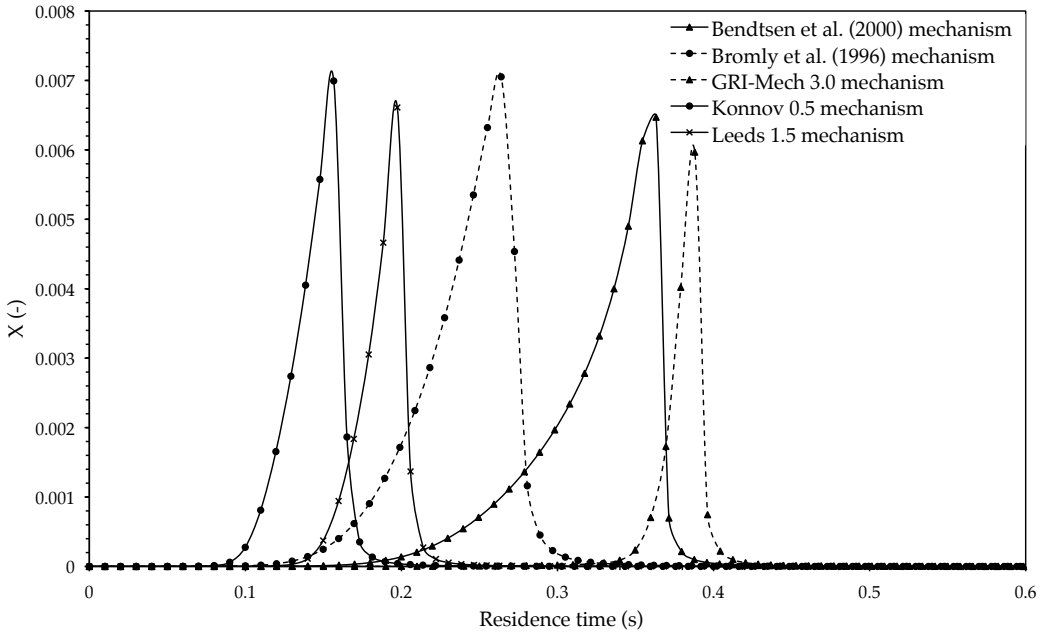

Figure 7.2 Comparison of CO concentration profiles (mass fractions) predicted by five different detailed kinetic mechanisms for CH_4 combustion in an adiabatic PFR at atmospheric pressure, for an initial CH_4 concentration of 1 vol%, and inlet temperature of 1000K.

Selection of an appropriate detailed mechanism as the starting point for the reduction is therefore crucial if a skeletal mechanism capable of accurately predicting combustion behaviour in the porous burner is to be developed.

The mechanism developed by Bendtsen, Glarborg and Dam-Johansen (2000), henceforth referred to as the 'Bendtsen' mechanism, was selected. The Bendtsen mechanism is the more recent and comprehensive of the two low-temperature mechanisms considered. Furthermore, it has been validated experimentally in an adiabatic PFR over the temperature range 750–1250K, which corresponds fairly well to conditions expected in the porous burner. The full mechanism, which includes nitrogen (N_2) and argon (Ar) chemistry, consists of 484 reversible reactions and 78 chemical species, and is provided in Appendix D.

7.3 Mechanism reduction

The reduction of a detailed kinetic mechanism to produce a skeletal mechanism involves the elimination of species and reactions that are unimportant for a particular set of conditions (temperature, pressure, concentration and reactor type) of interest.

The current mechanism reduction was performed for an adiabatic PFR at atmospheric pressure, for conditions representative of those expected in the porous burner: a CH_4 concentration of 1 vol% in wet (1 vol% water) air, at an inlet temperature of 1000K. The PFR modelled was 90 cm in length, and an inlet velocity of 150 cms^{-1} was used (to

ensure that combustion occurred within the length of the reactor). The aim of the reduction was to produce a skeletal mechanism capable of accurately replicating the temperature profile, as well as the profiles of the major species, predicted by the full Bendtsen mechanism under these conditions.

The reduction was undertaken according to the methodology proposed by Turányi (1990a), namely: (1) selection of 'important' species; (2) identification of 'necessary' and 'redundant' species (and elimination of redundant species); and (3) identification of important reactions. The freely available Fortran program KINALC (Turányi and Zsely 2005), a post-processor to CHEMKIN that offers a number of routines useful in mechanism reduction, was used to carry out the necessary analyses.

7.3.1 Selection of important species

The important species were selected as being those entering the combustion process and the resulting stable combustion products: CH_4, H_2O, O_2, H_2, CO, CO_2 and CH_2O.

7.3.2 Elimination of redundant species

Necessary species are defined as those for which realistic concentrations are required in order to calculate accurate concentration profiles for the important species, or to reproduce other specific features of the combustion process—in this case the temperature profile. Redundant species are those that may be omitted from the mechanism without compromising the accuracy of the predictions.

Strong coupling between species means that identification of necessary and redundant species is not straightforward. Species connectivity was analysed at a number of residence times using the CONNECT routine in KINALC. An analysis of the effect of a change in concentration of a particular species on the rate of production of the important species was used to determine if that species was necessary.

The redundant species—and associated reactions—were then eliminated from the mechanism to create an 'intermediate' mechanism consisting of 138 reversible reactions and 26 species. The intermediate mechanism was tested against the full mechanism to confirm that it was able to accurately reproduce the temperature and concentration profiles. The effect of eliminating each individual species on the accuracy of the mechanism was also tested.

7.3.3 Identification of important reactions

Identification of the important reactions was carried out by means of a principal component analysis (PCA), an advanced sensitivity analysis technique. An important feature of PCA is that it can be used to explore interactions among reactions, thereby eliminating groups of reactions, rather than individual ones. KINALC was used to

perform the PCA on the normalised algebraic rate sensitivity matrix $\tilde{F}$, with the important species—along with temperature—in the objective function. $\tilde{F}$ is given by

$$\tilde{F} = \left\{ \frac{\partial \ln \omega_i}{\partial \ln k_j} \right\} = \left\{ \frac{\upsilon_{ij} r_j}{\omega_i} \right\} \tag{7.1}$$

where υ_{ij} is the stoichiometric coefficient of species i in the reaction j, k_j and r_j represent the rate coefficient and the rate respectively of reaction j, and ω_i is the rate of production of species i. The elements of the matrix $\tilde{F}$ are therefore the ratio of the rate of formation or consumption of species i in reaction j to the net rate of concentration change of species i. Reactions were considered to be important if they corresponded to a significant eigenvector element (>0.2), of a principal component characterised by a large eigenvalue (>0.0001).

Reactions determined to be unimportant by the PCA were eliminated from the mechanism. The resulting skeletal mechanism was tested against the full mechanism as before. Further reactions were then eliminated on a trial-and-error basis to produce a final skeletal mechanism about a tenth of the size of the original Bendtsen mechanism.

7.4 Skeletal mechanism

The final skeletal mechanism is shown in Table 7.1. It contains 47 reversible reactions and 26 chemical species.

Table 7.1 Skeletal kinetic mechanism for ultra-lean CH_4 combustion.

	Reaction	$k = AT^{\beta} \exp(E_a / RT)$		
		A (mol cm s K)	β	E_a (cal/mol)
1	$O + OH = O_2 + H$	2.00E + 14	–0.400	0
2	$OH + H_2 = H_2O + H$	2.10E + 08	1.520	3449.63
3	$2OH = O + H_2O$	4.30E + 03	2.700	–2485.73
4	$H + O_2 + M = HO_2 + M$	2.10E + 18	–1.000	0
	Enhanced third-body efficiencies: $H_2O = 10$; $N_2 = 0$			
5	$H + O_2 + N_2 = HO_2 + N_2$	6.70E + 19	–1.420	0
6	$H + HO_2 = H_2 + O_2$	4.30E + 13	0	1410.85
7	$H + HO_2 = 2OH$	1.70E + 14	0	873.91
8	$O + HO_2 = O_2 + OH$	3.30E + 13	0	0
9	$OH + HO_2 = H_2O + O_2$	1.90E + 16	–1.000	0
10	$2HO_2 = H_2O_2 + O_2$	4.20E + 14	0	11980.70
11	$H_2O_2 + M = 2OH + M$	1.30E + 17	0	45495.06
	Enhanced third-body efficiencies: $H_2O = 5$			
12	$H_2O_2 + OH = H_2O + HO_2$	7.80E + 12	0	1329.86
13	$H_2O_2 + OH = H_2O + HO_2$	5.80E + 14	0	9558.96
14	$CO + OH = CO_2 + H$	1.50E + 07	1.300	–757.92
15	$CH_2O + H = HCO + H_2$	1.30E + 08	1.620	2165.77
16	$CH_2O + O = HCO + OH$	1.80E + 13	0	3079.67

Reaction		$k = AT^{\beta}\exp(E_a/RT)$		
		A (mol cm s K)	β	E_a (cal/mol)
17	$CH_2O + OH = HCO + H_2O$	3.40E + 09	1.180	–446.95
18	$CH_2O + HO_2 = HCO + H_2O_2$	3.00E + 12	0	12998.59
19	$CH_2O + O_2 = HCO + HO_2$	6.00E + 13	0	40655.59
20	$HCO + M = H + CO + M$	1.90E + 17	–1.000	16998.16
	Enhanced third-body efficiencies: $H_2O = 5$			
21	$HCO + O_2 = HO_2 + CO$	7.60E + 12	0	399.96
22	$CH_4 + H = CH_3 + H_2$	1.30E + 04	3.000	8039.13
23	$CH_4 + O = CH_3 + OH$	1.00E + 09	1.500	8599.07
24	$CH_4 + OH = CH_3 + H_2O$	1.60E + 06	2.100	2459.73
25	$CH_4 + O_2 = CH_3 + HO_2$	7.90E + 13	0	55993.92
26	$CH_3 + O = CH_2O + H$	8.40E + 13	0	0
27	$CH_3 + OH + (M) = CH_3OH + (M)$	6.30E + 13	0	0
	Low pressure limit:	1.89E + 38	–6.300	3099.66
	TROE parameters: 2.1050E–01; 8.3500E+01; 5.3980E+03; 8.3700E+03			
	Enhanced third-body efficiencies: $H_2O = 8.58$; $N_2 = 1.43$			
28	$CH_3 + HO_2 = CH_3O + OH$	8.00E + 12	0	0
29	$CH_3 + O_2 = CH_3O + O$	2.90E + 13	0	30476.69
30	$CH_3 + O_2 = CH_2O + OH$	3.60E + 10	0	8939.03
31	$2CH_3 + (M) = C_2H_6 + (M)$	2.10E + 16	–0.970	619.93
	Low pressure limit:	1.26E + 50	–9.670	6219.33
	TROE parameters: 5.3250E-01; 1.5100E+02; 1.0380E+03; 4.9700E+03			
	Enhanced third-body efficiencies: $H_2O = 8.59$; $N_2 = 1.43$; $H_2 = 2$; $CO = 2$; $CO_2 = 3$			
32[†]	$CH_2(S) + N_2 = CH_2 + N_2$	1.30E + 13	0	429.95
33	$CH_2(S) + O_2 = CO + OH + H$	7.00E + 13	0	0
34	$CH_3OH + OH = CH_3O + H_2O$	1.32E + 04	2.530	959.90
35	$CH_2O + H + (M) = CH_3O + (M)$	5.40E + 11	0.454	2599.72
	Low pressure limit:	1.54E + 30	–4.800	5559.40
	TROE parameters: 7.5800E-01; 9.4000E+01; 1.5550E+03; 4.2000E+03			
	Enhanced third-body efficiencies: $H_2O = 8.58$; $N_2 = 1.43$			
36	$CH_3O + O_2 = CH_2O + HO_2$	6.30E + 10	0	2599.72
37	$C_2H_6 + OH = C_2H_5 + H_2O$	7.20E + 06	2	863.91
38	$C_2H_4 + H + (M) = C_2H_5 + (M)$	1.10E + 12	0.454	1821.80
	Low pressure limit:	1.112E + 34	–5.000	4447.52
	TROE parameters: 5.0000E-01; 9.5000E+01; 9.5000E+01; 2.0000E+02			
	Enhanced third-body efficiencies: $H_2O = 5$			
39	$C_2H_5 + O_2 = C_2H_4 + HO_2$	1.00E + 10	0	–2189.76
40	$C_2H_4 + O = CH_2HCO + H$	4.70E + 06	1.880	179.98
41	$C_2H_4 + OH = C_2H_3 + H_2O$	2.00E + 13	0	5939.36
42	$C_2H_3 + O_2 = CH_2HCO + O$	2.50E + 15	–0.780	3134.66
43	$CH_2HCO + O_2 = CH_2O + CO + OH$	2.20E + 11	0	1499.84
44	$CH_3 + O_2 + (M) = CH_3O_2 + (M)$	7.80E + 08	1.200	0
	Low pressure limit:	5.40E + 25	–3.300	0
	Enhanced third-body efficiencies: $H_2O = 10$; $N_2 = 1.1$			
45	$CH_3O_2 + OH = CH_3OH + O_2$	6.00E + 13	0	0
46	$CH_3O_2 + CH_3 = 2CH_3O$	2.40E + 13	0	0
47	$CH_3OOH = CH_3O + OH$	6.30E + 14	0	42295.41

[†] The methylene radical is an example of a carbene, a carbon radical with two unpaired electrons. It can exist in either the triplet state (CH_2), in which the electrons have parallel spins (and the net spin angular momentum is non-zero); or the singlet state ($CH_2(S)$), in which the electrons are spin-paired (and the spin momentums cancel each other to give zero net spin). The triplet state has a lower energy than the singlet state (Atkins 1994; Solomons 1996).

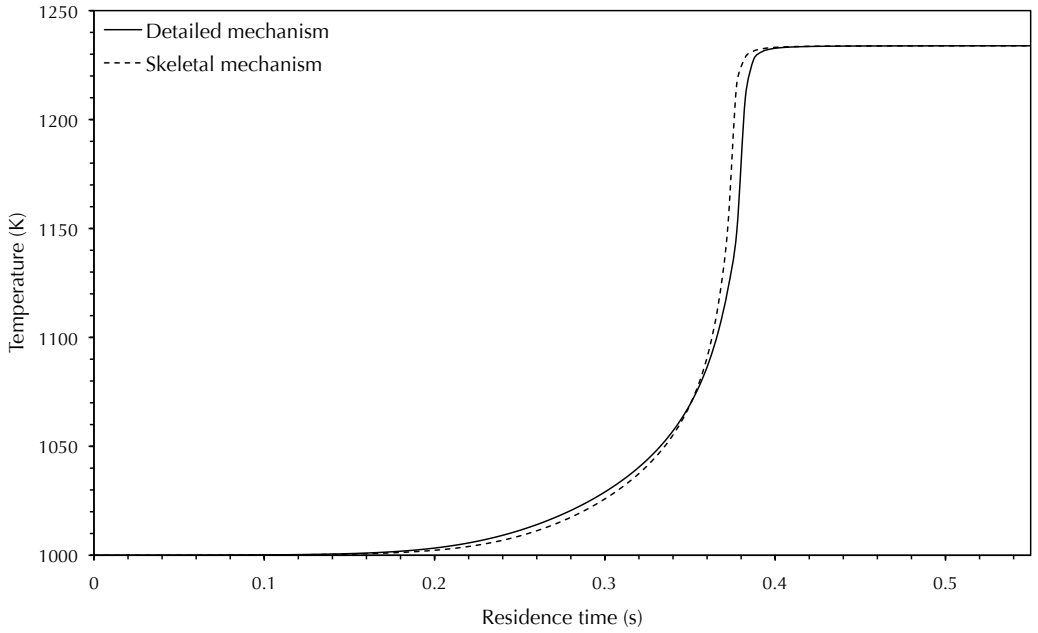

Figure 7.3 Comparison of temperature profiles predicted by the detailed (Bendtsen et al. 2000) and skeletal mechanisms for CH_4 combustion in an adiabatic PFR, for the mechanism reduction conditions: 1 vol% CH_4 in wet (1 vol% H_2O) air, inlet temperature 1000K, pressure 1 atm.

Figures 7.3 and 7.4 compare the predictions of the skeletal mechanism with those of the detailed mechanism, for the conditions at which the skeletal mechanism was reduced; Figure 7.3 shows the temperature profile, and Figure 7.4 the concentration profiles of the major species (CH_4, CO and CO_2). It can be seen that the skeletal mechanism accurately replicates the predictions of the full Bendtsen mechanism to within ±2%.

The reaction set, along with the necessary chemical kinetic and thermodynamic data, is provided in CHEMKIN format in Appendix E. Concentration profiles for all of the chemical species in the skeletal mechanism are given in Appendix F.

7.5 Validation of skeletal mechanism

The reduction of a detailed kinetic mechanism to a skeletal mechanism can only be achieved by sacrificing comprehensiveness: the skeletal mechanism will only be valid for a restricted range of conditions similar to those at which it was reduced. Using CHEMKIN, a series of simulations was carried out to determine the range of conditions (temperature, CH_4 concentration, pressure, and moisture content of the air) for which the current skeletal mechanism successfully reproduces the combustion behaviour predicted by the detailed mechanism, to an acceptable degree of accuracy. As per the reduction process itself, these simulations were carried out for an adiabatic PFR of length 90 cm. The results of this validation are summarised by Figures 7.5 to 7.8.

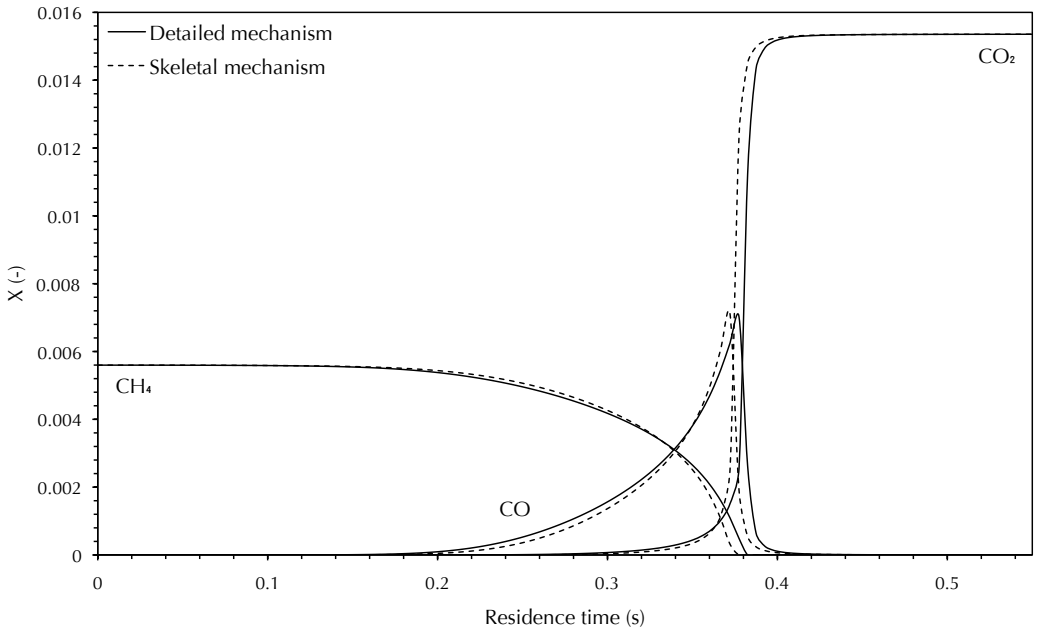

Figure 7.4 Comparison of major species (CH_4, CO and CO_2) concentration profiles (mass fractions) predicted by the detailed (Bendtsen et al. 2000) and skeletal mechanisms for CH_4 combustion in an adiabatic PFR, for the mechanism reduction conditions: 1 vol% CH_4 in wet (1 vol% H_2O) air, inlet temperature 1000K, pressure 1 atm.

Figure 7.5 illustrates the effect of CH_4 concentration on the accuracy of the skeletal mechanism. It shows temperature profiles obtained for CH_4 concentrations ranging from 0.1 to 5 vol%. The inlet velocities were adjusted for each case such that combustion occurred within the length of the reactor.

It can be seen that for the CH_4 concentrations below the reduction concentration, the combustion profile is accurate to within ±10% of the detailed mechanism predictions. An accuracy of ±10% is also obtained for higher CH_4 concentrations of between 1 and 3 vol%. The accuracy of the skeletal mechanism decreases as concentration increases, as would be expected; for a CH_4 concentration of 5 vol%, the accuracy is only ±25%.

Figure 7.6 illustrates the effect of temperature on the accuracy of the skeletal mechanism. It shows the temperature profiles for inlet temperatures ranging from 900 to 1200K. Again, it was necessary to adjust the inlet velocities so that combustion occurred within the length of the reactor for each case. It can be seen that for temperatures other than the reduction temperature, ignition is predicted to occur slightly later by the skeletal mechanism. For temperatures 100K above or below the reduction temperature, the predictions are still accurate to ±10%. At 1200K the error is ±20%.

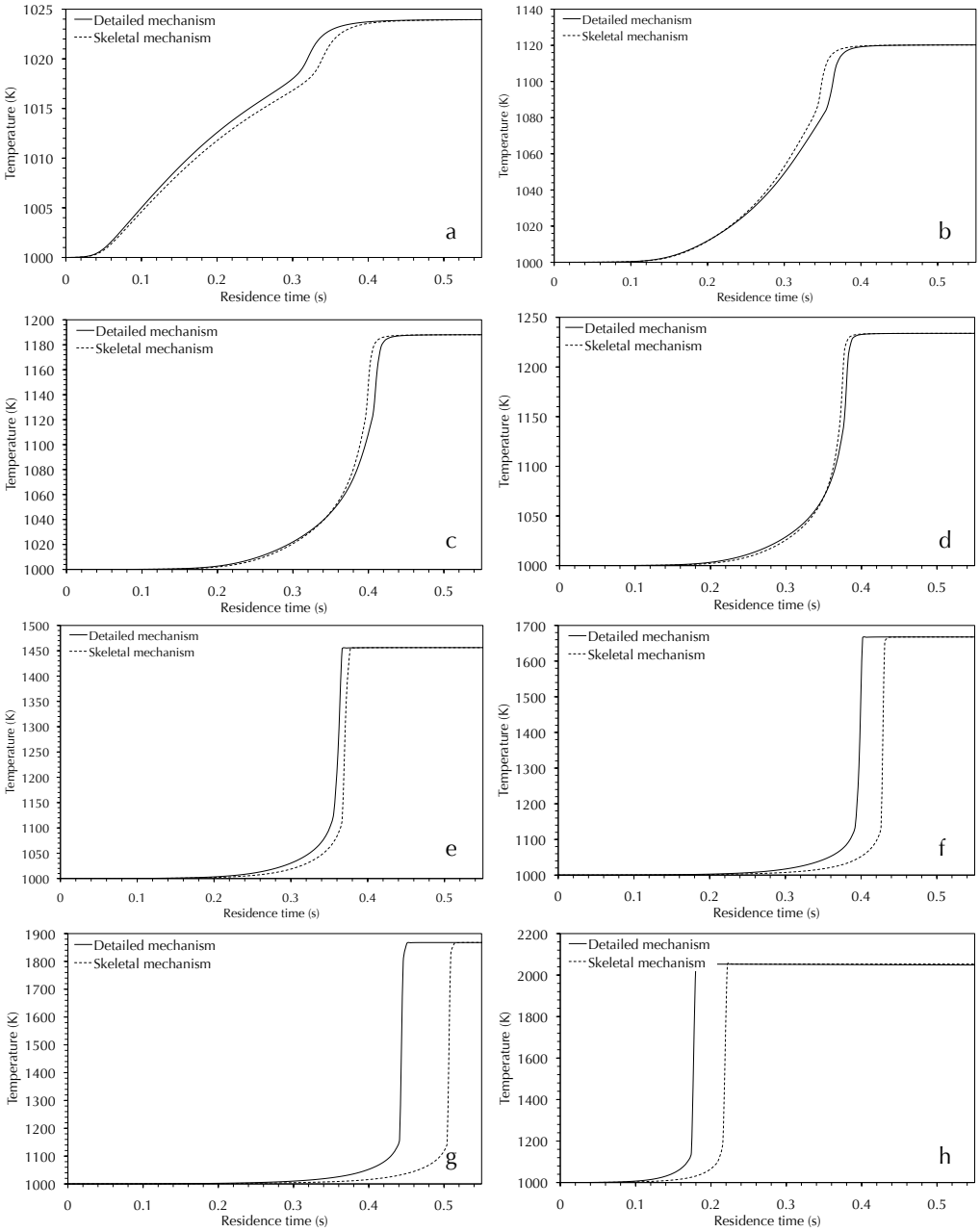

Figure 7.5 Effect of CH_4 concentration on skeletal mechanism accuracy: Comparison of temperature profiles predicted by the detailed (Bendtsen et al. 2000) and skeletal mechanisms for CH_4 combustion in a 90 cm long adiabatic PFR, at a pressure of 1 atm and inlet temperature of 1000K, at CH_4 concentrations (in wet (1 vol% H_2O) air) of (a) 0.1 vol% (inlet velocity 20 cms^{-1}) (b) 0.5 vol% (inlet velocity 100 cms^{-1}) (c) 0.8 vol% (inlet velocity 150 cms^{-1}) (d) 1 vol% (reduction conditions; inlet velocity 150 cms^{-1}) (e) 2 vol% (inlet velocity 150 cms^{-1}) (f) 3 vol% (inlet velocity 150 cms^{-1}) (g) 4 vol% (inlet velocity 150 cms^{-1}) and (h) 5 vol% (inlet velocity 50 cms^{-1}). Note the difference in temperature scales.

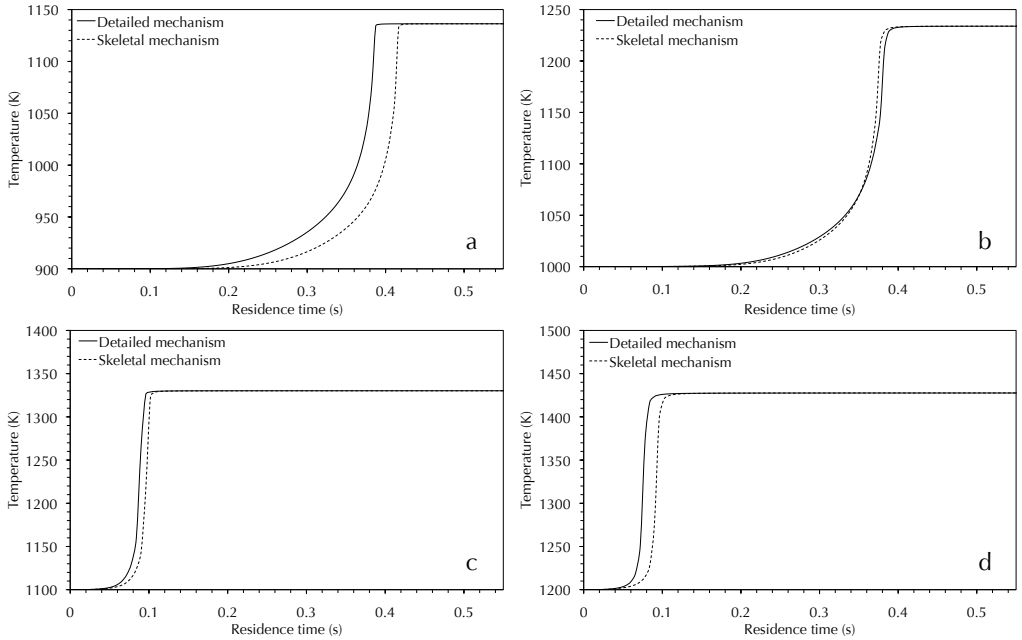

Figure 7.6 Effect of temperature on skeletal mechanism accuracy: Comparison of temperature profiles predicted by the detailed (Bendtsen et al. 2000) and skeletal mechanisms for CH_4 combustion in a 90 cm long adiabatic PFR, for 1 vol% CH_4 in wet (1 vol% H_2O) air at a pressure of 1 atm and inlet temperatures of (a) 900K (inlet velocity 20 cms^{-1}) (b) 1000K (reduction conditions; inlet velocity 150 cms^{-1}) (c) 1100K (inlet velocity 150 cms^{-1}) and (d) 1200K (inlet velocity 500 cms^{-1}). Note the difference in temperature scales.

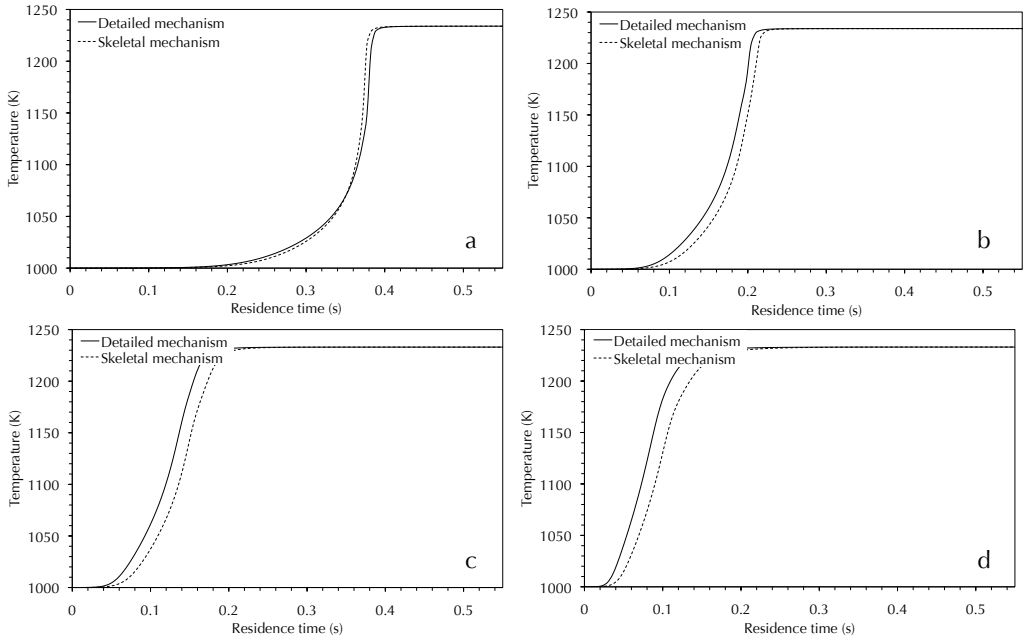

Figure 7.7 Effect of reactor pressure on skeletal mechanism accuracy: Comparison of temperature profiles predicted by the detailed (Bendtsen et al. 2000) and skeletal mechanisms for CH_4 combustion in a 90 cm long adiabatic PFR, for 1 vol% CH_4 in wet (1 vol% H_2O) air at an inlet temperature of 1000 K, inlet velocity of 150 cms^{-1}, and pressures of (a) 1 atm (reduction conditions) (b) 5 atm (c) 10 atm and (d) 20 atm.

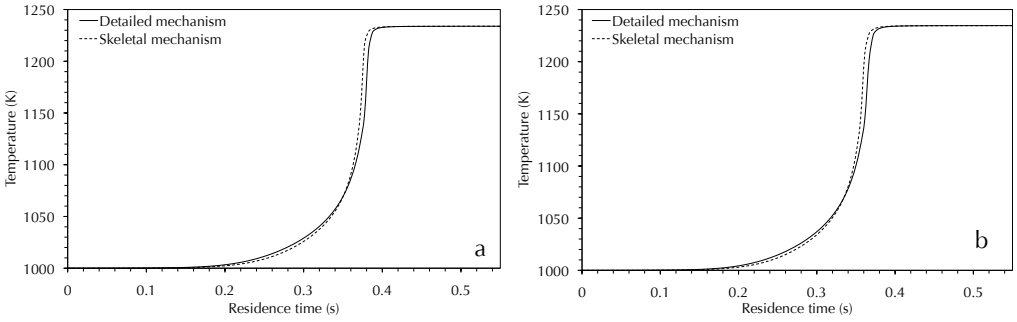

Figure 7.8 Effect of moisture content on skeletal mechanism accuracy: Comparison of temperature profiles predicted by the detailed (Bendtsen et al. 2000) and skeletal mechanisms for CH_4 combustion in an adiabatic PFR, at an inlet temperature of 1000 K and pressure of 1 atm for 1 vol% CH_4 in (a) wet (1 vol% H_2O) air (reduction conditions) and (b) dry air.

Figure 7.7 illustrates the effect of reactor pressure on the accuracy of the skeletal mechanism. It shows the temperature profiles for pressures ranging from 1 to 20 atm. It can be seen that for pressures above the reduction pressure of 1 atm, the skeletal mechanism predicts that ignition occurs later than when the detailed mechanism is used. For pressures up to 10 atm, the temperature profiles are accurate to ±10% of those predicted by the detailed mechanism. At 20 atm the error is ±20%.

The mechanism reduction was carried out for CH_4 in wet air with a moisture content of 1 vol% water. The temperature profiles shown in Figure 7.8 confirm that the skeletal mechanism is also valid for dry air.

In summary, the skeletal mechanism is able to successfully replicate the combustion behaviour predicted by the full Bendtsen mechanism, to within ±10%, for the following conditions:

- CH_4 concentrations of 0.1 to 3 vol%.
- Temperatures of 900 to 1100K.
- Pressures of 1 to 10 atm.
- Wet or dry air feeds.

As would be expected, the deviation of the predictions of the skeletal mechanism from those of the detailed mechanism increases as the conditions modelled diverge from the conditions under which the skeletal mechanism was reduced.

In the following chapter, the implementation of the skeletal mechanism in a CFD model of a porous burner will be discussed.

Chapter 8

DEVELOPMENT OF A CFD MODEL

8.1 Introduction

This chapter describes the development of a computational fluid dynamics (CFD) model of a porous burner.

It is hoped that eventually a multi-dimensional model capable of accurately simulating and predicting the operation of practical burners will be developed. However, the modelling of complex physics, such as combustion, in extensive geometries, is computationally demanding. The first step in the development process is therefore to demonstrate the viability of a modelling approach based on CFD, by successfully implementing the necessary physical models in a simple 1-dimensional system. The development of this initial 1-dimensional model is described here; combustion in a porous burner involves an intimate coupling of the combustion, heat transfer and fluid dynamics processes, so this is not a trivial problem.

In the following section the methodology used in developing the model is discussed. A complete description of the model is given, including details of the geometry and mesh; the governing equations; the physical models used to describe the flow, heat transfer and combustion processes in the system; the material properties of both the gas and solid phases; the boundary conditions applied; and the solution method employed. Some preliminary results from the model are then presented, and the predictions compared to the experimental results obtained from the pilot-scale demonstration described in Part 2 of this thesis.

8.2 Methodology

The CFD analysis was performed using the general-purpose commercial CFD code ANSYS CFX 12.0 (ANSYS n.d.). All simulations were performed on an HP xw8400 workstation running Microsoft Windows XP with an available RAM of 3.25 GB.

8.2.1 Geometry and mesh

A simple cylindrical geometry was created using ANSYS DesignModeler (ANSYS n.d.). The dimensions of the cylinder were set to represent the combustion chamber of the experimental pilot-scale porous burner: length 90 cm and cross-sectional diameter 26 cm[†]. The model domain is composed of a single porous region representing the main porous bed of saddles in the experimental burner.

A relatively coarse 1-dimensional mesh composed of 1 cm elements was applied to the model domain, as illustrated in Figure 8.1. The mesh was generated using the sweep mesh functionality in ANSYS DesignModeler.

8.2.2 Governing equations

The conservation equations for mass, momentum, gas and solid phase energy, and species conservation at steady-state are given by

Continuity equation:

$$\nabla \cdot (\Phi_g \rho_g \mathbf{u}) = 0 \tag{8.1}$$

Momentum equation:

$$\nabla \cdot (\Phi_g \rho_g \mathbf{u} \otimes \mathbf{u}) = -\Phi_g \nabla p + \nabla \cdot (\Phi_g \mu \nabla \mathbf{u}) \tag{8.2}$$

Gas phase energy equation:

$$\nabla \cdot (\Phi_g \rho_g H_g \mathbf{u}) = \nabla \cdot (\Phi_g k_g \nabla T_g) + S_{Eg} - \Phi_g \sum_{k=1}^{N_s} \omega_k H_k W_k \tag{8.3}$$

Solid phase energy equation:

$$0 = \nabla \cdot (\Phi_s k_s \nabla T_s) + S_{Es} \tag{8.4}$$

Species conservation equation:

$$\begin{aligned} &\nabla \cdot (\rho_g X_k \mathbf{u}) = (\nabla . \rho_g D_{km} \nabla X_k) + \omega_k W_k, \\ &k \in [1, N_s] \end{aligned} \tag{8.5}$$

[†] The diameter is unimportant for the initial model development described here, as a 1-dimensional mesh is applied. However, realistic dimensions are used to facilitate extending the current model to use a 2- or 3-dimensional mesh in future.

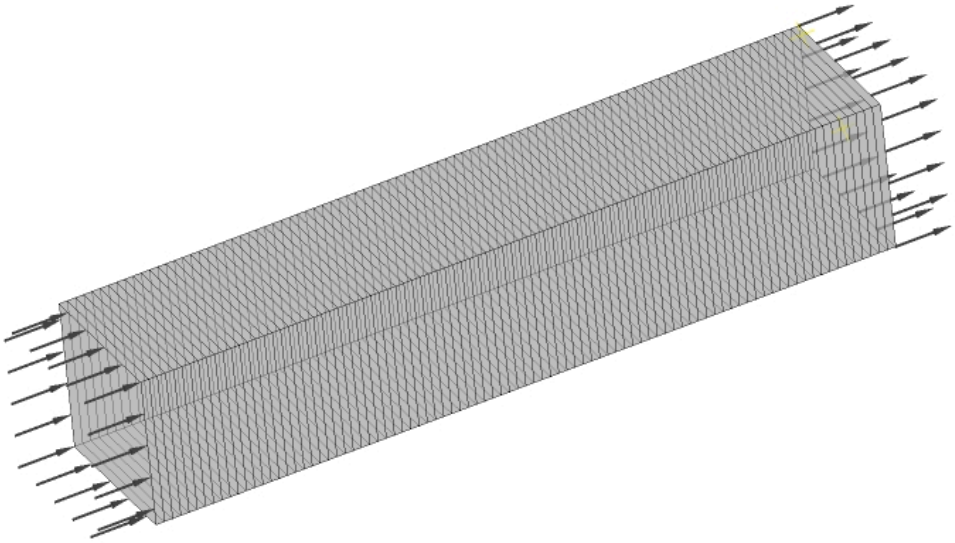

Figure 8.1 1-dimensional mesh used in the porous burner model.

8.2.3 Physical models

8.2.3.1 Flow model

The fluid was modelled as a reacting ideal gas mixture. Buoyancy was neglected, laminar flow was assumed, and adiabatic and free-slip conditions were applied at the walls. A reference pressure of 1 atm was used.

Pressure loss due to the presence of the porous solid was accounted for by an isotropic loss model based on Darcy's law, using the values for the porosity and permeability given in Table 8.1.

8.2.3.2 Heat transfer model

In order to accurately model heat recirculation in a porous burner, it is necessary to use a model that accounts for local temperature differences between the gas and the porous solid. Separate energy equations for the gas (equation 8.3) and solid (equation 8.4) phases were therefore applied.

A heat transfer model that accounted for the transport of thermal energy, but not for kinetic energy effects, was employed in the gas phase, as is evident from equation 8.3.

However, ANSYS CFX 12.0 does not support heat transfer in a porous solid, so it was necessary to add models for conductive heat transfer within the solid phase, and for convective heat transport within the porous region.

Convective heat transport. To model convective heat transfer between the solid and gas phases, the source term in the solid phase energy equation becomes

$$S_{Es} = h_v(T_g - T_s) \tag{8.6}$$

and that in the gas phase energy equation

$$S_{Eg} = h_v(T_s - T_g) \tag{8.7}$$

where the volumetric heat transfer coefficient h_v is calculated from the heat transfer coefficient h by

$$h_v = A_v h \tag{8.8}$$

using the value for A_v given in Table 8.1.

The heat transfer coefficient h is calculated from the Nusselt number according to

$$h = Nu\frac{k_s}{d_h} \tag{8.9}$$

using the values of k_s and d_h given in Table 8.1 .

Nu is derived from the Reynolds and Prandtl numbers based on the following correlation for forced convection in a packed bed (Bird, Stewart and Lightfoot 2007):

$$Nu = 2.19(Re\,Pr)^{1/3} \tag{8.10}$$

Conductive heat transfer in the solid phase. Conductive heat transfer in the solid phase was modelled via the use of an additional diffusive variable Ψ, which is described by the conservation equation

$$\nabla\cdot(\rho_g\Phi_g\Gamma\nabla\Psi) + \Phi_g S_\Psi = 0 \tag{8.11}$$

If Ψ is set to be the solid temperature T_s, then equation 8.11 becomes

$$\nabla\cdot(\rho_g\Phi_g\Gamma_s\nabla T_s) + \Phi_g S_\Psi = 0 \tag{8.12}$$

and will correctly represent conduction in the solid if the diffusivity Γ is defined as

$$\Gamma_s = \frac{k_s\Phi_s}{\rho_g\Phi_g c_{ps}} \tag{8.13}$$

The source term S_Ψ is then related to the source term for convective heat transport S_{Es} by

$$S_\Psi = \frac{S_{Es}}{c_{ps}\Phi_g} \tag{8.14}$$

Radiative heat transport. A complete description of heat transfer in a porous medium would also include a model for radiation. However, it has been shown that the contribution of radiation to the heat recirculation process declines for leaner mixtures (Barra and Ellzey 2004). For the low combustion temperatures produced by the ultra-lean mixtures of interest here, it was assumed that conduction would be the dominant mode of heat transport, so radiative heat transport was not included in the initial model.

8.2.3.3 Combustion model

Combustion was modelled using a finite rate chemistry model, which is suitable in this system as the reaction rate is limited by the chemical kinetics of the reaction. The CH_4 combustion reaction was described using the multi-step skeletal kinetic mechanism developed in the previous chapter (Table 7.1). The mechanism consists of 47 elementary reversible reactions.

The rate constant k for the forward reaction step of each reversible reaction was specified in Arrhenius form

$$k = AT^{\beta} \exp\left(\frac{E_a}{RT}\right) \tag{8.15}$$

using the values for A, β and E_a given in Table 7.1, with the backward reaction rates calculated from the equilibrium constant for each reaction. The enhanced third body efficiencies shown for some of the reactions in Table 7.1 were also included.

It can also be seen from Table 7.1 that the rates of certain reactions in the mechanism are dependant on pressure, as well as temperature. ANSYS CFX 12.0 does not support pressure-dependant reactions via the GUI, so extra expressions were added to the model to calculate the pressure-dependant reaction rates according to the method described by Gilbert, Luther and Troe (1982), using the TROE parameters specified in Table 7.1.

8.2.4 Material properties

8.2.4.1 Gas properties

The gas mixture is composed of the 26 chemical species included in the skeletal mechanism. These are: H, H_2, O, O_2, OH, H_2O, HO_2, H_2O_2, CH_2, $CH_2(S)$, CH_3, CH_4, CO, CO_2, HCO, CH_2O, CH_3O, CH_3OH, CH_3O_2, CH_3OOH, C_2H_3, C_2H_4, C_2H_5, C_2H_6, CH_2HCO and N_2.

The specific heat capacity of each species was defined using a temperature dependant polynomial expression in NASA format. The polynomial coefficients were taken from the thermodynamic database provided with the full chemical kinetic mechanism (Bendtsen, Glarborg and Dam-Johansen 2000) from which the skeletal mechanism employed in this model was reduced.

The thermal conductivity and viscosity of each species were also specified using temperature dependant polynomial expressions, and the binary diffusion coefficients by temperature and pressure dependant polynomial expressions, in the manner described by Kee et al. (1986). The polynomial coefficients were derived from the transport properties database that accompanies the GRI-Mech chemical mechanism (Smith et al. 1999)[†].

8.2.4.2 Porous solid properties

The properties of the porous solid were set to represent a packed bed of ½" alumina (Al_2O_3) saddles, as in the experimental burner. The relevant material properties are given in Table 8.1.

Table 8.1 Material properties for a packed bed of ½" Al_2O_3 saddles.

Property	Value
Porosity Φ_s (%)[a]	66
Permeability κ (m^2)[b]	2×10^{-6}
Area density A_v (m^{-1})[a]	540
Hydraulic diameter d_h (m)[c]	1.1×10^{-2}
Thermal conductivity k_s ($Wm^{-1}K^{-1}$)[d]	6
Heat capacity c_{ps} ($Jkg^{-1}K^{-1}$)[e]	765

[a] The values for porosity and area density are as specified by the manufacturer (RVT Process Equipment n.d.).

[b] The permeability was calculated using Darcy's law combined with the Ergun equation for flow through a packed bed of non-spherical particles, in the manner described by Kay and Nedderman (1985). See appendix B for details.

[c] The hydraulic diameter was calculated according to the method described by Kay and Nedderman (1985) for a packed bed on non-spherical particles. See appendix B for details.

[d] The thermal conductivity is that for Al_2O_3 given by Pickenäcker et al. (1999a).

[e] The value for the specific heat capacity is that for Al_2O_3 given by Perry and Green (1997).

[†] The GRI-Mech transport data was used as no transport properties were provided with the mechanism (Bendtsen, Glarborg and Dam-Johansen 2000) from which the skeletal mechanism used in the model is derived.

8.2.5 Boundary conditions

The boundary conditions applied at the inlet were

$$\mathbf{u} = \mathbf{u}_{in}\,;\, T_g = T_{g,in}\,;\, X_k = X_{k,in} \tag{8.16}$$

and those at the outlet were

$$\frac{\partial T_g}{\partial n} = \frac{\partial X_k}{\partial n} = 0 \tag{8.17}$$

The solid temperature boundary condition at the inlet was specified as

$$-\Phi_s \lambda_s \frac{\partial T_s}{\partial n} + h_s (T_{g,in} - T_s) = 0 \tag{8.18}$$

and at the outlet as

$$-\Phi_s \lambda_s \frac{\partial T_s}{\partial n} + h_s (T_{inf} - T_s) = 0 \tag{8.19}$$

8.2.6 Simulation conditions

In order to validate the predictions of the model, simulations were carried out over the same range of conditions (firing rates and CH_4 concentrations) as were used in the experimental pilot-scale demonstration, as shown on the burner map in Figure 6.8. The preheat temperatures achieved in the experimental system (500–800K) were specified as the inlet temperatures in the model.

8.2.7 Solution method

ANSYS CFX 12.0 solves the conservation equations using a finite volume method.

In order to deal with the short timescales of some of the chemical reactions, it was necessary to use the stiff chemistry solver. This approach effectively decouples the flow and chemistry, allowing appropriate solvers and timesteps to be used for each model; in this case the highly coupled non-linear equations for the chemical species and enthalpy were solved using a Newton method (Holm-Christensen et al. 2001).

All simulations were performed at steady-state. A physical timestep of 1×10^{-3} s was specified.

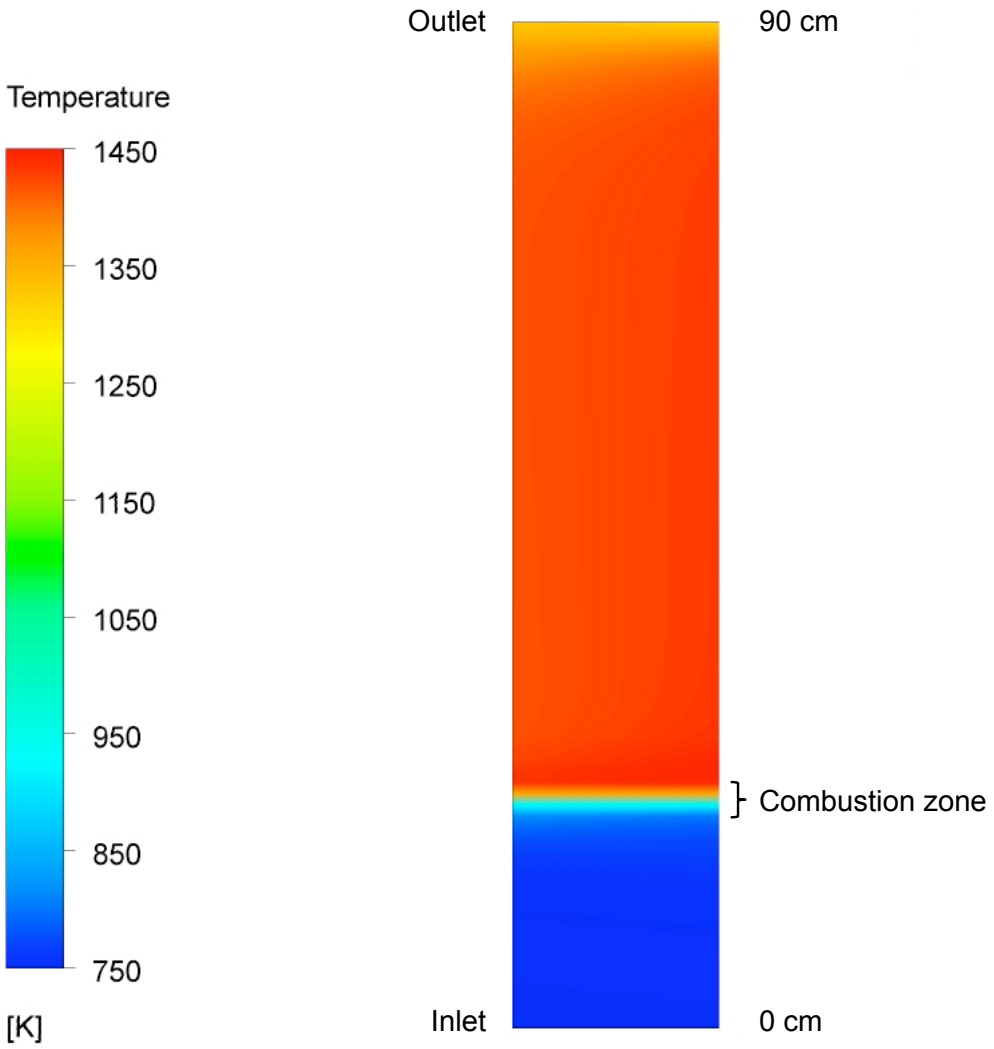

Figure 8.2 Example of CFD results: Predicted temperature profile for a firing rate of 300 kWm^{-2}, CH_4 concentration of 2.9 vol%, and preheat temperature of 750K.

8.3 Results and analysis

8.3.1 Typical temperature profiles

Figure 8.2 provides an example of the output obtained from the CFD porous burner model. It shows the steady-state temperature distribution in the burner for a firing rate of 300 kWm^{-2}, CH_4 concentration of 2.9 vol%, and preheat temperature of 750K. The location of the combustion zone is clearly visible. The adiabatic nature of the system is also apparent.

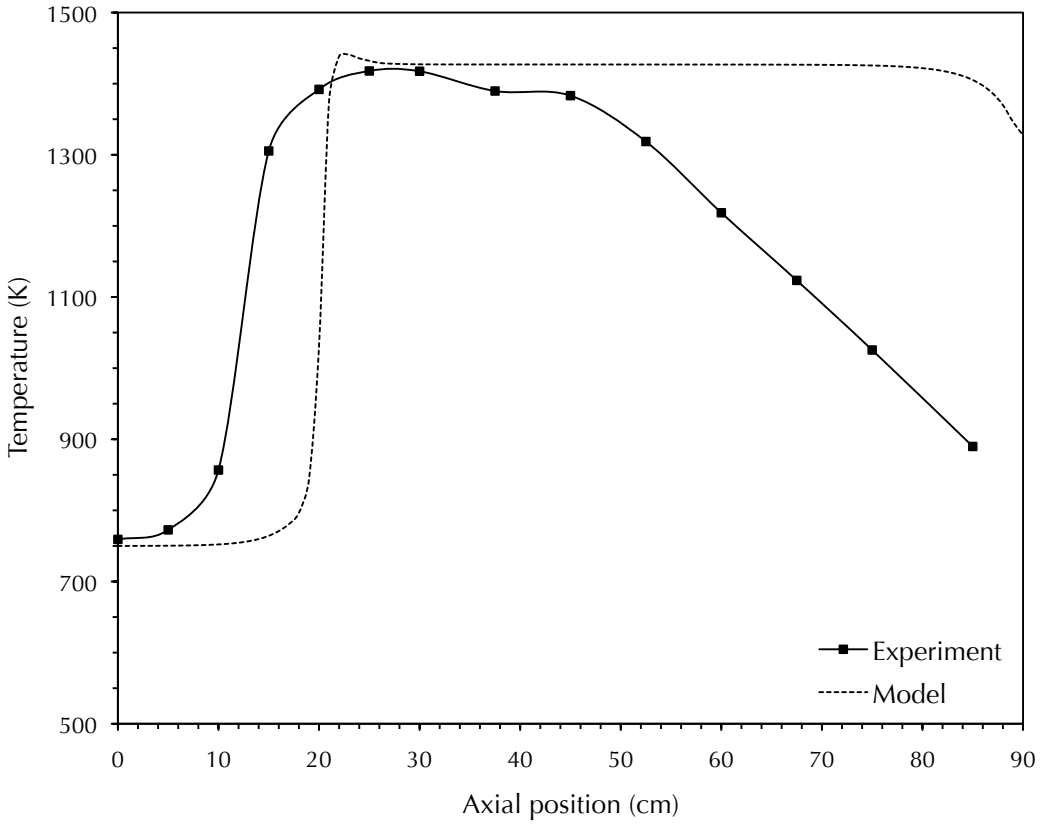

Figure 8.3 Comparison of predicted temperature profile for a firing rate of 300 kWm^{-2}, CH_4 concentration of 2.9 vol%, and preheat temperature of 750K, to that obtained in the experimental burner under similar conditions.

Figure 8.3 compares the same temperature profile—displayed in the conventional format used elsewhere in this thesis—to that obtained in the experimental pilot-scale burner under similar conditions; the temperature shown for the model is the gas temperature. It can be seen that there is a fairly pronounced difference in the location of the onset of combustion between the predicted and measured profiles. The model also predicts a much sharper temperature rise.

A perfect match between model and experiment would not be expected however, due to a number of simplifications applied in this initial model, including: (1) the walls of the model burner are assumed to be adiabatic, whereas the experimental burner experienced significant radial heat losses; (2) the model describes CH_4 combustion, whereas the experimental burner ran on natural gas; (3) the combustion chamber is modelled as a single porous region, whereas the experimental burner was of a multi-section design incorporating a layer of flint clay below the main porous bed; (4) radiative heat transfer was not included in the model; and (5) there is a possible error of ±10% in the predictions of the chemical kinetic mechanism under these conditions.

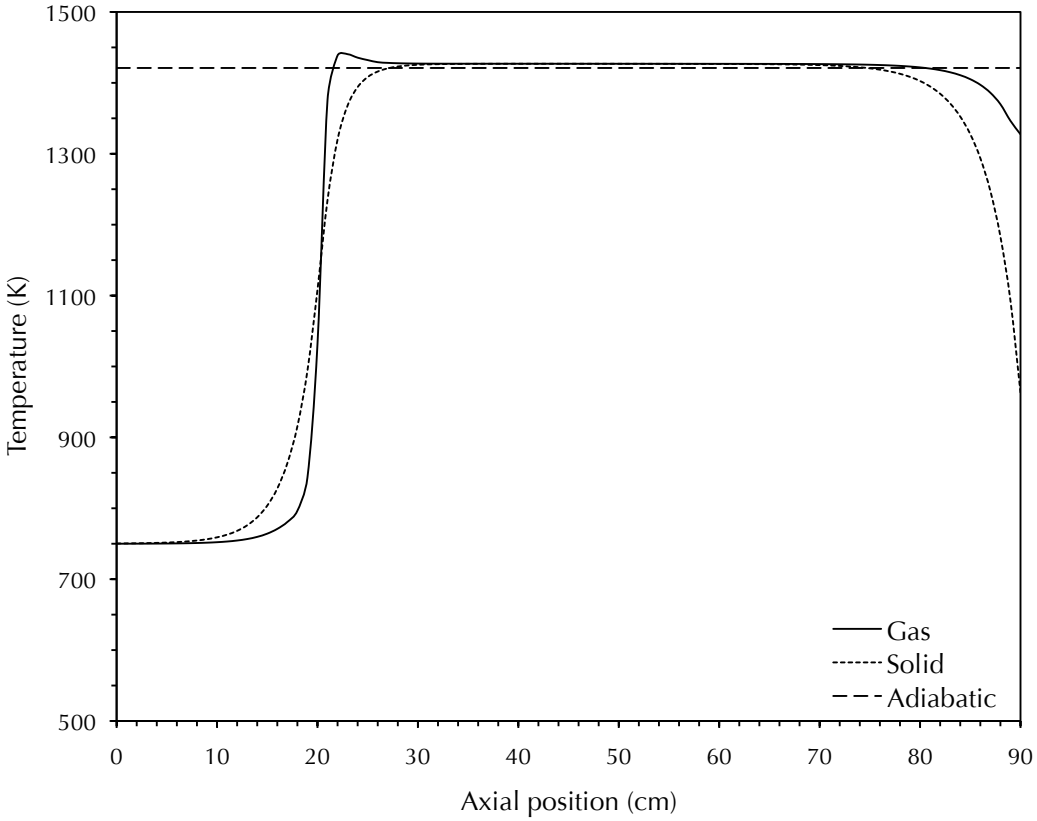

Figure 8.4 Predicted solid and gas temperature profiles for a firing rate of 300 kWm^{-2}, CH_4 concentration of 2.9 vol%, and preheat temperature of 750K. The adiabatic flame temperature is also indicated.

There is also a high degree of uncertainty in the temperature measurements obtained in the experimental burner, as previously discussed (§5.2.2).

Figure 8.4 again illustrates the temperature profiles predicted for a firing rate of 300 kWm^{-2}, CH_4 concentration of 2.9 vol%, and preheat temperature of 750K. Separate profiles for the gas and solid phases are shown. The heat recirculation process that characterises combustion in a porous medium is indicated by the differences between the two temperature profiles: It can be seen that upstream of the combustion zone, the solid is hotter than the gas, due to conductive heat transport from the combustion zone via the solid phase. In this upstream region, there is solid-to-gas convective heat transfer, thus preheating the incoming gas. Downstream of the combustion zone, it can be seen that the gas is hotter than the solid. There is therefore gas-to-solid convective heat transfer in this downstream region; the hot solid then conducts heat in the upstream direction; and thus the cycle continues.

It can also be seen from Figure 8.4 that the gas temperature exhibits a definite peak. This coincides with the release of energy from the combustion reaction.

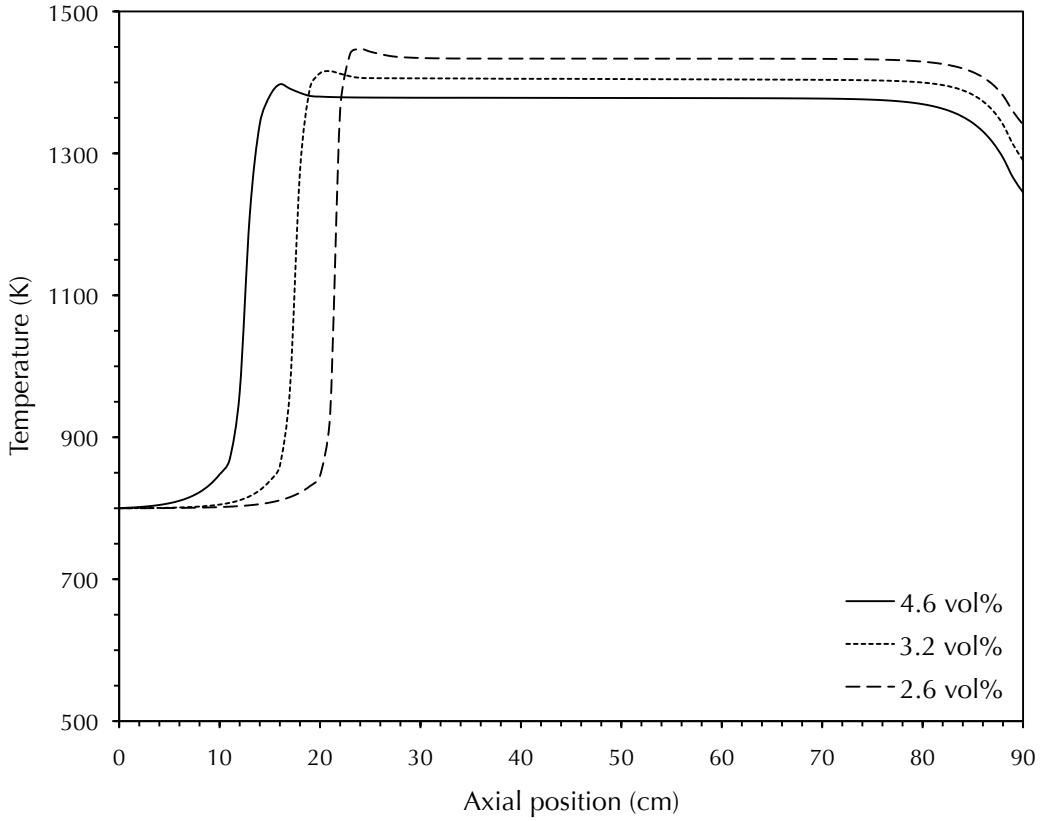

Figure 8.5 Effect of CH_4 concentration: Predicted temperature profiles for CH_4 concentrations of 2.6, 3.2 and 4.6 vol%, at a firing rate of 300 kWm^{-2}, and preheat temperature of 800K.

The adiabatic flame temperature for the system is also indicated. It can be seen that the gas temperature peaks above the adiabatic temperature. In other words, the combustion process is super-adiabatic, as would be expected for a mixture this lean (§3.2).

8.3.2 Effect of methane concentration

Figure 8.5 illustrates the effect of changing the CH_4 concentration whilst keeping the firing rate and preheat temperature constant. Temperature profiles at CH_4 concentrations of 2.6, 3.2 and 4.6 vol% are shown, at a firing rate of 300 kWm^{-2}, and preheat temperature of 800K. It can be seen that a decrease in CH_4 concentration causes the flame to stabilise further downstream. This confirms the trend observed in the experimental burner (see Figure 6.4 for comparison).

It is also interesting to note that the corresponding adiabatic flame temperatures for the system at these concentrations are 1401K, 1527K and 1806K at 2.6, 3.2 and 4.6 vol% CH_4 respectively[†]. The peak temperatures predicted by the model therefore indicate that the system is operating sub-adiabatically at the higher CH_4 concentrations.

[†] Note that the adiabatic flame temperature also depends on the preheat temperature.

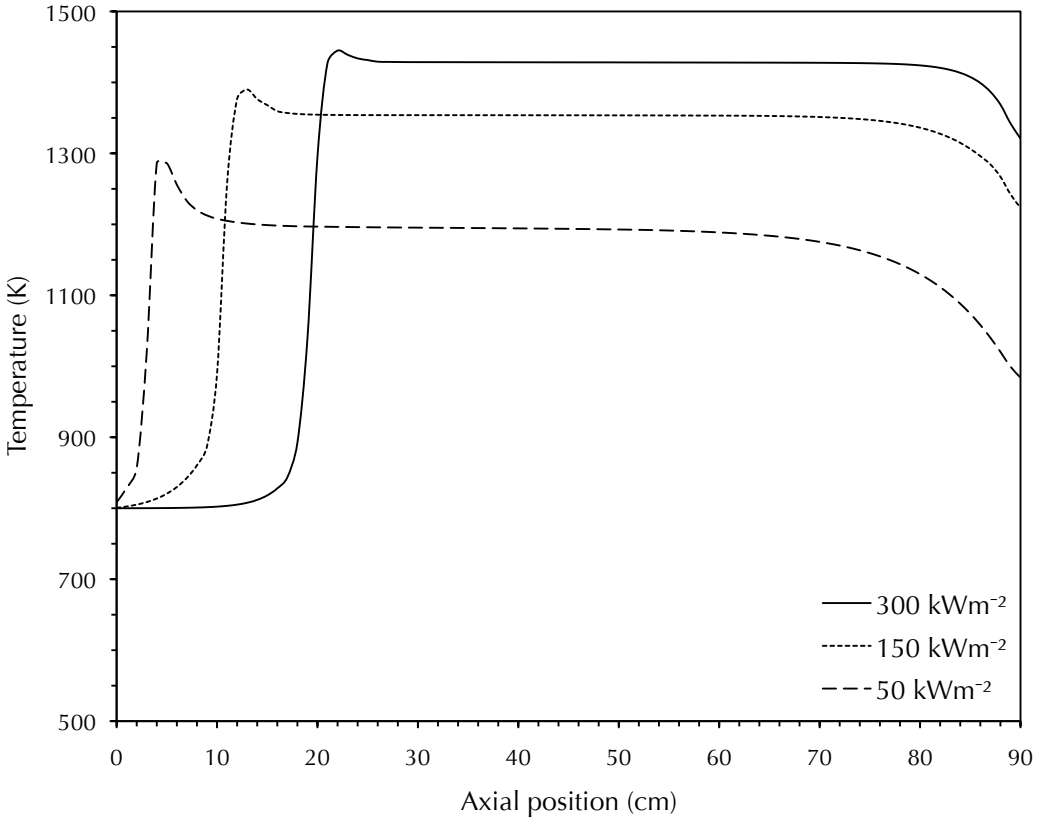

Figure 8.6 Effect of firing rate: Predicted temperature profiles for firing rates of 50, 150 and 300 kWm^{-2}, at a CH_4 concentration of 2.9 vol%, and preheat temperature of 800K.

This is consistent with what has been observed in previous studies (§3.2.2.4), and suggests that heat losses from the system boundaries exceed the heat recirculation provided by the porous solid under these conditions.

At CH_4 concentrations below those shown, corresponding to the transient combustion regime in the experimental system, stable solutions could not be otained using the model.

8.3.3 Effect of firing rate

Figure 8.6 illustrates the effect of changing the firing rate whilst keeping the CH_4 concentration and preheat temperature constant. Temperature profiles at firing rates of 50, 150 and 300 kWm^{-2} are shown, at a CH_4 concentration of 2.9 vol%, and preheat temperature of 800K. It can be seen that an increase in firing rate causes the flame to stabilise further downstream, as well as resulting in higher peak temperatures. Again, the model correctly predicts the observed experimental trend (as shown in Figure 6.6).

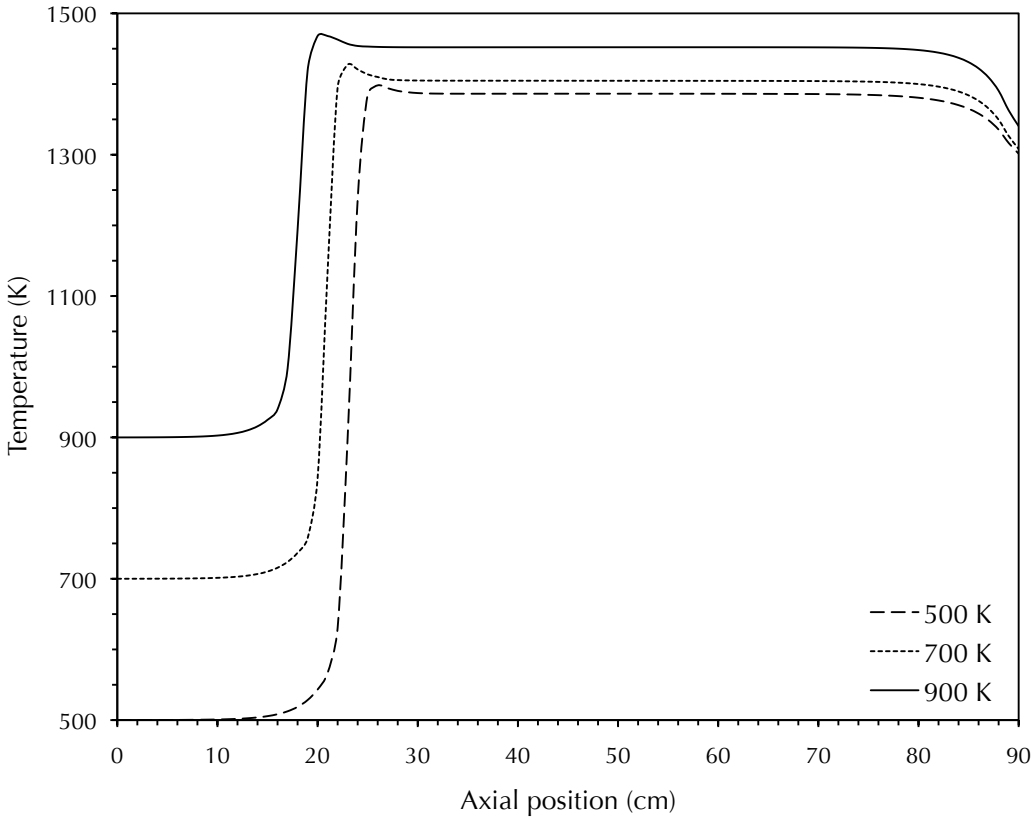

Figure 8.7 Effect of preheat temperature: Predicted temperature profiles for preheat temperatures of 500, 700 and 900K, at a firing rate of 300 kWm^{-2}, and a CH_4 concentration of 2.9 vol%.

8.3.4 Effect of preheat temperature

Figure 8.7 illustrates the effect of changing the preheat temperature whilst keeping the CH_4 concentration and firing rate constant. Temperature profiles at preheat temperatures of 500, 700 and 900K are shown, at a firing rate of 300 kWm^{-2} and a CH_4 concentration of 2.9 vol%. It can be seen that a decrease in preheat temperature causes the flame to stabilise further downstream. Lower maximum temperatures are also predicted for lower preheat temperatures, as would be expected.

In the model, a specified value for the preheat temperature is applied. In the experimental pilot-scale system the situation is more complex, as the amount of preheating is not an independent variable, but is determined by the effectiveness of the heat exchanger positioned at the outlet of the porous bed. This would be influenced by both the location of the combustion zone and the peak temperature, which in turn are influenced by the inlet conditions. Such an analysis as provided by Figure 8.7 was therefore not possible in the experimental system.

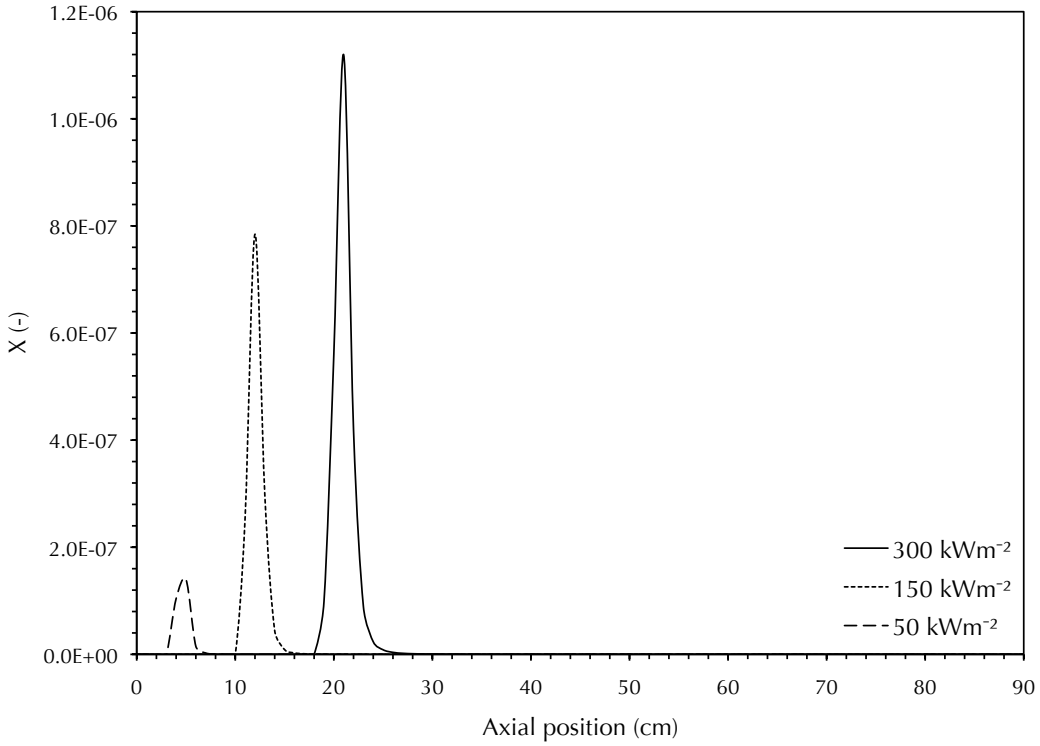

Figure 8.8 Effect of firing rate: Predicted H radical mass fraction profiles for firing rates of 50, 150 and 300 kWm^{-2}, at a CH_4 concentration of 2.9 vol%, and preheat temperature of 800K.

8.3.5 Typical species concentration profiles

Figure 8.8 again shows the effect of firing rate for the set of conditions previously described by the temperature profiles in Figure 8.6. In this case, however, the concentration profiles (in terms of mass fraction) of the hydrogen radical (H) are shown. Concentration profiles of the H radical are useful in studying ignition behaviour in combustion systems, as this species is associated with decomposition of the fuel.

The increased intensity of the combustion process at higher firing rates is clearly indicated by the increasing size of the H radical peaks as the firing rate increases.

In the experimental system, accurate measurements from within the combustion chamber are difficult to obtain due to the restrictive presence of the porous solid. The CFD model developed in this chapter is therefore a useful analytical tool: it is capable of providing additional data, such as the local solid and gas temperatures and species concentrations illustrated by the examples in Figures 8.4 and 8.8 respectively, that would not otherwise be available.

CONCLUSIONS AND FUTURE WORK

CONCLUSIONS AND FUTURE WORK

As shown in Chapter 1, although most discussions of greenhouse gas mitigation focus on energy-related carbon dioxide (CO_2) emissions, it is estimated that a quarter of the enhanced greenhouse effect observed since pre-industrial times is actually due to methane (CH_4). Emissions of CH_4—a potent greenhouse gas with a global warming potential (GWP) 25 times greater than that of CO_2, but a relatively short atmospheric lifetime of only 12 years—currently constitute 14.3% of total global anthropogenic greenhouse gas emissions. Due to the high GWP but short lifetime of CH_4, mitigation of these emissions should translate quickly into reductions in atmospheric concentrations. Anthropogenic emissions sources identified as having the greatest mitigation potential include coal mining, oil and gas distribution, and landfills.

As discussed in Chapter 2, emissions from coal mining in particular are some of the most challenging to mitigate from a technical perspective, because the CH_4 in the mine ventilation air (MVA)—which accounts for the majority of the emissions—is present at extremely low concentrations (typically less than 1 vol%). Lean-burn combustion systems, capable of combusting mixtures with the very low energy contents typical of MVA and other CH_4 emissions, were identified as a key mitigation technology, and a worthy topic for further research.

Although most often used for radiant heating applications, porous burners were identified as a possible lean-burn mitigation technology. They have not previously been considered for this purpose. Chapter 3 reviewed the use of porous burners for lean-burn applications. It was concluded that further research, both experimental and modelling, is required in the area of ultra-lean combustion, and particularly as regards the optimisation of burner designs for this purpose.

Pilot-scale demonstration

Part 2 of this thesis described the pilot scale demonstration of a porous burner system. The aims of the pilot-scale study were to demonstrate the concept of ultra-lean CH_4 combustion in porous burners; to determine the lowest practical lean flammability limit at which stable operation could be achieved; and to obtain the performance data needed to evaluate porous burners as a potential CH_4 mitigation technology.

In Chapter 4, the design of a porous burner for ultra-lean CH_4 combustion was described. The design incorporated a number of innovative features including: the integration of a heat exchanger into the system to recuperate additional heat from the combustion process; a modular structure, to enable the depth of the porous bed to be

adjusted; and the use of a randomly packed bed of saddles (which increased the porosity of the bed compared with commonly used spherical packing, whilst still retaining the durability of a packed bed over a rigid structure). A two-section design, incorporating a thin layer of flint clay below the main bed of alumina (Al_2O_3) saddles, was used. A CFD model was developed to assess two different design configurations and proved to be a useful design tool. The pilot-scale burner was successfully constructed and commissioned; the experimental set-up and procedure for its demonstration were described in Chapter 5.

In Chapter 6, the results of the pilot-scale demonstration were presented and analysed. It was found that combustion could be stabilised over the widest range of conditions when the largest possible porous bed depth was used. By analysing the temperature profiles in the bed, it was also found that either a decrease in natural gas (NG) concentration, or an increase in firing rate, caused the flame to stabilise further downstream from the inlet. Previous research has indicated that the use of a two-section design acts to stabilise the combustion process (§3.4.2). However, other than at relatively high NG concentrations, the flame did not stabilise at the interface between the flint clay and the main porous bed of saddles, indicating that this element of the design did not play a role in combustion stability in the current system.

A burner map describing the complete operating range of the system was developed. In summary, the stable lean flammability limit of the system operating on NG was found to be 2.3 vol%. This is a considerable extension of the conventional lean limit for NG (4.3 vol% in air), and is comparable with the results obtained in the limited number of previous studies that have focused on ultra-lean combustion in porous burners (Christo et al. 2002; Kotani, Behbahani and Takeno 1984). Operating in the transient combustion regime allowed the lean limit to be reduced further still, to 1.1 vol%.

The chosen arrangement of heat exchangers was demonstrated to be effective in preheating the incoming mixture; preheat temperatures of 500–800K were achieved. The efficiency of the heat exchanger system was estimated to be around 60–70%.

Emissions of the combustion related pollutants carbon monoxide (CO) and unburned hydrocarbons (UHC) were found to be negligible, indicating that the combustion process was complete. A full exhaust gas analysis would also include nitrogen oxide (NO_X) emissions, and this could be incorporated into any future work.

For this thesis, the temperature profile in the porous bed was measured using a series of thermocouples. A number of alternative non-intrusive experimental techniques have recently been applied in porous burner research, and could also be considered for use in the future to gain additional information on temperature and species concentrations. These include coherent anti-Stokes Raman scattering (CARS) (Kiefer et al. 2009);

electrical capacitance tomography (ECT) imaging (Liu et al. 2008); and laser induced fluorescence (LIF) (Voß 2008).

A major limitation of the current system was identified as being the extensive radial heat losses—accounting for approximately 10% of burner output—occurring through the burner walls, indicating that the Al_2O_3 fibre insulation employed was not sufficiently effective. This is a relatively straightforward issue to deal with however, and the use of additional or more effective insulation material should allow the achievable lean limit to be reduced further.

The use of a more effective material for the main porous bed of the burner should also allow the stable operating range of the burner to be further extended. The packed bed of 60% Al_2O_3, ½" ceramic saddles used in the current burner was chosen due to the favourable overall collection of attributes—good heat transfer characteristics, high application temperature, durability, and cost—that characterises this combination of material and structure. However, other materials, such as silicon carbide (SiC) foams or particles, and various high temperature metal alloys, exhibit superior heat transfer properties, and should be considered in future.

Computational fluid dynamics model

Part 3 of this thesis concerned the development of a CFD model. The ultimate aim was to create a comprehensive model capable of accurately describing ultra-lean CH_4 combustion in a porous burner.

In Chapter 7, the development of a skeletal kinetic mechanism for ultra-lean CH_4 combustion was described. The comprehensive mechanism describing CH_4 oxidation chemistry at low temperatures published by Bendtsen, Glarborg and Dam-Johansen (2000) was used as the starting point for the reduction. The reduction was performed for an adiabatic plug flow reactor (PFR) at atmospheric pressure, for a CH_4 concentration of 1 vol% in wet (1 vol% water) air, and an inlet temperature of 1000 K. The skeletal mechanism developed contained 47 reversible reactions and 26 chemical species. This is about a tenth of the size of the original mechanism, making it suitable for incorporation into a CFD code. The skeletal mechanism accurately reproduced the combustion behaviour predicted by the full mechanism at the conditions under which it was produced.

One of the drawbacks of using a reduced mechanism of any sort is that the reduction is accompanied by a loss of comprehensiveness, so the mechanism is no longer universally applicable. However, the skeletal mechanism developed in this thesis was found to be accurate to within ±10% over a range of conditions: CH_4 concentrations of 0.1–3 vol%; temperatures of 900–1100K; pressures of 1–10 atm; and wet or dry air feeds.

For conditions further from those under which it was reduced, the predictions of the mechanism are less accurate, but the main features of the combustion process are still described.

The skeletal mechanism could therefore be used with confidence in the porous burner model. It could also potentially be used for describing CH_4 combustion in other lean-burn technologies, for example the thermal flow reversal reactors (TFRR) described in Chapter 2 (§2.4.3.3). Moreover, the predictions of the mechanism are still accurate at pressures above atmospheric, so it might be suitable for modelling high-pressure combustion devices such as stationary gas turbines, which operate at pressures of 10–15 atm (Borman and Ragland 1998).

For the purposes of this thesis, the prediction of NO_X emissions was not considered necessary, as significant NO_X formation was not expected under the ultra-lean operating conditions of interest. The nitrogen chemistry contained in the original full mechanism was therefore removed as part of the reduction process. If predictions of NO_X were required for future work, the reduction would have to be repeated, with NO and NO_2 included in the objective function of the principal component analysis used to identify important reactions. Alternatively, it might be simpler to predict NO_X formation using a post-processing method, as previously demonstrated by Eggels and de Goey (1996).

Although modelling CH_4 chemistry is a good starting point, future work might involve creating a skeletal mechanism describing more complex mixtures, with compositions typical of actual CH_4 emissions or NG. This would most likely lead to a significant increase in the size of the mechanism required however, making implementation in CFD more challenging.

Furthermore, mechanism reduction of the sort undertaken for this thesis is a time consuming process, and is only semi-automated. If additional mechanisms were required for future work, the use of an automated generation procedure, such as that recently proposed by Løvas (2009), should be investigated.

In Chapter 8, the development of a 1-dimensional CFD model of a porous burner was described. Additional models describing heat transfer in a porous solid were successfully added to the commercial CFD code ANSYS CFX 12.0, and relatively detailed combustion chemistry was incorporated via the use of the skeletal mechanism described previously. The use of separate solid and gas energy equations accounted for non-equilibrium between the solid and gas phases, allowing the heat recirculation process—fundamental to porous burner operation—to be described.

Comparison of the burner temperature profiles predicted by the model with experimental data from the pilot-scale demonstration revealed a number of

discrepancies between the two, the most noteworthy being the exact location of the combustion zone. However, a perfect match was not expected, due to a number of simplifications applied in this initial model; the most significant of these is that the walls of the model burner were assumed to be adiabatic, whereas the experimental burner experienced significant radial heat losses.

Nevertheless, the model successfully predicted the main features of burner behaviour. The existence of a preheat zone due to heat recirculation via the solid was demonstrated, and the combustion process was shown to be superadiabatic, as expected. The main trends—the behaviour of the process on changing the firing rate or CH_4 concentration, and the approximate limits of stable combustion—were also predicted correctly.

Although the initial model development described in this thesis used only a simple 1-dimensional mesh, the feasibility of the CFD approach in modelling porous burners was demonstrated. The computational effort required was within realistic boundaries; a situation that will only improve in the future. The adaptation of a commercial CFD code for this purpose is novel. Although in recently published research by Liu, Xie and Wu (2009b), the ANSYS FLUENT code was used to model combustion in a porous medium, this work was restricted by the use of a single-step global reaction to describe the combustion chemistry.

There is much potential for future work in extending and improving the CFD model. The most obvious next step would be to take full advantage of the capabilities of CFD by extending the model to include 2- or 3-dimensional geometry. The effect of radial heat losses, and of flow inhomogeneities in the feed, could then be investigated. It would also be reasonably straightforward to add additional domains to the model to represent a multi-section burner design, and to investigate the effect of the length of the porous bed.

A complete description of heat transfer in a porous medium would also include a model for radiation. Radiative heat transfer in porous burners in commonly modelled by assuming that the solid is a grey, diffuse, homogenous medium, that can be described by a radiative transfer equation for isotropic scattering that accounts for the effects of emission, absorption and scattering (Viskanta 1966). The radiative transfer equation can be solved using the Schuster-Schwarzchild approximation (also known as the two-flux model) (Modest 2003). Such a model could be incorporated into the CFD code by means of an additional governing equation and appropriate source terms.

The current model applies the simplifying assumption that flow through the porous region is laminar. This is a topic on which knowledge is limited, as it is clearly difficult to obtain local velocity measurements from within a porous burner, however there is

experimental evidence to suggest that this assumption may not be valid (Wharton, Ellzey and Bogard 2005), particularly for porous beds with large pore sizes, such as the packed bed of saddles simulated in the current model. CFX supports a number of turbulence models, including the commonly used and generally applicable k-ε model (Launder and Spalding 1974). It would be an interesting exercise to investigate the effect of the inclusion of turbulence on the predictions of the model.

Alternative techniques for efficiently incorporating the combustion chemistry into the model could also be investigated. Examples of possible methods include the adaptive chemistry approach, whereby several different, simpler mechanisms are used in a single simulation, with each mechanism only being applied under those reaction conditions where it is faithful to the original full mechanism (Schwer, Lu and Green 2003); in-situ adaptive tabulation (ISAT) (Yang and Pope 1998); and the use of artificial neural networks (Cerri et al. 2003). Another proposed method, that of post-processing detailed chemical kinetics mechanisms onto CFD simulations (Skjøth-Rasmussen et al. 2004), would not be suitable for modelling porous burners (with the possible exception of predicting NO_X emissions, as already mentioned), due to the strong interdependence of combustion and heat transfer.

The initial CFD model described in this thesis considers the combustion chamber of the porous burner in isolation, and a specified preheat temperature is applied to the incoming reactants. A full model of the pilot-scale system would also need to incorporate the interaction between the combustion chamber and the surrounding heat exchanger, however this is clearly a much more computationally demanding proposal.

Thus far, only steady-state simulations of the system have been performed. It would be worthwhile to perform some transient simulations, in order to better understand the behaviour of the porous burner for leaner mixtures, when it operates in the transient combustion regime. Again, this would be more computationally expensive.

An extended, multi-dimensional CFD model based on the simplified 1-dimensional description of the porous burner described here would be a powerful investigative tool, and, if the accuracy of the model predictions could be improved, it could also be used to refine burner design. The models developed to describe heat transfer in a porous medium could also be applicable to other systems in the minerals and process industries.

Evaluation of porous burners as a methane mitigation technology

Based on the extension of the lean limit achieved here, porous burners show potential as a CH_4 mitigation technology. Simply improving insulation to reduce heat losses should allow the lean limit to be reduced further. The transient combustion regime

offers advantages where the energy content of the emission stream is extremely low (in the case of MVA for example), although significant alteration of the current system would be required to allow continuous operation in transient mode, for example via reciprocal flow operation. Otherwise, supplementation of the emission stream with additional fuel might be necessary. The alternative design configuration considered in Chapter 4 (§4.3), which included an additional fuel inlet directly below the porous bed, could be reconsidered under this scenario. For emissions with a higher energy content—such as MVA from coal mine bleeder shafts, landfill gas, and low quality biogas from anaerobic digestion—the process could essentially be used as is.

Using NG rather than CH_4 as the fuel is significant in the context of mitigation applications, as the presence of the higher alkanes in NG alters its combustion characteristics. Crucially, the lean flammability limit of NG (4.3 vol%) is already lower than that of CH_4 (5 vol%), and this must be considered when evaluating burner performance with respect to any potential CH_4 mitigation application. Further demonstration of the burner using a mixture with the characteristics of a particular emission stream (including any impurities) would be required. The use of NG as a demonstration fuel is valid however, as emissions regularly contain gases other than CH_4. Coal bed methane (CBM), for example, is very similar to NG in composition and calorific value.

It was also found that the combustion process in the pilot-scale burner appeared relatively stable against fluctuations in the firing rate or fuel concentration. This would be of benefit for CH_4 mitigation applications, as it would mean that the system would be resilient enough to cope with the variability in flow rate and energy content that characterises many emissions. This needs to be investigated systematically in the future.

The high thermal mass of the porous bed, which gives the burner this resilience, also results in the system having a long start-up phase however. This means that it might not be suitable for applications involving frequent on-and-off operation. A means of accelerating the warm-up period, for example by embedding an electric heater in the porous bed, could be investigated for future use.

Another design limitation of the burner in its current form is the pressure drop imposed by the arrangement of heat exchanger tubing. For CH_4 emissions at ambient pressure, the use of a compressor would be required to overcome this, imposing a negative energy cost. For MVA mitigation, the pressure drop would additionally impact on the safety of the ventilation system.

Scale-up and adaptation of the current pilot-scale system for industrial utilization, including the incorporation of automated data acquisition and process control, would of course be necessary. The use of active flame stabilisation (§3.4.7) to deal with the

expected supply fluctuations might be appropriate. High-pressure operation should be considered where a high throughput is needed. Preprocessing of the emissions, for example to remove moisture or particulates, might also be needed; this was not considered in the current study.

In conclusion, based on the results obtained thus far, porous burners show potential as a lean-burn technology for the mitigation of CH_4 emissions. In order to assess the suitability of a porous burner system for the mitigation of emissions from a particular source, a further demonstration of the system under the conditions specific to that source—ideally on site—would be required.

APPENDICES

Appendix A

NATURAL GAS SYSTEM MITIGATION OPTIONS

Possible procedural and hardware improvements in the natural gas system are listed below (EPA 2006b; Fernandez et al. 2005; Gillis et al. 2007; Robinson, Fernandez and Kantamaneni 2003).

Production. The production system includes wells, compressors, dehydrators, pneumatic devices, chemical injection pumps, heaters, meters, pipeline, and central gathering facilities. Mitigation options in the production system include:

- Use of catalytic converters for well field engines and compressors.
- Replacement of wet seals with dry seals in centrifugal compressors.
- Installation of flare systems at gas wells.
- Installation of plunger-lift systems in gas wells.
- Replacement of high-bleed pneumatic devices with low-bleed devices.
- Introduction of direct inspection and maintenance (DI&M) programs at production sites.

Processing. The processing system includes gas plant facilities that incorporate the use of vessels, compressors, dehydrators, pneumatic devices, acid gas removal units and heaters. Mitigation options in the processing system include:

- Retrofit of fuel gas for reciprocating compressors.
- Replacement of wet seals with dry seals in centrifugal compressors.
- Optimisation of glycol recirculation rates (glycol is used in dehydrators to remove water from the natural gas).
- Installation of flash tank separation in glycol dehydration systems.
- Replacement of glycol dehydrators with desiccant dehydrators.
- Use of lower heater-treater temperatures.
- Installation of automatic shutoff valves on pilot burners.
- Conversion of gas pneumatic controls to instrument air.

- Introduction of DI&M programs at gas processing plants.

Transmission. The transmission system includes transmission pipeline networks, compressor stations, and meter and pressure-regulating stations. Mitigation options in the transmission system include:

- Use of pipeline pumpdown techniques to lower gas line pressure before maintenance.
- Replacement of wet seals with dry seals in centrifugal compressors.
- Replacement of compressor rod packing systems.
- Replacement of gas-expansion starter turbines with electric starters on compressors and pumps.
- Conversion of gas pneumatic controls to instrument air.
- Introduction of DI&M programs at compressor stations and surface facilities.
- Repair of pipeline defects using composite wrap.

Distribution. The distribution system includes main and service pipeline networks, meter and pressure regulating stations, pneumatic devices, and customer meters. Mitigation options in the distribution system include:

- Use of hot taps in service pipeline connections.
- Use of composite wrap for non-leaking pipeline defects.
- Use of pipeline pumpdown techniques to lower gas line pressure before maintenance.
- Introduction of DI&M programs at gate stations.
- Repair of pipeline defects using composite wrap.

Appendix B

MATERIAL PROPERTIES CALCULATIONS

B.1 Permeability calculations

The permeabilities of the porous regions included in the CFD model of the porous burner described in Chapter 4 (§4.5) were calculated using Darcy's law combined with the Ergun equation for turbulent flow through a packed bed of non-spherical particles, in the manner described by Kay and Nedderman (1985).

Darcy's law for flow through a porous medium is given by

$$\frac{\Delta p}{L} = \frac{\mu u}{\kappa} \tag{B.1}$$

where u refers to the superficial velocity of the gas.

The Ergun equation (Ergun 1952) for turbulent flow through a packed bed of non-spherical particles of equivalent spherical diameter d_s and shape factor λ is given by

$$\frac{\Delta p}{L} = 150\lambda^2 \frac{(1-\Phi)^2}{\Phi^3} \frac{\mu u}{d_s^2} + 1.75\lambda \frac{(1-\Phi)}{\Phi^3} \frac{\rho_g u^2}{d_s} \tag{B.2}$$

λ is defined as the surface-volume ratio of the particle divided by the surface-volume ratio of a sphere of diameter d_s, and hence is given by

$$\lambda = \frac{d_s}{6} \frac{A_p}{V_p} \tag{B.3}$$

where A_p/V_p is the surface area to volume ratio of the porous material.

The permeabilities for each porous region were thus obtained by combining equations B.1 and B.2, using the values for μ, ρ, u, d_s, A_p/V_p, λ and Φ given in Table B.1.

B.2 Hydraulic diameter calculations

The hydraulic diameter (d_h) was calculated according to the method described by Kay and Nedderman (1985) for a packed bed of non-spherical particles.

d_h is given by

$$d_h = 4m \tag{B.4}$$

where

$$m = \frac{\Phi}{(1-\Phi)}\frac{d_s}{6\lambda} \tag{B.5}$$

λ is as defined by equation B.3. The relevant values of Φ, d_s and λ are given in Table B.1.

Table B.1 Material properties of the porous regions.

Property	Saddles	Flint clay	Cordierite tiles
Viscosity μ ($kgm^{-1}s^{-1}$)[a]	4.153×10^{-5}	4.153×10^{-5}	4.153×10^{-5}
Density ρ_g (kgm^{-3})[a]	3.53×10^{-1}	3.53×10^{-1}	3.53×10^{-1}
Superficial velocity u (ms^{-1})[b]	1.665	1.665	1.665
Equivalent spherical diameter d_s (m)[c]	1.27×10^{-2}	3.00×10^{-2}	1.00×10^{-3}
Surface area to volume ratio A_p/V_p (m^{-1})[d]	540	-	-
Shape factor λ (-)[e]	1.143	1.538	3.300
Porosity Φ (-)[f]	0.66	0.48	0.70

[a] Values for μ and ρ are those for air at 1000K (Rogers and Mayhew 1995).

[b] The values for u corresponds to a mass flow rate of 115 kgh^{-1}.

[c] For the saddles, d_s is taken as the nominal size as specified by the manufacturer (RVT Process Equipment n.d.), as suggested by McCabe, Smith and Harriot (2005). For the flint clay, d_s is estimated based on measurements provided by Lynch (2001).

[d] For the saddles, the value of A_p/V_p is as specified by the manufacturer (RVT Process Equipment n.d.).

[e] For the saddles, λ is calculated from the value of A_p/V_p according to equation B.3. For the flint clay and cordierite tiles, the value for λ is taken from McCabe, Smith and Harriot (2005).

[f] Values for Φ are as specified by the manufacturer (RVT Process Equipment n.d.) in the case of the saddles, as previously measured (Lynch 2001) for the flint clay, and as given by García, Miranzo and Osendi (2003) for the cordierite tiles.

Appendix C

BURNER OPERATING PROCEDURE

This operating procedure should be referred to in conjunction with the manufacturer supplied user manuals for the equipment and software used. For the Alicat MC series mass flow controllers (MFCs) and associated Flow Vision software these are available from http://www.alicatscientific.com, and for the DataTaker DT600 data acquisition system and associated DeLogger software from http://www.datataker.com.

Software menu commands are given in parentheses.

Start-up procedure

Start-up of temperature data logging system

1 Connect DataTaker to power source.

2 Ensure DataTaker is connected to PC.

3 Start DeLogger software and load Porous Burner program.[†]

4 *In DeLogger:* Connect DeLogger to DataTaker (*Connections*/*Connect* then select the relevant COM port from the list). If unable to connect, reset DataTaker manually and try again.

5 *In DeLogger:* Send Porous Burner program to DataTaker (*Program*/*Send to Connection*).

6 *In DeLogger:* Check status of DataTaker internal memory (*DataTaker*/*Status*) and clear any old data if necessary (*DataTaker*/*Clear* then select *Internal Memory* and *All Data*).

7 *In DeLogger:* Start logging temperature data (*DataTaker*/*Datalogging*/*Data Logging On*).

Start-up of flow data logging and control system

8 Connect MFCs to power source. To prevent overheating, do not leave MFCs connected to power source for extended periods with no flow.

[†] The Porous Burner program contains the saved DataTaker configuration for the porous burner system, including details of schedules, channel assignments and so on, as described in §5.2.2.

9 Ensure MFCs are connected to PC.

10 Start Flow Vision software.

11 *In Flow Vision:* Connect Flow Vision to MFCs (*File/New Session*). Once connected, new windows corresponding to each MFC will appear. This may take a few minutes to complete.

12 *In Flow Vision:* Ensure gas type is set correctly (*Configure/Gas Select* then select *Methane* or *Air* as appropriate).

13 *In Flow Vision:* Ensure plotting rate is set correctly (*Configure/Polling Rate/30 seconds*).

14 *In Flow Vision:* Specify which flow data to log (*Capture/Capture Path* then enter a suitable file location to which to save logged data, select *Capture Data from All Devices* and select the properties (*mass flow rate, volumetric flow rate, temperature, pressure, set point, time, date*) to be logged).

15 *In Flow Vision:* Start logging flow data (*Capture/Start Capturing*).

Start-up of main porous burner system

16 Turn ON extractor fan.

17 Turn ON air compressor.

18 OPEN manual valve to start air flow.

19 *In Flow Vision:* Set air flow to ignition conditions (*Configure/Set Point/Other* then enter a flow rate of *500 splm*).

20 OPEN manual valve to start NG flow.

21 Turn ON pilot burner.

22 *In Flow Vision:* Set NG flow to ignition conditions (*Configure/Set Point/Other* then enter a flow rate of *50 slpm*).

23 *In DeLogger:* Monitor the temperature profile of the porous bed. Once the combustion zone has migrated to the base of the porous bed, and the temperature at the base of the bed has reached ~1200K, ignition is complete.

24 Turn OFF pilot burner.

25 *In Flow Vision:* Set NG and air flows to start-up conditions (*Configure/Set Point/Other* then enter a flow rate of *50 slpm* for NG and *1000 slpm* for air).

26 *In DeLogger*: Monitor the temperature profile of the porous bed. Once the bed has reached the desired temperature (dependent on operating requirements), start-up is complete. This may take up to 2–3 hours depending on the initial and desired temperatures of the bed.

Normal operating procedure

27 *In Flow Vision*: Set NG and air flows to desired operating conditions (*Configure/Set Point/Other* then enter the desired flow rate).

28 *In DeLogger:* Monitor the temperature profile of the porous bed.

Shut-down procedure

Shut-down of main porous burner system

29 *In Flow Vision:* Reduce NG flow to zero (*Configure*/*Set Point*/*Other* then enter a flow rate of *0 slpm*).

30 CLOSE manual value to shut off NG flow.

31 *In Flow Vision:* Reduce air flow to zero (*Configure*/*Set Point*/*Other* then enter a flow rate of *0 slpm*).

32 CLOSE manual value to shut off air flow.

33 Turn OFF air compressor.

Shut-down of flow data logging and control system

34 Shut down Flow Vision software to stop logging flow data.

35 Disconnect MFCs from power source.

Shut-down of temperature data logging system

36 *In DeLogger:* Stop logging temperature data (*DataTaker*/*Halt*).

37 *In DeLogger:* Save temperature data from DataTaker internal memory to file (*DataTaker*/*Unload* then select *Unload to File*, select *CSV* as the file type and enter a suitable file name). This may take a few minutes to complete.

38 *In DeLogger:* Clear data from the DataTaker internal memory (*DataTaker*/*Clear*).

39 *In DeLogger:* Disconnect DeLogger from DataTaker (*DataTaker*/*Disconnect*).

40 Shut down DeLogger software.

41 Disconnect DataTaker from power source.

Appendix D

DETAILED KINETIC MECHANISM

The reaction set and rate coefficients for the comprehensive kinetic mechanism developed by Bendtsen, Glarborg and Dam-Johansen (2000) for low-temperature methane combustion, and used as the starting point for the mechanism reduction described in Chapter 7, is given below.

	REACTIONS CONSIDERED			(k = A T**b exp(-E/RT)) A	b	E
1.	O+OH=O2+H			2.00E+14	-0.4	0.0
2.	O+H2=OH+H			5.00E+04	2.7	6290.0
3.	OH+H2=H2O+H			2.10E+08	1.5	3450.0
4.	2OH=O+H2O			4.30E+03	2.7	-2486.0
5.	H+H+M=H2+M			1.00E+18	-1.0	0.0
	H2O	Enhanced by	0.000E+00			
6.	H+H+H2O=H2+H2O			6.00E+19	-1.2	0.0
7.	H+O+M=OH+M			6.20E+16	-0.6	0.0
	H2O	Enhanced by	5.000E+00			
8.	H+OH+M=H2O+M			1.60E+22	-2.0	0.0
	H2O	Enhanced by	5.000E+00			
9.	O+O+M=O2+M			1.90E+13	0.0	-1788.0
	H2O	Enhanced by	5.000E+00			
10.	H+O2+M=HO2+M			2.10E+18	-1.0	0.0
	H2O	Enhanced by	1.000E+01			
	N2	Enhanced by	0.000E+00			
11.	H+O2+N2=HO2+N2			6.70E+19	-1.4	0.0
12.	H+HO2=H2+O2			4.30E+13	0.0	1411.0
13.	H+HO2=2OH			1.70E+14	0.0	874.0
14.	H+HO2=O+H2O			3.00E+13	0.0	1721.0
15.	O+HO2=O2+OH			3.30E+13	0.0	0.0
16.	OH+HO2=H2O+O2			1.90E+16	-1.0	0.0
17.	HO2+HO2=H2O2+O2			4.20E+14	0.0	11982.0
	Declared duplicate reaction...					
18.	HO2+HO2=H2O2+O2			1.30E+11	0.0	-1629.0
	Declared duplicate reaction...					
19.	H2O2+M=OH+OH+M			1.30E+17	0.0	45500.0
	H2O	Enhanced by	5.000E+00			
20.	H2O2+H=HO2+H2			1.70E+12	0.0	3755.0
21.	H2O2+H=OH+H2O			1.00E+13	0.0	3576.0
22.	H2O2+O=OH+HO2			6.60E+11	0.0	3974.0
23.	H2O2+OH=H2O+HO2			7.80E+12	0.0	1330.0
	Declared duplicate reaction...					
24.	H2O2+OH=H2O+HO2			5.80E+14	0.0	9560.0
	Declared duplicate reaction...					
25.	CO+O+M=CO2+M			6.20E+14	0.0	3000.0
	H2O	Enhanced by	5.000E+00			
26.	CO+OH=CO2+H			1.50E+07	1.3	-758.0
27.	CO+O2=CO2+O			2.50E+12	0.0	47700.0
28.	HO2+CO=CO2+OH			5.80E+13	0.0	22934.0
29.	CH2O+M=HCO+H+M			3.30E+16	0.0	81000.0

```
    H2O             Enhanced by    5.000E+00
 30. CH2O+H=HCO+H2                                  1.30E+08    1.6     2166.0
 31. CH2O+O=HCO+OH                                  1.80E+13    0.0     3080.0
 32. CH2O+OH=HCO+H2O                                3.40E+09    1.2     -447.0
 33. CH2O+HO2=HCO+H2O2                              3.00E+12    0.0    13000.0
 34. CH2O+O2=HCO+HO2                                6.00E+13    0.0    40660.0
 35. HCO+M=H+CO+M                                   1.90E+17   -1.0    17000.0
    H2O             Enhanced by    5.000E+00
 36. HCO+H=CO+H2                                    1.20E+13    0.2        0.0
 37. HCO+O=CO+OH                                    3.00E+13    0.0        0.0
 38. HCO+O=CO2+H                                    3.00E+13    0.0        0.0
 39. HCO+OH=H2O+CO                                  1.00E+14    0.0        0.0
 40. HCO+O2=HO2+CO                                  7.60E+12    0.0      400.0
 41. CH3+H(+M)=CH4(+M)                              1.30E+16   -0.6      383.0
    Low pressure limit:  0.17500E+34 -0.47600E+01  0.24400E+04
    TROE centering:      0.78300E+00  0.74000E+02  0.29410E+04  0.69640E+04
    H2O             Enhanced by    8.570E+00
    N2              Enhanced by    1.430E+00
 42. CH4+H=CH3+H2                                   1.30E+04    3.0     8040.0
 43. CH4+O=CH3+OH                                   1.00E+09    1.5     8600.0
 44. CH4+OH=CH3+H2O                                 1.60E+06    2.1     2460.0
 45. CH4+HO2=CH3+H2O2                               1.80E+11    0.0    18700.0
 46. CH4+O2=CH3+HO2                                 7.90E+13    0.0    56000.0
 47. CH3+H=CH2+H2                                   9.00E+13    0.0    15100.0
 48. CH2(S)+H2=CH3+H                                7.20E+13    0.0        0.0
 49. CH3+O=CH2O+H                                   8.40E+13    0.0        0.0
 50. CH3+OH=CH2+H2O                                 7.50E+06    2.0     5000.0
 51. CH2(S)+H2O=CH3+OH                              3.00E+15   -0.6        0.0
 52. CH2OH+H=CH3+OH                                 1.00E+14    0.0        0.0
 53. CH3O+H=CH3+OH                                  1.00E+14    0.0        0.0
 54. CH3+OH(+M)=CH3OH(+M)                           6.30E+13    0.0        0.0
    Low pressure limit:  0.18900E+39 -0.63000E+01  0.31000E+04
    TROE centering:      0.21050E+00  0.83500E+02  0.53980E+04  0.83700E+04
    N2              Enhanced by    1.430E+00
    H2O             Enhanced by    8.580E+00
 55. CH3+HO2=CH3O+OH                                8.00E+12    0.0        0.0
 56. CH3+O2=CH3O+O                                  2.90E+13    0.0    30480.0
 57. CH3+O2=CH2O+OH                                 3.60E+10    0.0     8940.0
 58. CH3+CH3(+M)=C2H6(+M)                           2.10E+16   -1.0      620.0
    Low pressure limit:  0.12600E+51 -0.96700E+01  0.62200E+04
    TROE centering:      0.53250E+00  0.15100E+03  0.10380E+04  0.49700E+04
    N2              Enhanced by    1.430E+00
    H2O             Enhanced by    8.590E+00
    H2              Enhanced by    2.000E+00
    CO              Enhanced by    2.000E+00
    CO2             Enhanced by    3.000E+00
 59. CH3+CH2O=CH4+HCO                               7.80E-08    6.1     1967.0
 60. CH3+HCO=CH4+CO                                 1.20E+14    0.0        0.0
 61. CH2+H=CH+H2                                    1.00E+18   -1.6        0.0
 62. CH2+O=CO+H+H                                   5.00E+13    0.0        0.0
 63. CH2+O=CO+H2                                    3.00E+13    0.0        0.0
 64. CH2+OH=CH+H2O                                  1.10E+07    2.0     3000.0
 65. CH2+OH=CH2O+H                                  2.50E+13    0.0        0.0
 66. CH2+O2=CO+H2O                                  2.20E+22   -3.3     2867.0
 67. CH2+O2=CO2+H+H                                 3.30E+21   -3.3     2867.0
 68. CH2+O2=CH2O+O                                  3.30E+21   -3.3     2867.0
 69. CH2+O2=CO2+H2                                  2.60E+21   -3.3     2867.0
 70. CH2+O2=CO+OH+H                                 1.60E+21   -3.3     2867.0
 71. CH2+CO2=CH2O+CO                                1.10E+11    0.0     1000.0
 72. CH2+CH4=CH3+CH3                                4.30E+12    0.0    10030.0
 73. CH2+CH3=C2H4+H                                 4.20E+13    0.0        0.0
 74. CH2+CH2=C2H2+H+H                               4.00E+13    0.0        0.0
 75. CH2+HCCO=C2H3+CO                               3.00E+13    0.0        0.0
 76. CH2(S)+M=CH2+M                                 1.00E+13    0.0        0.0
    H               Enhanced by    0.000E+00
    H2O             Enhanced by    0.000E+00
    N2              Enhanced by    0.000E+00
    AR              Enhanced by    0.000E+00
 77. CH2(S)+N2=CH2+N2                               1.30E+13    0.0      430.0
 78. CH2(S)+AR=CH2+AR                               1.50E+13    0.0      884.0
 79. CH2(S)+H=CH2+H                                 2.00E+14    0.0        0.0
 80. CH2(S)+H2O=CH2+H2O                             3.00E+13    0.0        0.0
 81. CH2(S)+H=CH+H2                                 3.00E+13    0.0        0.0
```

```
 82. CH2(S)+O=CO+H+H                                   3.00E+13    0.0         0.0
 83. CH2(S)+OH=CH2O+H                                  3.00E+13    0.0         0.0
 84. CH2(S)+O2=CO+OH+H                                 7.00E+13    0.0         0.0
 85. CH2(S)+CO2=CH2O+CO                                3.00E+12    0.0         0.0
 86. CH2(S)+CH4=CH3+CH3                                4.30E+13    0.0         0.0
 87. CH2(S)+CH3=C2H4+H                                 2.00E+13    0.0         0.0
 88. CH2(S)+CH2CO=C2H4+CO                              1.60E+14    0.0         0.0
 89. CH2(S)+C2H6=CH3+C2H5                              1.20E+14    0.0         0.0
 90. CH+H=C+H2                                         1.50E+14    0.0         0.0
 91. CH+O=CO+H                                         5.70E+13    0.0         0.0
 92. CH+OH=HCO+H                                       3.00E+13    0.0         0.0
 93. CH+OH=C+H2O                                       4.00E+07    2.0      3000.0
 94. CH+O2=HCO+O                                       3.30E+13    0.0         0.0
 95. CH+H2O=CH2O+H                                     5.70E+12    0.0      -751.0
 96. CH+CO2=HCO+CO                                     3.40E+12    0.0       690.0
 97. CH+CH4=C2H4+H                                     6.00E+13    0.0         0.0
 98. CH+CH3=C2H3+H                                     3.00E+13    0.0         0.0
 99. CH+CH2=C2H2+H                                     4.00E+13    0.0         0.0
100. CH+CH2O=CH2CO+H                                   9.50E+13    0.0      -515.0
101. CH+HCCO=C2H2+CO                                   5.00E+13    0.0         0.0
102. C+OH=CO+H                                         5.00E+13    0.0         0.0
103. C+O2=CO+O                                         2.00E+13    0.0         0.0
104. C+CH3=C2H2+H                                      5.00E+13    0.0         0.0
105. C+CH2=C2H+H                                       5.00E+13    0.0         0.0
106. CH3OH+H=CH2OH+H2                                  1.70E+07    2.1      4868.0
107. CH3OH+H=CH3O+H2                                   4.20E+06    2.1      4868.0
108. CH3OH+O=CH2OH+OH                                  3.90E+05    2.5      3080.0
109. CH3OH+OH=CH2OH+H2O                                5.30E+04    2.5       960.0
110. CH3OH+OH=CH3O+H2O                                 1.32E+04    2.5       960.0
111. CH3OH+HO2=CH2OH+H2O2                              9.60E+10    0.0     12578.0
112. CH2O+H(+M)=CH3O(+M)                               5.40E+11    0.5      2600.0
     Low pressure limit:  0.15400E+31 -0.48000E+01  0.55600E+04
     TROE centering:      0.75800E+00  0.94000E+02  0.15550E+04  0.42000E+04
     N2              Enhanced by    1.430E+00
     H2O             Enhanced by    8.580E+00
113. CH3O+H=CH2O+H2                                    2.00E+13    0.0         0.0
114. CH3O+O=CH2O+OH                                    1.00E+13    0.0         0.0
115. CH3O+OH=CH2O+H2O                                  1.00E+13    0.0         0.0
116. CH3O+O2=CH2O+HO2                                  6.30E+10    0.0      2600.0
117. H+CH2O(+M)=CH2OH(+M)                              5.40E+11    0.5      3600.0
     Low pressure limit:  0.91000E+32 -0.48200E+01  0.65300E+04
     TROE centering:      0.71870E+00  0.10300E+03  0.12910E+04  0.41600E+04
     N2              Enhanced by    1.430E+00
     H2O             Enhanced by    8.580E+00
     CO              Enhanced by    2.000E+00
     CO2             Enhanced by    3.000E+00
     H2              Enhanced by    2.000E+00
118. CH2OH+H=CH2O+H2                                   2.00E+13    0.0         0.0
119. CH2OH+O=CH2O+OH                                   1.00E+13    0.0         0.0
120. CH2OH+OH=CH2O+H2O                                 1.00E+13    0.0         0.0
121. CH2OH+O2=CH2O+HO2                                 1.60E+15   -1.0         0.0
     Declared duplicate reaction...
122. CH2OH+O2=CH2O+HO2                                 7.20E+13    0.0      3577.0
     Declared duplicate reaction...
123. C2H6+H=C2H5+H2                                    5.40E+02    3.5      5210.0
124. C2H6+O=C2H5+OH                                    3.00E+07    2.0      5115.0
125. C2H6+OH=C2H5+H2O                                  7.20E+06    2.0       864.0
126. C2H6+HO2=C2H5+H2O2                                1.30E+13    0.0     20460.0
127. C2H6+O2=C2H5+HO2                                  5.00E+13    0.0     55000.0
128. C2H6+CH3=C2H5+CH4                                 5.50E-01    4.0      8300.0
129. C2H4+H(+M)=C2H5(+M)                               1.10E+12    0.5      1822.0
     Low pressure limit:  0.11120E+35 -0.50000E+01  0.44480E+04
     TROE centering:      0.50000E+00  0.95000E+02  0.95000E+02  0.20000E+03
     H2O             Enhanced by    5.000E+00
130. C2H5+H(+M)=C2H6(+M)                               5.20E+17   -1.0      1580.0
     Low pressure limit:  0.20000E+42 -0.70800E+01  0.66850E+04
     TROE centering:      0.84220E+00  0.12500E+03  0.22190E+04  0.68820E+04
     N2              Enhanced by    1.000E+00
     H2O             Enhanced by    6.000E+00
     AR              Enhanced by    7.000E-01
131. C2H5+H=CH3+CH3                                    4.90E+12    0.3         0.0
132. C2H5+O=CH3+CH2O                                   4.20E+13    0.0         0.0
133. C2H5+O=CH3HCO+H                                   5.30E+13    0.0         0.0
```

```
134. C2H5+O=C2H4+OH                                   3.00E+13    0.0        0.0
135. C2H5+OH=C2H4+H2O                                 2.40E+13    0.0        0.0
136. C2H5+O2=C2H4+HO2                                 1.00E+10    0.0    -2190.0
137. C2H5+CH2O=C2H6+HCO                               5.50E+03    2.8     5860.0
138. C2H5+HCO=C2H6+CO                                 1.20E+14    0.0        0.0
139. C2H5+CH3=C2H4+CH4                                1.10E+12    0.0        0.0
140. C2H5+C2H5=C2H6+C2H4                              1.50E+12    0.0        0.0
141. C2H3+H(+M)=C2H4(+M)                              6.10E+12    0.3      280.0
     Low pressure limit:  0.98000E+30 -0.38600E+01  0.33200E+04
     TROE centering:      0.78200E+00  0.20750E+03  0.26630E+04  0.60950E+04
     H2              Enhanced by    2.850E+00
     CO              Enhanced by    2.100E+00
     CO2             Enhanced by    2.850E+00
     H2O             Enhanced by    7.140E+00
     CH4             Enhanced by    2.850E+00
     C2H6            Enhanced by    4.290E+00
     N2              Enhanced by    1.430E+00
142. C2H4+M=C2H2+H2+M                                 3.50E+16    0.0    71500.0
     N2              Enhanced by    1.500E+00
     H2O             Enhanced by    1.000E+01
143. C2H4+H=C2H3+H2                                   5.40E+14    0.0    14900.0
144. C2H4+O=CH2HCO+H                                  4.70E+06    1.9      180.0
145. C2H4+O=CH3+HCO                                   8.10E+06    1.9      180.0
146. C2H4+O=CH2CO+H2                                  6.80E+05    1.9      180.0
147. C2H4+OH=C2H3+H2O                                 2.00E+13    0.0     5940.0
148. C2H4+HO2=CH3HCO+OH                               2.20E+12    0.0    17200.0
149. C2H4+O2=CH2HCO+OH                                2.00E+08    1.5    39000.0
150. C2H4+CH3=C2H3+CH4                                5.00E+11    0.0    15000.0
151. H+C2H2(+M)=C2H3(+M)                              3.10E+11    0.6     2590.0
     Low pressure limit:  0.22540E+41 -0.72690E+01  0.65770E+04
     TROE centering:      0.50000E+00  0.67500E+03  0.67500E+03
     H2              Enhanced by    2.000E+00
     CO              Enhanced by    2.000E+00
     CO2             Enhanced by    3.000E+00
     H2O             Enhanced by    5.000E+00
152. C2H3+H=C2H2+H2                                   4.00E+13    0.0        0.0
153. C2H3+O=CH2CO+H                                   3.00E+13    0.0        0.0
154. C2H3+OH=C2H2+H2O                                 2.00E+13    0.0        0.0
155. C2H3+O2=CH2O+HCO                                 1.10E+23   -3.3     3890.0
156. C2H3+O2=CH2HCO+O                                 2.50E+15   -0.8     3135.0
157. C2H3+O2=C2H2+HO2                                 5.20E+15   -1.3     3310.0
158. C2H3+CH2O=C2H4+HCO                               5.40E+03    2.8     5860.0
159. C2H3+HCO=C2H4+CO                                 9.00E+13    0.0        0.0
160. C2H3+CH3=C2H2+CH4                                2.10E+13    0.0        0.0
161. C2H3+C2H3=C2H4+C2H2                              1.50E+13    0.0        0.0
162. C2H2+M=C2H+H+M                                   9.10E+30   -3.7   127138.0
     H2              Enhanced by    2.000E+00
     CO              Enhanced by    2.000E+00
     CO2             Enhanced by    3.000E+00
     H2O             Enhanced by    5.000E+00
163. H2+C2H=C2H2+H                                    4.10E+05    2.4      864.0
164. C2H2+O=CH2+CO                                    6.10E+06    2.0     1900.0
165. C2H2+O=HCCO+H                                    1.40E+07    2.0     1900.0
166. C2H2+O=C2H+OH                                    3.20E+15   -0.6    15000.0
167. OH+C2H2=C2H+H2O                                  3.40E+07    2.0    14000.0
168. OH+C2H2=HCCOH+H                                  5.00E+05    2.3    13500.0
169. OH+C2H2=CH2CO+H                                  2.20E-04    4.5    -1000.0
170. OH+C2H2=CH3+CO                                   4.80E-04    4.0    -2000.0
171. OH+C2H2(+M)=C2H2OH(+M)                           1.50E+08    1.7     1000.0
     Low pressure limit:  0.18100E+24 -0.20000E+01  0.00000E+00
     H2              Enhanced by    2.000E+00
     CO              Enhanced by    2.000E+00
     CO2             Enhanced by    3.000E+00
     H2O             Enhanced by    5.000E+00
172. HO2+C2H2=CH2HCO+O                                1.00E+12    0.0    10000.0
173. HO2+C2H2=CH2O+HCO                                1.00E+12    0.0    10000.0
174. C2H2+O2=HCO+HCO                                  2.00E+08    1.5    30100.0
175. C2+H2=C2H+H                                      4.00E+05    2.4     1000.0
176. C2H+O=CH+CO                                      5.00E+13    0.0        0.0
177. C2H+OH=HCCO+H                                    2.00E+13    0.0        0.0
178. C2H+OH=C2+H2O                                    4.00E+07    2.0     8000.0
179. C2H+O2=CO+CO+H                                   2.50E+13    0.0        0.0
180. C2H+CH4=CH3+C2H2                                 7.20E+12    0.0      976.0
```

```
181. C2+OH=C2O+H                                       5.00E+13    0.0        0.0
182. C2+O2=CO+CO                                       5.00E+13    0.0        0.0
183. CH3HCO=CH3+HCO                                    7.10E+15    0.0    81280.0
184. CH3HCO+H=CH3CO+H2                                 4.10E+09    1.2     2400.0
185. CH3HCO+O=CH3CO+OH                                 5.80E+12    0.0     1800.0
186. CH3HCO+OH=CH3CO+H2O                               2.30E+10    0.7    -1110.0
187. CH3HCO+HO2=CH3CO+H2O2                             3.00E+12    0.0    12000.0
188. CH3HCO+O2=CH3CO+HO2                               3.00E+13    0.0    39000.0
189. CH3HCO+CH3=CH3CO+CH4                              2.00E-06    5.6     2464.0
190. CH2HCO=CH3+CO                                     1.00E+13    0.0    42000.0
191. CH2HCO+H=CH3+HCO                                  1.00E+14    0.0        0.0
192. CH2HCO+H=CH3CO+H                                  3.00E+13    0.0        0.0
193. CH2HCO+O=CH2O+HCO                                 5.00E+13    0.0        0.0
194. CH2HCO+OH=CH2CO+H2O                               2.00E+13    0.0        0.0
195. CH2HCO+OH=CH2OH+HCO                               1.00E+13    0.0        0.0
196. CH2HCO+O2=CH2O+CO+OH                              2.20E+11    0.0     1500.0
197. CH2HCO+CH3=C2H5CHO                                5.00E+13    0.0        0.0
198. CH2HCO+CH2=C2H4+HCO                               5.00E+13    0.0        0.0
199. CH2HCO+CH=C2H3+HCO                                1.00E+14    0.0        0.0
200. C2H5+HCO=C2H5CHO                                  1.80E+13    0.0        0.0
201. C2H5CHO+H=C2H5CO+H2                               8.00E+13    0.0        0.0
202. C2H5CHO+O=C2H5CO+OH                               7.80E+12    0.0     1730.0
203. C2H5CHO+OH=C2H5CO+H2O                             1.20E+13    0.0        0.0
204. C2H5+CO=C2H5CO                                    1.50E+11    0.0     4800.0
205. C2H2OH+H=CH2HCO+H                                 5.00E+13    0.0        0.0
206. C2H2OH+O=OCHCHO+H                                 5.00E+13    0.0        0.0
207. C2H2OH+O2=OCHCHO+OH                               1.00E+12    0.0     5000.0
208. CH3CO(+M)=CH3+CO(+M)                              2.80E+13    0.0    17100.0
     Low pressure limit:  0.21000E+16  0.00000E+00  0.14000E+05
     TROE centering:      0.50000E+00  0.10000E-29  0.10000E+31
     H2              Enhanced by    2.000E+00
     CO              Enhanced by    2.000E+00
     CO2             Enhanced by    3.000E+00
     H2O             Enhanced by    5.000E+00
209. CH3CO+H=CH3+HCO                                   2.10E+13    0.0        0.0
210. CH3CO+H=CH2CO+H2                                  1.20E+13    0.0        0.0
211. CH3CO+O=CH3+CO2                                   1.50E+14    0.0        0.0
212. CH3CO+O=CH2CO+OH                                  4.00E+13    0.0        0.0
213. CH3CO+OH=CH2CO+H2O                                1.20E+13    0.0        0.0
214. CH2+CO(+M)=CH2CO(+M)                              8.10E+11    0.5     4510.0
     Low pressure limit:  0.18800E+34 -0.51100E+01  0.70950E+04
     TROE centering:      0.59070E+00  0.27500E+03  0.12260E+04  0.51850E+04
     H2              Enhanced by    2.000E+00
     CO              Enhanced by    2.000E+00
     CO2             Enhanced by    3.000E+00
     H2O             Enhanced by    8.580E+00
     N2              Enhanced by    1.430E+00
215. CH2CO+H=CH3+CO                                    5.90E+06    2.0     1300.0
216. CH2CO+H=HCCO+H2                                   3.00E+07    2.0    10000.0
217. CH2CO+O=CO2+CH2                                   1.80E+12    0.0     1350.0
218. CH2CO+O=HCCO+OH                                   2.00E+07    2.0    10000.0
219. CH2CO+OH=HCCO+H2O                                 1.00E+07    2.0     3000.0
220. CH2CO+OH=CH2OH+CO                                 7.20E+12    0.0        0.0
221. CH2CO+OH=CH3+CO2                                  3.00E+12    0.0        0.0
222. HCCOH+H=HCCO+H2                                   3.00E+07    2.0     1000.0
223. HCCOH+OH=HCCO+H2O                                 1.00E+07    2.0     1000.0
224. HCCOH+O=HCCO+OH                                   2.00E+07    3.0     1900.0
225. OCHCHO+M=HCO+HCO+M                                1.00E+17    0.0    58000.0
226. OCHCHO+H=CH2O+HCO                                 3.00E+13    0.0        0.0
227. CH+CO(+M)=HCCO(+M)                                5.00E+13    0.0        0.0
     Low pressure limit:  0.18800E+29 -0.37400E+01  0.19360E+04
     TROE centering:      0.57570E+00  0.23700E+03  0.16520E+04  0.50690E+04
     N2              Enhanced by    1.430E+00
     H2O             Enhanced by    8.580E+00
     CO              Enhanced by    2.000E+00
     CO2             Enhanced by    3.000E+00
     H2              Enhanced by    2.000E+00
228. H+HCCO=CH2(S)+CO                                  1.00E+14    0.0        0.0
229. O+HCCO=H+CO+CO                                    1.00E+14    0.0        0.0
230. HCCO+OH=C2O+H2O                                   6.00E+13    0.0        0.0
231. HCCO+O2=CO2+CO+H                                  1.40E+07    1.7     1000.0
232. HCCO+O2=CO+CO+OH                                  2.90E+07    1.7     1000.0
233. HCCO+HCCO=C2H2+CO+CO                              1.00E+13    0.0        0.0
```

```
234. C2O+H=CH+CO                                      1.00E+13    0.0        0.0
235. C2O+O=CO+CO                                      5.00E+13    0.0        0.0
236. C2O+OH=CO+CO+H                                   2.00E+13    0.0        0.0
237. C2O+O2=CO+CO+O                                   2.00E+13    0.0        0.0
238. H+NO+M=HNO+M                                     4.00E+20   -1.8        0.0
     H2O              Enhanced by    4.100E+00
     H2               Enhanced by    1.250E+00
     N2               Enhanced by    1.000E+00
239. NO+O+M=NO2+M                                     7.50E+19   -1.4        0.0
     N2               Enhanced by    1.700E+00
     O2               Enhanced by    1.500E+00
     H2O              Enhanced by    1.000E+01
240. OH+NO+M=HONO+M                                   5.10E+23   -2.5      -68.0
     H2O              Enhanced by    5.000E+00
241. HO2+NO=NO2+OH                                    2.10E+12    0.0     -479.0
242. NO2+H=NO+OH                                      8.40E+13    0.0        0.0
243. NO2+O=NO+O2                                      3.90E+12    0.0     -238.0
244. NO2+O(+M)=NO3(+M)                                1.30E+13    0.0        0.0
     Low pressure limit:  0.10000E+29 -0.40800E+01  0.24700E+04
     N2               Enhanced by    1.500E+00
     O2               Enhanced by    1.500E+00
     H2O              Enhanced by    1.860E+01
245. NO2+NO2=NO+NO+O2                                 1.60E+12    0.0    26123.0
246. NO2+NO2=NO3+NO                                   9.60E+09    0.7    20900.0
247. NO3+H=NO2+OH                                     6.00E+13    0.0        0.0
248. NO3+O=NO2+O2                                     1.00E+13    0.0        0.0
249. NO3+OH=NO2+HO2                                   1.40E+13    0.0        0.0
250. NO3+HO2=NO2+O2+OH                                1.50E+12    0.0        0.0
251. NO3+NO2=NO+NO2+O2                                5.00E+10    0.0     2940.0
252. HNO+H=H2+NO                                      4.50E+11    0.7      655.0
253. HNO+O=NO+OH                                      1.00E+13    0.0        0.0
254. HNO+OH=NO+H2O                                    3.60E+13    0.0        0.0
255. HNO+O2=HO2+NO                                    1.00E+13    0.0    25000.0
256. HNO+NO2=HONO+NO                                  6.00E+11    0.0     2000.0
257. HNO+HNO=N2O+H2O                                  9.00E+08    0.0     3100.0
258. HNO+NH2=NH3+NO                                   3.63E+06    1.6    -1252.0
259. H2NO+M=HNO+H+M                                   2.50E+15    0.0    50000.0
     H2O              Enhanced by    5.000E+00
     N2               Enhanced by    2.000E+00
260. H2NO+H=HNO+H2                                    3.00E+07    2.0     2000.0
261. H2NO+H=NH2+OH                                    5.00E+13    0.0        0.0
262. H2NO+O=HNO+OH                                    3.00E+07    2.0     2000.0
263. H2NO+O=NH2+O2                                    2.00E+14    0.0        0.0
264. H2NO+OH=HNO+H2O                                  2.00E+07    2.0     1000.0
265. H2NO+NO=HNO+HNO                                  2.00E+04    2.0    13000.0
266. H2NO+NO2=HNO+HONO                                6.00E+11    0.0     2000.0
267. HONO+H=H2+NO2                                    1.20E+13    0.0     7352.0
268. HONO+O=OH+NO2                                    1.20E+13    0.0     5961.0
269. HONO+OH=H2O+NO2                                  4.00E+12    0.0        0.0
270. NH3+M=NH2+H+M                                    2.20E+16    0.0    93470.0
271. NH3+H=NH2+H2                                     6.40E+05    2.4    10171.0
272. NH3+O=NH2+OH                                     9.40E+06    1.9     6460.0
273. NH3+OH=NH2+H2O                                   2.00E+06    2.0      566.0
274. NH3+HO2=NH2+H2O2                                 3.00E+11    0.0    22000.0
275. NH2+H=NH+H2                                      4.00E+13    0.0     3650.0
276. NH2+O=HNO+H                                      6.60E+14   -0.5        0.0
277. NH2+O=NH+OH                                      6.80E+12    0.0        0.0
278. NH2+OH=NH+H2O                                    4.00E+06    2.0     1000.0
279. NH2+HO2=H2NO+OH                                  5.00E+13    0.0        0.0
280. NH2+HO2=NH3+O2                                   1.00E+13    0.0        0.0
281. NH2+NO=NNH+OH                                    8.90E+12   -0.3        0.0
282. NH2+NO=N2+H2O                                    1.72E+19   -2.3     1058.0
283. NH2+NO2=N2O+H2O                                  3.20E+18   -2.2        0.0
284. NH2+NO2=H2NO+NO                                  3.50E+12    0.0        0.0
285. NH2+H2NO=NH3+HNO                                 3.00E+12    0.0     1000.0
286. HONO+NH2=NO2+NH3                                 7.11E+01    3.0    -4941.0
287. NH2+NH2=N2H2+H2                                  8.50E+11    0.0        0.0
288. NH2+NH=N2H2+H                                    5.00E+13    0.0        0.0
289. NH2+N=N2+H+H                                     7.20E+13    0.0        0.0
290. NH+H=N+H2                                        3.00E+13    0.0        0.0
291. NH+O=NO+H                                        9.20E+13    0.0        0.0
292. NH+OH=HNO+H                                      2.00E+13    0.0        0.0
293. NH+OH=N+H2O                                      5.00E+11    0.5     2000.0
```

```
294. NH+O2=HNO+O                                      4.60E+05    2.0     6500.0
295. NH+O2=NO+OH                                      1.30E+06    1.5      100.0
296. NH+NO=N2O+H                                      3.19E+14   -0.5        0.0
297. NH+NO=N2+OH                                      2.20E+13   -0.2        0.0
298. NH+NO2=N2O+OH                                    1.00E+13    0.0        0.0
299. NH+NH=N2+H+H                                     2.50E+13    0.0        0.0
300. NH+N=N2+H                                        3.00E+13    0.0        0.0
301. N+OH=NO+H                                        3.80E+13    0.0        0.0
302. N+O2=NO+O                                        6.40E+09    1.0     6280.0
303. N+NO=N2+O                                        3.30E+12    0.3        0.0
304. N2H2+M=NNH+H+M                                   5.00E+16    0.0    50000.0
     H2O             Enhanced by    1.500E+01
     O2              Enhanced by    2.000E+00
     N2              Enhanced by    2.000E+00
     H2              Enhanced by    2.000E+00
305. N2H2+H=NNH+H2                                    5.00E+13    0.0     1000.0
306. N2H2+O=NH2+NO                                    1.00E+13    0.0        0.0
307. N2H2+O=NNH+OH                                    2.00E+13    0.0     1000.0
308. N2H2+OH=NNH+H2O                                  1.00E+13    0.0     1000.0
309. N2H2+NO=N2O+NH2                                  3.00E+12    0.0        0.0
310. N2H2+NH2=NH3+NNH                                 1.00E+13    0.0     1000.0
311. N2H2+NH=NNH+NH2                                  1.00E+13    0.0     1000.0
312. NNH=N2+H                                         1.00E+07    0.0        0.0
313. NNH+H=N2+H2                                      1.00E+14    0.0        0.0
314. NNH+O=N2+OH                                      8.00E+13    0.0        0.0
315. NNH+O=N2O+H                                      1.00E+14    0.0        0.0
316. NNH+O=NH+NO                                      5.00E+13    0.0        0.0
317. NNH+OH=N2+H2O                                    5.00E+13    0.0        0.0
318. NNH+O2=N2+HO2                                    2.00E+14    0.0        0.0
319. NNH+O2=N2+O2+H                                   5.00E+13    0.0        0.0
320. NNH+NO=N2+HNO                                    5.00E+13    0.0        0.0
321. NNH+NH2=N2+NH3                                   5.00E+13    0.0        0.0
322. NNH+NH=N2+NH2                                    5.00E+13    0.0        0.0
323. N2O+M=N2+O+M                                     4.00E+14    0.0    56100.0
     N2              Enhanced by    1.700E+00
     O2              Enhanced by    1.400E+00
     H2O             Enhanced by    1.200E+01
     CO              Enhanced by    1.500E+00
     CO2             Enhanced by    3.000E+00
324. N2O+H=N2+OH                                      3.30E+10    0.0     4729.0
     Declared duplicate reaction...
325. N2O+H=N2+OH                                      4.40E+14    0.0    19254.0
     Declared duplicate reaction...
326. N2O+O=NO+NO                                      6.60E+13    0.0    26630.0
327. N2O+O=N2+O2                                      1.00E+14    0.0    28000.0
328. N2O+OH=N2+HO2                                    1.30E-02    4.7    36561.0
329. N2O+OH=HNO+NO                                    1.20E-04    4.3    25081.0
330. N2O+NO=NO2+N2                                    5.30E+05    2.2    46281.0
331. CN+H2=HCN+H                                      3.00E+05    2.5     2237.0
332. HCN+O=NCO+H                                      1.40E+04    2.6     4980.0
333. HCN+O=NH+CO                                      3.50E+03    2.6     4980.0
334. HCN+O=CN+OH                                      2.70E+09    1.6    29200.0
335. HCN+OH=CN+H2O                                    3.90E+06    1.8    10300.0
336. HCN+OH=HOCN+H                                    5.90E+04    2.4    12500.0
337. HCN+OH=HNCO+H                                    2.00E-03    4.0     1000.0
338. HCN+OH=NH2+CO                                    7.80E-04    4.0     4000.0
339. HCN+CN=C2N2+H                                    1.50E+07    1.7     1530.0
340. CN+O=CO+N                                        7.70E+13    0.0        0.0
341. CN+OH=NCO+H                                      4.00E+13    0.0        0.0
342. CN+O2=NCO+O                                      7.50E+12    0.0     -389.0
343. CN+CO2=NCO+CO                                    3.70E+06    2.2    26884.0
344. CN+NO2=NCO+NO                                    5.30E+15   -0.8      344.0
345. CN+NO2=CO+N2O                                    4.90E+14   -0.8      344.0
346. CN+NO2=N2+CO2                                    3.70E+14   -0.8      344.0
347. CN+HNO=HCN+NO                                    1.80E+13    0.0        0.0
348. CN+HONO=HCN+NO2                                  1.20E+13    0.0        0.0
349. CN+N2O=NCN+NO                                    3.90E+03    2.6     3696.0
350. CN+HNCO=HCN+NCO                                  1.50E+13    0.0        0.0
351. CN+NCO=NCN+CO                                    1.80E+13    0.0        0.0
352. HNCO+M=NH+CO+M                                   1.10E+16    0.0    86000.0
353. HNCO+H=NH2+CO                                    2.20E+07    1.7     3800.0
354. HNCO+O=HNO+CO                                    1.50E+08    1.6    44012.0
355. HNCO+O=NH+CO2                                    9.80E+07    1.4     8524.0
```

356.	HNCO+O=NCO+OH	2.20E+06	2.1	11425.0
357.	HNCO+OH=NCO+H2O	6.40E+05	2.0	2563.0
358.	HNCO+HO2=NCO+H2O2	3.00E+11	0.0	22000.0
359.	HNCO+O2=HNO+CO2	1.00E+12	0.0	35000.0
360.	HNCO+NH2=NH3+NCO	5.00E+12	0.0	6200.0
361.	HNCO+NH=NH2+NCO	3.00E+13	0.0	23700.0
362.	HOCN+H=NCO+H2	2.00E+07	2.0	2000.0
363.	HOCN+O=NCO+OH	1.50E+04	2.6	4000.0
364.	HOCN+OH=NCO+H2O	6.40E+05	2.0	2563.0
365.	HCNO+H=HCN+OH	1.00E+14	0.0	12000.0
366.	HCNO+O=HCO+NO	2.00E+14	0.0	0.0
367.	HCNO+OH=CH2O+NO	4.00E+13	0.0	0.0
368.	NCO+M=N+CO+M	3.10E+16	-0.5	48000.0
369.	NCO+H=NH+CO	5.00E+13	0.0	0.0
370.	NCO+O=NO+CO	4.70E+13	0.0	0.0
371.	NCO+OH=NO+HCO	5.00E+12	0.0	15000.0
372.	NCO+O2=NO+CO2	2.00E+12	0.0	20000.0
373.	NCO+H2=HNCO+H	7.60E+02	3.0	4000.0
374.	NCO+HCO=HNCO+CO	3.60E+13	0.0	0.0
375.	NCO+NO=N2O+CO	6.20E+17	-1.7	763.0
376.	NCO+NO=N2+CO2	7.80E+17	-1.7	763.0
377.	NCO+NO2=CO+NO+NO	2.50E+11	0.0	-707.0
378.	NCO+NO2=CO2+N2O	3.00E+12	0.0	-707.0
379.	NCO+HNO=HNCO+NO	1.80E+13	0.0	0.0
380.	NCO+HONO=HNCO+NO2	3.60E+12	0.0	0.0
381.	NCO+N=N2+CO	2.00E+13	0.0	0.0
382.	NCO+NCO=N2+CO+CO	1.80E+13	0.0	0.0
383.	C2N2+O=NCO+CN	4.60E+12	0.0	8880.0
384.	C2N2+OH=HOCN+CN	1.90E+11	0.0	2900.0
385.	NCN+O=CN+NO	1.00E+14	0.0	0.0
386.	NCN+OH=HCN+NO	5.00E+13	0.0	0.0
387.	NCN+H=HCN+N	1.00E+14	0.0	0.0
388.	NCN+O2=NO+NCO	1.00E+13	0.0	0.0
389.	H+CH3CN=HCN+CH3	4.00E+07	2.0	2000.0
390.	H+CH3CN=CH2CN+H2	3.00E+07	2.0	1000.0
391.	O+CH3CN=NCO+CH3	1.50E+04	2.6	4980.0
392.	OH+CH3CN=CH2CN+H2O	2.00E+07	2.0	2000.0
393.	CH2CN+O=CH2O+CN	1.00E+14	0.0	0.0
394.	CN+CH2OH=CH2CN+OH	5.00E+13	0.0	0.0
395.	H2CN+M=HCN+H+M	3.00E+14	0.0	22000.0
396.	CO+NO2=CO2+NO	9.00E+13	0.0	33779.0
397.	CO+N2O=N2+CO2	3.20E+11	0.0	20237.0
398.	CO2+N=NO+CO	1.90E+11	0.0	3400.0
399.	CH2O+NCO=HNCO+HCO	6.00E+12	0.0	0.0
400.	CH2O+NO2=HCO+HONO	8.00E+02	2.8	13730.0
401.	HCO+NO=HNO+CO	7.20E+12	0.0	0.0
402.	HCO+NO2=CO+HONO	1.20E+23	-3.3	2355.0
403.	HCO+NO2=H+CO2+NO	8.40E+15	-0.8	1930.0
404.	HCO+HNO=CH2O+NO	6.00E+11	0.0	2000.0
405.	CH4+CN=CH3+HCN	6.20E+04	2.6	-437.0
406.	NCO+CH4=CH3+HNCO	9.80E+12	0.0	8120.0
407.	CH3+NO=HCN+H2O	1.50E-01	3.5	3950.0
408.	CH3+NO=H2CN+OH	1.50E-01	3.5	3950.0
409.	CH3+NO2=CH3O+NO	4.00E+13	-0.2	0.0
410.	CH3+N=H2CN+H	7.10E+13	0.0	0.0
411.	CH3+CN=CH2CN+H	1.00E+14	0.0	0.0
412.	CH3+HOCN=CH3CN+OH	5.00E+12	0.0	2000.0
413.	CH2+NO=HCN+OH	2.20E+12	0.0	-378.0
414.	CH2+NO=HCNO+H	1.30E+12	0.0	-378.0
415.	CH2+NO2=CH2O+NO	5.90E+13	0.0	0.0
416.	CH2+N=HCN+H	5.00E+13	0.0	0.0
417.	CH2+N2=HCN+NH	1.00E+13	0.0	74000.0
418.	H2CN+N=N2+CH2	2.00E+13	0.0	0.0
419.	CH2(S)+NO=HCN+OH	2.00E+13	0.0	0.0
420.	CH2(S)+NO=CH2+NO	1.00E+14	0.0	0.0
421.	CH2(S)+HCN=CH3+CN	5.00E+13	0.0	0.0
422.	CH+NO2=HCO+NO	1.00E+14	0.0	0.0
423.	CH+NO=HCN+O	4.80E+13	0.0	0.0
424.	CH+NO=HCO+N	3.40E+13	0.0	0.0
425.	CH+NO=NCO+H	1.90E+13	0.0	0.0
426.	CH+N=CN+H	1.30E+13	0.0	0.0
427.	CH+N2=HCN+N	3.70E+07	1.4	20723.0
428.	CH+N2O=HCN+NO	1.90E+13	0.0	-511.0

```
429. C+NO=CN+O                                         2.00E+13    0.0        0.0
430. C+NO=CO+N                                         2.80E+13    0.0        0.0
431. C+N2=CN+N                                         6.30E+13    0.0    46019.0
432. C+N2O=CN+NO                                       5.10E+12    0.0        0.0
433. C2H6+CN=C2H5+HCN                                  1.20E+05    2.8    -1788.0
434. C2H6+NCO=C2H5+HNCO                                1.50E-09    6.9    -2910.0
435. C2H4+CN=C2H3+HCN                                  5.90E+14   -0.2        0.0
436. C2H3+NO=C2H2+HNO                                  1.00E+12    0.0     1000.0
437. C2H3+N=HCN+CH2                                    2.00E+13    0.0        0.0
438. C2H2+NCO=HCCO+HCN                                 1.40E+12    0.0     1815.0
439. C2H+NO=CN+HCO                                     2.10E+13    0.0        0.0
440. CH2CO+CN=HCCO+HCN                                 2.00E+13    0.0        0.0
441. HCCO+NO=HCNO+CO                                   7.20E+12    0.0        0.0
442. HCCO+NO=HCN+CO2                                   1.60E+13    0.0        0.0
443. HCCO+NO2=HCNO+CO2                                 1.60E+13    0.0        0.0
444. HCCO+N=HCN+CO                                     5.00E+13    0.0        0.0
445. CH3+O2(+M)=CH3O2(+M)                              7.80E+08    1.2        0.0
     Low pressure limit:  0.54000E+26 -0.33000E+01  0.00000E+00
     N2              Enhanced by    1.100E+00
     H2O             Enhanced by    1.000E+01
446. CH3O2+H=CH3O+OH                                   1.00E+14    0.0        0.0
447. CH3O2+O=CH3O+O2                                   3.60E+13    0.0        0.0
448. CH3O2+OH=CH3OH+O2                                 6.00E+13    0.0        0.0
449. CH3O2+HO2=CH3OOH+O2                               2.50E+11    0.0    -1570.0
450. CH3O2+H2O2=CH3OOH+HO2                             2.40E+12    0.0     9940.0
451. CH3O2+CH2O=CH3OOH+HCO                             2.00E+12    0.0    11665.0
452. CH3O2+CH4=CH3OOH+CH3                              1.80E+11    0.0    18500.0
453. CH3O2+CH3=CH3O+CH3O                               2.40E+13    0.0        0.0
454. CH3O2+CH3O=CH2O+CH3OOH                            3.00E+11    0.0        0.0
455. CH3O2+CH2OH=CH2O+CH3OOH                           1.20E+13    0.0        0.0
456. CH3O2+CH3OH=CH3OOH+CH2OH                          1.80E+12    0.0    13700.0
457. CH3O2+CH3O2=CH3O+CH3O+O2                          1.00E+11    0.0      300.0
458. CH3O2+CH3O2=CH3OH+CH2O+O2                         4.00E+09    0.0    -2210.0
459. CH3OOH=CH3O+OH                                    6.30E+14    0.0    42300.0
460. CH3OOH+H=CH3O2+H2                                 8.80E+10    0.0     1860.0
461. CH3OOH+H=CH3O+H2O                                 8.20E+10    0.0     1860.0
462. CH3OOH+O=CH3O2+OH                                 1.00E+12    0.0     3000.0
463. CH3OOH+OH=CH3O2+H2O                               1.80E+12    0.0     -378.0
464. CH3O2+NO=CH3O+NO2                                 2.53E+12    0.0     -358.0
465. CH4+NO2=CH3+HONO                                  1.20E+13    0.0    30000.0
466. CH3NO2(+M)=CH3+NO2(+M)                            1.80E+16    0.0    58500.0
     Low pressure limit:  0.13000E+18  0.00000E+00  0.42000E+05
     TROE centering:      0.18300E+00  0.10000E-29  0.10000E+31
467. CH3NO2+H=HONO+CH3                                 3.30E+12    0.0     3730.0
468. CH3NO2+H=CH3NO+OH                                 1.40E+12    0.0     3730.0
469. CH3NO2+H=H2CNO2+H2                                5.40E+02    3.5     5200.0
470. CH3NO2+O=H2CNO2+OH                                1.50E+13    0.0     5350.0
471. CH3NO2+OH=H2CNO2+H2O                              5.00E+05    2.0     1000.0
472. CH3NO2+OH=CH3OH+NO2                               2.00E+10    0.0    -1000.0
473. CH3NO2+HO2=H2CNO2+H2O2                            3.00E+12    0.0    23000.0
474. CH3NO2+O2=H2CNO2+HO2                              2.00E+13    0.0    57000.0
475. CH3NO2+CH3=CH4+H2CNO2                             5.50E-01    4.0     8300.0
476. CH3NO2+CH2(S)=CH3+H2CNO2                          1.20E+14    0.0        0.0
477. CH3NO2+CH2=CH3+H2CNO2                             6.50E+12    0.0     7900.0
478. CH3NO2+CH3O=H2CNO2+CH3OH                          3.00E+11    0.0     7000.0
479. CH3NO2+NO2=H2CNO2+HONO                            3.00E+11    0.0    32000.0
480. H2CNO2=CH2O+NO                                    1.00E+13    0.0    36000.0
481. H2CNO2+H=CH3+NO2                                  5.00E+13    0.0        0.0
482. H2CNO2+O=CH2O+NO2                                 5.00E+13    0.0        0.0
483. H2CNO2+OH=CH2OH+NO2                               1.00E+13    0.0        0.0
484. H2CNO2+OH=CH2O+HONO                               1.00E+13    0.0        0.0

 NOTE: A units mole-cm-sec-K, E units cal/mole
```

Appendix E

SKELETAL KINETIC MECHANISM

The chemical kinetics and thermodynamic data for the skeletal mechanism for ultra-lean methane combustion developed in Chapter 7 are given below in CHEMKIN format.

```
ELEMENTS
H
O
C
N
END
SPECIES
H       H2      O       O2      OH      H2O     HO2     H2O2    CH2     CH2(S)
CH3     CH4     CO      CO2     HCO     CH2O    CH3O    CH3OH   CH3O2   CH3OOH
C2H3    C2H4    C2H5    C2H6    N2      CH2HCO
END
THERMO ALL
   200.000  1000.000  6000.000
C2H5                83194H   5C   2    0    0G   300.000  4000.000 1400.00    0 1
 0.87349157E+01 0.54537677E-02-0.37647177E-06-0.31297920E-09 0.52844000E-13    2
 0.10265269E+05-0.23104086E+02 0.24398923E+01 0.13747212E-01-0.85500653E-06    3
-0.31469924E-08 0.93754355E-12 0.13158588E+05 0.13099146E+02                   4
C2H3                83194H   3C   2    0    0G   300.000  4000.000 1400.00    0 1
 0.71861677E+01 0.34552682E-02-0.29435373E-06-0.20681942E-09 0.36797774E-13    2
 0.32229627E+05-0.15977573E+02 0.24955740E+01 0.10269993E-01-0.10226917E-05    3
-0.27594382E-08 0.96919825E-12 0.34232813E+05 0.10614626E+02                   4
CH2(S)              83194H   2C   1    0    0G   300.000  4000.000 1400.00    0 1
 0.40752106E+01 0.15779120E-02-0.10806129E-06-0.84592437E-10 0.14033284E-13    2
 0.50007492E+05-0.15480316E+01 0.35932946E+01 0.13151238E-02 0.30756846E-06    3
 0.42637904E-09-0.34178712E-12 0.50451547E+05 0.17780241E+01                   4
CH2                 83194H   2C   1    0    0G   300.000  4000.000 1400.00    0 1
 0.39737520E+01 0.16097502E-02-0.10785119E-06-0.86399922E-10 0.14301196E-13    2
 0.45608973E+05 0.75549729E-01 0.36872995E+01 0.15066403E-02 0.69679857E-07    3
 0.23537297E-09-0.19397147E-12 0.45863672E+05 0.20267601E+01                   4
CH3O2      9/08/94 LIG/CC   1H   3O   2    0G   300.000  5000.000 1381.000    11
 8.04008290E+00 6.53779443E-03-2.30284850E-06 3.64660532E-10-2.14511604E-14    2
-2.27775197E+03-1.73557764E+01 1.46355059E+00 2.09318664E-02-1.40862480E-05    3
 4.66682187E-09-6.15228667E-13 1.08022981E+02 1.83173980E+01                   4
CH3OOH             BUR95 H   4C   1O   2   00G   200.000  6000.000  1000.000    1
 0.61600316E+01 0.10239957E-01-0.36101507E-05 0.57550301E-09-0.34178147E-13    2
-0.17654526E+05-0.61911544E+01 0.49652507E+01 0.92343510E-03 0.34455956E-04    3
-0.44469600E-07 0.17456120E-10-0.16726970E+05 0.29880275E+01                   4
H                   120186H   1               G   300.000  5000.000 1000.00      1
 2.50000000e+00 0.00000000e+00 0.00000000e+00 0.00000000e+00 0.00000000e+00    2
 2.54716300e+04-4.60117600e-01 2.50000000e+00 0.00000000e+00 0.00000000e+00    3
 0.00000000e+00 0.00000000e+00 2.54716300e+04-4.60117600e-01                   4
H2                  121286H   2               G   300.000  5000.000 1000.00      1
 2.99142300e+00 7.00064400e-04-5.63382900e-08-9.23157800e-12 1.58275200e-15    2
-8.35034000e+02-1.35511000e+00 3.29812400e+00 8.24944200e-04-8.14301500e-07    3
-9.47543400e-11 4.13487200e-13-1.01252100e+03-3.29409400e+00                   4
O                   120186O   1               G   300.000  5000.000 1000.00      1
```

```
 2.54206000e+00-2.75506200e-05-3.10280300e-09 4.55106700e-12-4.36805200e-16    2
 2.92308000e+04 4.92030800e+00 2.94642900e+00-1.63816600e-03 2.42103200e-06    3
-1.60284300e-09 3.89069600e-13 2.91476400e+04 2.96399500e+00                   4
O2                121386O   2               G   300.000  5000.000 1000.00     1
 3.69757800e+00 6.13519700e-04-1.25884200e-07 1.77528100e-11-1.13643500e-15    2
-1.23393000e+03 3.18916600e+00 3.21293600e+00 1.12748600e-03-5.75615000e-07    3
 1.31387700e-09-8.76855400e-13-1.00524900e+03 6.03473800e+00                   4
OH                121286O   1H   1          G   300.000  5000.000 1000.00     1
 2.88273000e+00 1.01397400e-03-2.27687700e-07 2.17468400e-11-5.12630500e-16    2
 3.88688800e+03 5.59571200e+00 3.63726600e+00 1.85091000e-04-1.67616500e-06    3
 2.38720300e-09-8.43144200e-13 3.60678200e+03 1.35886000e+00                   4
H2O                20387H   2O   1          G   300.000  5000.000 1000.00     1
 2.67214600e+00 3.05629300e-03-8.73026000e-07 1.20099600e-10-6.39161800e-15    2
-2.98992100e+04 6.86281700e+00 3.38684200e+00 3.47498200e-03-6.35469600e-06    3
 6.96858100e-09-2.50658800e-12-3.02081100e+04 2.59023300e+00                   4
HO2                20387H   1O   2          G   300.000  5000.000 1000.00     1
 4.07219100e+00 2.13129600e-03-5.30814500e-07 6.11226900e-11-2.84116500e-15    2
-1.57972700e+02 3.47602900e+00 2.97996300e+00 4.99669700e-03-3.79099700e-06    3
 2.35419200e-09-8.08902400e-13 1.76227400e+02 9.22272400e+00                   4
H2O2              120186H   2O   2          G   300.000  5000.000 1000.00     1
 4.57316700e+00 4.33613600e-03-1.47468900e-06 2.34890400e-10-1.43165400e-14    2
-1.80069600e+04 5.01137000e-01 3.38875400e+00 6.56922600e-03-1.48501300e-07    3
-4.62580600e-09 2.47151500e-12-1.76631500e+04 6.78536300e+00                   4
CH3               121286C   1H   3          G   300.000  5000.000 1000.00     1
 2.84405200e+00 6.13797400e-03-2.23034500e-06 3.78516100e-10-2.45215900e-14    2
 1.64378100e+04 5.45269700e+00 2.43044300e+00 1.11241000e-02-1.68022000e-05    3
 1.62182900e-08-5.86495300e-12 1.64237800e+04 6.78979400e+00                   4
CH4               121286C   1H   4          G   300.000  5000.000 1000.00     1
 1.68347900e+00 1.02372400e-02-3.87512900e-06 6.78558500e-10-4.50342300e-14    2
-1.00807900e+04 9.62339500e+00 7.78741500e-01 1.74766800e-02-2.78340900e-05    3
 3.04970800e-08-1.22393100e-11-9.82522900e+03 1.37221900e+01                   4
CO                121286C   1O   1          G   300.000  5000.000 1000.00     1
 3.02507800e+00 1.44268900e-03-5.63082800e-07 1.01858100e-10-6.91095200e-15    2
-1.42683500e+04 6.10821800e+00 3.26245200e+00 1.51194100e-03-3.88175500e-06    3
 5.58194400e-09-2.47495100e-12-1.43105400e+04 4.84889700e+00                   4
CO2               121286C   1O   2          G   300.000  5000.000 1000.00     1
 4.45362300e+00 3.14016900e-03-1.27841100e-06 2.39399700e-10-1.66903300e-14    2
-4.89669600e+04-9.55395900e-01 2.27572500e+00 9.92207200e-03-1.04091100e-05    3
 6.86668700e-09-2.11728000e-12-4.83731400e+04 1.01884900e+01                   4
HCO               121286H   1C   1O   1     G   300.000  5000.000 1000.00     1
 3.55727100e+00 3.34557300e-03-1.33500600e-06 2.47057300e-10-1.71385100e-14    2
 3.91632400e+03 5.55229900e+00 2.89833000e+00 6.19914700e-03-9.62308400e-06    3
 1.08982500e-08-4.57488500e-12 4.15992200e+03 8.98361400e+00                   4
CH2O              121286C   1H   2O   1     G   300.000  5000.000 1000.00     1
 2.99560600e+00 6.68132100e-03-2.62895500e-06 4.73715300e-10-3.21251700e-14    2
-1.53203700e+04 6.91257200e+00 1.65273100e+00 1.26314400e-02-1.88816800e-05    3
 2.05003100e-08-8.41323700e-12-1.48654000e+04 1.37848200e+01                   4
CH3O              121686C   1H   3O   1     G   300.000  3000.000 1000.00     1
 3.77080000e+00 7.87149700e-03-2.65638400e-06 3.94443100e-10-2.11261600e-14    2
 1.27832500e+02 2.92957500e+00 2.10620400e+00 7.21659500e-03 5.33847200e-06    3
-7.37763600e-09 2.07561100e-12 9.78601100e+02 1.31521800e+01                   4
CH3OH             121686C   1H   4O   1     G   300.000  5000.000 1000.00     1
 4.02906100e+00 9.37659300e-03-3.05025400e-06 4.35879300e-10-2.22472300e-14    2
-2.61579100e+04 2.37819600e+00 2.66011500e+00 7.34150800e-03 7.17005100e-06    3
-8.79319400e-09 2.39057000e-12-2.53534800e+04 1.12326300e+01                   4
C2H4              121286C   2H   4          G   300.000  5000.000 1000.00     1
 3.52841900e+00 1.14851800e-02-4.41838500e-06 7.84460100e-10-5.26684800e-14    2
 4.42828900e+03 2.23038900e+00-8.61488000e-01 2.79616300e-02-3.38867700e-05    3
 2.78515200e-08-9.73787900e-12 5.57304600e+03 2.42114900e+01                   4
C2H6              121686C   2H   6          G   300.000  4000.000 1000.00     1
 4.82593800e+00 1.38404300e-02-4.55725900e-06 6.72496700e-10-3.59816100e-14    2
-1.27177900e+04-5.23950700e+00 1.46253900e+00 1.54946700e-02 5.78050700e-06    3
-1.25783200e-08 4.58626700e-12-1.12391800e+04 1.44322900e+01                   4
N2                121286N   2               G   300.000  5000.000 1000.00     1
 2.92664000e+00 1.48797700e-03-5.68476100e-07 1.00970400e-10-6.75335100e-15    2
-9.22797700e+02 5.98052800e+00 3.29867700e+00 1.40824000e-03-3.96322200e-06    3
 5.64151500e-09-2.44485500e-12-1.02090000e+03 3.95037200e+00                   4
CH2HCO            110393O   1H   3C   2     G   300.000  5000.000 1000.00     1
 5.97567000e+00 8.13059100e-03-2.74362400e-06 4.07030400e-10-2.17601700e-14    2
 4.90321800e+02-5.04525100e+00 3.40906200e+00 1.07385700e-02 1.89149200e-06    3
-7.15858300e-09 2.86738500e-12 1.52147700e+03 9.55829000e+00                   4
END
REACTIONS    MOLES  CAL/MOLE
```

```
O+OH =  O2+H                                      2.000E+14  -0.4000       0.00
OH+H2 =  H2O+H                                    2.100E+08   1.5200    3449.63
2OH =  O+H2O                                      4.300E+03   2.7000   -2485.73
H+O2+M =  HO2+M                                   2.100E+18  -1.0000       0.00
 H2O/10/ N2/0/
H+O2+N2 =  HO2+N2                                 6.700E+19  -1.4200       0.00
H+HO2 =  H2+O2                                    4.300E+13   0.0000    1410.85
H+HO2 =  2OH                                      1.700E+14   0.0000     873.91
O+HO2 =  O2+OH                                    3.300E+13   0.0000       0.00
OH+HO2 =  H2O+O2                                  1.900E+16  -1.0000       0.00
2HO2 =  H2O2+O2                                   4.200E+14   0.0000   11980.70
H2O2+M =  2OH+M                                   1.300E+17   0.0000   45495.06
 H2O/5/
H2O2+OH =  H2O+HO2                                7.800E+12   0.0000    1329.86
DUPLICATE
H2O2+OH =  H2O+HO2                                5.800E+14   0.0000    9558.96
DUPLICATE
CO+OH =  CO2+H                                    1.500E+07   1.3000    -757.92
CH2O+H =  HCO+H2                                  1.300E+08   1.6200    2165.77
CH2O+O =  HCO+OH                                  1.800E+13   0.0000    3079.67
CH2O+OH =  HCO+H2O                                3.400E+09   1.1800    -446.95
CH2O+HO2 =  HCO+H2O2                              3.000E+12   0.0000   12998.59
CH2O+O2 =  HCO+HO2                                6.000E+13   0.0000   40655.59
HCO+M =  H+CO+M                                   1.900E+17  -1.0000   16998.16
 H2O/5/
HCO+O2 =  HO2+CO                                  7.600E+12   0.0000     399.96
CH4+H =  CH3+H2                                   1.300E+04   3.0000    8039.13
CH4+O =  CH3+OH                                   1.000E+09   1.5000    8599.07
CH4+OH =  CH3+H2O                                 1.600E+06   2.1000    2459.73
CH4+O2 =  CH3+HO2                                 7.900E+13   0.0000   55993.92
CH3+O =  CH2O+H                                   8.400E+13   0.0000       0.00
CH3+OH(+M) =  CH3OH(+M)                           6.300E+13   0.0000       0.00
 N2/1.43/ H2O/8.58/
    LOW /  1.890E+38  -6.30    3099.66 /
    TROE /   2.1050E-01  8.3500E+01  5.3980E+03  8.3700E+03 /
CH3+HO2 =  CH3O+OH                                8.000E+12   0.0000       0.00
CH3+O2 =  CH3O+O                                  2.900E+13   0.0000   30476.69
CH3+O2 =  CH2O+OH                                 3.600E+10   0.0000    8939.03
2CH3(+M) =  C2H6(+M)                              2.100E+16  -0.9700     619.93
 N2/1.43/ H2O/8.59/ H2/2/ CO/2/ CO2/3/
    LOW /  1.260E+50  -9.67    6219.33 /
    TROE /   5.3250E-01  1.5100E+02  1.0380E+03  4.9700E+03 /
CH2(S)+N2 =  CH2+N2                               1.300E+13   0.0000     429.95
CH2(S)+O2 =  CO+OH+H                              7.000E+13   0.0000       0.00
CH3OH+OH =  CH3O+H2O                              1.320E+04   2.5300     959.90
CH2O+H(+M) =  CH3O(+M)                            5.400E+11   0.4540    2599.72
 N2/1.43/ H2O/8.58/
    LOW /  1.540E+30  -4.80    5559.40 /
    TROE /   7.5800E-01  9.4000E+01  1.5550E+03  4.2000E+03 /
CH3O+O2 =  CH2O+HO2                               6.300E+10   0.0000    2599.72
C2H6+OH =  C2H5+H2O                               7.200E+06   2.0000     863.91
C2H4+H(+M) =  C2H5(+M)                            1.100E+12   0.4540    1821.80
 H2O/5/
    LOW /  1.112E+34  -5.00    4447.52 /
    TROE /   5.0000E-01  9.5000E+01  9.5000E+01  2.0000E+02 /
C2H5+O2 =  C2H4+HO2                               1.000E+10   0.0000   -2189.76
C2H4+O =  CH2HCO+H                                4.700E+06   1.8800     179.98
C2H4+OH =  C2H3+H2O                               2.000E+13   0.0000    5939.36
C2H3+O2 =  CH2HCO+O                               2.500E+15  -0.7800    3134.66
CH2HCO+O2 =  CH2O+CO+OH                           2.200E+11   0.0000    1499.84
CH3+O2(+M) =  CH3O2(+M)                           7.800E+08   1.2000       0.00
 N2/1.1/ H2O/10/
    LOW /  5.400E+25  -3.30       0.00 /
CH3O2+OH =  CH3OH+O2                              6.000E+13   0.0000       0.00
CH3O2+CH3 =  2CH3O                                2.400E+13   0.0000       0.00
CH3OOH =  CH3O+OH                                 6.300E+14   0.0000   42295.41
END
```

Appendix F

SKELETAL MECHANISM VALIDATION

This appendix compares the predictions of the skeletal mechanism for ultra-lean methane combustion developed in Chapter 7 with those of the detailed mechanism (Bendtsen, Glarborg and Dam-Johansen 2000) from which it was reduced. Predictions of the concentration profiles for all of the chemical species in the skeletal mechanism are provided in the figures below (Figures F.1–F.25); each figure shows the profiles for a single species.

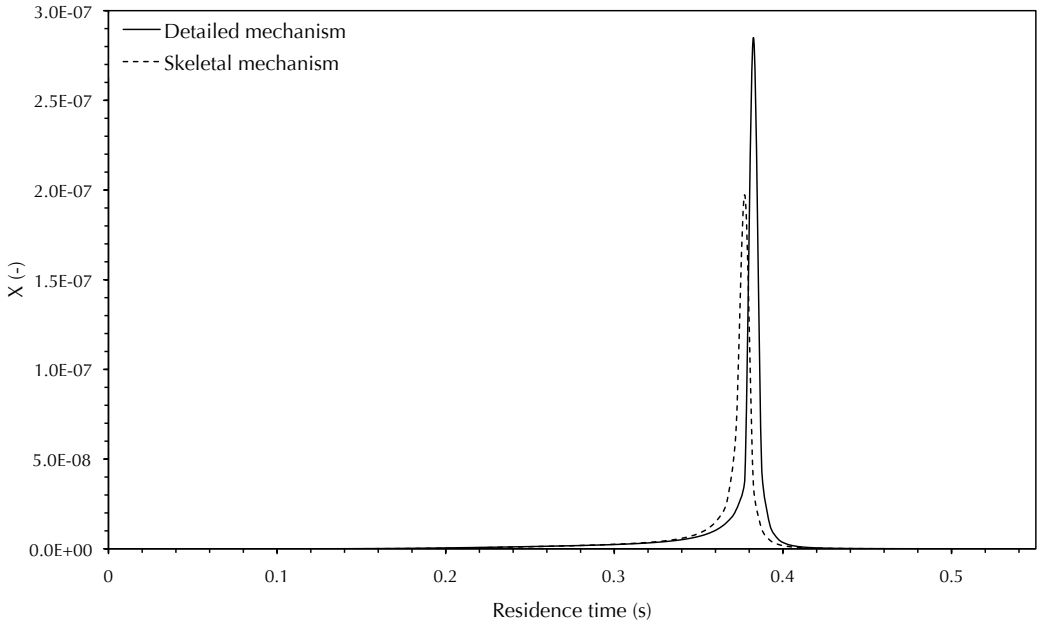

Figure F.1 Comparison of H radical concentration profiles (mass fractions) predicted by the detailed and skeletal mechanisms for CH_4 combustion in an adiabatic PFR, for the mechanism reduction conditions: 1 vol% CH_4 in wet (1 vol% H_2O) air, inlet temperature 1000K, pressure 1 atm.

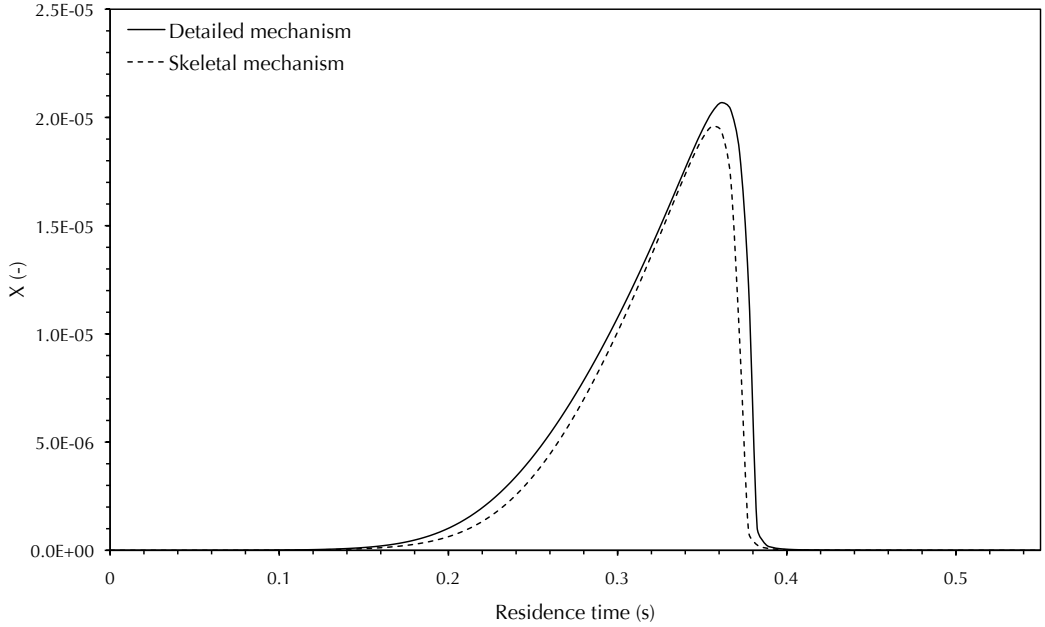

Figure F.2 Comparison of H_2 concentration profiles (mass fractions) predicted by the detailed and skeletal mechanisms for CH_4 combustion in an adiabatic PFR, for the mechanism reduction conditions: 1 vol% CH_4 in wet (1 vol% H_2O) air, inlet temperature 1000K, pressure 1 atm.

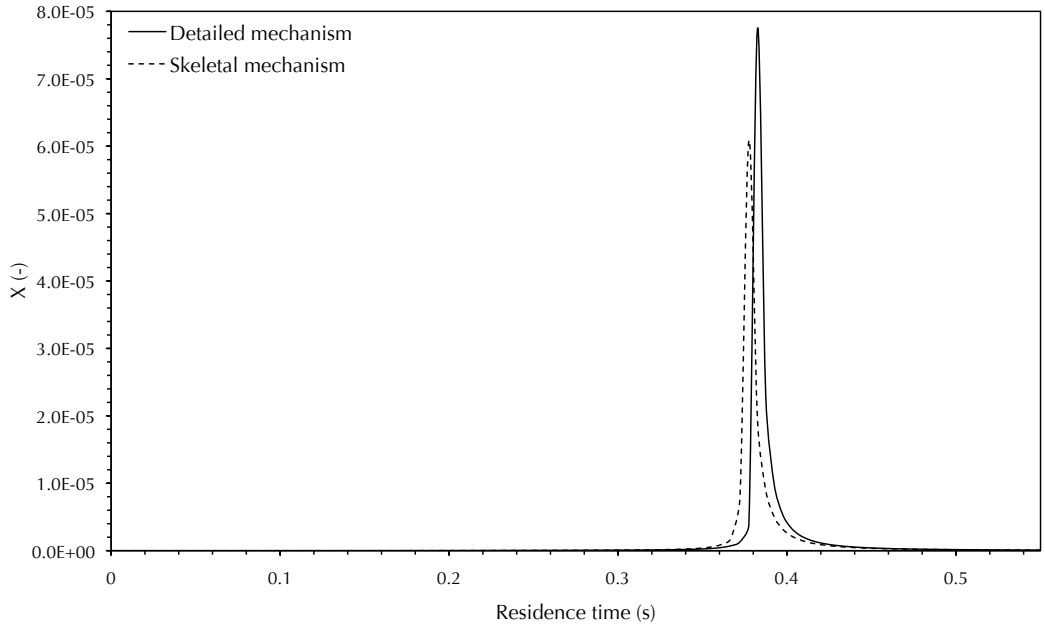

Figure F.3 Comparison of O radical concentration profiles (mass fractions) predicted by the detailed and skeletal mechanisms for CH_4 combustion in an adiabatic PFR, for the mechanism reduction conditions: 1 vol% CH_4 in wet (1 vol% H_2O) air, inlet temperature 1000K, pressure 1 atm.

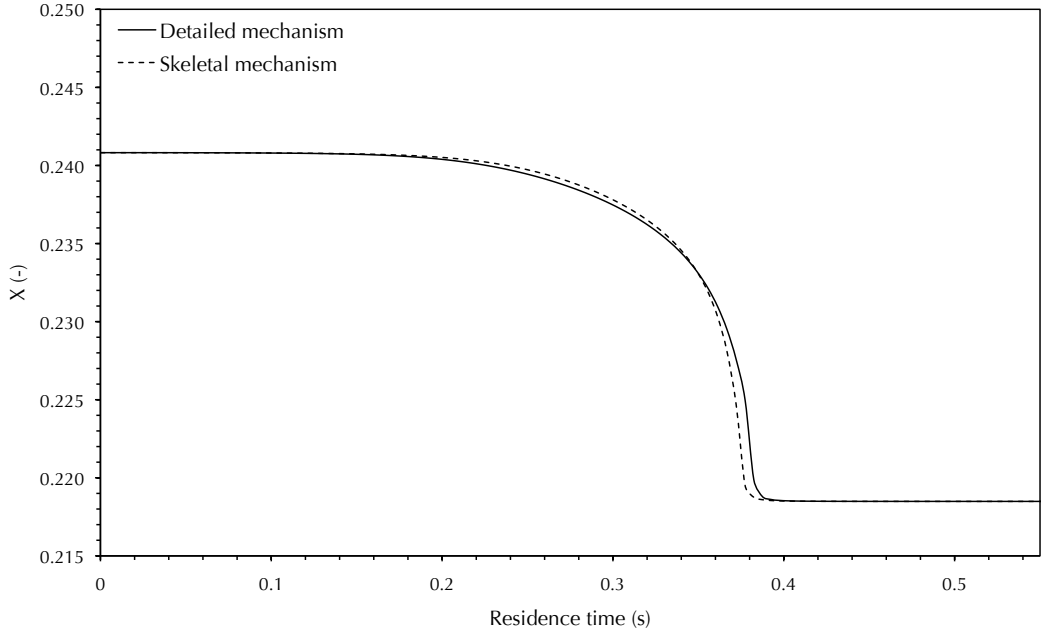

Figure F.4 Comparison of O_2 concentration profiles (mass fractions) predicted by the detailed and skeletal mechanisms for CH_4 combustion in an adiabatic PFR, for the mechanism reduction conditions: 1 vol% CH_4 in wet (1 vol% H_2O) air, inlet temperature 1000K, pressure 1 atm.

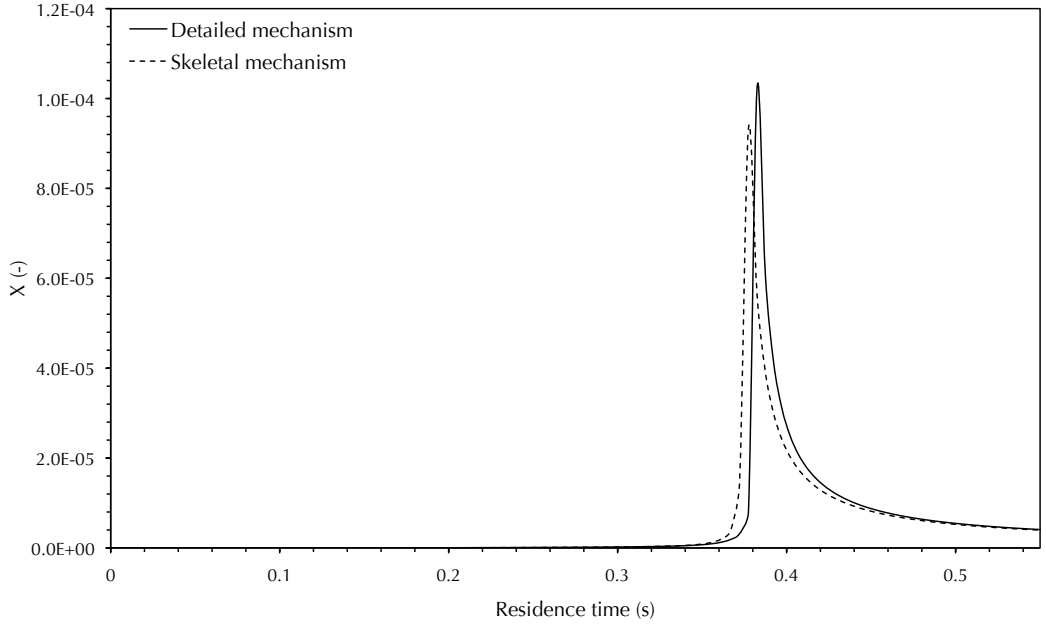

Figure F.5 Comparison of OH radical concentration profiles (mass fractions) predicted by the detailed and skeletal mechanisms for CH_4 combustion in an adiabatic PFR, for the mechanism reduction conditions: 1 vol% CH_4 in wet (1 vol% H_2O) air, inlet temperature 1000K, pressure 1 atm.

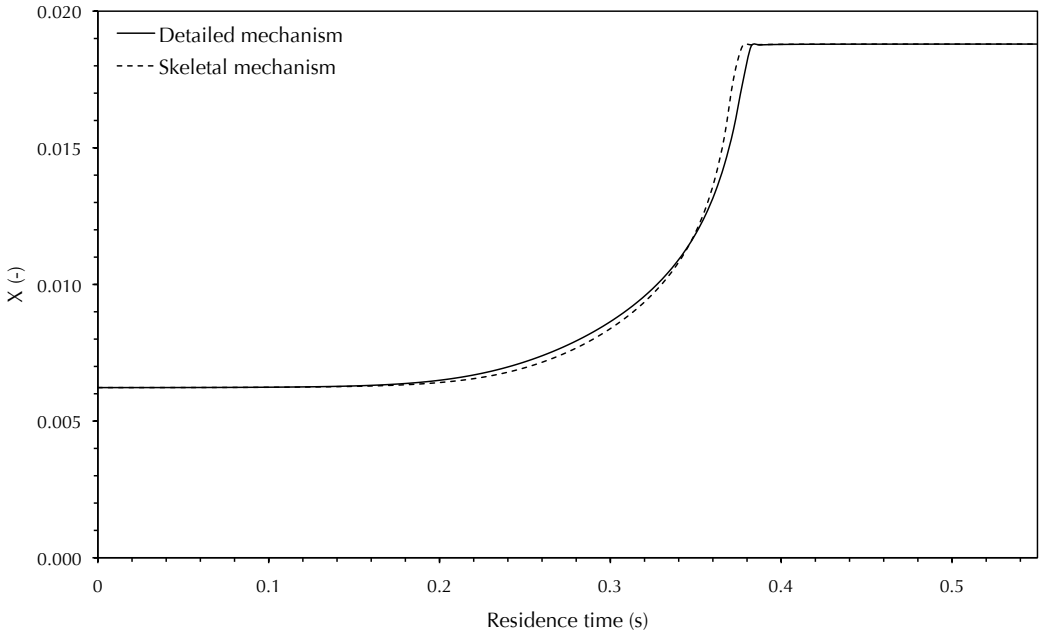

Figure F.6 Comparison of H_2O concentration profiles (mass fractions) predicted by the detailed and skeletal mechanisms for CH_4 combustion in an adiabatic PFR, for the mechanism reduction conditions: 1 vol% CH_4 in wet (1 vol% H_2O) air, inlet temperature 1000K, pressure 1 atm.

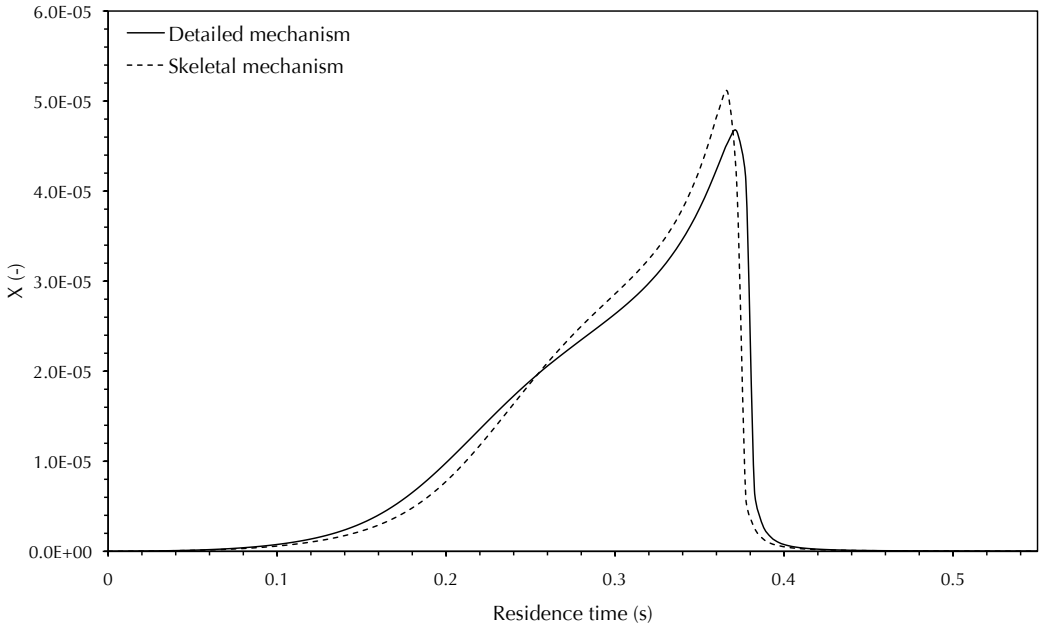

Figure F.7 Comparison of HO_2 radical concentration profiles (mass fractions) predicted by the detailed and skeletal mechanisms for CH_4 combustion in an adiabatic PFR, for the mechanism reduction conditions: 1 vol% CH_4 in wet (1 vol% H_2O) air, inlet temperature 1000K, pressure 1 atm.

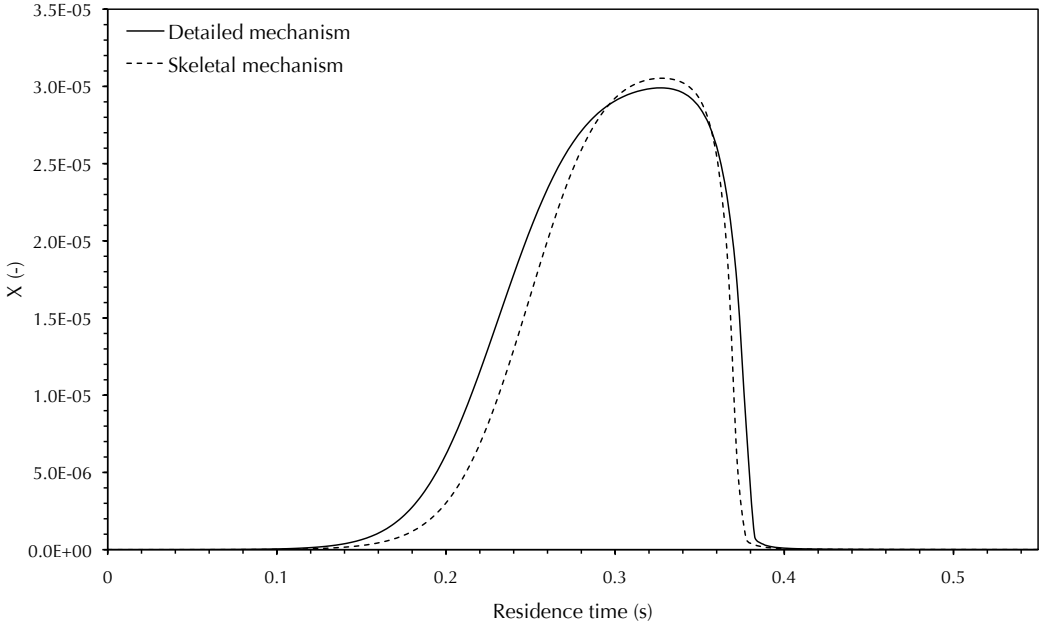

Figure F.8 Comparison of H_2O_2 radical concentration profiles (mass fractions) predicted by the detailed and skeletal mechanisms for CH_4 combustion in an adiabatic PFR, for the mechanism reduction conditions: 1 vol% CH_4 in wet (1 vol% H_2O) air, inlet temperature 1000K, pressure 1 atm.

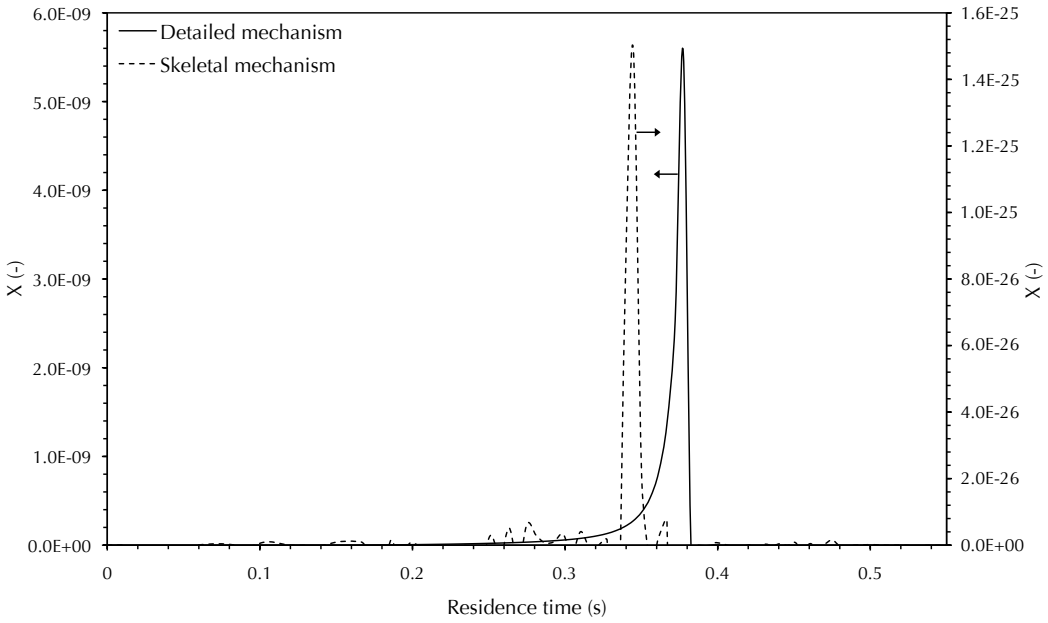

Figure F.9 Comparison of CH_2 radical concentration profiles (mass fractions) predicted by the detailed and skeletal mechanisms for CH_4 combustion in an adiabatic PFR, for the mechanism reduction conditions: 1 vol% CH_4 in wet (1 vol% H_2O) air, inlet temperature 1000K, pressure 1 atm. Note the different vertical axes.

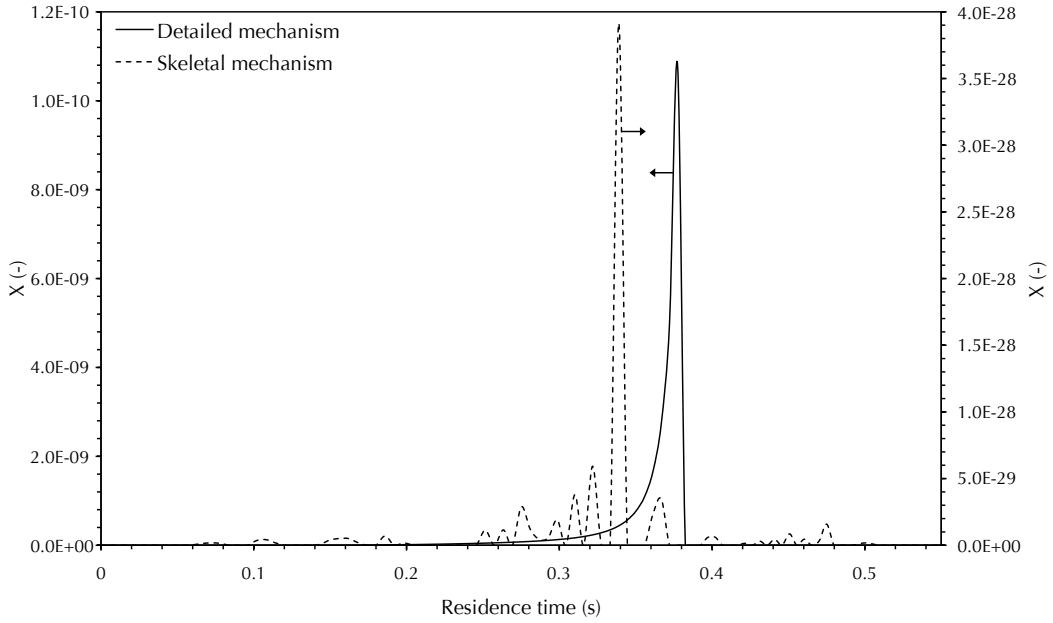

Figure F.10 Comparison of $CH_2(S)$ radical concentration profiles (mass fractions) predicted by the detailed and skeletal mechanisms for CH_4 combustion in an adiabatic PFR, for the mechanism reduction conditions: 1 vol% CH_4 in wet (1 vol% H_2O) air, inlet temperature 1000K, pressure 1 atm. Note the different vertical axes.

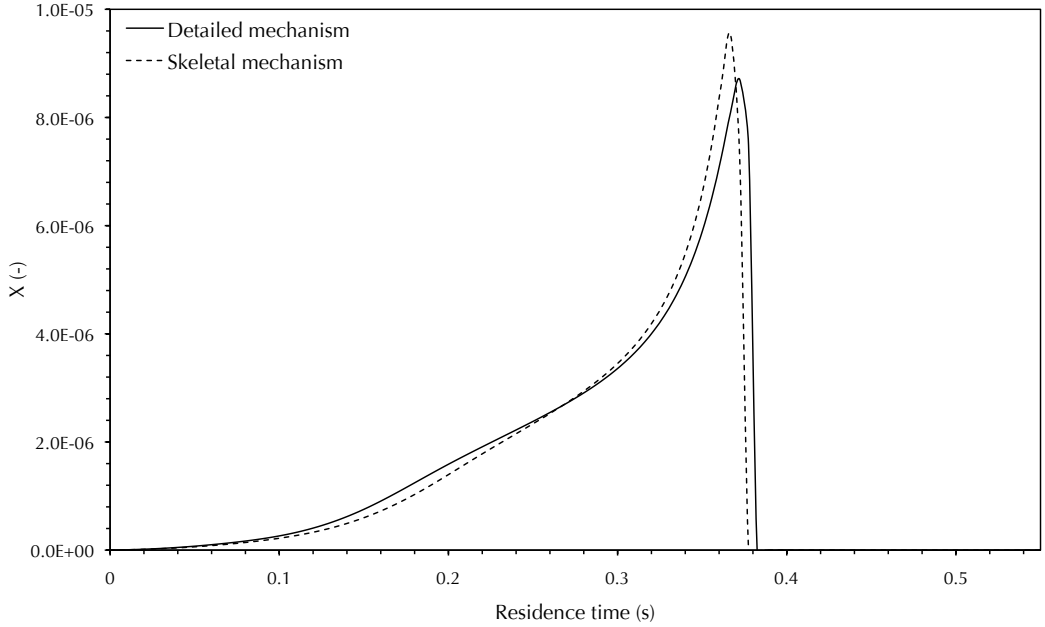

Figure F.11 Comparison of CH_3 radical concentration profiles (mass fractions) predicted by the detailed and skeletal mechanisms for CH_4 combustion in an adiabatic PFR, for the mechanism reduction conditions: 1 vol% CH_4 in wet (1 vol% H_2O) air, inlet temperature 1000K, pressure 1 atm.

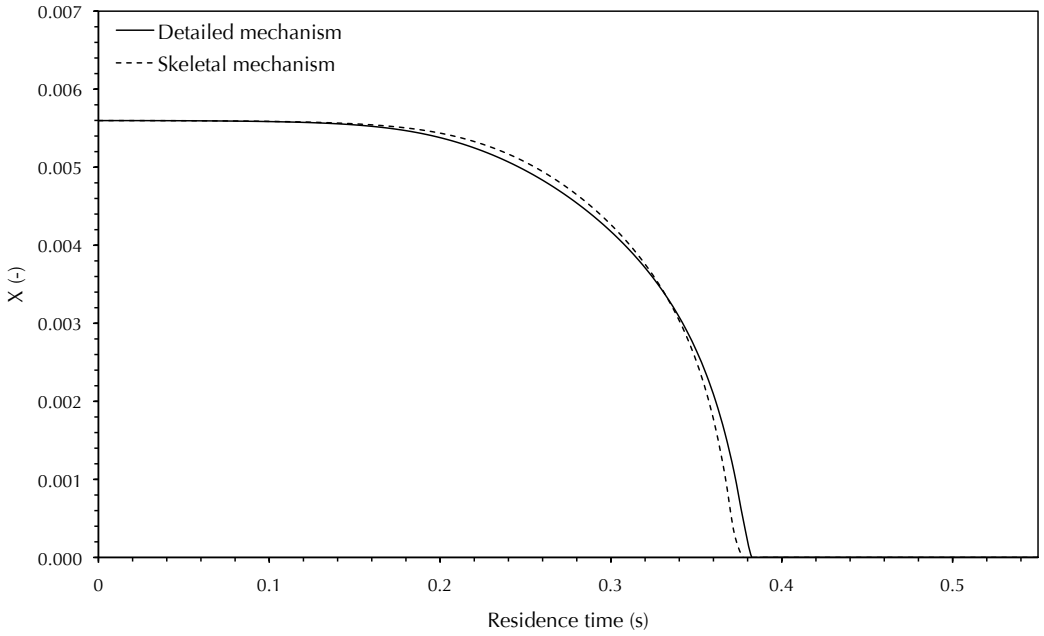

Figure F.12 Comparison of CH_4 concentration profiles (mass fractions) predicted by the detailed and skeletal mechanisms for CH_4 combustion in an adiabatic PFR, for the mechanism reduction conditions: 1 vol% CH_4 in wet (1 vol% H_2O) air, inlet temperature 1000K, pressure 1 atm.

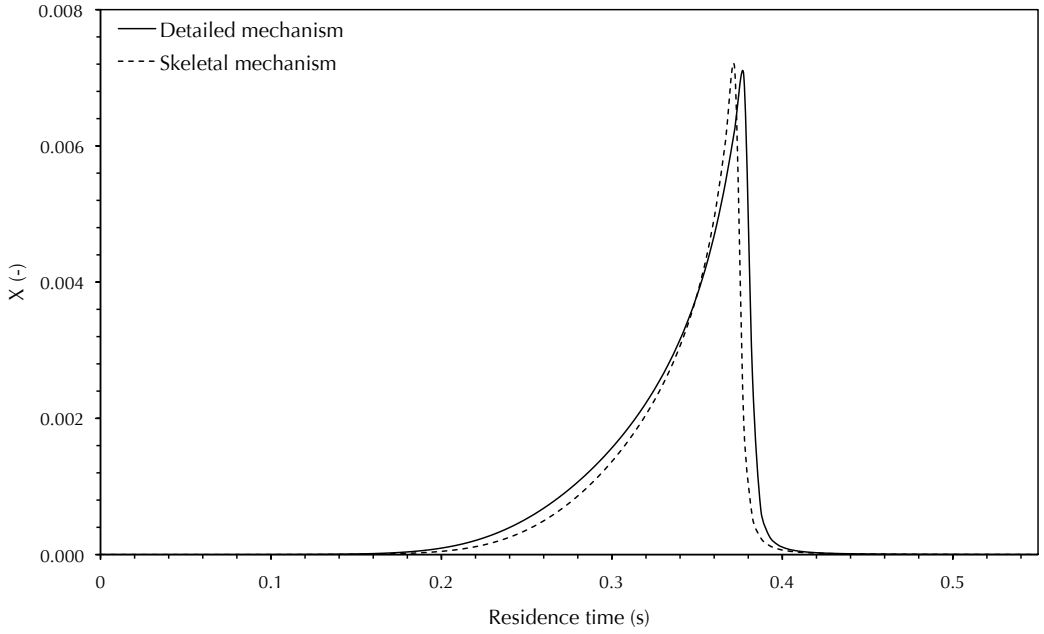

Figure F.13 Comparison of CO concentration profiles (mass fractions) predicted by the detailed and skeletal mechanisms for CH_4 combustion in an adiabatic PFR, for the mechanism reduction conditions: 1 vol% CH_4 in wet (1 vol% H_2O) air, inlet temperature 1000K, pressure 1 atm.

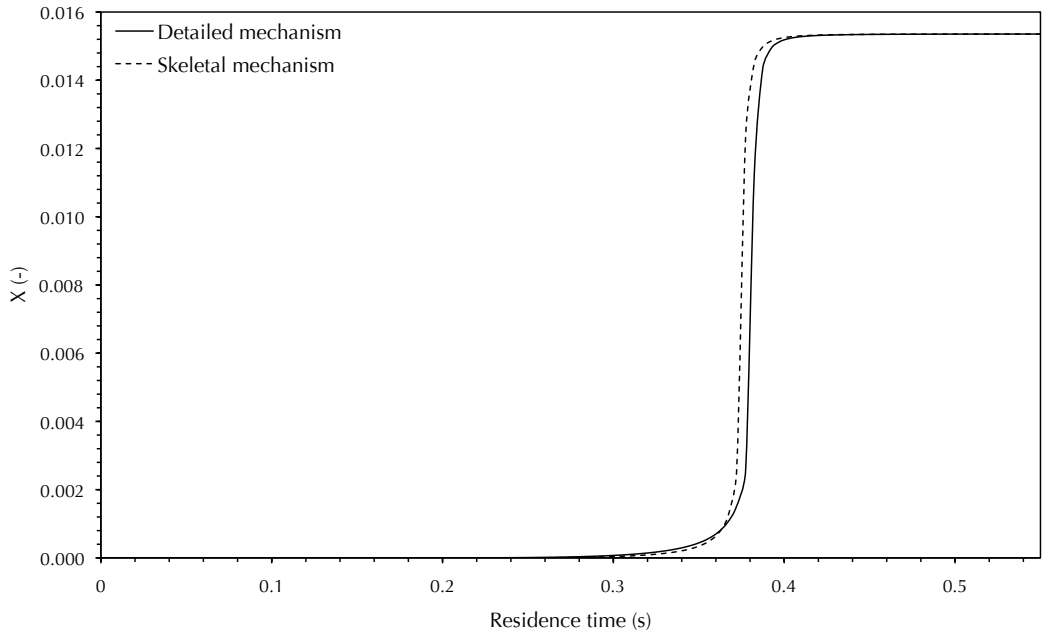

Figure F.14 Comparison of CO_2 concentration profiles (mass fractions) predicted by the detailed and skeletal mechanisms for CH_4 combustion in an adiabatic PFR, for the mechanism reduction conditions: 1 vol% CH_4 in wet (1 vol% H_2O) air, inlet temperature 1000K, pressure 1 atm.

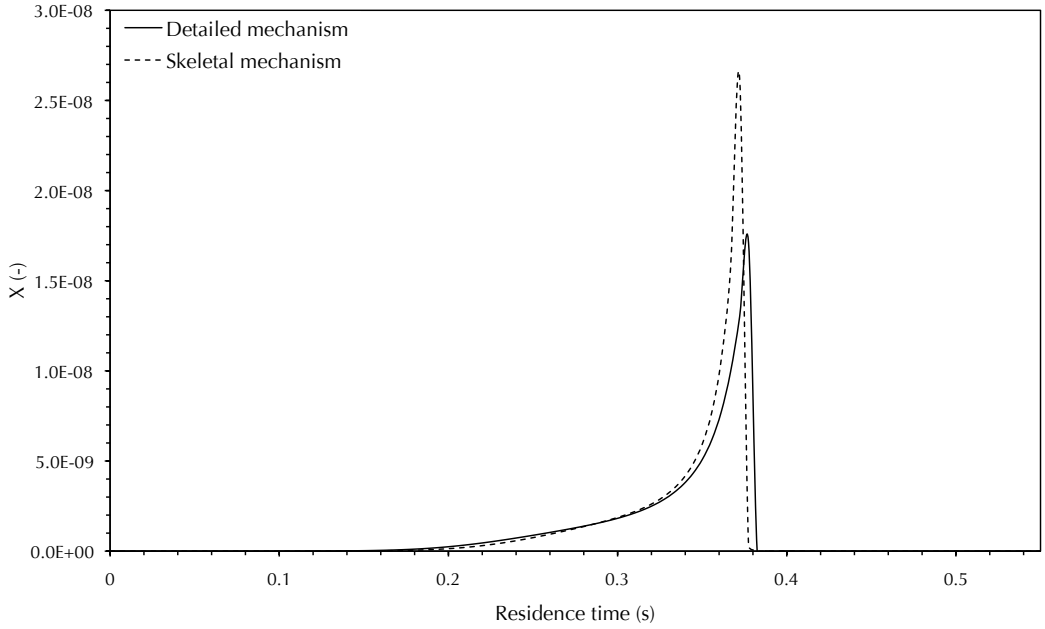

Figure F.15 Comparison of HCO radical concentration profiles (mass fractions) predicted by the detailed and skeletal mechanisms for CH_4 combustion in an adiabatic PFR, for the mechanism reduction conditions: 1 vol% CH_4 in wet (1 vol% H_2O) air, inlet temperature 1000K, pressure 1 atm.

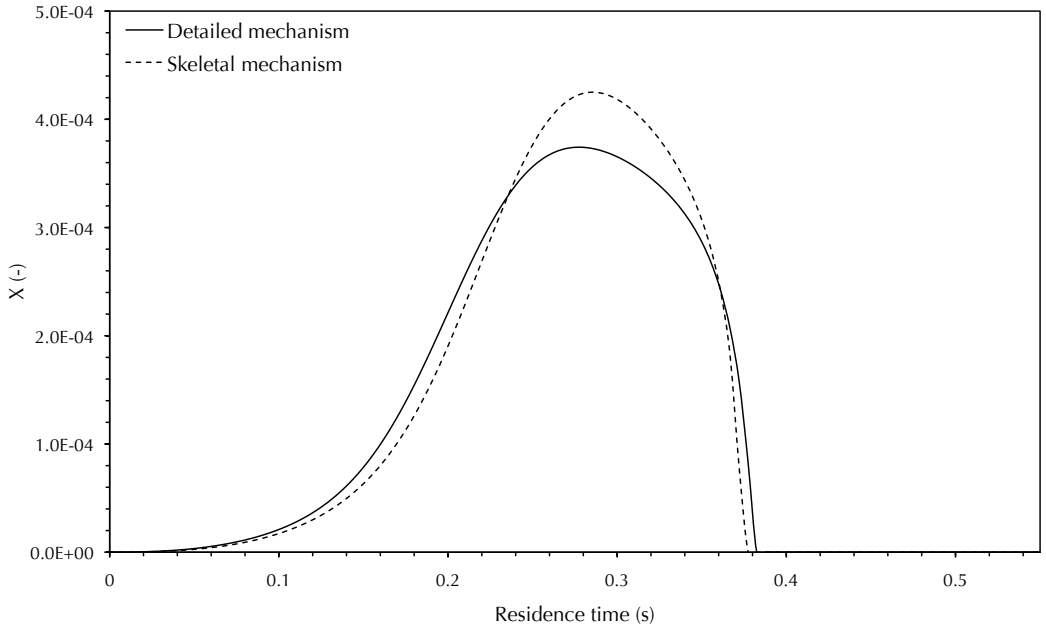

Figure F.16 Comparison of CH_2O concentration profiles (mass fractions) predicted by the detailed and skeletal mechanisms for CH_4 combustion in an adiabatic PFR, for the mechanism reduction conditions: 1 vol% CH_4 in wet (1 vol% H_2O) air, inlet temperature 1000K, pressure 1 atm.

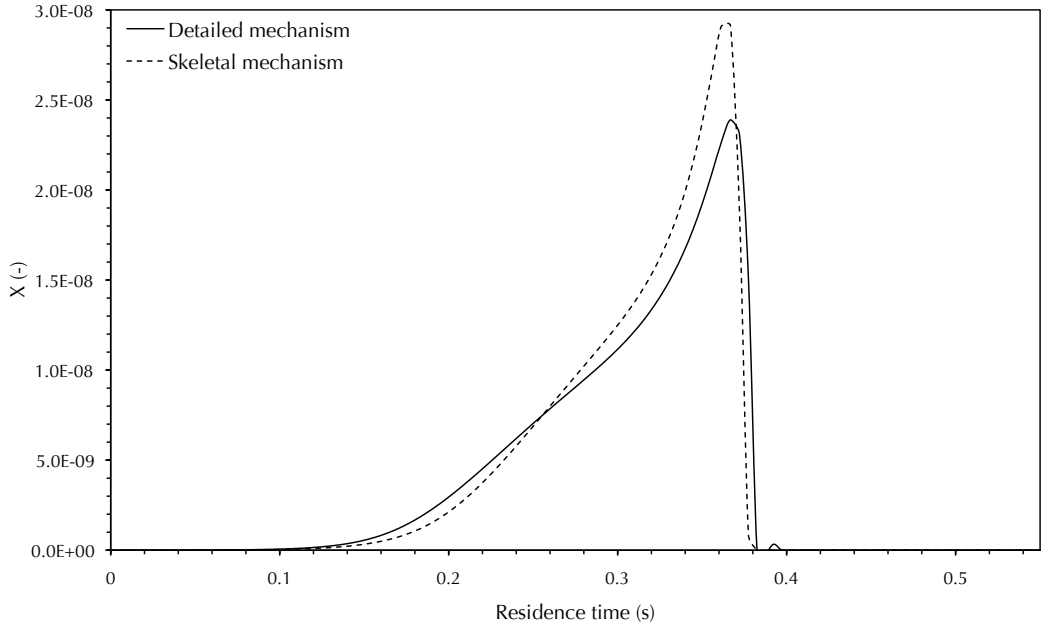

Figure F.17 Comparison of CH_3O radical concentration profiles (mass fractions) predicted by the detailed and skeletal mechanisms for CH_4 combustion in an adiabatic PFR, for the mechanism reduction conditions: 1 vol% CH_4 in wet (1 vol% H_2O) air, inlet temperature 1000K, pressure 1 atm.

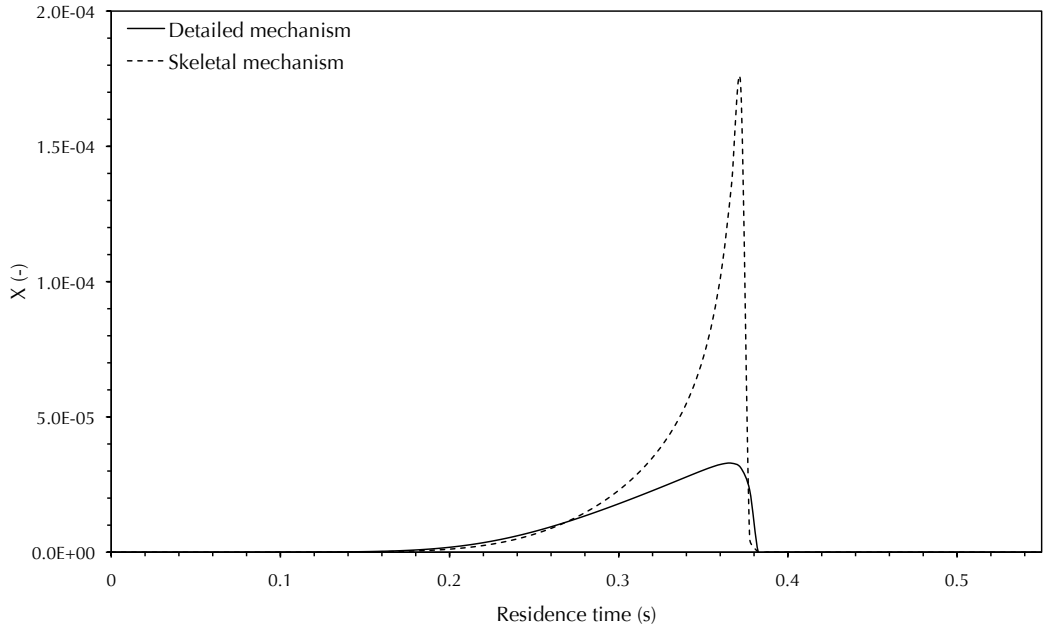

Figure F.18 Comparison of CH_3OH concentration profiles (mass fractions) predicted by the detailed and skeletal mechanisms for CH_4 combustion in an adiabatic PFR, for the mechanism reduction conditions: 1 vol% CH_4 in wet (1 vol% H_2O) air, inlet temperature 1000K, pressure 1 atm.

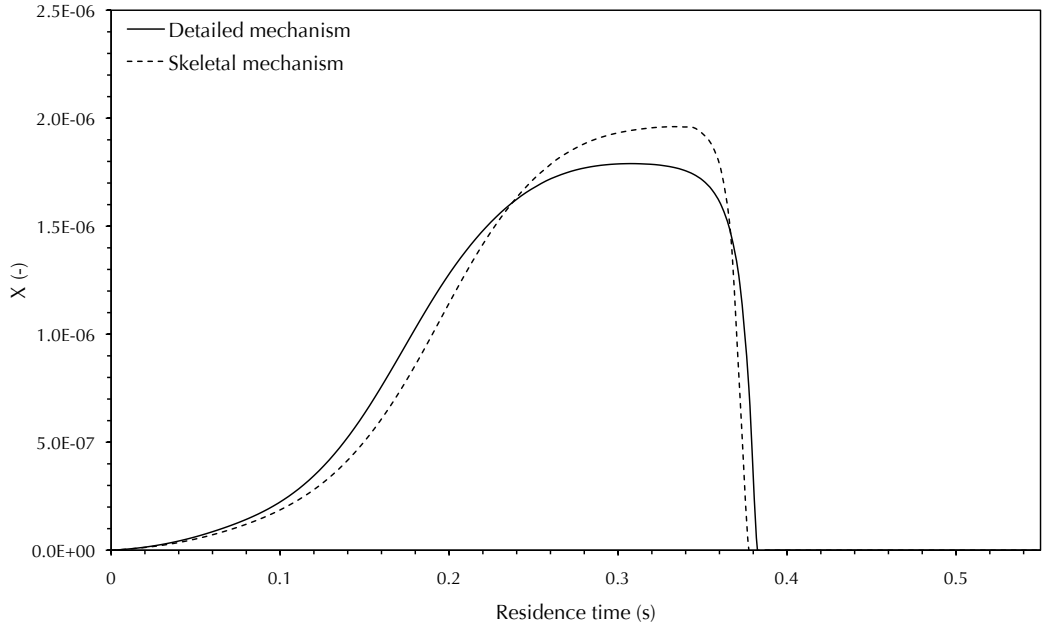

Figure F.19 Comparison of CH_3O_2 radical concentration profiles (mass fractions) predicted by the detailed and skeletal mechanisms for CH_4 combustion in an adiabatic PFR, for the mechanism reduction conditions: 1 vol% CH_4 in wet (1 vol% H_2O) air, inlet temperature 1000K, pressure 1 atm.

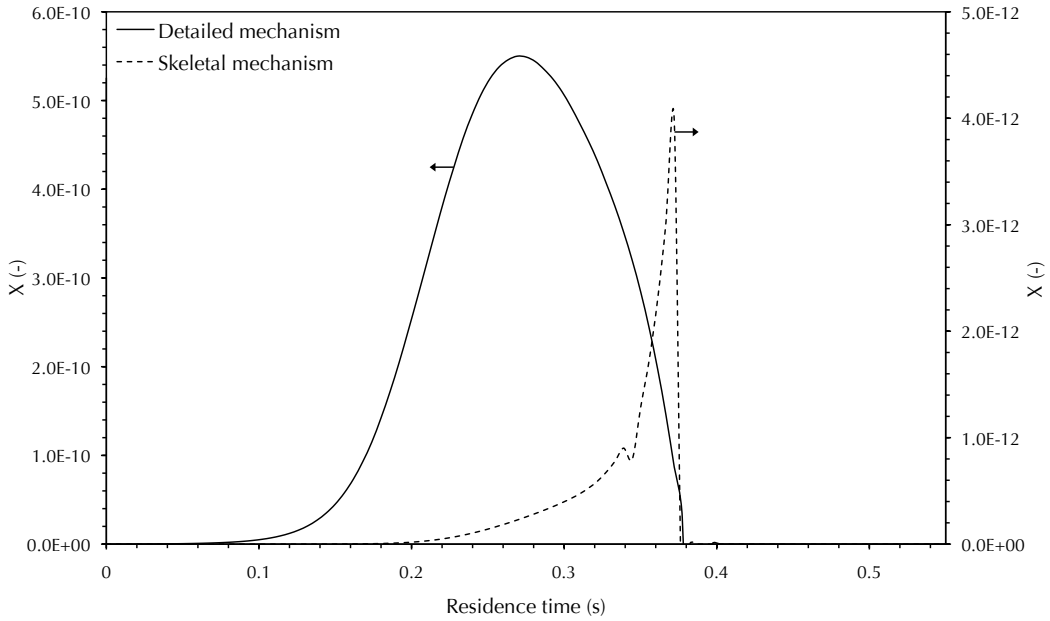

Figure F.20 Comparison of CH_3OOH concentration profiles (mass fractions) predicted by the detailed and skeletal mechanisms for CH_4 combustion in an adiabatic PFR, for the mechanism reduction conditions: 1 vol% CH_4 in wet (1 vol% H_2O) air, inlet temperature 1000K, pressure 1 atm. Note the different vertical axes.

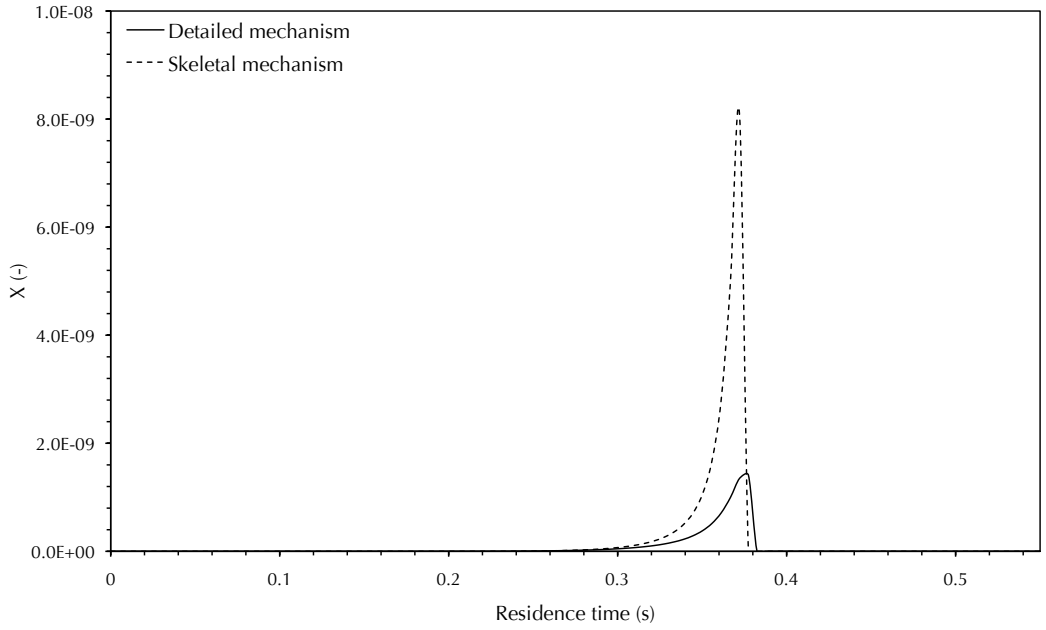

Figure F.21 Comparison of C_2H_3 radical concentration profiles (mass fractions) predicted by the detailed and skeletal mechanisms for CH_4 combustion in an adiabatic PFR, for the mechanism reduction conditions: 1 vol% CH_4 in wet (1 vol% H_2O) air, inlet temperature 1000K, pressure 1 atm.

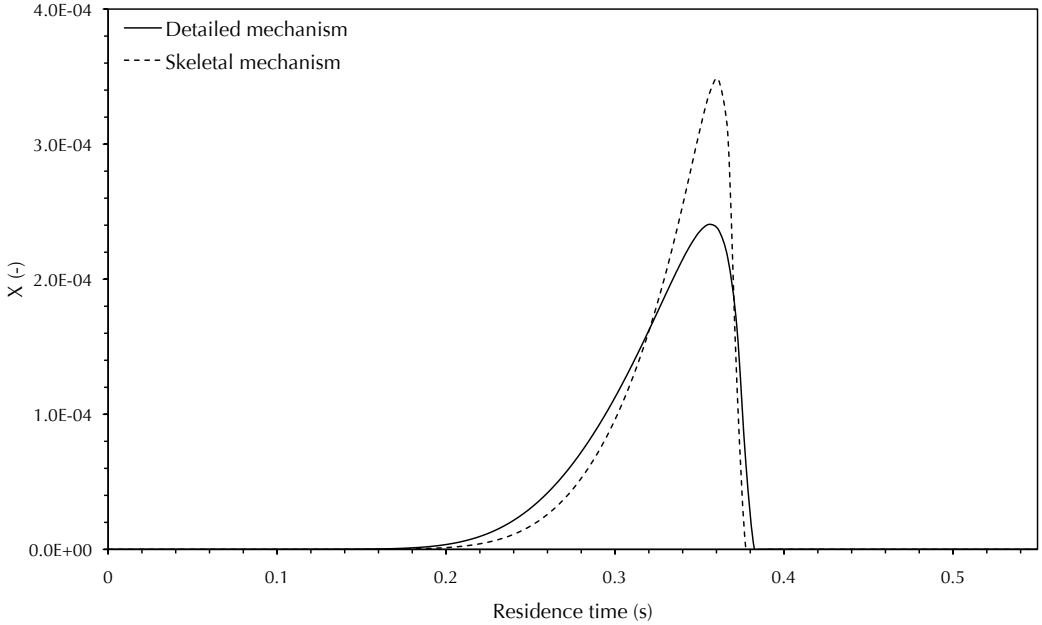

Figure F.22 Comparison of C_2H_4 concentration profiles (mass fractions) predicted by the detailed and skeletal mechanisms for CH_4 combustion in an adiabatic PFR, for the mechanism reduction conditions: 1 vol% CH_4 in wet (1 vol% H_2O) air, inlet temperature 1000K, pressure 1 atm.

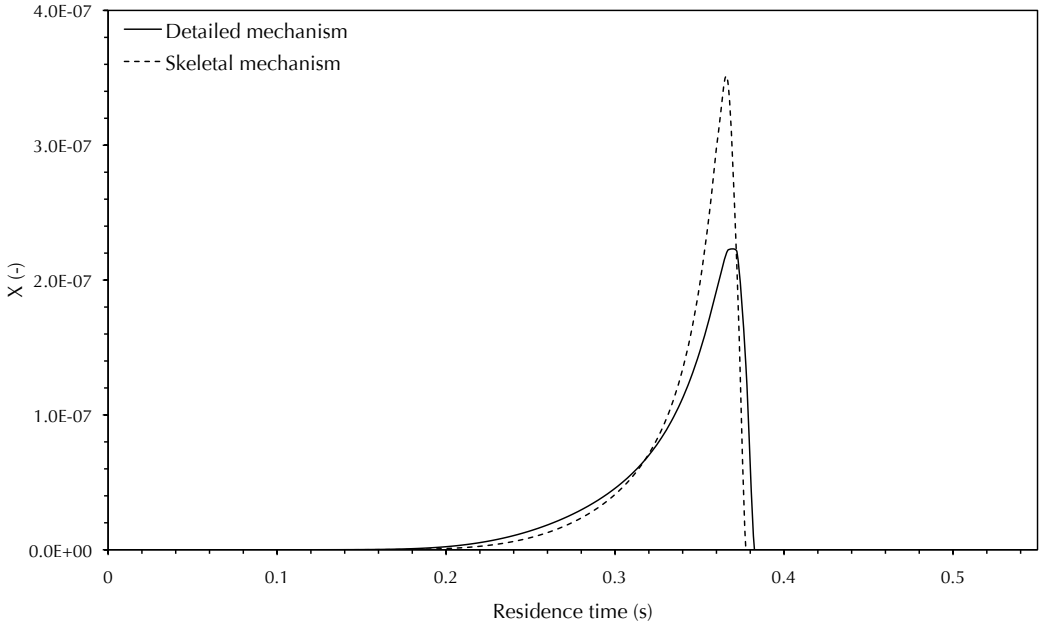

Figure F.23 Comparison of C_2H_5 radical concentration profiles (mass fractions) predicted by the detailed and skeletal mechanisms for CH_4 combustion in an adiabatic PFR, for the mechanism reduction conditions: 1 vol% CH_4 in wet (1 vol% H_2O) air, inlet temperature 1000K, pressure 1 atm.

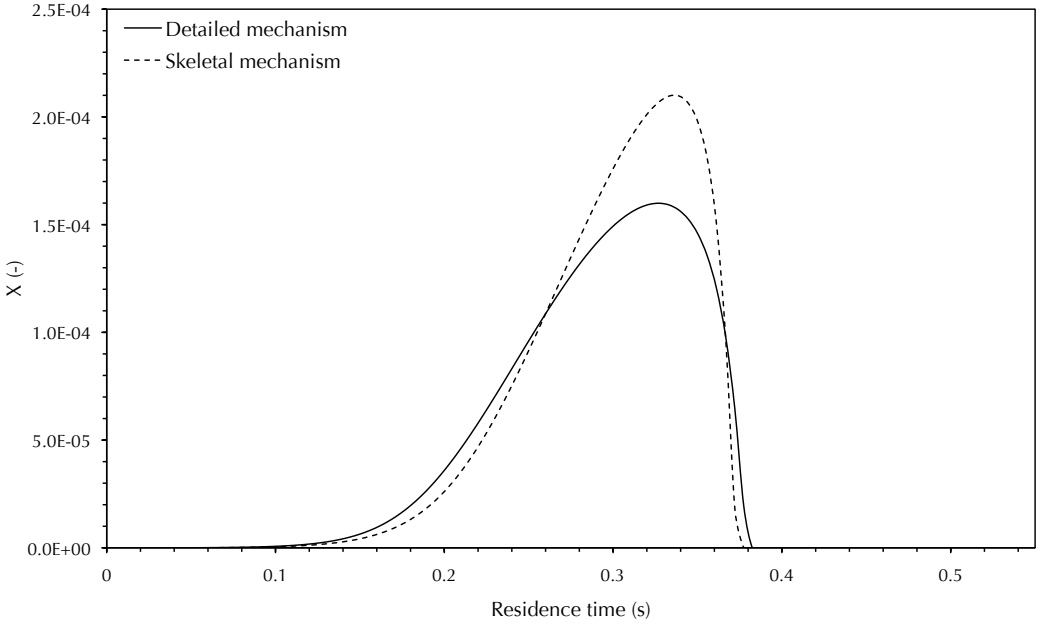

Figure F.24 Comparison of C_2H_6 concentration profiles (mass fractions) predicted by the detailed and skeletal mechanisms for CH_4 combustion in an adiabatic PFR, for the mechanism reduction conditions: 1 vol% CH_4 in wet (1 vol% H_2O) air, inlet temperature 1000K, pressure 1 atm.

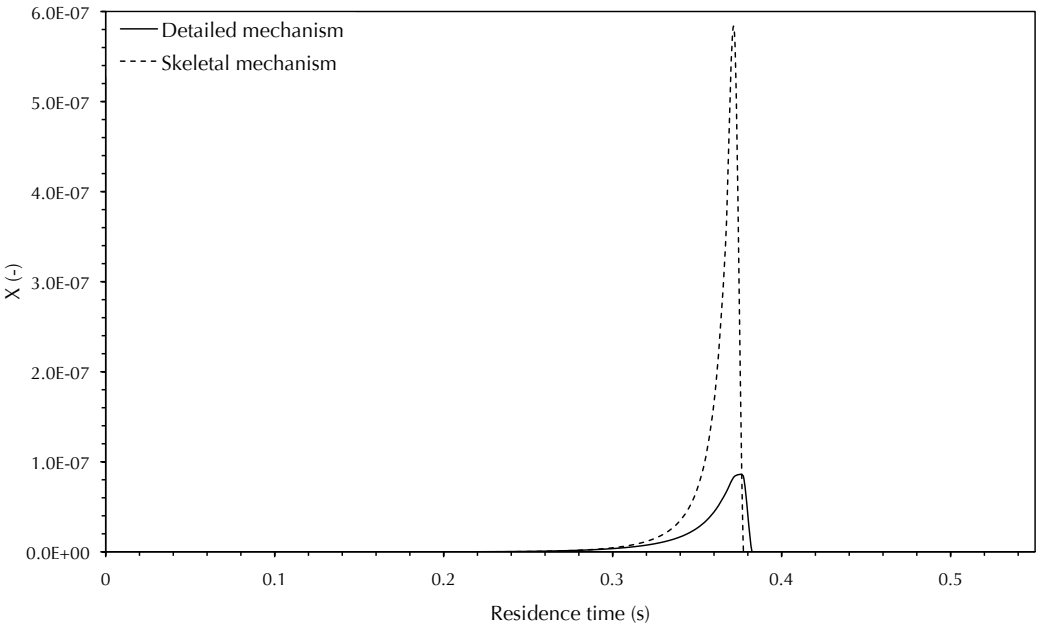

Figure F.25 Comparison of CH_2HCO radical concentration profiles (mass fractions) predicted by the detailed and skeletal mechanisms for CH_4 combustion in an adiabatic PFR, for the mechanism reduction conditions: 1 vol% CH_4 in wet (1 vol% H_2O) air, inlet temperature 1000K, pressure 1 atm.

REFERENCES

REFERENCES

Afsharvahid S, Ashman PJ and Dally BB. 2008. Investigation of NO_X conversion characteristics in a porous medium. *Combustion and Flame* 152:604–15.

Afsharvahid S, Dally BB and Christo FC. 2003a. Numerical study of flame stabilization inside porous burner. Paper presented at the 2003 Australian Symposium on Combustion, Melbourne, Australia. December 8–9.

Afsharvahid S, Dally BB and Christo FC. 2003b. On the stabilisation of ultra-lean methane and propane flames in porous media. Paper presented at the 4th Asia-Pacific Conference on Combustion, Nanjing, China. August 18–21.

Afsharvahid S, Lanspeary PV, Dally BB and Christo FC. 2002. On the design of an ultra lean porous burner. Paper presented at the 2002 Australian Symposium on Combustion, Adelaide, Australia. February 7–8.

Alavandi SK and Agrawal AK. 2008. Experimental study of combustion of hydrogen-syngas/methane fuel mixtures in a porous burner. *International Journal of Hydrogen Energy* 33:1407–15.

Aldushin AP. 1993. New results in the theory of filtration combustion. *Combustion and Flame* 94:308–20.

Al-Hamamre Z, Diezinger S, Talukdar P, von Issendorff F and Trimis D. 2006. Combustion of low calorific value gases from landfills and waste pyrolysis using porous medium burner technology. *Process Safety and Environmental Protection* 84:297–308.

Al-Hamamre Z, Voß S and Trimis D. 2007. Detailed experimental and numerical investigation of the partial oxidation of methane in a porous reactor. Paper presented at the 3rd European Combustion Meeting, Chania, Crete. April 11–13.

Al-Hamamre Z, Voß S and Trimis D. 2009. Hydrogen production by thermal partial oxidation of hydrocarbon fuels in porous media based reformer. *International Journal of Hydrogen Energy* 34:827–32.

Alicat. http://www.alicatscientific.com (accessed June 4, 2009).

Altendorfner M, von Issendorf F and Dannehl M. 2007. Development of a high pressure burner for industrial applications using inert porous media. Paper presented at the 9th International Conference on Energy for a Clean Environment (Clean Air IX), Póvoa de Varzim, Portugal. July 2–5.

American Society for Testing and Materials (ASTM). 1993. *Manuel on the use of thermocouples in temperature measurement*. 4th ed. Philadelphia: ASTM.

Anastas PT and Zimmerman JB. 2003. Design through the 12 principles of green engineering. *Environmental Science & Technology* 37:94A–101A.

ANSYS. http://www.ansys.com (accessed March 10, 2009).

ASM International. 1995. Engineering tables: Ceramics and glasses. In *Engineered materials handbook desk edition*. Materials Park, OH: ASM International.

Atkins PW. 1994. *Physical chemistry*. 5th ed. Oxford: Oxford University Press.

Australian Greenhouse Office (AGO). 2002. *Developing a strategic framework for greenhouse and agriculture: An issues paper*. Canberra, Australia: Australian Greenhouse Office.

Autodesk. *AutoCAD 2002*. http://www.autodesk.com.au (accessed May 1, 2009).

Babkin VS. 1993. Filtrational combustion of gases: Present state of affairs and prospects. *Pure and Applied Chemistry* 65:335–44.

Babkin VS, Drobyshevich VI, Laevskii, YM and Potytnyakov SI. 1983. Filtration combustion of gases. *Combustion, Explosion and Shock Waves* 19:147–55.

Babkin VS, Korzhavin AA and Bunev VA. 1991. Propagation of premixed gaseous explosion flames in porous media. *Combustion and Flame* 87:182–90.

Babkin VS and Laevskii YM. 1987. Seepage gas combustion. *Combustion, Explosion and Shock Waves* 23:531–47.

Babkin VS, Wierzba I and Karim GA. 2003. The phenomenon of energy concentration in combustion waves and its applications. *Chemical Engineering Journal* 91:279–85.

Bakry A. 2008. Stabilized premixed combustion within atmospheric gas porous inert medium (PIM) burner. *Proceedings of the Institution of Mechanical Engineers Part A: Journal of Power and Energy* 222:781–9.

Bakry A, Genenger B, Schmidt V and Trimis D. 2000. Low emission combustion of vegetable oils with the porous burner technology. In *New and renewable technologies for sustainable development*, ed. NH Afgan and MdG Carvalho, 541–55. Boston, MA: Kluwer Academic Publishers.

Bambace LAW, Ramos FM, Lima IBT and Rosa RR. 2007. Mitigation and recovery of methane emissions from tropical hydroelectric dams. *Energy* 32:1038–46.

Barra AJ, Diepvens G, Ellzey JL and Henneke MR. 2003. Numerical study of the effects of material properties on flame stabilization in a porous burner. *Combustion and Flame* 134:369–79.

Barra AJ and Ellzey JL. 2004. Heat recirculation and heat transfer in porous burners. *Combustion and Flame* 137:230–41.

Bartz DF, Moreno FE and Duggan PA. 1992. Ultra-low NO_x, ultra-high VOC destruction with adiabatic radiant combustors. *ASME PD* 39:7–12.

Baukal CE. 2001. *The John Zink combustion handbook*. Boca Raton, FL: CRC Press.

Bell RD, Chaffin C and Koeroghlian M. 1992. Experimental investigation of a staged porous ceramic burner. *ASME PD* 39:41–46.

Bendtsen AB, Glarborg P and Dam-Johansen K. 2000. Low temperature oxidation of methane: The influence of nitrogen oxides. *Combustion Science and Technology* 151:31–71.

Berlin AA, Shteinberg AS, Frolov SM, Belyaev AA, Posvyanskii VS and Basevich VY. 2006. Extension of the combustion limits for a porous burner by external heating. *Doklady Physical Chemistry* 406:43–8.

Bibler CJ, Marshall JS and Pilcher RC. 1998. Status of worldwide coal mine methane emissions and use. *International Journal of Coal Geology* 35:283–310.

Bilger RW and Stårner SH. 1990. On reduced mechanisms for methane-air combustion in nonpremixed flames. *Combustion and Flame* 80:135–49.

Bingue JP, Saveliev AV, Fridman AA and Kennedy LA. 2002a. Hydrogen production in ultra-rich filtration combustion of methane and hydrogen sulfide. *International Journal of Hydrogen Energy* 27:643–49.

Bingue JP, Saveliev AV, Fridman AA and Kennedy LA. 2002b. Hydrogen sulfide filtration combustion: Comparison of theory and experiment. *Experimental Thermal and Fluid Science* 26:409–15.

Bingue JP, Saveliev AV, Fridman AA and Kennedy LA. 2002c. NO_X and CO emissions of lean and ultra-lean filtration combustion of methane/air mixtures in an inert porous media. *Clean Air* 3:199–210.

Bingue JP, Saveliev AV and Kennedy LA. 2004. Optimization of hydrogen production by filtration combustion of methane by oxygen enrichment and depletion. *International Journal of Hydrogen Energy* 29:1365–70.

Bingue JP, Saveliev AV and Kennedy LA. 2007. NO reburning in ultrarich filtration combustion of methane. *Proceedings of the Combustion Institute* 31:3417–24.

Bird RB, Stewart WE and Lightfoot EW. 2007. *Transport Phenomena*. 2nd ed. New York: Wiley.

Boone DR. 2000. Biological formation and consumption of methane. In *Atmospheric methane: Its role in the global environment*, ed. MAK Khalil, 42–62. Berlin, Germany: Springer-Verlag.

Borman GL and Ragland KW. 1998. *Combustion engineering*. Singapore: McGraw-Hill.

Bouma PH and de Goey LPH. 1996. The stability of flames on a ceramic foam surface burner. Paper presented at the 1st European Conference on Small Burner Technology and Heating Equipment, Zurich, Switzerland. September 25–26.

Bouma PH and de Goey LPH. 1999. Premixed combustion on ceramic foam burners. *Combustion and Flame* 119:133–43.

Bouma PH, Eggels RLGM and de Goey LPH. 1995. NO emissions of ceramic foam surface gas burners in the radiation mode. Paper presented at the 3rd International Conference on Combustion Technologies for a Clean Environment (Clean Air III), Lisbon, Portugal. July 3–6.

Bouma PH, Eggels RLGM, de Goey LPH, Nieuwenhuizen JK and van der Drift A. 1995a. A numerical and experimental study of the NO-emission of ceramic foam surface burners. *Combustion Science and Technology* 108:193–203.

Bouma PH, Somers LMT, de Goey LPH and Nieuwenhuizen JK. 1995b. Modelling of methane-air combustion on ceramic foam surface burners in the radiation mode. *Heat and Technology* 13:127–39.

Bowen HK. 1980. Basic research needs on high temperature ceramics for energy applications. *Materials Science and Engineering* 44:1–56.

BP. 2009. *BP Statistical review of world energy 2009*. http://www.bp.com (accessed August 6, 2009).

Brenkley D and Bennett SC. 1996. An integrated approach to coal mine methane estimation, recovery and utilisation. *Energy Conversion and Management* 37:807–12.

Brenner G, Pickenäcker K, Pickenäcker O, Trimis D, Wawrzinek K and Weber T. 2000. Numerical and experimental investigation of matrix-stabilized methane/air combustion in porous inert media. *Combustion and Flame* 123:201–13.

Bromly JH, Barnes FJ, Muris S, You X and Haynes BS. 1996. Kinetic and thermodynamic sensitivity analysis of the NO-sensitised oxidation of methane. *Combustion Science and Technology* 115:259–96.

Bröckerhoff P and Emonts B. 1994. Test of a premixing radiant burner for the low NO_X combustion of natural gas/hydrogen mixtures. *International Journal of Hydrogen Energy* 19:395–98.

Bubnovich V, Toledo M, Henríquez L, Rosas C and Romero J. 2010. Flame stabilization between two beds of alumina balls in a porous burner. *Applied Thermal Engineering* 30:92–95.

Buckmaster J and Takeno T. 1981. Blow-off and flashback of an excess enthalpy flame. *Combustion Science and Technology* 25:153–58.

Burgoyne JH and Hirsch H. 1954. The combustion of methane at high temperatures. *Proceedings of the Royal Society of London, Series A, Mathematical and Physical Sciences* 227:73–93.

Calabrò PS. 2009. Greenhouse gases emission from municipal waste management: The role of separate collection. *Waste Management* 29:2178–87.

Cannon RW, Gugel E, Leimer G and Woetting G. 2000. Ceramics, advanced structural products. In *Ullmann's Enclyclopedia of Industrial Chemistry*. 7th ed. New York: Wiley.

Carothers FP, Schultz HL and Talkington CC. 2004. Mitigation of methane emissions from coal mine ventilation air: An update. Paper presented at the 10th US/North American Mine Ventilation Symposium, Anchorage, AK. May 16–19.

Carras JN, Day SJ, Saghafi A and Williams DJ. 2009. Greenhouse gas emissions from low-temperature oxidation and spontaneous combustion at open-cut coal mines in Australia. *International Journal of Coal Geology* 78:161–8.

Cathonnet M. 1994. Chemical kinetic modelling of combustion from 1969 to 2019. *Combustion Science and Technology* 98:265–79.

Casy M and Wintergerste T. 2000. *ERCOFTAC Special Interest Group on 'Quality and Trust in Industrial CFD' Best Practice Guidelines*. Brussels: ERCOFTAC.

Catalano A. 1996. Thermophotovoltaics: A new paradigm for power generation? *Renewable Energy* 8:495–99.

Cerri G, Michelassi V, Monacchia S and Pica S. 2003. Kinetic combustion neural modelling integrated into computational fluid dynamics. *Proceedings of the Institution of Mechanical Engineers Part A: Journal of Power and Energy* 217:185–92.

Chadwick MJ, Highton NH and Lindman N. 1987. *Environmental impacts of coal mining and utilization*. Oxford: Pergamon Press.

Chaffin C, Koenig M, Koeroghlian M, Matthews RD, Hall MJ, Nichols SP and Lim I-G. 1991. Experimental investigation of premixed combustion within highly porous media. Paper presented at the 3rd ASME/JSME Thermal Engineering Joint Conference, Reno, NV. March 17–22.

Chappellaz J and Raynaud D. 2000. The ice core record of atmospheric methane. In *Atmospheric methane: Its role in the global environment*, ed. MAK Khalil, 9–24. Berlin, Germany: Springer-Verlag.

Chevalier C. 1993. Entwicklung eines detaillierten Reaktionsmechanismus zur Modellierung der Verbrennungsprozesse von Kohlenwasserstoffen bei Hoch- und Niedertemperaturbedingungen. PhD thesis, University of Stuttgart.

Christo FC, Dally BB, Lanspeary PV, Afsharvahid S and Joseph SD. 2002. *Development of porous burner technology for ultra-lean combustion systems*. Report GC-FR-F-220202. Adelaide, Australia: Galilee Consulting.

Chumakov YA and Knyazeva AG. 2009. Regimes of gas combustion in a porous body of a cylindrical heat generator. *Combustion, Explosion and Shock Waves* 45:14–24.

Churchill SW. 1989. Thermally stabilized combustion. *Chemical Engineering and Technology* 12:249–54.

Chynoweth DP, Owens JM and Legrand R. 2001. Renewable methane from anaerobic digestion of biomass. *Renewable Energy* 22:1–8.

Coal Industry Advisory Board (CIAB). 1994. *Global methane and the coal industry: A two-part report on methane emissions from the coal industry and coalbed methane recovery and use*. Paris: Coal Industry Advisory Board, International Energy Agency.

Coal Industry Advisory Board (CIAB). 2003. *Coal and sustainable development: Attitudes and activity*. Paris: Coal Industry Advisory Board (CIAB), International Energy Agency.

Coal Industry Advisory Board (CIAB). 2005. *Reducing greenhouse gas emissions: The potential of coal*. Paris: Coal Industry Advisory Board, International Energy Agency.

Coal Industry Advisory Board (CIAB). 2006. *Case studies in sustainable development in the coal industry*. Paris: Coal Industry Advisory Board, International Energy Agency.

Coal Industry Advisory Board (CIAB). 2008. *Clean coal technologies: Accelerating commercial and policy drivers for deployment*. Paris: Coal Industry Advisory Board, International Energy Agency.

Connell Wagner. 2007. *Mitigation of methane in mine ventilation air 2006 status report*. Report C16049. Brisbane, Australia: Australian Coal Association Research Program (ACARP).

CONSOL Energy. 2008. Capture and use of coal mine ventilation air methane. http://www.consolresearch.com/pollution/pollution-control.html (accessed August 1, 2008).

Contarin F, Barcellos WM, Saveliev AV and Kennedy LA. 2005. Energy extraction from a porous media reciprocal flow burner with embedded heat exchangers. *Journal of Heat Transfer* 127:123–30.

Contarin F, Saveliev AV, Fridman AA and Kennedy LA. 2003. A reciprocal flow filtration combustor with embedded heat exchangers: Numerical study. *International Journal of Heat and Mass Transfer* 46:949–61.

Cookson EJ and Floyd DE. 2007. Application of reticulated metal foam to gas fired infrared burners. *High Temperature Materials and Processes* 26:269–74.

Coward HF and Jones GW. 1952. Limits of flammability of gases and vapors. In *Bureau of Mines Bulletin 503*, Washington, DC: United States Bureau of Mines.

CSIRO. 2006. Cooperation on capturing China's mine methane emissions. *ECOS Magazine* 130:34.

Cunhill F, van de Beld L and Westerterp KR. 1997. Catalytic combustion of very lean mixtures in a reverse flow reactor using an internal electric heater. *Industrial and Engineering Chemistry Research* 36:4198–4206.

Danell R, Nunn J and Källstrand Å. 2002. *Demonstration of MEGTEC VOCSIDIZER for methane utilisation*. Report C9065. Brisbane, Australia: Australian Coal Association Research Program (ACARP).

DataTaker. http://www.datataker.com/products/dt500.html (accessed June 4, 2009).

De Gioannis G, Muntoni A, Cappai G and Milia S. 2009. Landfill gas generation after mechanical biological treatment of municipal solid waste: Estimation of gas generation rate constants. *Waste Management* 29:1026–34.

de la Chesnaye FC, Delhotal C, DeAngelo B, Ottinger-Schaefer D and Godwin D. 2007. Past, present, and future of non-CO_2 gas mitigation analysis. In *Human induced climate change: An interdisciplinary assessment*, ed. ME Schlesinger, HSKheshgi, J Smith, FC de la Chesnaye, JM Reilly, T Wilson and C Kolstad, 266–81. New York: Cambridge University Press.

de la Chesnaye FC, Harvey R, Kruger D and Laitner JA. 2001. Cost-effective reductions of non-CO_2 greenhouse gases. *Energy Policy* 29:1325–31.

Delalic N, Mulahasanovic D and Ganic EN. 2004. Porous media compact heat exchanger unit: Experiment and analysis. *Experimental Thermal and Fluid Science* 28:185–92.

Department of Climate Change (DCC). 2008. *Fugitive sector greenhouse gas emissions projections 2007*. Canberra, Australia: Australian Government Department of Climate Change.

Department of Climate Change (DCC). 2009. *National greenhouse gas inventory 2009: Accounting for the Kyoto target*. Canberra, Australia: Australian Government Department of Climate Change.

Department of Trade and Industry (DTI). 2004. *Coal mine methane: Review of the mechanisms for control of emissions*. Report COAL R256. London: UK Government Department of Trade and Industry.

DePoorter GL, Brog TK and Readey MJ. 1992. Properties and applications of structural ceramics. In *Properties and selection: Nonferrous alloys and special-purpose materials*, vol. 2 of the *ASM handbook*. Materials Park, Ohio: ASM International.

Dhamrat RS and Ellzey JL. 2006. Numerical and experimental study of the conversion of methane to hydrogen in a porous media reactor. *Combustion and Flame* 144:698–709.

di Mare L, Mihalik TA, Continillo G and Lee JHS. 2000. Experimental and numerical study of flammability limits of gaseous mixtures in porous media. *Experimental Thermal and Fluid Science* 21:117–23.

Diniz da Costa JC, Prasad P and Pagan RJ. 2004. Modern environmental improvement pathways for the coal power generation industry in Australia. *Process Safety and Environmental Protection* 82:191–9.

Dixon MJ, Schoegel I, Hull CB and Ellzey JL. 2008. Experimental and numerical conversion of liquid heptane to syngas through combustion in a porous media. *Combustion and Flame* 154:217–31.

Dobrego KV, Gnesdilov NN, Kozlov IM, Bubnovich VI and Gonzalez HA. 2005. Numerical investigation of the new regenerator-recuperator scheme of VOC oxidizer. *International Journal of Heat and Mass Transfer* 48:4695–4703.

Dobrego KV, Gnesdilov NN, Lee SH and Choi HK. 2008a. Lean combustibility limit of methane in reciprocal flow filtration combustion reactor. *International Journal of Heat and Mass Transfer* 51:2190–98.

Dobrego KV, Gnesdilov NN, Lee SH and Choi HK. 2008b. Methane partial oxidation reverse flow reactor scale up and optimization. *International Journal of Hydrogen Energy* 33:5501–09.

Dobrego KV, Gnesdilov NN, Lee SH and Choi HK. 2008c. Partial oxidation of methane in a reverse flow porous media reactor: Water admixing optimization. *International Journal of Hydrogen Energy* 33:5535–44.

Dobrego KV, Kozlov IM and Bubnovich VI. 2003. Dynamics of filtration combustion front perturbation in the tubular porous media burner. *International Journal of Heat and Mass Transfer* 46:3279–89.

Drayton MK, Saveliev AV, Kennedy LA, Fridman AA and Li Y. 1998. Syngas production using superadiabatic combustion of ultra-rich methane-air mixtures. *Proceedings of the Combustion Institute* 27:1361–67.

Du L and Xie M. 2006. The influences of thermophysical properties of porous media on superadiabatic combustion with reciprocating flow. *Heat Transfer—Asian Research* 35:336–50.

Dunn-Rankin D. 2008. *Lean combustion: Technology and control*. San Diego, CA: Academic Press.

Duplessis N. 2009. Ventilation air methane oxidation using a VAMOX system at an active coal mine in the USA. Paper presented at the International Coalbed and Shale Gas Symposium, Tuscaloosa, AL. May 18.

Duran A and Rost M. 2005. Flameless thermal oxidation for chlorinated waste vent gas destruction: A case history. Paper presented at the 24th International Conference on Incineration and Thermal Treatment Technologies (IT3 2005), Galveston, TX. May 9–13.

Durst F. 2006. Porous medium combustion and applications. Paper presented at the 5th Indo-German Winter Academy, Digha, India. December 9–16.

Durst F and Trimis D. 2002. Combustion by free flames versus combustion reactors. *Clean Air* 3:1–20.

Durst F, Trimis D and Dimaczek G. 1993. Brenner. Ger. Offen. DE 4322109.2, filed July 2, 1993 and issued January 12, 1995.

Durst F and Weclas M. 2001. A new type of internal combustion engine based on the porous-medium combustion technique. *Proceedings of the Institution of Mechanical Engineers Part D: Journal of Automobile Engineering* 215:63–81.

Echigo R, Kurusu M, Ichimiya K and Yoshizawa Y. 1983. Combustion augmentation of extremely low calorific gases (application of the effective energy conversion method from gas enthalpy to thermal radiation). Paper presented at the ASME/JSME Thermal Engineering Joint Conference, Honolulu, HI. March 20–24.

Eggels RLGM and de Goey LPH. 1996. Post-processing method for predicting NO formation in one- and two-dimensional premixed methane-air flames. *Combustion and Flame* 107:65–71.

Ellzey JL and Goel R. 1995. Emissions of CO and NO from a two stage porous media burner. *Combustion Science and Technology* 107:81–91.

Elverum PJ, Ellzey JL and Kovar D. 2005. Durability of YZA ceramic foams in a porous burner. *Journal of Materials Science* 40:155–64.

Environmental Protection Agency (EPA). 1997. *Use of coal mine methane in greenhouses?* Fact sheet EPA 430-F-98-085. Washington, DC: US Environmental Protection Agency.

Environmental Protection Agency (EPA). 1998. *Use of coal mine methane in coal dryers*. Draft. Washington, DC: US Environmental Protection Agency.

Environmental Protection Agency (EPA). 1999. *US Methane emissions 1990–2020: Inventories, projections, and opportunities for reductions*. Report EPA 430-R-99-013. Washington, DC: US Environmental Protection Agency.

Environmental Protection Agency (EPA). 2000. *Technical and economic assessment: Mitigation of methane emissions from coal mine ventilation air*. Report EPA 430-R-001. Washington, DC: US Environmental Protection Agency.

Environmental Protection Agency (EPA). 2002. *Powering microturbines with landfill gas*. Fact sheet EPA 430-F-02-012. Washington, DC: US Environmental Protection Agency.

Environmental Protection Agency (EPA). 2003a. *Assessment of the worldwide market potential for oxidizing coal mine ventilation air methane*. Report EPA 430-R-03-002. Washington, DC: US Environmental Protection Agency.

Environmental Protection Agency (EPA). 2003b. *International analysis of methane and nitrous oxide abatement opportunities*. Report to Energy Modeling Forum, Working Group 21 (EMF-21). Washington, DC: US Environmental Protection Agency.

Environmental Protection Agency (EPA). 2004a. *Using coal mine methane to heat mine ventilation air*. Revised draft. Washington, DC: US Environmental Protection Agency.

Environmental Protection Agency (EPA). 2004b. *Using ventilation air methane (VAM) as combustion air in reciprocating engines and turbines*. Revised draft. Washington, DC: US Environmental Protection Agency.

Environmental Protection Agency (EPA). 2006a. *Global anthropogenic non-CO_2 greenhouse gas emissions: 1990–2020*. Report EPA 430-R-06-003. Washington, DC: US Environmental Protection Agency.

Environmental Protection Agency (EPA). 2006b. *Global mitigation of non-CO_2 greenhouse gases*. Report EPA 430-R-06-005. Washington, DC: US Environmental Protection Agency.

Environmental Protection Agency (EPA). 2006c. *Market opportunities for biogas recovery systems: A guide to identifying candidates for on-farm and centralized systems*. Report EPA-430-8-06-004. Washington, DC: US Environmental Protection Agency.

Environmental Protection Agency (EPA). 2007. *Voluntary programs*. http://epa.gov/methane/voluntary.html (accessed August 17, 2009).

Environmental Protection Agency (EPA). 2008. *US surface coal mine methane recovery project opportunities*. Report EPA 430-R-08-001. Washington, DC: US Environmental Protection Agency.

Ergun S. 1952. Fluid flow through packed columns. *Chemical Engineering Progress* 48:89–94.

Evans RL. 2007. *Fueling our future: An introduction to sustainable energy*. New York: Cambridge University Press.

Fay M, Dhamrat R and Ellzey JL. 2005. Effect of porous reactor design on conversion of methane to hydrogen. *Combustion Science and Technology* 177:2171–89.

Fend T, Trimis D, Pitz-Paal R, Hoffschmidt B and Reutter O. 2005. Thermal properties. In *Cellular ceramics: Structure, manufacturing, properties and applications*, ed. M Scheffler and P Colombo, 342–60. Weinheim, Germany: Wiley.

Fernandez R, Petrusak R, Robinson D and Zavadil D. 2005. Cost-effective methane emissions reductions for small and midsize natural gas producers. *Journal of Petroleum Technology* 57:34–42.

Flores RM. 1998. Coalbed methane: From hazard to resource. *International Journal of Coal Geology* 35:3–26.

Food and Agriculture Organization (FAO). 2006. *Livestock's long shadow: Environmental issues and options*. Rome, Italy: United Nations Food and Agriculture Organization.

Fouteko SI, Shabunya SI, Zhdanok SA and Kennedy LA. 1996. Superadiabatic combustion wave in a diluted methane-air mixture under filtration in a packed bed. *Proceedings of the Combustion Institute* 26:3377–82.

Franco A and Diaz AR. 2009. The future challenges for 'clean coal technologies': Joining efficiency increase and pollutant emission control. *Energy* 34:348–54.

Fu X, Viskanta R and Gore JP. 1998. Modeling of thermal performance of a porous radiant burner. *ASME HTD* 361:11–18.

Fuse T, Kobayashi N and Hasatani M. 2005. Combustion characteristics of ethanol in a porous ceramic burner and ignition improved by enhancement of liquid-fuel intrusion in the pore with ultrasonic irradiation. *Experimental Thermal and Fluid Science* 29:467–76.

García E, Miranzo P and Osendi MI. 2003. Alterations in cordierite based burners subjected to radiant mode ageing conditions. *Journal of the European Ceramic Society* 23:3097–3103.

Gauthier S, Lebas E and Baillis D. 2007. SFGP 2007: Natural gas/hydrogen mixture combustion in a porous radiant burner. *International Journal of Chemical Reactor Engineering* 5:A114.

Gershtein VY and Baukal CE. 2001. CFD in burner development. In *Computational fluid dynamics in industrial combustion*, ed. CE Baukal, VY Gershtein and L Xianming, 249–85. Boca Raton, FL: CRC Press.

Gibson LJ and Ashby MF. 1997. *Cellular solids: Structure and properties*. 2nd ed. Cambridge, UK: Cambridge University Press.

Gilbert RG, Luther K and Troe J. 1982. Theory of thermal unimolecular reactions in the fall-off range, II: Weak collision rate constants. *Berichte der Bunsengesellschaft: Physical Chemistry Chemical Physics* 87:169–77.

Gillis B, Waltzer S, Heath MW, Cormack J and Ravishankar K. 2007. Technology drives methane emissions down, profits up. *Oil & Gas Journal* 105:20–28.

Glarborg P, Alzueta MU, Dam-Johansen K and Miller JA. 1998. Kinetic modelling of hydrocarbon/nitric oxide interactions in a flow reactor. *Combustion and Flame* 115:1–27.

Glassman I. 1996. *Combustion*. 3rd ed. San Diego, CA: Academic Press.

Gnesdilov NN, Dobrego KV, Kozlov IM and Shmelev ES. 2006. Numerical study and optimization of the porous media VOC oxidizer with electric heating elements. *International Journal of Heat and Mass Transfer* 40:5062–69.

GoGas. *Porous burner RADIMAX*. http://www.gogas.de (accessed March 18, 2008).

Gokulakrishnan P, McLellan PJ, Lawrence AD and Grandmaison EW. 2005. Kinetic analysis of NO-sensitized methane oxidation. *Chemical Engineering Science* 60:3683–92.

Golombok M, Prothero A and Shirvill LC. 1991. Surface combustion in metal fibre burner. *Combustion Science and Technology* 77:203–23.

Gómez SY, Escobar JA, Alvarez OA, Rambo CR, de Oliveira APN and Hotza D. 2009. ZrO_2 foams for porous radiant burners. *Journal of Materials Science* 44:3466–71.

Greil P. 2002. Advanced engineering ceramics. *Advanced Materials* 14:709–16.

Griffiths FJ. 1995. Reduced kinetic models and their application to practical combustion systems. *Progress in Energy and Combustion Science* 21:25–107.

Gude VG and Nirmalakhandan N. 2008. Desalination using low-grade heat sources. *Journal of Energy Engineering* 134:95–101.

Gunning PM. 2005. The methane to markets partnership: An international framework to advance the recovery and use of methane as a clean energy source. *Environmental Sciences* 2:361–6.

Hall MJ and Peroutka XN. 1995. A porous media burner for reforming methanol for fuel cell powered electric vehicles. *Society of Automotive Engineers Special Publications* SP-1108:101–9.

Hanamura K, Bohda K and Miyairi Y. 1997. A study of super-adiabatic combustion engine. *Energy Conversion and Management* 38:1259–66.

Hanamura K and Echigo R. 1991. An analysis of flame stabilization mechanisms in radiation burners. *Wärme und Stoffübertragung* 26:377–83.

Hanamura K, Echigo R and Zhdanok SA. 1993. Superadiabatic combustion in a porous medium. *International Journal of Heat and Mass Transfer* 36:3201–9.

Hanamura K, Kumano T and Iida Y. 2005. Electric power generation by super-adiabatic combustion in thermoelectric porous element. *Energy* 30:347–57.

Hanamura K and Nishio S. 2003. A feasibility study of reciprocating-flow super-adiabatic combustion engine. *JSME International Journal Series B* 46:579–85.

Hansen J, Sato M, Ruedy R, Lacis A and Oinas V. 2000. Global warming in the twenty-first century: An alternative scenario. *PNAS* 97:9875–80.

Hao X, Yang H and Zhang G. 2008. Trigeneration: A new way for landfill gas utilzation and its feasibility in Hong Kong. *Energy Policy* 36:3662–73.

Hardesty DR and Weinberg FJ. 1974. Burners producing large excess enthalpies. *Combustion Science and Technology* 8:201–14.

Haubrichs R and Widmann R. 2006. Evaluation of aerated biofilter systems for microbial methane oxidation of poor landfill gas. *Waste Management* 26:408–16.

Hayes RE. 2004. Catalytic solutions for fugitive methane emissions in the oil and gas sector. *Chemical Engineering Science* 59:4073–80.

Hayhoe K, Jain A, Pitcher H, MacCracken C, Gibbs M, Wuebbles D, Harvey R and Kruger D. 1999. Costs of multigreenhouse gas reduction targets for the USA. *Science* 29:905–6.

Henneke MR and Ellzey JL. 1997. A numerical study of re-ignition in porous media burners. *ASME HTD* 341:155–63.

Henneke MR and Ellzey JL. 1999. Modeling of filtration combustion in a packed bed. *Combustion and Flame* 117:832–40.

Ho TC. 2008. Kinetic modelling of large-scale reaction systems. *Catalysis reviews* 50:287–378.

Hoffmann JG, Echigo R, Yoshida H and Tada S. 1997. Experimental study on combustion in porous media with a reciprocating flow system. *Combustion and Flame* 111:32–46.

Holm-Christensen O, Jones IP, Wilkes NS, Splawski BA, Stopford PJ, Creemers B and Fletcher DF. 2001. The solution of coupled flow and chemistry problems. *Progress in Computational Fluid Dynamics* 1:43–9.

Howell JR, Hall MJ and Ellzey JL. 1996. Combustion of hydrocarbon fuels within porous inert media. *Progress in Energy and Combustion Science* 22:121–45.

Hsu P-F. 1996. Experimental study of the premixed combustion within the nonhomogeneous porous ceramic media. *ASME HTD* 329:1–10.

Hsu P-F, Evans WD and Howell JR. 1993. Experimental and numerical study of premixed combustion within nonhomogeneous porous ceramics. *Combustion Science and Technology* 90:149–72.

Hsu P-F, Howell JR and Matthews RD. 1993. A numerical investigation of premixed combustion within porous inert media. *Journal of Heat Transfer* 115:744–50.

Hsu P-F and Matthews RD. 1993. The necessity of using detailed kinetics in models for premixed combustion within porous media. *Combustion and Flame* 93:457–466.

Huang Y, Chao CYH and Cheng P. 2002. Effects of preheating and operation conditions on combustion in a porous medium. *International Journal of Heat and Mass Transfer* 45:4315–24.

Hughes KI, Turányi T, Clague AR and Pilling MJ. 2001. Development and testing of a comprehensive chemical mechanism for the oxidation of methane. *International Journal of Chemical Kinetics* 33:513–38.

InterGen. *Millmerran*. http://www.intergen.com/global/millmerran.php (accessed August 12, 2009).

Intergovernmental Panel on Climate Change (IPCC). 2005. *IPCC special report on carbon dioxide capture and storage*, ed. B Metz, O Davidson, H de Coninck, M Loos and L Meyer. New York: Cambridge University Press.

Intergovernmental Panel on Climate Change (IPCC). 2007a. *Climate change 2007: Impacts, adaptation and vulnerability. Contribution of Working Group II to the Fourth Assessment Report of the Intergovernmental Panel of Climate Change*, ed. ML Parry, OF Canziani, JP Palutikof, PJ van der Linden and CE Hanson. New York: Cambridge University Press.

Intergovernmental Panel on Climate Change (IPCC). 2007b. *Climate change 2007: Mitigation. Contribution of Working Group III to the Fourth Assessment Report of the Intergovernmental Panel*

on Climate Change, ed. B Metz, OR Davidson, PR Bosch, R Dave, LA Meyer. New York: Cambridge University Press.

Intergovernmental Panel on Climate Change (IPCC). 2007c. *Climate change 2007: Synthesis report*. Geneva, Switzerland: Intergovernmental Panel on Climate Change (IPCC).

Intergovernmental Panel on Climate Change (IPCC). 2007d. *Climate change 2007: The physical science basis. Contribution of Working Group I to the Fourth Assessment Report of the Intergovernmental Panel on Climate Change*, ed. S Solomon, D Qin, M Manning, Z Chen, M Marquis, KB Averyt, M Tignor and HL Miller. New York: Cambridge University Press.

International Energy Agency (IEA). 2002. *Solutions for the 21st century: Zero emissions technologies for fossil fuels.* Paris: International Energy Agency.

International Energy Agency (IEA). 2005. *Energy policies of IEA countries: Australia 2005 review*. Paris: International Energy Agency.

International Energy Agency (IEA). 2007a. Energy sector methane recovery and use initiative. http://www.iea.org/textbase/papers/2007/methane_fact.pdf (accessed July 30, 2008).

International Energy Agency (IEA). 2007b. *Key world energy statistics 2007*. Paris: International Energy Agency.

Isaacson R. 1990. *Methane from community wastes*. Oxford: Elsevier.

Ismagilov ZR, Pushkarev VV, Podyacheva OY, Koryabkina NA and Veringa H. 2001. A catalytic heat-exchanging tubular reactor for combining of high temperature exothermic and endothermic reactions. *Chemical Engineering Journal* 82:355–60.

Itaya Y, Miyoshi K, Maeda S and Hasatani M. 1992. Surface combustion of a premixed methane-air gas on a porous ceramic. *International Chemical Engineering* 32:123–31.

Jacobson NS. 1993. Corrosion of silicon-based ceramics in combustion environments. *Journal of the American Ceramic Society* 76:3–28.

Jardine CN, Boardman B, Osman A, Vowles J and Palmer J. 2004. *Methane UK*. Oxford: Environmental Change Institute, University of Oxford.

Jazbec M, Fletcher DF and Haynes BS. 2000. Simulation of the ignition of lean methane mixtures using CFD modelling and a reduced chemistry mechanism. *Applied Mathematical Modelling* 24:689–96.

Johnson DE, Johnson KA, Ward GM and Branine ME. 2000. Ruminants and other animals. In *Atmospheric methane: Its role in the global environment*, ed. MAK Khalil, 112–33. Berlin, Germany: Springer-Verlag.

Johnson PW, Novak T, White DJ, Stevenson JW, Mills RA, Lasseter EL and Boyer CM. 1998. Use of mine ventilation exhaust as combustion air in gas-fired turbo-electric generators. *IEEE Transactions of Industry Applications* 34: 399–405.

Jones JC. 2002. Suggestions towards improved reliability of thermocouple temperature measurement in combustion tests. In *Thermal measurements: The foundation of fire standards*. West Conshohocken, PA: ASTM International.

Jones AR, Lloyd SA and Weinberg FJ. 1978. Combustion in heat exchangers. *Proceedings of the Royal Society of London Series A: Mathematical and Physical Sciences* 360:97–115.

Judd AG. 2000. Geological sources of methane. In *Atmospheric methane: Its role in the global environment*, ed. MAK Khalil, 280–303. Berlin, Germany: Springer-Verlag.

Jugjai S and Chuenchit C. 2001. A study of energy conversion by a porous combustor-heat exchanger with cyclic flow reversal combustion. *International Energy Journal* 2:95–104.

Jugjai S and Nungniyom V. 2009. Cyclic operation of porous combustor-heater (PCH). *Fuel* 88:553–9.

Jugjai S and Phothiya C. 2007. Liquid fuels-fired porous combustor-heater. *Fuel* 86:1062–8.

Jugjai S and Polmart N. 2003. Enhancement of evaporation and combustion of liquid fuels through porous media. *Experimental Thermal and Fluid Science* 27:901–9.

Jugjai S and Pongsai C. 2007. Liquid fuels-fired porous burner. *Combustion Science and Technology* 179:1823–40.

Jugjai S and Sawananon A. 2004. The surface combustor-heater with cyclic flow reversal combustion embedded with water tube bank. *Fuel* 83:2369–79.

Jugjai S, Wongpanit N, Laoketkan T and Nokkaew S. 2002. The combustion of liquid fuels using a porous medium. *Experimental Thermal and Fluid Science* 26:15–23.

Jung Y, Imhoff PT, Augenstein DC and Yazdani R. 2009. Influence of high-permeability layers for enhancing landfill gas capture and reducing fugitive methane emissions from landfills. *Journal of Environmental Engineering* 135:138–46.

Kakutkina NA, Korzhavin AA and Mbarawa M. 2006. Filtration combustion of hydrogen-air, propane-air and methane-air mixtures in inert porous media. *Combustion, Explosion and Shock Waves* 42:372–83.

Kamal MM and Mohamad AA. 2005. Enhanced radiation output from foam burners operating with a nonpremixed flame. *Combustion and Flame* 140:233–48.

Kamal MM and Mohamad AA. 2006a. Combustion in porous media. *Proceedings of the Institution of Mechanical Engineers Part A: Journal of Power Engineering* 220:487–508.

Kamal MM and Mohamad AA. 2006b. Development of a Cylindrical Porous-Medium Burner. *Journal of Porous Media* 9:469–81.

Kamal MM and Mohamad AA. 2006c. Effect of swirl on performance of foam porous medium burners. *Combustion Science and Technology* 178:729–61.

Kaplan M and Hall MJ. 1995. Combustion of liquid fuels within a porous media radiant burner. *Experimental Thermal and Fluid Science* 11:13–20.

Karim GA, Hanafi AS and Zhou G. 1993. A kinetic investigation of the oxidation of low heating value fuel mixtures of methane and dilutents. *Journal of Energy Resources Technology* 115:301–6.

Kawaguchi O, Otoh T, Nakamura S, Todoroki A and Murayama Y. 1990. Premixed combustion at a fiber mat. *Proceedings of the Combustion Institute* 20:1019–24.

Kay JM and Nedderman RM. 1985. *Fluid mechanics and transfer processes*. Cambridge, UK: Cambridge University Press.

Kayal TK and Chakravarty M. 2007. Combustion of suspended fine solid fuel in air inside inert porous medium: A heat transfer analysis. *International Journal of Heat and Mass Transfer* 50:3359–65.

Kee RJ, Dixon-Lewis G, Warnatz J, Coltrin ME and Miller JA. 1986. *A Fortran computer code package for the evaluation of gas-phase, multicomponent transport properties*. Report SAND-86-8246. Livermore, CA: Sandia National Laboratories.

Kee RJ, Rupley FM, Miller JA, Coltrin ME, Grcar JF, Meeks E, Moffat HK, Lutz AE, Dixon-Lewis G, Smooke MD, Warnatz J, Evans GH, Larson RS, Mitchell RE, Petzold LR, Reynolds WC, Caracotsios M, Stewart WE, Glarborg P, Wang C, Adigun O, Houf WG, Chou CP, Miller SF, Ho P and Young DJ. 2005. *CHEMKIN Release 4.0.2*. http://www.reactiondesign.com/products/open/chemkin.html (accessed August 24, 2009).

Kennedy LA, Bingue JP, Saveliev AV, Fridman AA and Foutko SI. 2000. Chemical structures of methane-air filtration combustion waves for fuel-lean and fuel-rich conditions. *Proceedings of the Combustion Institute* 28:1431–38.

Kennedy LA, Fridman AA and Saveliev AV. 1995. Superadiabatic combustion in porous media: Wave propagation, instabilities, new type of chemical reactor. *Fluid Mechanics Research* 22:1–26.

Kennedy LA, Saveliev AV, Bingue JP and Fridman AA. 2002. Filtration combustion of a methane wave in air for oxygen-enriched and oxygen-depleted environments. *Proceedings of the Combustion Institute* 29:835–41.

Keppler F, Hamilton JTG, Brass M and Röckmann T. 2006. Methane emissions from terrestrial plants under aerobic conditions. *Nature* 439:187–91.

Kesting A, Pickenäcker K, Trimis D, Cerri I, Krieger R and Schneider H. 2001. Development of a highly efficient gas infrared heater by means of combustion in inert porous media. Paper presented at the International Gas Research Conference, Amsterdam, The Netherlands. November 5–8.

Kesting A, Pickenäcker O, Trimis D and Durst F. 1999. Development of a radiation burner for methane and pure oxygen using the porous burner technology. Paper presented at the 5th International Conference on Technologies and Combustion for a Clean Environment (Clean Air V), Lisbon, Portugal. July 12–15.

Khalil MAK. 2000. Atmospheric methane: An introduction. In *Atmospheric methane: Its role in the global environment*, ed. MAK Khalil, 1–8. Berlin, Germany: Springer-Verlag.

Khalil MAK, Rasmussen RA, Shearer MJ, Ge S and Rau JA. 1993. Methane from coal burning. *Chemosphere* 26:473–77.

Khalil MAK and Shearer MJ. 2000. Sources of methane: An overview. In *Atmospheric methane: Its role in the global environment*, ed. MAK Khalil, 98–111. Berlin, Germany: Springer-Verlag.

Khalil MAK, Shearer MJ and Rasmussen RA. 2000. Methane sinks, distributions, and trends. In *Atmospheric methane: Its role in the global environment*, ed. MAK Khalil, 86–97. Berlin, Germany: Springer-Verlag.

Khanna V, Goel R and Ellzey JL. 1994. Measurement of emissions and radiation for methane combustion within a porous medium burner. *Combustion Science and Technology* 99:133–42.

Kiefer J, Weikl MC, Seeger T, von Issendorff F, Beyrau F and Leipertz A. 2009. Non-intrusive gas-phase temperature measurements inside a porous burner using dual-pump CARS. *Proceedings of the Combustion Institute* 32:3123–29.

Kirchgessner DA. 2000. Fossil fuel industries. In *Atmospheric methane: Its role in the global environment*, ed. MAK Khalil, 263–279. Berlin, Germany: Springer-Verlag.

Kirchgessner DA, Masemore SS and Piccot SD. 2002. Engineering and economic evaluation of gas recovery and utilization technologies at selected US mines. *Environmental Science and Policy* 5:397–409.

Konnov AA. 2000. *Detailed reaction mechanism for small hydrocarbons combustion release 0.5.* http://homepages.vub.ac.be/~akonnov/ (accessed September 1, 2006).

Korzhavin AA, Bunev VA, Abdullin RK and Babkin VS. 1982. Flame zone in gas combustion in an inert porous medium. *Combustion, Explosion and Shock Waves* 18:628–31.

Kosmack DA, Winschel RA and Zak KP. 2003. Capture and use of coal mine ventilation air methane. Paper presented at the 20th International Coal Conference, Pittsburgh, PA. September 15–19.

Kotani Y, Behbahani HF and Takeno T. 1984. An excess enthalpy flame combustor for extended flow ranges. *Proceedings of the Combustion Institute* 20:2025–33.

Kotani Y and Takeno T. 1982. An experimental study on stability and combustion characteristics of an excess enthalpy flame. *Proceedings of the Combustion Institute* 19:1503–09.

Kuik O, Brander L and Tol RSJ. 2009. Marginal abatement costs of greenhouse gas emissions: A meta-analysis. *Energy Policy* 37:1395–1403.

Kulkarni MR and Peck RE. 1996. Analysis of a bilayered porous radiant burner. *Numerical Heat Transfer Part A: Applications* 30:219–32.

Kushwaha A, Poirier M, Hayes RE and Spoundjiev H. 2005. Heat extraction from a flow reversal reactor in lean methane combustion. *Chemical Engineering Research and Design* 83:205–13.

Kushwaha A, Poirier M, Sapoundjiev H and Hayes RE. 2004. Effect of reactor internal properties on the performance of a flow reversal catalytic reactor for methane combustion. *Chemical Engineering Science* 59:4081–93.

Laevski YM and Babkin VS. 2008. Stabilized gas combustion wave in an inert porous medium. *Combustion, Explosion and Shock Waves* 44:502–8.

Lai GY. 1992. Basic metallurgy and product forms. In *Heat treating*, vol. 4 of the *ASM handbook*. Materials Park, Ohio: ASM International.

Launder BE and Spalding DB. 1972. *Lectures in mathematical models of turbulence*. London: Academic Press.

Launder BE and Spalding DB. 1974. The numerical computation of turbulent flows. *Computer methods in applied mechanics and engineering* 3:269–89.

Law CK, Sung CJ, Wang H and Lu TF. 2003. Development of comprehensive detailed and reduced reaction mechanisms for combustion modelling. *AIAA Journal* 41:1629–46.

Le Chatelier H. 1891. Estimation of firedamp by flammability limits. *Annales des Mines* 19:388–95.

Lee SY and Holder GD. 2001. Methane hydrates potential as a future energy source. *Fuel Processing Technology* 71:181.

Leonardi SA, Gore JP and Viskanta R. 2001. Experimental investigation of partially-premixed combustion in a novel porous radiant burners. Paper presented at the 35th National Heat Transfer Conference (NHTC2001), Anaheim, CA. June 10–12.

Leonardi SA, Viskanta R and Gore JP. 2002. Radiation and thermal performance measurements of a metal fiber burner. *Journal of Quantitative Spectroscopy & Radiative Transfer* 73:491–501.

Levenspeil O. 1999. *Chemical reaction engineering*. 3rd ed. New York: Wiley.

Levine JS, Cofer WR III and Pinto JP. 2000. Biomass burning. In *Atmospheric methane: Its role in the global environment*, ed. MAK Khalil, 190–201. Berlin, Germany: Springer-Verlag.

Li SC and Williams FA. 2002. Reaction mechanisms for methane ignition. *Journal of Engineering for Gas Turbines and Power* 124:471–80.

Lim I-G and Matthews RD. 1993. Predictions of NO_X and CO emissions from porous media burners. *ASME PD* 50:77–84.

Litto R, Hayes RE, Sapoundjiev H, Fuxman A, Forbes F, Liu B and Bertrand F. 2006. Optimization of a flow reversal reactor for the catalytic combustion of lean methane mixtures. *Catalysis Today* 117:536–42.

Liu S, Chen Q, Xiong X, Zhang Z and Lei J. 2008. Preliminary study on ECT imaging of flames in porous media. *Measurement Science and Technology* 19:1–7.

Liu H, Dong S, Li B-W and Chen H-G. 2009. Parametric investigations of premixed methane-air combustion in two-section porous media by numerical simulation. *Fuel*. In press.

Liu H, Xie M and Wu D. 2009a. Thermodynamic analysis of the heat regenerative cycle in porous medium engine. *Energy Conversion and Management* 50:297–303.

Liu H, Xie M and Wu D. 2009b. Simulation of a porous medium (PM) engine using a two-zone combustion model. *Applied Thermal Engineering* 29:3189–97.

Liu JF and Hsieh WH. 2004. Experimental investigation of combustion in porous heating burners. *Combustion and Flame* 138:295–303.

Lloyd SA and Weinberg FJ. 1974. A burner for mixtures of very low heat content. *Nature* 251:47–49.

Lockwood FC, Abbas T, Kandamby NH and Sakthitharan V. 2001. CFD experience on industrial combustors. *Progress in Computational Fluid Dynamics* 1:1–13.

Lombardi L, Carnevale E and Corti A. 2006. Greenhouse effect reduction and energy recovery from waste landfill. *Energy* 31:3208–19.

Løvas T. 2009. Automatic generation of skeletal mechanism for ignition combustion based on level of importance analysis. *Combustion and Flame* 156:1348–58.

Lu T and Law CK. 2009. Towards accommodating realistic fuel chemistry in large-scale computations. *Progress in Energy and Combustion Science* 35:192–215.

Lucas PL, van Vuuren DP, Olivier JGJ and den Elzen MGJ. 2007. Long-term reduction potential of non-CO_2 greenhouse gases. *Environmental Science and Policy* 10:85–103.

MacDonald ME, Chadwick MJ and Aslanian GS. 1996. *The environmental management of low-grade fuels*. London: Earthscan.

Mach A, Herzog A, von Issendorff F, Kanka B, Krieger R, Mößbauer S, Ortona A, Pritzkow W, Schäfer J, Schmidt J, Schmücker M, Schneider H, Starke J, Trimis D, Vogt U and zur Megede D. 2005. CERPOR project: Optimization of ceramic components for the porous burner technology. Paper presented at the Conference on Porous Ceramic Materials (PCM 2005), Bruges, Belgium. October 20–21.

Mach A, Inayat A, von Issendorff F and Delgado A. 2007. Oxidation processes of SiSiC foams used in porous burners. Paper presented at the 10th International Conference and Exhibition of the European Ceramic Society, Berlin, Germany. June 17–21.

Malico I and Pereira JCF. 1999. Numerical predictions of porous burners with integrated heat exchanger for household applications. *Journal of Porous Media* 2:153–62.

Marbach TL and Agrawal AK. 2005. Experimental study of surface and interior combustion using composite porous inert media. *Journal of Engineering for Gas Turbines and Power* 127:307–13.

Marbach TL, Sadasivuni V and Agrawal AK. 2007. Investigation of a miniature combustor using porous media surface stabilized flame. *Combustion Science and Technology* 179:1901–22.

Martin RJ, Stilger JD and Holst MR. 1991. Method and apparatus for controlled reaction in a reaction matrix. US Patent 5,165,884, filed July 5, 1991 and issued November 24, 1992.

Massachusetts Institute of Technology (MIT). 2007. *The future of coal: Options for a carbon-constrained world*. Cambridge, MA: Massachusetts Institute of Technology.

Mathis WM Jr and Ellzey JL. 2003. Flame stabilization, operating range, and emissions for a methane/air porous burner. *Combustion Science and Technology* 175:825–39.

Matthews E. 2000. Wetlands. In *Atmospheric methane: Its role in the global environment*, ed. MAK Khalil, 202–233. Berlin, Germany: Springer-Verlag.

Mattus R. 2005. Major coal mine greenhouse gas emission converted to electricity: 1st large scale installation. *Environmental Sciences* 2:377–82.

MatWeb. *Fecralloy TM 145 electrical resistance steel*. http://www.matweb.com (accessed March 18, 2008).

Mbarawa M, Kakutkina NA and Korzhavin AA. 2007. Experimental investigation on peculiarities of the filtration combustion of the gaseous fuel-air mixtures in the porous inertia media. *Journal of Mechanical Science and Technology* 21:1799–1806.

McCabe WL, Smith JC and Harriot P. 2005. *Unit operations of chemical engineering*. 7th ed. New York: McGraw-Hill.

MEGTEC. 2008. *Energy from coal mine ventilation air methane*. http://www.megtec.com/energy-from-coal-mine-ventilation-methane-p-682-l-en.html (accessed August 1, 2008).

Mendes MAA, Pereira JMC and Pereira JCF. 2008. On the stability of ultra-lean H_2/CO combustion in inert porous burners. *International Journal of Hydrogen Energy* 33:3416–25.

Mendiara T, Alzueta MU, Millera A and Bilbao R. 2004. An augmented reduced mechanism for methane combustion. *Energy & Fuels* 18:619–27.

Meng WH, McCordic C, Gore JP and Herold KE. 1991. A study of effects of porous ceramic inserts on heat transfer and combustion in a fired heat exchanger. Paper presented at the 3rd ASME/JSME Thermal Engineering Joint Conference, Reno, NV. March 17–22.

Methane to Markets. *Methane technologies for mitigation and utilization*. http://www.methanetomarkets.org/resources/coalmines/docs/cmm_tech_database.pdf (accessed July 28, 2008).

Methane to Markets. 2006. *CMM global overview*. http://www.methanetomarkets.org/resources/coalmines/overview.htm (accessed July 31, 2008).

Miller JA and Bowman CT. 1989. Mechanism and modeling of nitrogen chemistry in combustion. *Progress in Energy and Combustion Science* 15:287–338.

Miller JA and Kee RJ. 1990. Chemical kinetics and combustion modelling. *Annual Review of Physical Chemistry* 41:345–87.

Min DK and Shin HD. 1991. Laminar premixed flame stabilized inside a honeycomb ceramic. *International Journal of Heat and Mass Transfer* 34:341–56.

Mital R, Gore JP and Viskanta R. 1997. A study of the structure of submerged reaction zone in porous ceramic radiant burners. *Combustion and Flame* 111:175–84.

Mital R, Gore JP and Viskanta R. 1998. A radiation efficiency measurement procedure for gas-fired radiant burners. *Experimental Heat Transfer* 11:3–21.

Modest MF. 2003. *Radiative heat transfer*. San Diego, CA: Elsevier.

Mohamad AA. 2002. Numerical simulation of combustion in a cylindrical porous medium. Paper presented at the 2002 Engineering Technology Conference On Energy (ETCE 2002), Houston, TX. February 4–5.

Mohamad AA. 2003. Fundamentals of combustion in porous burners. Paper presented at the NATO Advanced Study Institute on Porous Media, Neptun-Olimp, Romania. June 9–20.

Mohamad AA. 2005. Combustion in porous media: Fundamentals and applications. In *Transport phenomena in porous media*, vol. 3, ed. DB Ingham and I Pop. Amsterdam, The Netherlands: Elsevier.

Mohamad AA, Ramadhyani S and Viskanta R. 1994. Modelling of combustion and heat transfer in a packed bed with embedded coolant tubes. *International Journal of Heat and Mass Transfer* 37:1181–91.

Mohamad AA, Viskanta R and Ramadhyani S. 1994. Numerical predictions of combustion and heat transfer in a packed bed with embedded coolant tubes. *Combustion Science and Technology* 96:387–407.

Mößbauer S, Grüber W and Trimis D. 2001. Exhaust gas recirculation in porous burners for the target application zero emission steam engines. Paper presented at the 6th International Conference on Technologies and Combustion for a Clean Environment (Clean Air VI), Porto, Portugal. July 9–12.

Mößbauer S, Pickenäcker O and Trimis D. 1999. Application of the porous burner technology in energy- and heat-engineering. Paper presented at the 5th International Conference on Technologies and Combustion for a Clean Environment (Clean Air V), Lisbon, Portugal. July 12–15.

Mujeebu MA, Abdullah MZ, Abu Bakar MZ, Mohamad AA and Abdullah MK. 2009a. A review of investigations on liquid fuel combustion in porous inert media. *Progress in Energy and Combustion Science* 35:216–30.

Mujeebu MA, Abdullah MZ, Abu Bakar MZ, Mohamad AA and Abdullah MK. 2009b. Applications of porous media combustion technology: A review. *Applied Energy* 86:1365–75.

Mujeebu MA, Abdullah MZ, Abu Bakar MZ, Mohamad AA, Muhad RMN and Abdullah MK. 2009c. Combustion in porous media and its applications: A comprehensive survey. *Journal of Environmental Management* 90:2287–2312.

Nakos JT. 2002. Understanding the systematic error of a mineral-insulated, metal sheathed (MIMS) thermocouple attached to a heated flat surface. In *Thermal measurements: The foundation of fire standards*. West Conshohocken, Pennsylvania: ASTM International.

Neue H-U and Roger PA. 2000. Rice agriculture: Factors controlling emissions. In *Atmospheric methane: Its role in the global environment*, ed. MAK Khalil, 134–169. Berlin, Germany: Springer-Verlag.

Newburn ER and Agrawal AJ. 2007. Liquid fuel combustion using heat recirculation through annular porous media. *Transactions of the ASME* 129:914–9.

Nikiema J, Bibeau L, Lavoie J, Brzezinski R, Vigneux J and Heitz M. 2005. Biofiltration of methane: An experimental study. *Chemical Engineering Journal* 113:111–17.

Noordally E, Przybylski JM and Witton JJ. 2004. *Porous media combustors for clean gas turbine engines*. Report 9210/1-01/04. Bedford, UK: Cranfield University.

Oliveria FAC. 2008. Damage assessment of mullite ceramic foams in radiant gas burners. *Materials Science Forum* 587–8:99–103.

Oliveira AAM and Kaviany M. 2001. Nonequilibrium in the transport of heat and reactants in combustion in porous media. *Progress in Energy and Combustion Science* 27:523–45.

Patangi VK and Mishra SC. 2006. Combustion of gaseous hydrocarbon fuels within porous media: A review. In *Advances in energy research (AER-2006): Proceedings of the 1st national conference on advances in energy research*. Mumbai: India: Macmillan India.

Pedersen-Mjaanes H, Chan L and Mastorakos E. 2005. Hydrogen production from rich combustion in porous media. *International Journal of Hydrogen Energy* 30:579–92.

Perry RH and Green DW. 1997. *Perry's chemical engineers' handbook*. 7th ed. New York: McGraw-Hill.

Philopoulos A, Felske C and McCartney D. 2008. Field-scale treatment of landfill gas with a passive methane oxidizing biofilter. *Journal of Environmental Engineering and Science* 7:531–42.

Pickenäcker O, Pickenäcker K, Wawrzinek K, Trimis D, Pritzkow WEC, Müller C, Goedtke P, Papenburg U, Alder J, Standke G, Heymer H, Tauscher W and Jansen F. 1999a. Innovative ceramic materials for porous-medium burners. *Interceram* 48:326–30.

Pickenäcker O, Pickenäcker K, Wawrzinek K, Trimis D, Pritzkow WEC, Müller C, Goedtke P, Papenburg U, Alder J, Standke G, Heymer H, Tauscher W and Jansen F. 1999b. Innovative ceramic materials for porous-medium burners II, *Interceram* 48:424–33.

Pickenäcker O and Trimis D. 2001. Experimental study of a staged methane/air burner based on combustion in a porous inert medium. *Journal of Porous Media* 4:197–213.

Porvair. *Metal foam*. http://www.porvairadvancedmaterials.com (accessed March 18, 2008).

Prinn R, Reilly JM, Sarofim M, Wang C and Felzer B. 2007. Effects of air pollution control on climate: Results from an integrated global system model. In *Human induced climate change: An interdisciplinary assessment*, ed. ME Schlesinger, HS Kheshgi, J Smith, FC de la Chesnaye, JM Reilly, T Wilson and C Kolstad, 93–102. New York: Cambridge University Press.

Promeos. *Porous burner*. http://www.promeos.com (accessed March 18, 2008).

Qiu K and Hayden ACS. 2006. Premixed gas combustion stabilized in fiber felt and its application to a novel radiant burner. *Fuel* 85:1094–1100.

Qiu K and Hayden ACS. 2007. Thermophotovoltaic power generation systems using natural gas-fired radiant burners. *Solar Energy Materials and Solar Cells* 91:588–96.

Qui K and Hayden ACS. 2009. Increasing the efficiency of radiant burners by using polymer membranes. *Applied Energy* 86:349–54.

Ramos FM, Bambace LAW, Lima IBT, Ros RR, Mazzi EA and Fearnside PM. 2009. Methane stocks in tropical hydropower reservoirs as a potential energy source. *Climatic Change* 93:1–13.

Rasi S, Läntelä J, Veijanen A and Rintala J. 2008. Landfill gas upgrading with countercurrent water wash. *Waste Management* 28:1528–34.

Reilly JM, Jacoby HD and Prinn RG. 2003. *Multi-gas contributors to global climate change: Climate impacts and mitigation cost of non-CO_2 gases*. Arlington, Virginia: Pew Centre on Global Climate Change.

Reilly JM, Prinn RG, Harnisch J, Fitzmaurice J, Jacoby HD, Kicklighter D, Melillo J, Stone P, Sokolov A and Wang C. 1999. Multi-gas assessment of the Kyoto Protocol. *Nature* 401:549–55.

Rigby M, Prinn RG, Fraser PJ, Simmonds PG, Langenfelds RL, Huang J, Cunnold DM, Steele LP, Krummel PB, Weiss RF, O'Doherty S, Salameh PK, Wang HJ, Harth CM, Mühle J and Porter LW. 2008. Renewed growth of atmospheric methane. *Geophysical Research Letters* 35:L22805.

Robinson DR, Fernandez R and Kantamaneni RK. 2003. Methane emissions mitigation options in the global oil and natural gas industries. Paper presented at the 3rd International Methane and Nitrous Oxide Mitigation Conference, Beijing, China. November 17–21.

Rogers GFC and Mayhew YR. 1995. *Thermodynamic and transport properties of fluids: SI units*. 5th ed. Oxford: Blackwell.

Romero CE. 1998. Reduced kinetic mechanism for NO_X formation in laminar premixed CH_4/air flames. *Fuel* 77:669–75.

Roxbee Cox H. 1951. Some fuel and power projects. *Proceedings of the Institution of Mechanical Engineers* 164: 407–24.

RVT Process Equipment. *Saddles ½" Ceramics*. http://www.rvtpe.net/wp-content/uploads/td_fk_en/Saddles_12_Stonew.pdf (accessed March 10, 2009).

Rumminger MD. 1996. Numerical and experimental investigation of heat transfer and pollutant formation in porous direct-fired radiant burners. PhD thesis, The University of California, Berkeley.

Rumminger MD, Dibble RW, Heberle NH and Crosley DR. 1996. Gas temperature above a porous radiant burner: Comparison of measurements and model predictions. *Proceedings of the Combustion Institute* 26:1755–62.

Sadasivuni V and Agrawal AK. 2009. A novel meso-scale combustion system for operation with liquid fuels. *Proceedings of the Combustion Institute* 32:3155–62.

San-Gobain NorPro. *Heat sink and heat transfer media products and materials*. http://www.norpro.saint-gobain.com (accessed March 18, 2008).

Sapoundjiev H and Aubé F. 1999. *Catalytic flow reversal reactor technology: An opportunity for heat recovery and greenhouse gas elimination from mine ventilation air*. CETC report 1999–51/1999–07–29. Varennes, Canada: Natural Resources Canada CANMET Energy Technology Centre.

Sapoundjiev H, Aubé F and Trottier R. 1999. *Elimination of dilute methane emissions from underground mine and oil and natural gas production sectors*. CETC report 1999–13/1999–02–12. Varennes, Canada: Natural Resources Canada CANMET Energy Technology Centre.

Sathe SB, Kulkarni MR, Peck RE and Tong TW. 1990. An experimental and theoretical study of porous radiant burner performance. *Proceedings of the Combustion Institute* 23:1011–18.

Sathe SB, Peck RE and Tong TW. 1990. A numerical analysis of heat transfer and combustion in porous radiant burners. *International Journal of Heat and Mass Transfer* 33:1331–38.

Sato A, Hashiba K, Hasatani M, Sugiyama S and Kimura J. 1975. A correctional calculation method for thermocouple measurements of temperatures in flames. *Combustion and Flame* 24:35–41.

Saveliev AV, Kennedy LA, Fridman AA and Puri IK. 1996. Structures of multiple combustion waves formed under filtration of lean hydrogen-air mixtures in a packed bed. *Proceedings of the Combustion Institute* 26:3369–75.

Schmidt J, Scheiffele M, Mach A and von Issendorff F. 2005a. Highly porous non-oxide ceramic matrix composites (C/SiSiC and SiSiC) for porous burner applications. Paper presented at the Conference on Porous Ceramic Materials (PCM 2005), Bruges, Belgium. October 20–21.

Schmidt J, Scheiffele M, Mach A, von Issendorff F and Ortona A. 2005b. Manufacturing, characterization and testing of SiSiC foams for porous burner applications. Paper presented at the Conference on Porous Ceramic Materials (PCM 2005), Bruges, Belgium. October 20–21.

Schmidt J, Scheiffele M, Mach A and von Issendorff F. 2007. Fabrication and testing of corrugated 3D SiSiC ceramics for porous burner applications. *Industrial Ceramics* 27:127–130.

Schreel KRAM, van den Tillaart EL and de Goey LPH. 2005. The influence of burner material properties on the acoustical transfer function of radiant surface burners. *Proceedings of the Combustion Institute* 30:1741–48.

Schwer DA, Lu P and Green WH. 2003. An adaptive chemistry approach to modeling complex kinetics in reacting flows. *Combustion and Flame* 133:451–65.

Scott Health & Safety. *Scout multi gas monitoring system*. http://www.scotthealthsafety.com/americas/en/Products/Instruments/Portable/scoutpid.aspx (accessed June 4, 2009).

Shearer MJ and Khalil MAK. 2000. Rice agriculture: Emissions. In *Atmospheric methane: Its role in the global environment*, ed. MAK Khalil, 170–89. Berlin, Germany: Springer-Verlag.

Shirley A, Porto J and Hawk EW. 1996. A demonstration of methane recovery from coal mine gases by pressure swing adsorption. Paper presented at the 1997 International Coalbed Methane Symposium, Tuscaloosa, AL. May 12–16.

Shrestha SOB and Narayanan G. 2008. Landfill gas with hydrogen addition: A fuel for SI engines. *Fuel* 87:3616–26.

Singer SF. 1971. Stratospheric water vapour increase due to human activities. *Nature* 233:543–5.

Sinnott RK. 1999. *Coulson & Richardson's chemical engineering*, vol. 6, 3rd ed. Oxford: Butterworth-Heinemann.

Skjøth-Rasmussen MS, Holm-Christensen O, Østberg M, Christensen TS, Johannessen T, Jensen AD, Glarborg P and Livbjerg H. 2004. Post-processing of detailed chemical kinetic mechanisms onto CFD simulations. *Computers and Chemical Engineering* 28:2351–61.

Slimane RB, Lau FS, Khinkis M, Bingue JP, Saveliev AV and Kennedy LA. 2004. Conversion of hydrogen sulfide to hydrogen by superadiabatic partial oxidation: Thermodynamic consideration. *International Journal of Hydrogen Energy* 29:1471–77.

Sly LI, Bryant LJ, Cox JM and Anderson JM. 1993. Development of a biofilter for the removal of methane from coal mine ventilation atmospheres. *Applied Microbiology and Biotechnology* 39:400–404.

Smart A and Aspinall A. 2009. *Water and the electricity generation industry: Implications of use*. Waterlines Report Series number 18. Canberra, Australia: Australian Government National Water Commission.

Smith GP, Golden DM, Frenklach M, Moriarty NW, Eiteneer B, Goldenberg M, Bowman CT, Hanson RK, Song S, Gardiner WCJ, Lissianski VV and Qin Z. 1999. *GRI-Mech 3.0*. http://www.me.berkeley.edu/gri-mech (accessed September 1, 2006).

Smucker MT and Ellzey JL. 2004. Computational and experimental study of a two-section porous burner. *Combustion Science and Technology* 176:1171–89.

Solomons TWG. 1996. *Organic chemistry*. 6th ed. New York: Wiley.

Srivastava M and Harpalani S. 2006. Systematic quantification of ventilation air methane and its evaluation as an energy source. *Mining Engineering* 58:52–6.

Stevens CM and Whalen M. 2000. The isotopic composition of atmospheric methane and its sources. In *Atmospheric methane: Its role in the global environment*, ed. MAK Khalil, 25–41. Berlin, Germany: Springer-Verlag.

Su S and Agnew J. 2006. Catalytic combustion of coal mine ventilation air. *Fuel* 85:1201–10.

Su S, Beath A, Guo H, Mallet C. 2005. An assessment of mine methane mitigation and utilization technologies. *Progress in Energy and Combustion Science* 31:123–70.

Su S, Chen H, Teakle P and Xue S. 2008. Characteristics of coal mine ventilation air flows. *Journal of Environmental Management* 86:44–62.

Takami H, Suzuki T, Itaya Y and Hasatani M. 1998. Performance of flammability of kerosene and NO_X emission in the porous burner. *Fuel* 77:165–71.

Takeno T and Sato K. 1979. An excess enthalpy flame theory. *Combustion Science and Technology* 20:73–84.

Temperature Controls. http://www.temperature.com.au (accessed June 4, 2009).

Thorneloe SA, Barlaz MA, Peer R, Huff LC, Davis L and Mangino J. 2000. Waste management. In *Atmospheric methane: Its role in the global environment*, ed. MAK Khalil, 234–262. Berlin, Germany: Springer-Verlag.

Tillman DA and Harding NS. 2004. *Fuels of opportunity: Characteristics and uses in combustion systems*. Oxford: Elsevier.

Toledo M, Bubnovich V, Saveliev A and Kennedy L. 2009. Hydrogen production in ultrarich combustion of hydrocarbon fuels in porous media. *International Journal of Hydrogen Energy* 34:1818–27.

Tomlin AS, Turányi T and Pilling MJ. 1997. Mathematical tools for the construction, investigation and reduction of combustion mechanism. In *Low temperature combustion and autoignition*, ed. MJ Pilling, 293–437. Amsterdam, The Netherlands: Elsevier.

Trimis D and Durst F. 1996. Combustion in a porous medium: Advances and applications. *Combustion Science and Technology* 121:153–68.

Trimis D, Pickenäcker O and Wawrzinek K. 2005. Porous burners. In *Cellular ceramics: Structure, manufacturing, properties and applications*, ed. M Scheffler and P Colombo, 484–508. Weinheim, Germany: Wiley.

Tseng C-J and Howell JR. 1996. Combustion of liquid fuels in a porous radiant burner. *Combustion Science and Technology* 112:141–61.

Turányi T. 1990a. Reduction of large reaction mechanisms. *New Journal of Chemistry* 14:795–803.

Turányi T. 1990b. Sensitivity analysis of complex kinetic systems: Tools and applications. *Journal of Mathematical Chemistry* 5:203–48.

Turányi T and Zsely IG. 2005. *KINALC Version 2.0*. http://garfield.chem.elte.hu/Combustion/Combustion.html (accessed September 1, 2006).

United Nations (UN). 1992. *United Nations Framework Convention on Climate Change*. New York: United Nations.

Venkatraman K and Ashwath N. 2009. Can phytocapping technique reduce methane emission form municipal landfills? *International Journal of Environmental Technology and Management* 10: 4–15.

Versteeg H and Malalasekra W. 2007. *An introduction to computational fluid dynamics: The finite volume method*. 2nd ed. Harlow, UK: Pearson Education.

Vijaykant S and Agrawal AK. 2007. Liquid fuel combustion within silicon-carbide coated carbon foam. *Experimental Thermal and Fluid Science* 32:117–25.

Viskanta R. 1991. Enhancement of heat transfer in industrial combustion systems: Problems and future challenges. Paper presented at the 3rd ASME/JSME Thermal Engineering Joint Conference, Reno, NV. March 17–22.

Viskanta R. 2005. Combustion and heat transfer in inert porous media. In *Handbook of porous media*, ed. K Vafai, 607–44. 2nd ed. New York: Marcel Dekker.

Viskanta R and Gore JP. 2000. Overview of cellular ceramics based porous radiant burners for supporting combustion. *Clean Air* 1:167–203.

Viskanta R. 1966. Radiation transfer and interaction of convection with radiation heat transfer. In *Advances in Heat Transfer*, vol.1, ed. TFJ Irvine and JP Hartnett. New York: Academic Press.

Vogel BJ and Ellzey JL. 2005. Subadiabatic and superadiabatic performance of a two-section porous burner. *Combustion Science and Technology* 177:1323–38.

von Issendorff F, Stamatov V, Mach A and Trimis D. 2005. Application of porous burners in industrial furnaces for glass production. Paper presented at the 8th International Conference on Technologies and Combustion for a Clean Environment (Clean Air VIII), Lisbon, Portugal. June 27–30.

Voß S. 2008. Private communication.

Voß S, Al-Hamamre Z and Trimis D. 2007a. Characterisation of the emissions behaviour and combustion stability in porous media burner by using low and medium calorific value gases. *Gaswärme International* 56: 200–204.

Voß S, Al-Hamamre Z and Trimis D. 2007b. Experimental and numerical investigations of a post combustion system on the base of the porous burner technology for the application in SOFC fuel cell systems. Paper presented at the 9th International Conference on Energy for a Clean Environment (Clean Air IX), Póvoa de Varzim, Portugal. July 2–5.

Voß S, Kautz M, Steinbrück R, Schiesswohl E, Turner H, tom Felde J, Volkert J and Trimis D. 2008. Modulating hydrogen combustion system based on a porous media burner for HT-PEM systems. Paper presented at the 17th World Hydrogen Energy Conference, Brisbane, Australia. June 15–19.

Wall TF. 2007. Combustion processes for carbon capture. *Proceedings of the Combustion Institute* 31:31–47.

Wang WC, Dudek MP, Liang MP and Kiehl JT. 1991. Inadequacy of effective CO_2 as a proxy in simulating the greenhouse effect of other radiatively active gases. *Nature* 350:573–7.

Watts RG. 1997. *Engineering response to global climate change: Planning a research and development agenda*. Boca Raton, FL: CRC Press.

Wawrzinek K, Kesting A, Künzel J, Pickenäcker K, Pickenäcker O, Trimis D, Franz M and Härtel G. 2001. Experimental and numerical study of applicability of porous combustors for HCl synthesis. *Catalysis Today* 2001:393–7.

Weclas M. *Potential of porous medium combustion technology as applied to internal combustion engines*. Sonderdruck Schriftenreihe der Georg-Simon-Ohm-Fachhochschule Nürnberg Nr. 32. Nuremberg, Germany: Georg Simon OHM University of Applied Sciences Nuremberg.

Weinberg FJ. 1971. Combustion temperatures: The future? *Nature* 233:239–41.

Wendt M, Glynn P, Condren J, Mallett C, Beath A, Van Hattem R, Allwood A, and Addinell S. 2003. *Externally fired turbines for mitigation of ventilation air and waste coal emissions*. Report C9064. Brisbane, Australia: Australian Coal Association Research Program (ACARP).

West JJ and Fiore AM. 2005. Management of tropospheric ozone by reducing methane emissions. *Environmental Science and Technology* 39:4685–91.

West JJ, Fiore AM, Horowitz LW and Mauzerall DL. 2006. Global health benefits of mitigating ozone pollution with methane emission controls. *PNAS* 103:3988–93.

Westbrook CK and Dryer FL. 1984. Chemical kinetic modelling of hydrocarbon combustion. *Progress in Energy and Combustion Science* 10:1–57.

Weyant JP, de la Chesnaye FC and Blanford GJ. 2006. Overview of EMF-21: Multigas mitigation and climate policy. *The Energy Journal* Multi-greenhouse Gas Mitigation and Climate Policy Special Issue:1–32.

Wharton JA, Ellzey JL and Bogard DG. 2005. An experimental study of turbulence intensities and non-uniformities in the exit flow from a porous combustor. *Experiments in Fluids* 38:701–7.

White CM, Smith DH, Jones KL, Goodman AL, Jikich SA, LaCount RB, DuBose SB, Ozdemir E, Morsi BI and Schroeder KT. 2005. Sequestration of carbon dioxide in coal with enhanced coalbed methane recovery: A review. *Energy & Fuels* 19:659–724.

Wood S and Harris AT. 2008. Porous burners for lean-burn applications. *Progress in Energy and Combustion Science* 34: 667–84.

Wuebbles DJ and Hayhoe KAS. 2002. Atmospheric methane and global change. *Earth-Science Reviews* 57:177–210.

Wuebbles DJ, Hayhoe KAS and Kotamarthi R. 2000. Methane in the global environment. In *Atmospheric methane: Its role in the global environment*, ed. MAK Khalil, 304–41. Berlin, Germany: Springer-Verlag.

Xiao F, Sohrabi A and Karim GA. 2008. Effects of small amounts of fugitive methane in the air on diesel engine performance and its combustion characteristics. *International Journal of Green Energy* 5:334–45.

Xie M-Z, Shi J-R, Deng Y-B, Liu H, Zhou L and Xu Y-N. 2009. Experimental and numerical investigation on performance of a porous medium burner with reciprocating flow. *Fuel* 88:206–213.

Xiong T-Y, Khinkis MJ and Fish FF. 1995. Experimental study of a high-efficiency, low emission porous matrix combustor-heater. *Fuel* 74:1641–47.

Yang H, Minaev S, Geynce E, Nakamura H and Maruta K. 2009. Filtration combustion of methane in high-porosity micro-fibrous media. *Combustion Science and Technology* 181:654–69.

Yang B and Pope SB. 1998. Treating chemistry in combustion with detailed mechanism: *In-situ* adaptive tabulation in principle directions. *Combustion and Flame* 112:85–112.

Zabetakis MG. 1965. Flammability characteristics of gases and vapors. In *Bureau of Mines Bulletin 627*, Washington, DC: United States Bureau of Mines.

Zhang G, Cai X, Liu M, Lin B, Chen Y and Wang L. 2006. Characteristic analysis of low-velocity gas filtration combustion in an inert packed bed. *Combustion Theory and Modelling* 10:683–700.

Zhao Z, Wang C and Xie M. 2009. Numerical study on the realization of compression ignition in a type of porous medium engine fueled with isooctane. *Fuel*. In press.

Zhdanok SA, Dobrego KV and Futko SI. 1998. Flame localization inside axis-symmetric cylindrical and spherical porous media burners. *International Journal of Heat and Mass Transfer* 41:3647–55.

Zhdanok SA, Dobrego KV and Futko SI. 2000. Effect of porous media transparency on spherical and cylindrical filtrational combustion heaters performance. *International Journal of Heat and Mass Transfer* 43:3469–80.

Zhdanok S, Kennedy LA and Koester G. 1995. Superadiabatic combustion of methane air mixtures under filtration in a packed bed. *Combustion and Flame* 100:221–31.

Zhou XY and Pereira JCF. 1998. Comparison of four combustion models for simulating the premixed combustion in inert porous media. *Fire and Materials* 22:187–97.